# Channel bar radar architecture and evolution in the wandering gravel-bed Fraser and Squamish Rivers, British Columbia, Canada

by

**Colin Wooldridge**
BSc (Hons), Simon Fraser University, 1999
GIT, Association of Professional Engineers and Geoscientists of BC, 1999

Thesis submitted in partial fulfillment of
the requirements for the degree of
MASTER OF SCIENCE
in the
Department of Geography

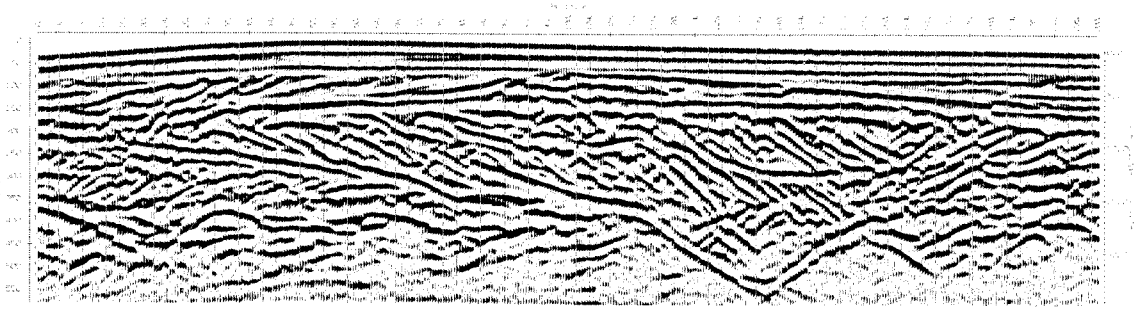


SIMON FRASER UNIVERSITY
April 2002

# APPROVAL

Name: Colin Lovell Wooldridge

Degree: Master of Science

Title of Thesis: Channel Bar Radar Architecture and Evolution in the Wandering Gravel-Bed Fraser and Squamish Rivers, British Columbia, Canada

Examining Committee:

Chair: I. Hutchinson, Associate Professor

Dr. E.J. Hickin, PGeo
Senior Supervisor
Professor, Departments of Geography and Earth Sciences
Simon Fraser University

Dr. T.A. Brennand
Committee Member
Associate Professor, Department of Geography
Simon Fraser University

Dr. M.A. Church, PGeo
External Examiner
Professor, Department of Geography
University of British Columbia

Date Approved: April 5, 2002

# Abstract

The three-dimensional (3D) subsurface alluvial architecture and evolution of four kilometer-scale gravel bars in the wandering gravel-bed Fraser and Squamish Rivers are described. Ground-penetrating radar (GPR) surveys, historic bathymetry soundings, and time-sequential aerial photographs are used to correlate the internal architecture (from basal scour surfaces to bartop deposits) to the evolution of unit bars, point bars, mid-channel bars, and bank-attached bars in the previous ~50 years.

Decimeter resolution and 3D reflection configurations were obtained from 15 km of GPR profiles shot with 50, 100, and 200 MHz antenna frequencies in ~200 m x ~200 m grids. GPR-imaged bounding surfaces matched bathymetric soundings and former bar positions mapped from historic photographs. Likewise, GPR-imaged sedimentary structures were coincident with patterns of bar translation and morphology evident in the photographic record.

The subsurface architecture of small (<1 km long, <3 m thick), mobile unit bars is characterized by internally consistent depositional packages of reflections, regardless of their in-channel position. Deeper scour surfaces below the stratigraphy of unit bars could not be correlated to photographic or bathymetric data, and are interpreted as storey boundaries delineating macroform architecture. The architecture of long-lived (>50 years) channel-scale macroforms is complex and consists of assemblages of configurations that are not genetically related. Unlike the case of unit bars, sediment is not uniformly transported, eroded, or deposited across macroforms.

Low-angle subhorizontal reflections are prominent throughout the alluvial architecture and record the migration of low-amplitude gravelly bedload sheets (2 to 3 grains thick) onto bar surfaces and in-channel. This style of stratified sheet-like sedimentation records the vertical, lateral, downstream, and upstream accretion of sediment (dependent on the dip of the strata). Of the five alluvial radar facies and two radar elements identified, the prevalence of small- to medium-scale (0.5 to 3 m), steeply inclined reflections (interpreted as slipface accretion) distinguishes wandering deposits from gravelly meandering or braiding successions. Two-dimensional, concave-up basal reflections identify channel and chute elements, which signify the multiple channeled character of wandering rivers. In contrast, channel scour elements produce 3D, scallop-shaped basal reflections, whose fill over-deepens alluvial successions.

Alluvial sediments (8 to 24 m thick) likely deposited in the last few hundred years overlie large-scale (>6.5 m), steeply dipping reflections, interpreted to be delta foresets deposited ~10,000 years ago during deglaciation. The style of fluvial sedimentation does not appear to have changed in this period, and the preservation of large-scale scour hollows indicates that wandering systems are vertically stable. Together, the unsteady episodic evolution of gravel barforms and their internal architecture confirm the transitional nature of the wandering type of river planform between meandering and braiding river types.

Hey boys,
your boat's riding a little high,
you must be empty.

old fishermen talk

**When force is necessary,**
**there it must be applied boldly, decisively and completely.**

**But one must know the limitations of force;**
**one must know when to blend force with a maneuver,**
**a blow with an agreement.**

Trotsky, *What Next?*

Risk! Risk anything!

Care no more for the opinion of others, for those voices.
Do the hardest thing on earth for you.
Act for yourself. Face the truth.

Katherine Mansfield, *Journal*

it is...natural for man to personify
everything that he wishes to comprehend,
in order that later he may control it

Freud, *The Future of an Illusion*

# Acknowledgements

The standard and spirit of this thesis was set long ago
by my good friend Carl Freeman, a petroleum geologist and climber.
Even though you be dead my man, I still haven't caught you.

Although my name sits in isolation on the front cover of this thesis - the work contained herein would not have been possible without the collaboration, ideas, and technical support of those named below. Handshakes and shifty looks to all of you.

**The Senior** Ted Hickin. Simply the best. The opportunity to work in my own backyard on big rivers has been fantastic. You challenge at the right moment and poise subtle comments that delve into unanswerable questions and grand concepts involving the genesis and maintenance of river behavior.

**The Second** Tracy Brennand continually questioned me, resulting in fuller explanations of the wandering phenomena. In the quest for TRUTH in advertising, your beliefs never wandered.

**The External** Thanks to Michael Church for inviting Ted and I to untangle the Fraser River's gravelly subsurface and for constraining some of the more speculative segments of the thesis.

**The Fraser Group** Darren Ham provided access to UBC resources and intriguing whole river comparisons within which to set my work. Steve Rice posed many questions and in doing so inadvertently directed a portion of my radar program. Marvin Rosenau and Laura Rempel, when not teasing me about our boat, opened my eyes to the interactive world of fish and gravel.

**Permission** Thanks to Valerie Cameron from the Ministry of Environment and Solvej Patschke from the Department of Fisheries and Oceans for securing permission to radar Fraser River bars.

**Advice** Sandy Vanderburgh and Olav Lian provided acute career insights early in my masters as we wandered drunkenly through the graveyards of Drynoch.

**SCUMM** To the rough and ready SCUMM out there - bring it on. The Hickin School of Cool Underwater Macroturbulent Motion contributed ideas, drinks and denial to the thesis. Porn Star Coke (aka Chris Simpson) wore sandy braids, Channa Pelpola dipped to the Fitz, Columbia Kevin Tabata got stressed, and Derek Ray fanned Charlotte.

**Data** Special thanks to UBC Geography and Michael Church for providing Fraser River bathymetry data and 2000 and 2001 aerial photographs. Dave Hutchinson from the Water Survey of Canada generously supplied the discharge data. Michael Jordan-Knox always came through with software. Mapping work got rolling with Craig Coburn's expertise in ER Mapper. Digital TRIM files were kindly provided by Adrian Hickin. Jasper Stoodley and Jeff Gutsell cranked me through the details of ArcView while Darren Ham offered publishing tips. Prof. Michael Roberts supplied photographs of the Fraser River and his interpretative style kept me American.

**Radar** This thesis would never have made the light of day without Chris Blay's unselfish and fearless attitude toward me in lending his bomber Compaq 486. Toast the Brit! I collected about 95% of the radar data by myself with the help of Asterix and Obelix, but to the plethora of young geo-apprentices who slaved as my radar jockeys, straining necks and backs under hot (and kold) skies and gravel wastelands: *I hope I have not stolen too much life from you.*

**Paid Radar Jockeys** My main mapper and radar man was Sean Todd whose disheveled morning getup and verbosity amused me. Joel Epp endured long Squamish days and lengthy gear hauls into the middle of the log sort yard. Sarah 'the tough girl' Baines pushed through all that deep cold water without rebellion.

**Volunteer Radar Jockeys** Solvej 'hyporheic' Patschke eliminated human error and kicked the Fraser to the big sky. Scott 'Stouhal' Babakaiff and his $2\pi d$ reminded me that water transports sediment. Matt Cleary ran the big number day and went numb. Cacti pricked Tim 'wetback' Johnsen as we discovered multiplication on the ancestral Deadman Delta. Quinn Jordan-Knox got deep and unresolved. Channa Pelpola broke his back dipping to Britannia. Crystal Huscroft staggered drunk under the spatially averaged load. Greg 'the brain' Matsuo stuffed rocks into his cranial void.

**The Written** Kathy Glen and Jennifer Lane provided motivation to finish the thesis, while the Yorkshire Motel in York, Nebraska provided an explosive setting to do so. Kevin Tabata caught critical copy-edit blunders. Prof. James MacEachern polished my american-english and harped on colloquialisms.

**The Unwritten** There is another component to this thesis that is unwritten within these pages: the agony, suffering, disillusionment, and utter frustration that accompany a fellow trying to motivate ground-penetrating radar to work for him. 2 dead laptops, 1 dead timing board, 9 dead batteries, 11 new batteries, 1 dead propeller, 1 pair of *stolen* size 15 runners, 1 rockslide, 1 dead car, and 2 dead car motors did the job - *barely*. GPR stole part of my life that I will never regain and for that I have to say sorry to all those I ignored, hurt, raged at, and destroyed - for you there will never be a next time.

Radar, radar all around,
can you feel the EM waves
bouncing underground?
Can you see the structure,
the dip, the trace?
And god damn,
the noise it makes.

Give it up.
The bar's too big.
The battery's down.
The wind's too strong
blowing silt all day long
filling hard drives, ports, and fans.

Fishers wonder at the sight
as their hooks bite
sockeye, chinook and Fin.
But the fibre-optics groan
as seaplanes are flown
throwing spray as they touch and go
only leaving their echo.
Yet the tugs are sprinting you know.
Pushing waves and swell
'cause the logs must flow.

The nite comes hard and cold.
Is the rain washing the keyboard clean?
Did you lose the data?
'Cause damn it Scott,
now the sun's too hot
and shit,
the laptop's stopped.

**Inspiration** Scott Babakaiff, Ted Hickin, and the Squamish River provided inspiration long ago to wade into fluvial settings and Diana Allen kept me stoked on hydro.

**Funding** The project was funded in part by a NSERC (Natural Sciences and Engineering Research Council of Canada) grant awarded to E.J. Hickin and a DEGIFS (Division of Engineers and Geoscientists in the Forest Sector) Bursary awarded to C.L. Wooldridge.

# Contents

# Figures

# Tables

# 1 Introduction

## 1.1 The Problem

The two- and three-dimensional architecture of channel-scale barforms provides sedimentary and stratigraphic evidence of depositional style from which fluvial style (*e.g.*, braiding, meandering) and paleohydraulics (*e.g.*, flow depth, channel multiplicity) are typically inferred and interpreted in the rock record. Inferences and interpretations are largely based on physical modeling and observations in modern/contemporary rivers. These observations, however, rarely link subsurface structure (*e.g.*, bedding geometries and lithofacies) to known patterns of sediment erosion and deposition (*e.g.*, the migration history and bed topography of barforms) (Bridge, 1993b; Willis, 1993). Instead, the internal stratification and external bounding geometries of ancient gravelly sediments are readily interpreted to represent specific bar morphologies (*e.g.*, longitudinal, transverse) while the contemporary architecture of these bars types is not well known. This is especially true of large gravel-bed (and sand-bed) modern rivers several hundred meters wide with channel depths greater than 4 m. Here, high water tables limit trenching and curtail detailed sedimentary analysis to bartop deposits. There has been little examination of the complete thickness of bar architecture from basal scour surfaces to bartop deposits.

The objectives of this study are to determine the subsurface architecture of four barforms and to link their internal architecture to the style of deposition revealed from historic aerial photographs during their evolution. Alluvial architecture is defined as the geometry, proportion, and spatial distribution of the various types of fluvial deposits in sedimentary basins (Stouthamer, 2001). For the purposes of this study, architecture is limited to the scale of a storey, defined as a deposit of a single channel bar and adjacent channel fill (Bridge and Mackey, 1993a).

## 1.2 Resolving the Problem

Ground-penetrating radar (GPR) is used to identify the large-scale subsurface architecture of four channel bars in the wandering gravel-bed Squamish and Fraser Rivers. The radar stratigraphy is compared to bar development over the past 50 to 58 years mapped from historic aerial photographs and bathymetric soundings. Integrating subsurface data with patterns of bar growth, erosion, and translation enables wandering barforms to be characterized, and provides a modern analog for the interpretation of wandering fluvial style in the rock record.

The concept of linking the subsurface (from GPR data) to the development of bars (from aerial photographs) is relatively new. Yet the technique is also being employed by Lunt *et al.* (2001) to describe channel bar deposits in the braiding Sagavanirktok River, Alaska, and was previously used to describe the

3D large-scale structure of point bar deposits in the meandering River South Esk, Scotland (Bridge *et al.*, 1995). This integrative method extends work in wandering gravel-bed rivers, in which Roberts *et al.* (1997) inferred patterns of bar development from the GPR-imaged internal structure of an active lateral bar. In this study, patterns of bar development are known, not inferred, allowing the subsurface architecture to be correlated with patterns of bar development. Squamish and Fraser River radar architectures are analyzed and compared for scale differences, complexity, geometry, and depositional style. Intra-river comparisons provide a wider spectrum of channel instability and bar development from which to construct an architectural framework.

The remainder of Chapter 1 reviews the geomorphology of wandering gravel-bed rivers, discusses barform typology, reviews the radar stratigraphy of braiding, meandering, and wandering river deposits, describes gravelly sedimentary structures (including their radar signatures) and associated depositional processes, and describes the study area. Chapter 2 describes the bathymetric, topographic, photographic, and GPR methods. Chapters 3, 4, 5, and 6 present the results, and discuss the radar stratigraphy of TFLENT Bar in Squamish River, and Calamity, Queens, and Wellington Bars in Fraser River. Chapter 7 concludes by synthesizing the results into a depositional framework. Appendix 1 contains 50, 100, and 200 MHz GPR profiles shot on each bar (written to a CD in *.pdf format).

## 1.3 Wandering Gravel-Bed Fluvial Style

The term wandering gravel-bed river was first used by Neill (1973) to describe the Athabasca River at Whitecourt, Alberta, and by Lewis and McDonald (1973) to describe the channel patterns of arctic rivers flowing across the Yukon north slope. Church (1983) entrenched the term in the literature by describing the character of channel instability and geomorphology of the Bella Coola River, British Columbia. Wandering rivers are multiple channeled with moderate bedload transport rates facilitating channel bar development in laterally unstable sedimentation zones (Church, 1983). Flow divides around mid-channel vegetated bars (islands), and is diverted into sloughs (abandoned channels) at moderate- and high-stage flows (Figs. 1.1A-D). Flow bifurcation leads to a hierarchy of channels with the main channel conveying the thalweg (the high velocity thread) and secondary channels carrying reduced flow volumes and velocities. Channels shift by progressively eroding banks opposite growing bars, by rapidly avulsing, or when flow diminishes around one side of a mid-channel bar (Desloges and Church, 1987). Avulsion and flow reduction through channels lead to channel abandonment and the infilling of sloughs.

Figures 1.1A-D clearly show the wandering style with multiple channels splitting around large (kilometer-scale), prominent gravel bars, including lateral bars that are attached to the channel bank or to islands, point bars at bends, and mid-channel bars in areas of flow expansion. The form of channel pattern in multiple channeled rivers is partly stage dependent (Knighton, 1984), and in this sense wandering rivers at mean annual discharge have intermediate sinuosity indexes between 1.2 and 1.5 (ratio of thalweg length to valley length) and braid indexes between 1 and 3 (number of braids per mean meander wavelength) (Brierley, 1989b).

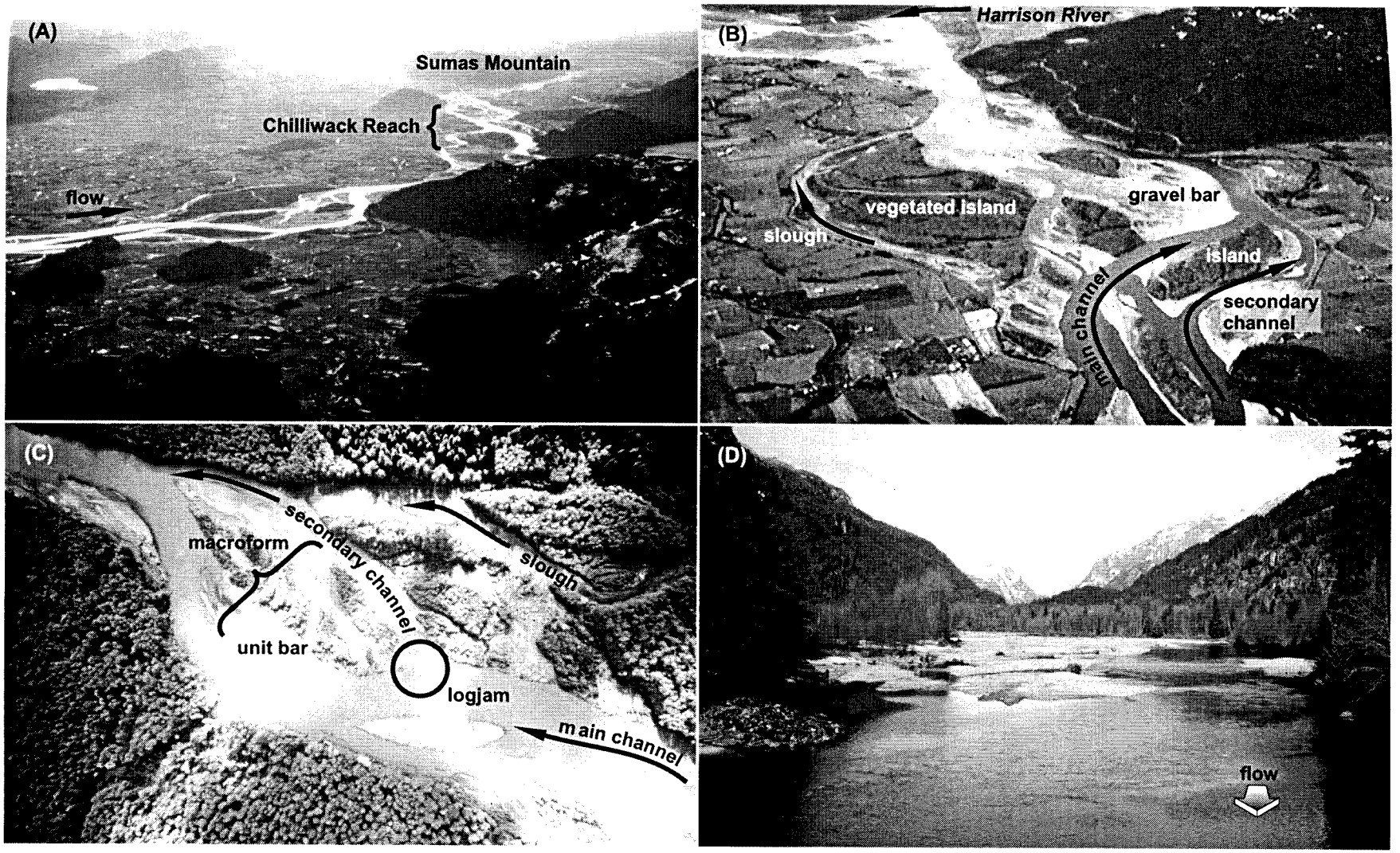


**Fig. 1.1** Wandering gravel-bed fluvial style. **(A)** Multiple channeled Fraser River flowing around bedrock knobs to the Strait of Georgia at the top of the photograph. Photograph courtesy of M.C. Roberts. **(B)** Downstream view of irregularly sinuous Fraser River splitting around channel bars and vegetated islands. Photograph courtesy of M.C. Roberts. **(C)** Mid-channel bars in Squamish River downstream of Ashlu River confluence. Photograph courtesy of E.J. Hickin. **(D)** Upstream view of the wandering river style immediately upstream of TFLENT Bar in the mountainous Squamish River valley.

The irregularly sinuous channels sporadically transport bedload and bar growth is largely accomplished by the attachment and incorporation of sediment waves (unit bars and gravelly bedload sheets) onto relatively stable bars (>50 years old; Figs. 1.1C, 1.2A, and 1.2B). The attachment of unit bars alters the geometry of the channel and deflects flow onto adjacent banks and bars instigating localized erosion and channel shifting. Eroded sediment is transported by the active channel and deposited downstream, initiating a new round of channel instability and bar growth (Desloges and Church, 1989; McLean *et al.*, 1999).

Bank erosion also incorporates complete trees, logs, and root wads into the channel. Large woody debris typically forms logjams on barheads, at the entrance to secondary channels (Gottesfeld and Gottesfeld, 1990), and in some cases builds extensive lateral jams fringing the exterior of channel bars (Fig. 1.2C). Logjams are hydraulically important structures, as they obstruct flow and promote bed scour upstream of jams (Fig. 1.2D). Conversely, the reduction of flow velocities in the lee of jams enhances sedimentation.

Floodplain formation is accomplished by three processes: (1) by the attachment of stable, vegetated islands to the floodplain after intervening sloughs have infilled, (2) by the lateral accretion of channel bars to the floodplain, and (3) by way of overbank sedimentation (Desloges and Church, 1987; Morningstar, 1987). Channel bank exposures are vertically limited (2 to 3 m in height), and show an island stratigraphy consisting of channel cobble-gravel overlain by 0 to 3 m of channel sands or overbank silty sand (Figs. 1.2E-G) (Desloges and Church, 1987; Roberts and Morningstar, 1989).

## 1.4 Barform Typology

Although there is no genetic classification of 'channel bars', the term bar is used in this study in reference to largely non-periodic, sedimentary bodies emergent at low-stage flow (*cf.* Smith, 1978). Channel bars are significant hydraulic and sedimentologic elements in gravelly rivers. They provide partial discrimination of braiding, wandering, and meandering channel patterns. Bars interact with, and influence the mean flow pattern through a reach (Church and Jones, 1982) reflecting sediment supply conditions and macro-scale channel processes rather than local fluid dynamics. Although the internal architecture of bars is largely controlled by high-stage flow conditions, falling-stage flow influences the local morphology of bar surfaces and small-scale depositional patterns (Miall, 1994).

Channel bars, in the most general sense, are "upstanding barriers of sediment emplaced across the current" (Allen, 1983). The identification of channel bars, however, is problematic because both periodic and non-periodic large-scale fluvial forms have been described as bars, with at least 32 specific bar types recognized in the fluvial literature (Smith, 1978). The indiscriminate and prolific use of morphologic bar descriptors (*e.g.*, longitudinal, diagonal) in the geological literature has led many workers to ignore the depositional processes and preserved sedimentary structures associated with such barforms (Smith, 1978).

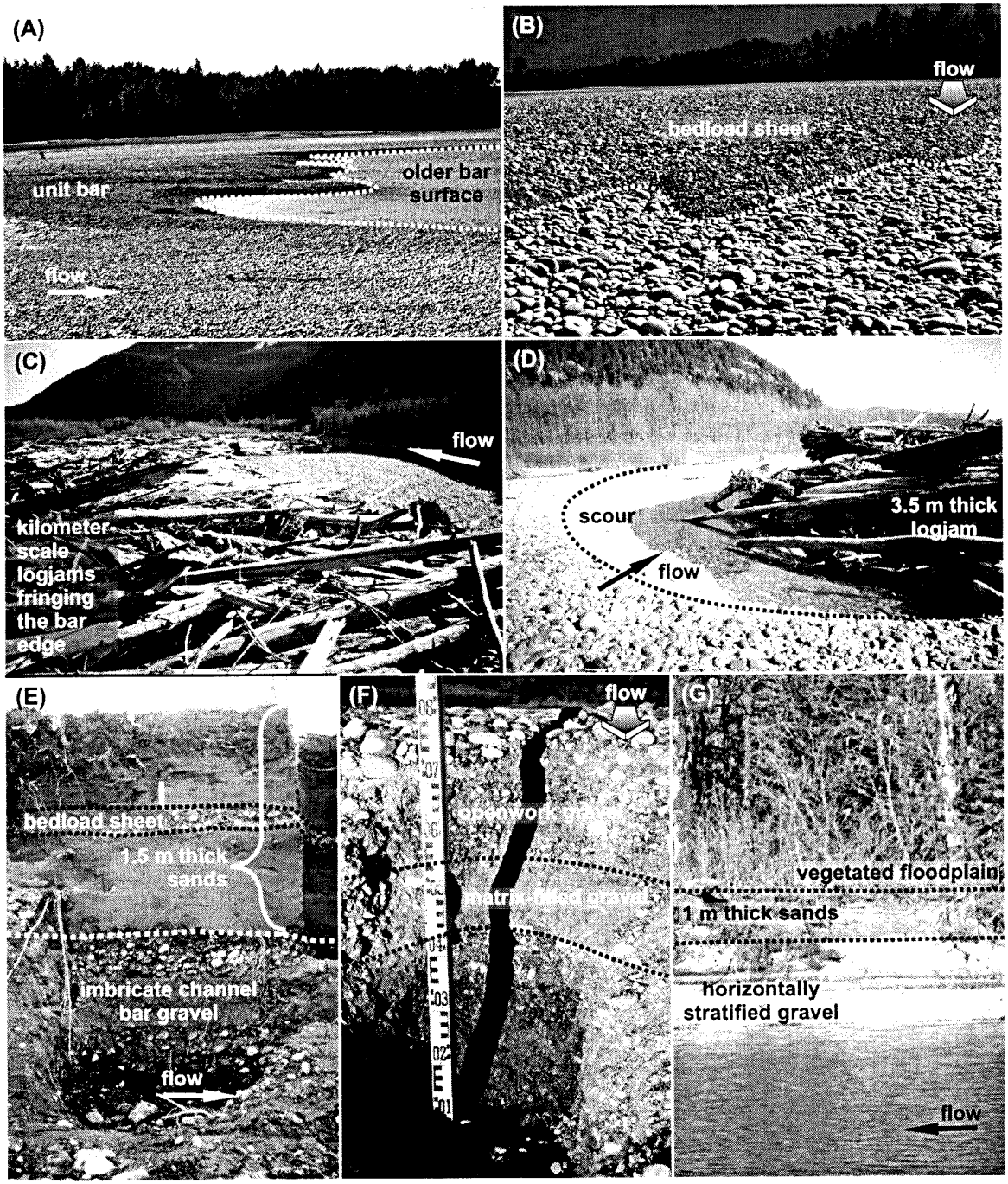


**Fig. 1.2** Characteristic gravelly bedforms, logjams, and island stratigraphy in wandering rivers. **(A)** Unit bar (0.3 to 0.4 m thick), and **(B)** bedload sheet (0.10 to 0.15 m thick), Gill Island Complex, Fraser River. Photographs courtesy of D.G. Ham. **(C)** Logjam morphology, and **(D)** logjams as hydraulic elements, TFLENT Bar, Squamish River. **(E)** Island stratigraphy, Fraser River. Photograph courtesy of M.C. Roberts. **(F)** Bar-margin slipface exposure (0.8 m high), Queens Bar, Fraser River. **(G)** Floodplain stratigraphy, Squamish River.

In an effort to standardize terminology, Ashley's (1990) report on large-scale subaqueous bedforms suggested a classification scheme of fluvially generated sedimentary bodies (Table 1.1). The scheme employs bedform descriptors that should be hydraulically important, so that a link between internal structure and genetically significant morphology can be established, especially in the interpretation of ancient facies. Ashley's (1990) classification highlights recognizable differences between barforms, which are used in identifying the scale and rhythmic nature of bars in subsurface geophysical profiles and in outcrop.

**Table 1.1** Classification of fluvially generated sedimentary bodies (Ashley, 1990), and their hierarchical ordering (Jackson, 1975).

| **Sedimentary Body** (commonly used terms) | **Periodicity** | **Hierarchical Ordering** | **Channel Position** (scaling) |
|---|---|---|---|
| **Ripples** | Periodic | Microform | In-channel (scaled to flow depth) |
| **Dunes** (linguoid bar, transverse bar) | Periodic | Mesoform | In-channel (scaled to flow depth) |
| **Unit bars** (lobe, longitudinal bar) | Quasi-periodic or solitary forms | Mesoform | In-channel (scaled to flow depth) |
| **Channel forms** (point bar, diagonal bar) | Periodic | Macroform | Part of channel (scaled to bankfull width) |
| **Braid bars, Compound bars** (longitudinal bar) | Quasi-periodic or solitary forms | Macroform | Part of channel (scaled to bankfull width) |

In this study bars are classified by their position within a channel (*e.g.*, point, mid-channel), and the hierarchical ordering of sedimentary bodies is deferred to in describing different types of channel bars (Table 1.1). Morphologic descriptors of bars are not used (*e.g.*, longitudinal, diagonal), as they connate particular depositional processes (*e.g.*, relative grain-size sorting, flow conditions) without describing preserved sedimentary structures (Smith, 1978). This study is concerned with mesoforms and macroforms, which can also be classified as simple and complex barforms, respectively.

### 1.4.1 Mesoforms (Unit Bars)

Non-periodic unit bars typically show relatively unmodified sedimentary structures whose morphologies are determined mainly by depositional processes (Smith, 1974). The internal structure of unit bars is *simple*, in the sense that depositional processes acting on a bar are largely coherent and unidirectional (Figs. 1.1C and 1.2A). Unit bars and dunes are both in-channel mesoforms (scaled to flow depth). The periodic nature of dunes ensures their preservation as spatially extensive trains at all stratigraphic levels, unlike solitary unit bars that are expected to be preserved as isolated packages.

### 1.4.2 Macroforms

Braid bars, compound bars, and channel forms are different types of macroforms that occupy substantial portions of the channel (scaled to bankfull width), and whose thickness is comparable to the mean depth of formative flows (Smith, 1985). Braid bars and compound bars are both largely non-periodic, *complex* sedimentary bodies produced by repeated cycles of deposition and erosion (including the accretion and incorporation of unit bars; Fig. 1.1C). In many cases, they are composed of several

individual bars that have become sutured together, and in fact are a complex of barforms. Braid bars divide flow into multiple channels, whereas compound bars are bank-attached forms. Channel forms, on the other hand, are periodic bars that display sequential facies associations and stratigraphy, thus facilitating (to some degree) the prediction of their spatial extent.

### 1.4.3 Islands

Vegetated channel bars, termed islands, are differentiated from topographically lower gravelly bar surfaces because vegetation influences the style of deposition across bartops and provides an indication of the relative stability of barforms (Fig. 1.1B). Some islands are dissected from the floodplain as channels reactivate abandoned sloughs, however, most islands are built from the vertical and lateral accretion of sediment onto bartops. Aggradation elevates bar surfaces to a point where flow depth is limited and shear stress is reduced allowing plant colonization (Boniface, 1985). Herbaceous willow and alder colonization provide greater flow resistance enhancing the deposition of sand and silt leading to an island stratigraphy of bar gravel overlain by channel sands. Alternatively, in the absence of active sediment transport over bar surfaces, vegetation can also become established on lower elevation bar surfaces indicating their stable nature.

## 1.5 GPR Profiling of Fluvial Deposits

Ground-penetrating radar has been used in fluvial geomorphology to identify the internal architecture and radar stratigraphy in a wide range of electrically resistive ancient and modern environments composed primarily of sand, gravel, or lithified rock. Examples include gravel bars in wandering gravel-bed rivers (Roberts *et al.*, 1997), braiding glaciofluvial outwash gravel (Huggenberger, 1993; Beres *et al.*, 1995; Olsen and Andreasen, 1995; Beres *et al.*, 1999), sandy braiding river deposits (Stephens, 1994; Bridge *et al.*, 1998; Bristow *et al.*, 1999), point bars in meander belts (Gawthorpe *et al.*, 1993; Bridge *et al.*, 1995; Leclerc and Hickin, 1997), anastomosing river channel geometry (Moorman *et al.*, 1991), and gravelly fan-delta and delta deposits (Jol and Smith, 1991; Smith and Jol, 1992, 1995, 1997; Ekes and Hickin, 2001; Pelpola, 2001).

Meandering and braiding river radar signatures and architectures have been compared by van Overmeeren (1998) and Ekes (2000). Transitional (wandering) channel architectures were identified by Vandenberghe and van Overmeeren (1999). The radar stratigraphies suggest distinct differences between braiding, meandering, and wandering deposits. Braiding river deposits are dominated by continuous, stratigraphically thick, stacked subhorizontal to horizontal reflections, and isolated (but in many cases overlapping) concave-up reflections interpreted to be gravelly bedload sheets and small channel fills, respectively. In contrast, meandering river deposits show channel-dipping, sigmoidal reflection packages interpreted to be point bar deposits, and minor occurrences of concave-up reflections representing small channel fills. The depositional style of wandering rivers appears somewhat intermediate between meandering and braiding deposits, as Vandenberghe and van Overmeeren's (1999) work shows multiple channel fills and dipping accretionary reflections. These radar signatures are similar to Roberts *et al.* (1997) GPR-imaged architecture from the wandering gravel-bed Rhone River.

# 1.6 Sedimentary and GPR Structures in Barforms

High magnitude flows transport sediment over bars as distinct bedforms. Gravelly bedforms such as bedload sheets (Fig. 1.2B) and dunes appear to migrate across, and are superimposed on bar surfaces (Gustavson, 1978; Massari, 1983; Lunt *et al.*, 2001) causing discordant flow directions within strata that delineate a single barform. In order to evaluate physical processes acting within a system, the form (structure) and texture of sediments is analyzed in this section from work on modern sediments and conglomeratic sections to identify the range of process-form relationships common to gravel-bedded rivers. Sedimentary processes and depositional environments are also inferred from the character of radar signatures rather than from the physical sedimentology of deposits. In this regard, this section also briefly documents the range of reflection configurations identified in fluvial sediments. (Table 1.2 outlines grain-sizes and the terminology used in this study.)

**Table 1.2** Grain-size scale for sediments. The Wentworth silt and sand classes have been condensed, eliminating the coarse, medium and fine subdivisions with emphasis given to gravel subdivisions (Boggs, 1995).

| Grain-size *b*-axis (mm) | Wentworth size class | Common names |
|---|---|---|
| <0.0039 | clay | mud |
| 0.0039 – 0.0625 | silt | |
| 0.0625 – 2 | sand | sand |
| 2 – 4 | granules | gravel |
| 4 – 64 | pebbles | |
| 64 – 256 | cobbles | |
| >256 | boulders | |

### 1.6.1 Crude Horizontal Stratification (*Vertical Accretion*)

Laterally continuous (100s of meters), massive (unstratified) to crude horizontally stratified conglomerate is the most dominant facies observed in ancient bedload dominated fluvial deposits, and is prevalent at all stratigraphic levels in modern river sections (Figs. 1.2E-G) (Forbes, 1983). Gravels are typically thinly stratified, poorly to moderately well sorted, clast-supported, and matrix-filled (Siegenthaler and Huggenberger, 1993). Stratification is horizontal to subhorizontal, and is discernable because of changes in grain-size, or because clast-supported, matrix-filled gravel alternates with clast-supported openwork gravel (Fig. 1.2F) (Steel and Thompson, 1983; Dawson and Bryant, 1987; Morison and Hein, 1987; Smith, 1990; Siegenthaler and Huggenberger, 1993; Bennett and Bridge, 1995).

Gravel strata show *b*-axis imbrication (*a*-axis transverse to flow direction, $a(t)$ imbrication) and are deposited from high-stage flow, grain to grain, low density tractional bedload (Eynon and Walker, 1974; Minter, 1978; Massari, 1983; Ramos and Sopena, 1983; Billi *et al.*, 1987; Karpeta, 1993; Todd, 1996). Bedload sheets are observed on Fraser and Squamish River bartop surfaces (Fig. 1.2B), but dunes are not. This suggests that horizontal gravelly stratification in bars is formed by successive deposition of bedload sheets 2 to 3 coarse grains thick (Bennett and Bridge, 1995), and 10s of meters wide prograding over bar surfaces, or deposited within channels (coarse grains $\approx D_{84}$, $D$ is the intermediate grain diameter, *b*-axis). Bedload sheets are equivalent to Hein and Walker's (1977) diffuse gravel sheets, but their terminology has been superseded (Hein, *pers. comm.*). Sedimentary evidence for bedload sheets comes

from strong, linear, graphical relations between stratal thickness and maximum particle size ($\sim D_{90}$). The relations show that stratal thickness is approximately 3 times greater than the diameter of the coarsest grains (Nemec and Steel, 1984).

Grain-size differences between sheets may be caused by fractional partitioning of grain-sizes within bedload sheets. Sheets with coarser crests (downstream margins) and finer tails have been observed in rivers (Whiting *et al.*, 1988; Lunt *et al.*, 2001), and in flumes (Dietrich *et al.*, 1989; Ashmore, 1991). Curiously, the reverse has also been noted with sheets displaying finer crests and coarser tails in rivers (Gustavson, 1978), and in flumes (Bennett and Bridge, 1995). In either case, bedload moves as pulses (sediment waves) with some sheets overtaking other sheets (Ashmore, 1991) forming larger low-relief bedforms (Livesey *et al.*, 1998) and unit bars (Fig. 1.2A).

Low density tractional bedload flow mechanisms dominate gravelly fluvial deposits, but in proximal or confined settings there are a range of processes that may interrupt normal fluvial sedimentation. High sediment concentrations and high flow velocities associated with hyperconcentrated flows and sediment gravity flows also deposit massive (unstratified) to crudely stratified sediments (Siegenthaler and Huggenberger, 1993). Hyperconcentrated flows tend to deposit thicker stratified, clast-supported, poorly to moderately sorted conglomerate with *a*-axis parallel to flow direction ($a(p)$) imbrication (Todd, 1989). In contrast, sediment gravity flows are internally chaotic (*ab*-axes are randomly oriented), poorly sorted, and typically matrix-supported (Smith, 1987; Sohn *et al.*, 1999).

*Radar Structure:* Flow-parallel and flow-normal horizontal to subhorizontal reflections have typically been interpreted as vertical accretion sediments (Huggenberger *et al.*, 1994).

### 1.6.2 Low-Angle Cross-Stratification (*Lateral, Downstream, or Upstream Accretion*)

***Lateral Accretion:*** Low-angle (5 to 15°) planar to sigmoidal gravelly cross-strata (up to 4 m thick and laterally continuous for 10 to 50 m) have been interpreted as lateral accretion surfaces. These strata demonstrate that bar surfaces built out laterally into channels while also aggrading vertically (Smith, 1974; Ori, 1982; Ramos and Sopena, 1983; Smith, 1990). Flow direction is normal to the dip of the strata (along strike) as shown by $a(t)$ imbrication.

*Radar Structure:* Flow-normal, low-angle (1 to 4°), channel-dipping, discontinuous, subparallel-to-surface reflections have typically been interpreted as lateral accretion deposits (Stephens, 1994; Naegeli *et al.*, 1996; Bridge *et al.*, 1998).

***Downstream Accretion:*** Massari (1983), Billi *et al.* (1987), and Smith (1990) interpreted low-angle (4 to 8°) inclined gravelly strata as deposits representing the downstream accretion of bars. These strata are differentiated from lateral accretion strata because the dip of the particle *b*-axis lies parallel to the dip of the inclined strata (rather than normal to dip) indicating the downstream accretion of strata.

*Radar Structure:* Downflow, low-angle (2°) dipping reflections as well as subhorizontal and undulatory reflections characterize downstream accretion radar signatures (Stephens, 1994; Bridge *et al.*, 1998).

***Upstream Accretion:*** Upstream dipping strata have not been identified in gravelly sediments to date; although they have been identified in braid bars in the sand-bed Brahmaputra River and were interpreted as upstream accretion deposits (Bristow, 1993).

*Radar Structure:* Flow-parallel, low-angle, upstream dipping reflections were interpreted as gravel dunes migrating and climbing onto a bar tip by Naegeli *et al.* (1996). The reflection pattern, however interpreted, does indicate the upstream accretion of sediment.

### 1.6.3 Planar Tabular Cross-Stratification (*Bar-Margin Slipface Accretion*)

Planar tabular cross-stratified gravelly sets are typically a minor facies occurring as solitary sets of steeply inclined (15 to 40°) planar tabular cross-strata ranging from 0.5 m thick (Karpeta, 1993) up to 4.5 m thick (Eynon and Walker, 1974; Massari, 1983). Thinner units of planar tabular cross-stratification tend to be less laterally continuous (on the scale of meters up to 30 m) than thicker units (10s of meters to >100 m parallel to the direction of transport) (Steel and Thompson, 1983; Smith, 1990). The tabular nature of the cross-strata and absence of well developed scour troughs suggests that the sets have a planar rather than trough geometry. Sets are typically interpreted as foresets deposited from sediments avalanching over migrating slipface margins of high relief barforms (Smith, 1974; Gustavson, 1978; Forbes, 1983; Massari, 1983; Ramos and Sopena, 1983; Steel and Thompson, 1983; Billi *et al.*, 1987; Morison and Hein, 1987; Smith, 1990).

Grain-size variations within, and between gravelly foreset strata can be formed by the unsteady transport of sediment (as sediment pulses or waves) to the bar-margin by migrating bedload sheets (Gustavson, 1978). Alternatively, distinct vertical assemblages of openwork and matrix-filled gravels are deposited in the lee of rapidly migrating bar-margins (Carling and Glaister, 1987; Carling, 1990). Flow separation in the lee of barforms effectively segregates the gravel from the sand and with the sand remaining in suspension it is transported through the system as suspended load. In this regard, the deposition of sand is insufficient to fill the interstices within the gravel foresets before another pulse of gravel is rapidly deposited, further advancing the barfront and burying the openwork gravels (Carling, 1990). Reactivation surfaces are commonly noted and probably record dissection of barfront margins during falling stage flows (Eynon and Walker, 1974; Karpeta, 1993).

*Radar Structure:* Oblique radar signatures have rarely been imaged in fluvial environments, a consequence of the sites profiled, rather than a lack of structures in the subsurface.

### 1.6.4 Trough Cross-Stratification (*Scour Fill or Gravel Dunes*)

***Scour Fill:*** Trough cross-stratified sediments are the second most common facies documented in outcrop, and in some successions can rival the abundance of horizontally stratified strata (Smith, 1985). Trough cross-stratified deposits typically occur as concave-up cross-strata (up to 2.5 m thick) with tangential lower contacts composed of clast-supported, matrix-filled gravel (Morison and Hein, 1987). They have also been found to alternate with openwork conglomerate (Siegenthaler and Huggenberger, 1993).

Scoop-shaped scours (pools) form where flow converges at channel confluences or between bars, and fill by sediment avalanching into pools (Massari, 1983; Steel and Thompson, 1983; Morison and Hein, 1987; Smith, 1990; Siegenthaler and Huggenberger, 1993). Scour hollows are uniquely identified on the basis of poor sorting, larger grain-sizes, and discordant fills. They are typically isolated or clustered in the sedimentary record, and along the length of the channel (Minter, 1978; Morison and Hein, 1987; Karpeta, 1993). Siegenthaler and Huggenberger (1993) note that scours are likely infilled by avalanching at the

upstream ends of the pools with sediments accreting laterally along pool edges as the pool shifts below the general level of the channel floor due to constriction of the channel. In contrast, Forbes (1983) documented shallow, gravelly scours (~1 m wide, ~10 m long, up to 1 m deep) on bartop surfaces, but in general scours are in-channel features that can over-deepen channel floors up to 6 times the mean flow depth (Best, 1987; Cowan, 1991; Ashmore, 1993; Salter, 1993; Best and Ashworth, 1997).

*Radar Structure:* Flow-normal, steeply inclined, trough-shaped reflections grading downstream into relatively low-angle reflections have been interpreted as scour hollows (Huggenberger, 1993). Beres *et al.* (1995) profiled a 300 $m^2$ area (15 m x 20 m) with a closely spaced grid (0.25 m x 0.5 m cell size) to generate 3D GPR data in the same gravel pit as Huggenberger (1993). Horizontal time slices confirmed the trough-shaped nature of a scour-pool structure and more clearly defined paleoflow direction through the pool. Scour-pools were ~2 m deep, 35 to 41 m long, and 20 to 23 m wide asymmetric structures. The multistorey, elongate scour-fill structures enclosed a fill composed of packages of oblique-tangential and sigmoidal reflections dipping between 18 and 33°, with a mean dip of 24° (Beres *et al.*, 1999).

***Gravel Dunes:*** Gravel dunes have been captured migrating along channel floors in kilometer- (Fahnestock and Bradley, 1973) and meter-scale streams (Dinehart, 1989). Although their sedimentary structures are largely unknown, trough cross-stratified sediments have been interpreted in outcrop as gravel dunes (Morison and Hein, 1987; Smith, 1990). Morison and Hein (1987) differentiated gravelly dunes from scour hollow deposits by the presence of higher proportions of sand and finer gravel with well defined sorting in cross-strata.

*Radar Structure:* Huggenberger (1993) interpreted packages of oblique-tangential and sigmoidal reflections (the fill within the scour hollows) as dune structures due to the absence of flow-normal trough structures seen in the scour hollows.

### 1.6.5 Basal, Concave-Up Forms (*Channel and Chute Floors*)

Concave-up forms grading into planar cross-stratification have been interpreted as chutes and represent deposition at, or near the bartop (Eynon and Walker, 1974; Gustavson, 1978; Massari, 1983). Where grain-size contrasts are obvious, such as conglomerate scoured into sandstone, channel floors are readily identified. In cases where gravelly floored channels scour into gravelly channel deposits, the lack of grain-size differentiation may cause contacts to appear conformable, or the contacts may be interpreted as internal scour surfaces merely separating growth intervals within a barform (Smith, 1990).

*Radar Structure:* Virtually all flow-normal radar profiles interpreted as channels or chutes are characterized by distinct concave-up basal reflections. The reflections indicate the depth of scour (Stephens, 1994), and approximate the scale of contemporary modern channels (Naegeli *et al.*, 1996). The radar stratigraphy in many cases shows concave-up reflections truncating lower concave-up reflections producing multistorey, cross-cutting relationships interpreted to be suites of complete or partial channel fills (Stephens, 1994; Roberts *et al.*, 1997; Bristow *et al.*, 1999).

### 1.6.6 Sandy Channel Sediments

Lenses of sandy deposits are found in lower velocity sites on bar surfaces, such as in the lee of logjams, at downstream bar-margins, in secondary channels and chutes, and capping vegetated islands. Similarly, they are found as discontinuous, sandy lenses interstratified in conglomeratic successions at all

stratigraphic levels. Desloges and Church (1987) and Brierley (1989b) document a range of sandy sedimentary structures typically found in wandering river channel and bar deposits, including (1) trough cross-stratification deposited by three-dimensional dunes, (2) planar tabular cross-strata deposited by two-dimensional dunes, (3) poorly defined cross-stratification indicative of scour-fill deposits, (4) horizontal stratification representing planar strata deposited under upper flow regime conditions, (5) small-scale cross-lamina deposited by lower flow regime ripples, and (6) massive sands deposited from suspension.

*Radar Structure:* Low-amplitude, gently dipping, occasionally curved, wavy, discontinuous reflections have been interpreted as small- and medium-scale sandy sets of trough cross-stratification deposited by dunes (Bristow *et al.*, 1999). Trough scores were interpreted on evidence of truncated underlying reflections (Bridge *et al.*, 1998).

# 1.7 Fraser River Study Area

Fraser River drains ~250,000 $km^2$ of south-central British Columbia, including the Rocky and Columbia Mountains, the Interior Plateau, and the Coast Mountain Range. It discharges into the Strait of Georgia adjacent to Vancouver. The annual pattern of runoff is dominated by a snowmelt freshet beginning in April, with high-stage flow occurring throughout late May, June, and early July. The mean annual flow at Hope is 2720 $m^3s^{-1}$ and at Mission it is 3410 $m^3s^{-1}$. The flood of record in 1894 is estimated to have reached 17 200 $m^3s^{-1}$ at Mission. The measured flood of record in 1948 was 15 200 $m^3s^{-1}$ at Hope, which would have been between 16 200 and 16 500 $m^3s^{-1}$ at Mission (McLean *et al.*, 1999).

The Fraser River exits from the confined bedrock Fraser River Canyon ~18 km upstream from Hope and begins depositing its gravelly bedload in a series of bars as it flows through the Fraser Lowland (Fig. 1.3). Between Hope and Laidlaw (150 km upstream from the mouth of the Fraser River), the river flows through a single channel confined by bedrock, landslide debris, and Pleistocene terraces. It emerges onto its alluvial fan at Laidlaw as a wandering gravel-bed river displaying mid-channel islands and multiple channels. The 55 km long wandering reach ends at Sumas Mountain near Chilliwack, coincident with the toe of the fan. Here, the river changes abruptly to a single-thread, sand-bed meandering channel with its entire gravel bedload deposited upstream of Sumas Mountain (McLean *et al.*, 1999).

### 1.7.1 Chilliwack Reach

Three gravel bars, Calamity, Queens, and Wellington, were profiled in the 17.5 km long Chilliwack Reach (Figs. 1.4A and 1.4B), which is a sub-reach of the wandering gravel-bed Fraser River. The upstream limit of the Chilliwack Reach is the Harrison River confluence and its downstream boundary is the Vedder River confluence, about 100 km from the Strait of Georgia. The Chilliwack Reach has a channel gradient of 0.00018 and its bed materials are 75 to 85% gravel with a $D_{50}$ of 10 to 18 mm (McLean *et al.*, 1999). Bimodal subsurface channel deposits consist of a coarse gravel fraction ($D_{50}$ is 25 to 30 mm) with a matrix of medium sand making up the fine fraction (Fig. 1.2F). Sediments exposed on bar surfaces are usually unimodal gravels, similar in composition to the subsurface clasts, except that the sand fraction is frequently missing (McLean *et al.*, 1999). Surface deposits of sand are found in sloughs, on the downstream side of bars, in shallow channels behind bars, and along some of the secondary channels.

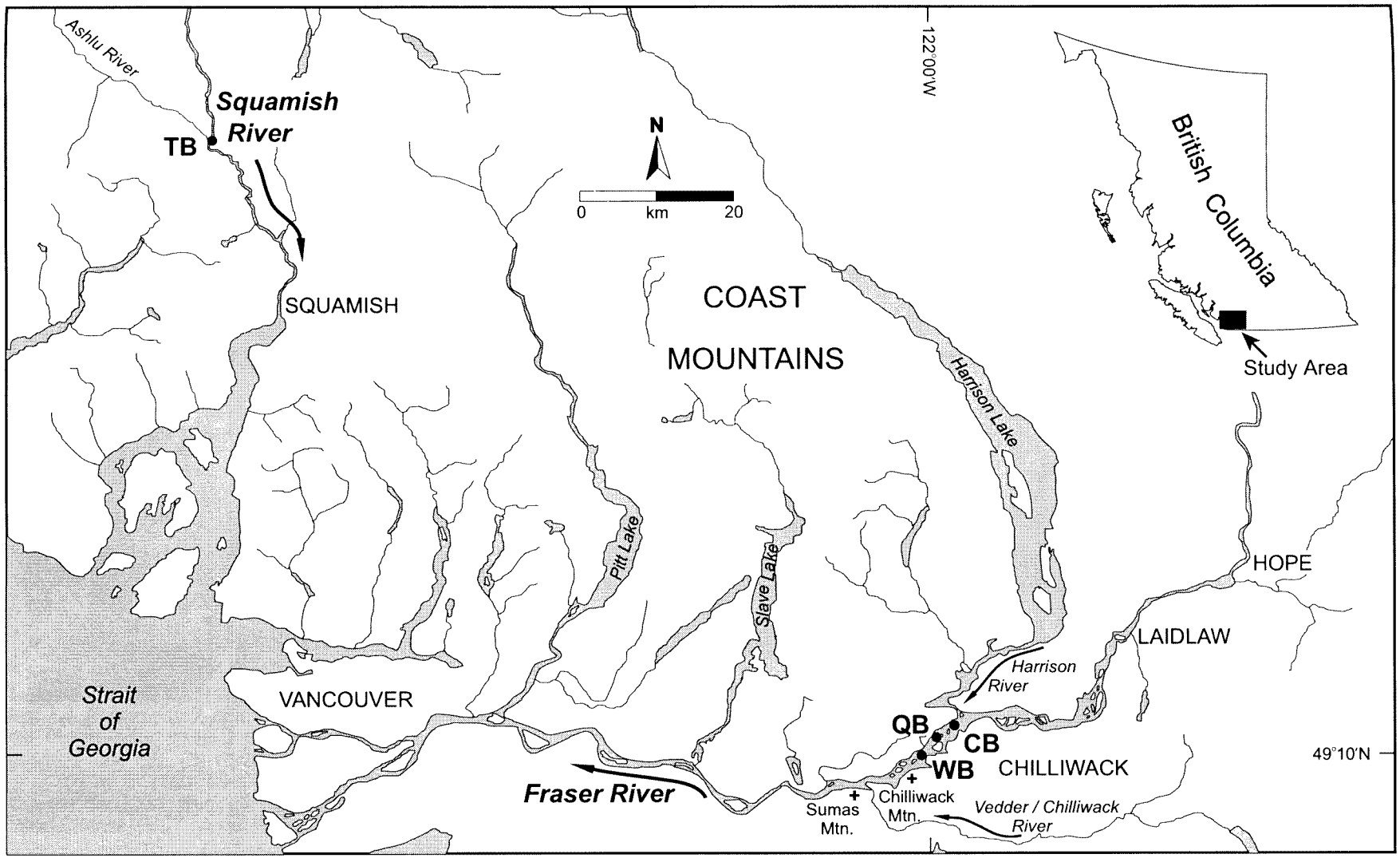


**Fig. 1.3** Location map of channel bar sites in the wandering gravel-bed Squamish and Fraser Rivers, southwestern British Columbia. TFLENT Bar (TB), Calamity Bar (CB), Queens Bar (QB), and Wellington Bar (WB) are indicated.

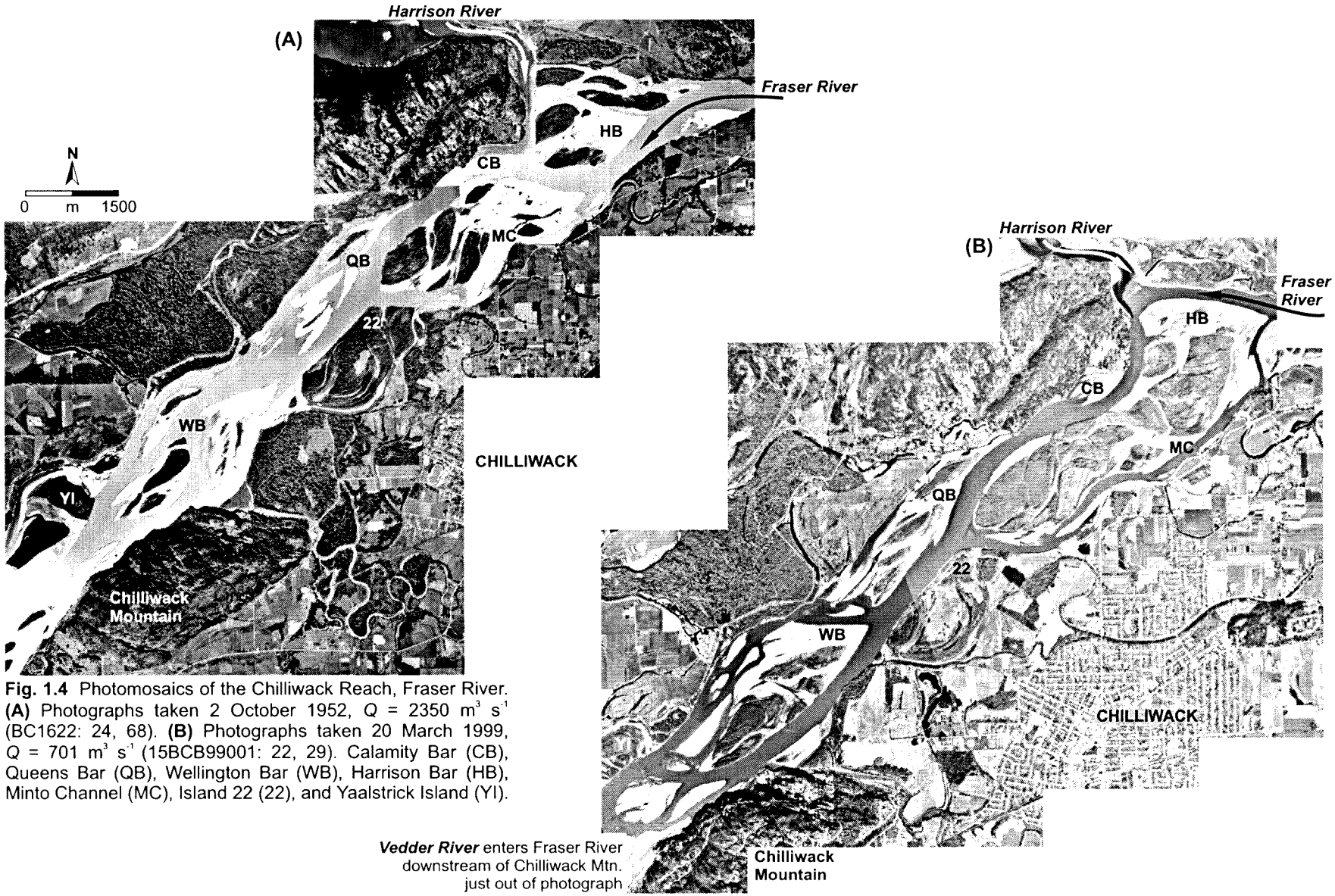


**Fig. 1.4** Photomosaics of the Chilliwack Reach, Fraser River. **(A)** Photographs taken 2 October 1952, $Q$ = 2350 $m^3$ $s^{-1}$ (BC1622: 24, 68). **(B)** Photographs taken 20 March 1999, $Q$ = 701 $m^3$ $s^{-1}$ (15BCB99001: 22, 29). Calamity Bar (CB), Queens Bar (QB), Wellington Bar (WB), Harrison Bar (HB), Minto Channel (MC), Island 22 (22), and Yaalstrick Island (YI).

## 1.8 Squamish River Study Area

The Squamish River is located in the southwestern corner of British Columbia and flows 150 km south through the Coast Mountain Range into the Howe Sound fjord, about 60 km north of Vancouver (Fig. 1.3). The river flows in a fault oriented, glacially scoured valley draining a 3600 $km^2$ basin, of which 20% is glacier covered. Headwaters rise to more than 3000 m elevation and are underlain primarily by quartz diorite and granodiorite with minor occurrences of gneiss and schist. Volcanic clasts are sourced to the river from extensive Holocene debris avalanche deposits at the base of the Mount Cayley volcanic pile.

The hydrological regime of Squamish River is dominated by fall rains and an early summer snowmelt peak (freshet). Fall rains (September to November) are short in duration (events last on the order of days), but are the highest magnitude discharges. The flood of record was generated from a winter rain-on-snow event with a maximum instantaneous discharge of 2610 $m^3s^{-1}$ on 8 October 1984 (Hickin and Sichingabula, 1988). The severe magnitude of individual events is important in governing bar formation throughout the river as gravel transport functions appear to behave exponentially above the critical threshold of motion for gravel (McLean *et al.*, 1999). The freshet is longer in duration, beginning in mid- to late April, peaking by mid-June, and extending until late July, but the mean peak freshet discharge (500 $m^3s^{-1}$) is of lesser magnitude than the fall rains. After the freshet, discharge declines until the end of the year to a mean minimum discharge of 60 $m^3s^{-1}$ in January. Mean annual discharge at Brackendale is 239 $m^3s^{-1}$.

Although the Fraser River also experiences fall rain events, their hydrologic signature is muted relative to the high magnitude and long duration of the freshet. In this sense, bed material transport occurs at different times and in each of the two river systems and for much longer in the Fraser system.

### 1.8.1 TFLENT Bar

One gravel bar, TFLENT (Tree Farm License Entrance), was profiled in the 10.5 km long wandering reach situated between braiding and meandering reaches (Fig. 1.5). The wandering reach begins 44 km upstream from the mouth of Squamish River at the downstream end of a 17 km long braiding reach. The wandering reach ends about 3 km downstream of the Ashlu River confluence, where the channel changes abruptly to a single-thread meandering channel. The irregularly sinuous channel in the wandering reach splits around channel islands and bars and is laterally unstable switching between channels. Channel gradient is 0.0015 and bed material throughout the reach is composed primarily of gravel up to large cobbles with lesser amounts of sand (Brierley, 1984).


**Fig. 1.5** Aerial photograph of the wandering gravel-bed Squamish River and the bank-attached TFLENT Bar (TB). The bar is downstream of the Ashlu Bridge and upstream of the Ashlu River confluence. Photograph taken 8 August 1996, $Q$ = 364 $m^3 s^{-1}$ (BCB96036: 19).

# 2 Methods

## 2.1 Bathymetry

### 2.1.1 Squamish River

Channel bottom surveys of Squamish River were completed using a Lowrance X-16 chart-recorder mounted on a 3 m long inflatable boat during low-stage flow (~50 $m^3 s^{-1}$) on 14 April 2001. Bathymetry of three representative cross-sections and one channel centerline sounding were recorded to determine the channel geometry. An engineering level was used to measure water surface, bar, and top of bank elevations to calculate scour depths.

### 2.1.2 Fraser River

Historic channel bottom survey data of Fraser River were acquired from the Department of Geography, UBC (courtesy of Dr. M. Church). Channel soundings were completed in 1952, 1984, and 1999, the details of which can be found in McLean (1990) and analytical results in McLean and Church (1999). The data are a series of UTM (Universal Transverse Mercator) geo-referenced (real world) *xyz* points, where *x* is the Easting, *y* is the Northing, and *z* is the elevation.

Vertical sediment aggradation rates were determined for each site directly beneath areas profiled with the GPR by differencing successive survey elevation data. Mean aggradation rates for the 32 year period between 1952 and 1984 were calculated and compared to rates calculated for the 15 year period between 1984 and 1999. Depth of scour at each site was also determined from the bathymetric soundings.

## 2.2 Topography

Bartop topography was surveyed at each site using a Duratech AL240 level and stadia rod. The data were collected in order to topographically correct GPR profiles. For this reason, the surveys were limited to the grid of lines profiled with GPR. Lines were generally surveyed every 10 m along their length, including the start and end points. The top and bottom of slope breaks associated with slipfaces were also surveyed to capture their geometry. Topographic elevations were accurate within 1 cm over 200 m of double-run leveling.

The topographic surveys were tied to real world space (*x* and *y* UTM coordinates) through GPS (global positioning system) surveys of the start and end points along the GPR lines. An Eagle Explorer GPS unit was used, and *x* and *y* coordinates were accurate to within 5 m of their true position. This permitted

the GPR grids to be positioned accurately on aerial photographs of each bar, and to be aligned with historic bathymetric soundings.

## 2.3 Aerial Photographs

### 2.3.1 Mapping and Photograph Selection

Gravel bars, vegetation, and channel boundaries were mapped from time sequential aerial photographs to identify patterns of change through time. Six maps were digitized for each bar using ArcView 3.2™ from rectified photographs spanning the period 1943 to 2001 (Table 2.1).

**Table 2.1** Catalog of aerial photographs used to map channel change. Aerial photographs acquired from the National Air Photo Library (A), Province of British Columbia (BC), and Selkirk Remote Sensing (SRS). Squamish and Fraser River discharge data from Water Survey of Canada stations 08GA022 (Brackendale) and 08MF005 (Hope), respectively. Channel bar abbreviations are TFLENT Bar (TB), Calamity Bar (CB), Queens Bar (QB), and Wellington Bar (WB).

| | Date | Discharge ($m^3 s^{-1}$) | Filmroll: Number (Channel Bar) |
|---|---|---|---|
| Squamish River | 1951 Jun. 14 | No data. 43 yr mean for June 14 is ~440 | BC1227: 22(TB) |
| | 1960 Jun. 22 | 334 | BC5012: 244(TB) |
| | 1964 Jul. 24 | 462 | BC5105: 217(TB) |
| | 1967 Apr. 06 | 60.6 | BC5225: 86(TB) |
| | 1976 Sep. 27 | 379 | BC5758: 73(TB) |
| | 1984 Nov. 05 | 123 | Hickin collection (TB) |
| | 1994 Jul. 27 | 467 | BCC94121: 34(TB) |
| | 1996 Aug. 08 | 364 | BCB96036: 19(TB) |
| Fraser River | 1943 Dec. 05 | 929 | A7075: 36(CB), 21(QB); A7074: 71(WB) |
| | 1952 Oct. 02 | 2350 | BC1622: 68(CB), 24(QB), 24(WB) |
| | 1967 Apr. 11 | 1120 | BC5226: 65(CB), 66(QB), 67(WB) |
| | 1971 Mar. 19 | 799 | BC5406: 155(CB), 155(QB), 134(WB) |
| | 1979 Mar. 22 | 1010 | BC79003: 114(CB), 116-118(QB), 84(WB) |
| | 1986 Sep. 03 | 2500 | BCC537: 150(CB), 146-148(QB), 144(WB) |
| | 1993 Aug. 15 | 3270 | 30BCB93030: 13(CB), 15(QB); 30BCB93032: 188(WB) |
| | 1999 Mar. 20 | 701 | 15BCB99001: 22(CB), 29(QB), 29(WB) |
| | 2000 Mar. 10 | 677 | SRS6164: 79(CB), 81-83(QB), 90(WB) |
| | 2001 Mar. 07 | 485 | SRS6348: 63(CB), 66-67(QB), 69(WB) |

Selection of suitable photographs was contingent upon four main considerations: (1) degree of morphologic change between photographs from different years, (2) river discharge level, (3) the scale of the photographs, and (4) photograph quality.

Firstly, to gain an indication of how quickly bars in wandering rivers change, photographs were chosen at unevenly spaced intervals of ten years or less. The time intervals between photographs were dictated by the frequency of photographs flown and by water level. Prior to 1960, photographic coverage was typically once or twice a decade, leaving little choice in selecting photographs. From the 1960s on, the Squamish River was typically flown twice a decade, whereas the Fraser River was photographed more than four times a decade. The increased coverage allowed selection of closely spaced photographs in order to characterize rates of change in wandering bars. Vertical aerial photographs of the Fraser River

date back to 1928 and to 1951 on the Squamish River. Numerous photographs from years between those chosen for digitization were examined in detail to build an inventory of surficial features found on gravel bars from different years. For instance, unit bar morphology was characterized from digitized photographs and compared to other photographs to ensure a fully generic morphologic description and redundancy in interpretation.

Secondly, photographs were chosen in which discharge was relatively low so that bars were emergent. The photographs display a range of water levels due to them being flown at different times of the year. Differing water levels pose problems in comparing absolute change in gravel area from one year to the next. Yet different water levels give an indication of vertical aggradation rates across bar areas through time, by comparing the amount of emergent area between photographs.

Thirdly, small-scale photographs (*e.g.*, 1:100 000) were not selected because meter-scale differences in barforms could not be resolved. At the other end of the spectrum, large-scale photographs (*e.g.*, 1:1000) were also not selected due to the large number of photographs required to capture a bar, and the lack of ground control points in each photograph necessary for rectification.

Fourthly, photographs with cloud cover, that were out of focus, or had sunlight glittering off the water obscuring barforms were not selected.

### 2.3.2 Photographic Rectification

Aerial photographs were rectified digitally using an image processing software program, ER Mapper 6.0™ (Leys and Werritty, 1999). Rectification (otherwise known as 'rubber-sheeting') manipulates the *xy* space of photographs thereby flattening the images by removing any distortions induced by plane tilt and yaw as the photographs were being shot. Rectification involves 'warping' the photograph to an orthorectified base map by picking coincident ground control points on both images. This process geo-codes the photograph by placing it into real world space with every cell on the photograph assigned a UTM coordinate. This allows each rectified photograph to be compared to any other photograph in real world space regardless of the scale of the original photography. Orthorectification (manipulation of *xyz* space) was not undertaken due to the lack of surface topography (the *z* direction) on bars, which rarely exceeds 3 m of relief.

Photographs were scanned as black and white, 300 dpi (dots per inch) images to provide adequate resolution while limiting the file size, which was typically about 6 to 7 Mb (megabytes). The base maps were of two varieties: 1:20 000 digital TRIM (Terrain Resource and Inventory Maps) data (92G084, 92G094 for Squamish River, and 92G020, 92G030, 92H021, 92H011 for Fraser River), and 1995 color orthophotographs based on, and as accurate as, 1:20 000 TRIM data produced by Selkirk Remote Sensing Ltd. and Triathlon Mapping Corporation (blocks D32, D33, E34, E35, and E36). Anthropogenic features such as roads, buildings, bridges, and high voltage transmission towers were used as ground control points to geo-reference the images, because their locations rarely change through time. Typically 14 to 20 control points were used to rectify the photographs. The oldest photographs (in particular the 1951 and 1960 Squamish River photographs) were the most difficult to rectify because of the scarcity of control points, and in these cases only ~7 points were used. All photographs were referenced to the NAD83 horizontal datum. The coincidence of channel boundaries through time shows that rectification was successful, as the edges of digitized features are accurate to within 1 m.

## 2.4 GPR Theory

Ground penetrating radar (GPR) is the general term applied to geophysical techniques that employ radio-frequency electromagnetic energy in the 10 MHz to 1 GHz frequency range to image the subsurface. GPR profiling is similar to seismic reflection profiling, except that GPR transmits electromagnetic (EM) energy and images the electrical properties of the ground. In contrast, seismic techniques transmit acoustic energy which images the ground's mechanical properties.

GPR repetitively transmits short pulses of radio-frequency EM energy into the ground. The energy propagates downwards as a wavefront traveling at the EM wave velocity of the medium through which it is passing. When the wavefront encounters changes in the bulk electrical properties of different subsurface strata some energy is reflected back to the surface and some is transmitted downward to deeper strata. Reflections are primarily controlled by contrasts in the relative dielectric constant ($\varepsilon_r$) between sediment types, and largely depend on the composition of the sediment, its water content, and the character of the interface between adjacent strata (van Dam, 2001). The strength of the reflected signal is approximately proportional to the difference in relative dielectric contrasts between the sediment interfaces. There is a strong relationship between electrical and physical properties of materials. For this reason radar reflections may be used to identify physical boundaries such as geologic interfaces (*e.g.*, bedding), saturation fronts (the water table), and erosional contacts.

Reflected energy is received at the surface and its arrival time is recorded. Profiles show the total travel time for a signal to pass through the subsurface, reflect from an electrical contrast and return to the surface. This is the two-way travel time which can be converted to a depth from measurement of the propagation velocity of the sediment.

### 2.4.1 EM Properties of Geologic Materials

The propagation velocity and attenuation of radar signals depends on the dielectric and conductive properties of the ground. The velocity ($V$) of radiowaves in sediment is explicitly given by:

$$V = \frac{c}{\left\{(\varepsilon_r \mu_r / 2)\left[\left(1 + P^2\right) + 1\right]\right\}^{0.5}} \quad (1)$$

where $c$ is the speed of light (0.3 m ns$^{-1}$), $\varepsilon_r$ is the relative dielectric constant (a dimensionless ratio that is a measure of the capacity of a material to store a charge), $\mu_r$ is the relative magnetic permeability (equal to 1 for non-magnetic sediments such as sand and gravel), and $P$ is the loss factor ($P = \sigma/\omega\varepsilon$, where $\sigma$ is the conductivity, $\varepsilon$ is the permittivity, and $\omega$ is the angular frequency ($\omega = 2\pi f$, where $f$ is the frequency)). In sediments with low electrical loss (low conductivity), $P \approx 0$ and the speed of radiowaves is simply:

$$V = \frac{c}{\varepsilon_r^{0.5}} \quad (2)$$

The dielectric constant ranges from 3 to 6 in dry sand to 25 to 30 in wet sand (Reynolds, 1997) showing that the water content of sediments strongly controls signal velocity. Sediments with high electrical conductivity, such as clays, attenuate radiowaves resulting in shallow penetration depths and

low velocities. In contrast, sand and gravel are resistant sediments enabling deep penetration and faster velocities, making sand and gravel deposits ideal radar targets.

## 2.5 GPR Instrumentation and Surveys

### 2.5.1 GPR Instrumentation

A Sensors and Software pulseEKKO™ IV GPR system was employed with a 400 V transmitter and three different antenna frequencies: 200, 100, and 50 MHz. For the 200, 100, and 50 MHz antennas, antenna separation and length were 0.5, 1.0, 2.0 m, trace spacing was 0.1, 0.25, 0.5 m, sampling rate was 800, 800, 1600 ps, respectively, and all traces were stacked 128 times (Table 2.2).

**Table 2.2** GPR trace spacing, antenna separation, sampling rate, wavelength, and vertical resolution of 200, 100, and 50 MHz antennas using a velocity of 0.085 m $ns^{-1}$.

| Frequency, *f* (MHz) | Trace Spacing (m) | Antenna Separation (m) | Sampling Rate (ps) | Wavelength, λ (m) | Vertical Resolution, *R* | | |
|---|---|---|---|---|---|---|---|
| | | | | | λ/4 (m) | λ/3 (m) | λ/2 (m) |
| 200 | 0.10 | 0.5 | 800 | 0.43 | 0.11 | 0.14 | 0.21 |
| 100 | 0.25 | 1.0 | 800 | 0.85 | 0.21 | 0.28 | 0.43 |
| 50 | 0.50 | 2.0 | 1600 | 1.70 | 0.43 | 0.57 | 0.85 |

A Toshiba Pentium II or a Compaq 486 PC laptop computer controlled the GPR system. The laptop was connected to the console unit and each was powered by a rechargeable 13 A, 12 V gelsel battery. Fibre-optic cables (15 m long) connected the console to the transmitting and receiving antennas, each of which was powered by two rechargeable 7 A, 6 V gelsel batteries (Figs. 2.1A and 2.1B).

The three different antenna frequencies were used at each site to give a range of resolutions, depths, and to provide for interpretative redundancy. High frequency antennas (200 MHz) provided greater resolution, but less depth penetration than low frequency antennas (50 MHz). The theoretical vertical resolution ($R$) is equal to $\lambda/4$ (Reynolds, 1997), but was found to vary between $\lambda/3$ and $\lambda/2$ (Table 2.2; the wavelength of the transmitted radiowave ($\lambda$) can be expressed as $\lambda = V/f$).

Antenna separation and trace spacing were set following Sensors and Software guidelines (Sensors and Software, 1996). Radar survey techniques included reflection profiling and velocity sounding with the antennas oriented perpendicular broadside in both cases. Constant offset reflection profiling was carried out with the antennas moved along the survey line at a fixed interval (trace spacing) and constant separation between the antennas. Reflection profiling records two-way travel time versus distance producing radargrams, in which the subsurface is imaged as a series of wiggle-traces (Fig. 2.1C).

The choice of 128 stacks was made on Squamish River bars early in the field program by comparing 32, 64, 128, and 256 stacks shot on the same line. Stacking 128 times improved the continuity of some dipping reflections compared to 64 stacks and made reflections discrete entities versus 32 stacks. These results showed that 128 stacks improved the signal-to-noise ratio as 128 traces were collected at each survey position, averaged, and output as one trace.

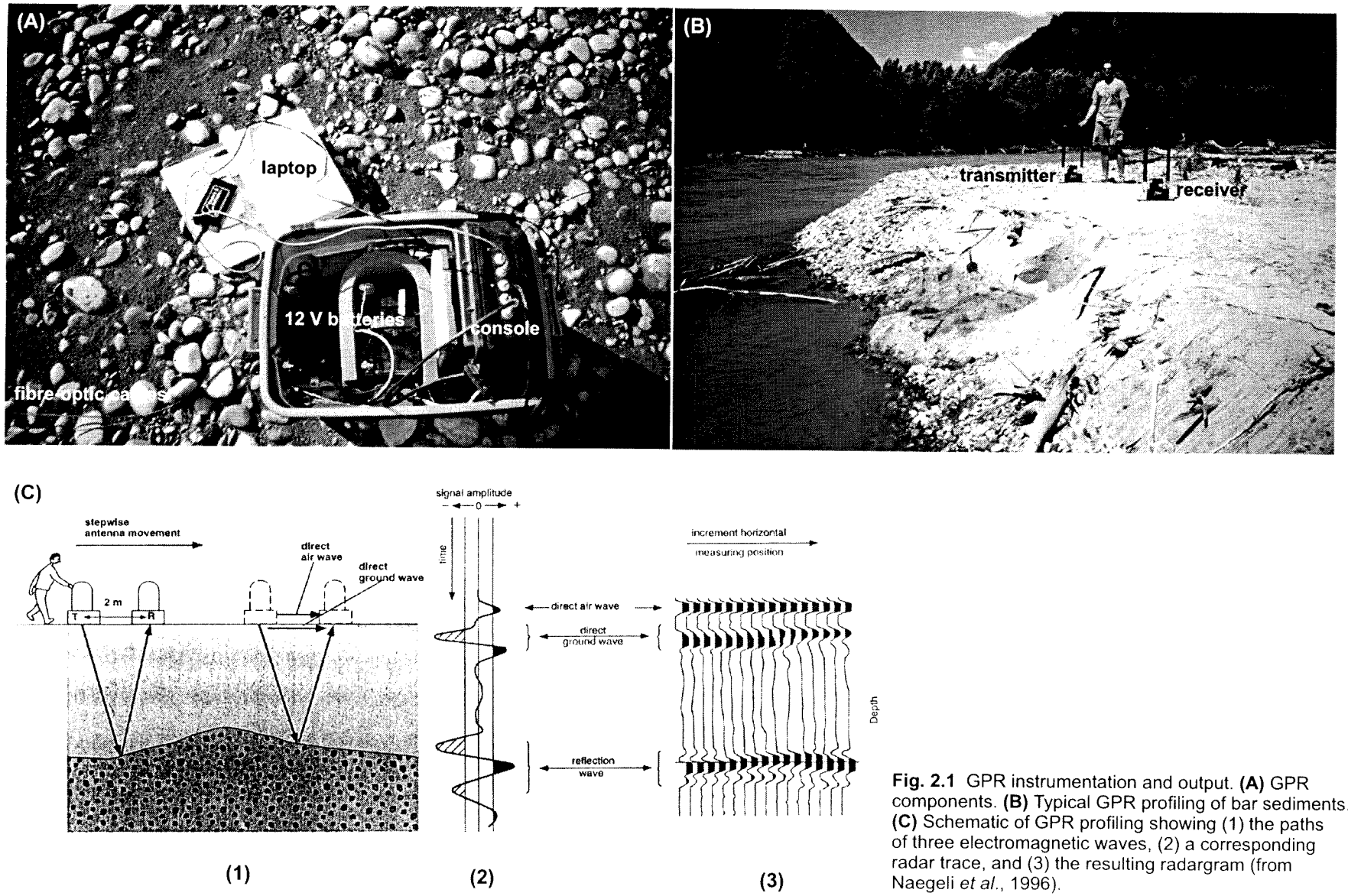


**Fig. 2.1** GPR instrumentation and output. **(A)** GPR components. **(B)** Typical GPR profiling of bar sediments. **(C)** Schematic of GPR profiling showing (1) the paths of three electromagnetic waves, (2) a corresponding radar trace, and (3) the resulting radargram (from Naegeli *et al.*, 1996).

256 stacks did not improve data quality and was not used for two reasons. Firstly, doubling stacks from 128 to 256 doubled the shot time (and total survey time) from over 4 hours to more than 8 hours for 200 m long surveys profiled with 200 MHz antennas. This was unfeasible due to battery constraints. Secondly, a high number of stacks can distort steeper sedimentary structures by laterally smearing and defocusing the radar image (Reynolds, 1997). Subsequent trials on Fraser River bars showed no difference between 64 and 128 stacks, but Fraser River bars were also shot at 128 stacks to maintain consistency in data collection between sites.

### 2.5.2 GPR Surveys

Approximately 1 km of ground was profiled in rectilinear grids (~200 m x 200 m) at each bar, totaling 15 km of radar profiles. Lines were shot orthogonal to each other in order to capture longitudinal and lateral subsurface changes, and to permit the 3D characterization of the radar stratigraphy. The GPR surveys were carried out between late July 2000 and early March 2001 on dry days without appreciable precipitation.

## 2.6 GPR Velocity Analysis

Velocity sounding or common midpoint (CMP) gathers involved moving the antennas incrementally away from the midpoint of the survey line, with each antenna moved half the trace spacing, thereby increasing the offset from the midpoint. CMP profiles record travel time versus offset and are used to calculate subsurface velocities. Eleven CMP pairs were shot at five of the sites with different combinations of the three antenna frequencies for comparative purposes. No CMPs were shot at the Inner Channel site, Queens Bar, Fraser River, because of the similar results from each of the other Fraser River bars. CMPs were shot in pairs, orthogonal to each other to ensure that one of the CMPs would produce focused reflections with minimal signal noise.

Figures 2.2A-D and 2.3A-D show the CMP gathers analyzed and their locations on the bars. The CMPs were shot along topographically flat, previously profiled lines, 1 to 2 m elevation above river level where subsurface reflections were known to be horizontal to subhorizontal. Horizontal reflections enabled subsurface velocities to be calculated without going through the DEVILISH (Dipping Event Velocity Inequality Licked (Judson *et al.*, 1978)) procedure of correcting for dipping reflections.

Radiowave velocities through sediment allow the depth to reflections to be calculated, and also reveal information about the nature of the sediments. Velocities were determined from analysis of the airwave, groundwave, and reflections captured by CMP gathers (Fig. 2.4A).

The airwave is the first transmitted pulse. It travels through the air to the receiver at the speed of radiowaves in air (0.3 m $ns^{-1}$). The groundwave (or direct wave) is the next signal received and it travels through the near-surface ground at the speed of radiowaves in the near-surface sediment. The airwave and groundwave are straight lines on *T-X* plots (two-way travel time (*T*) versus offset (*X*)) whose velocity is the inverse of the slope of the line ($T/X = 1/V$) (Fig. 2.4A).

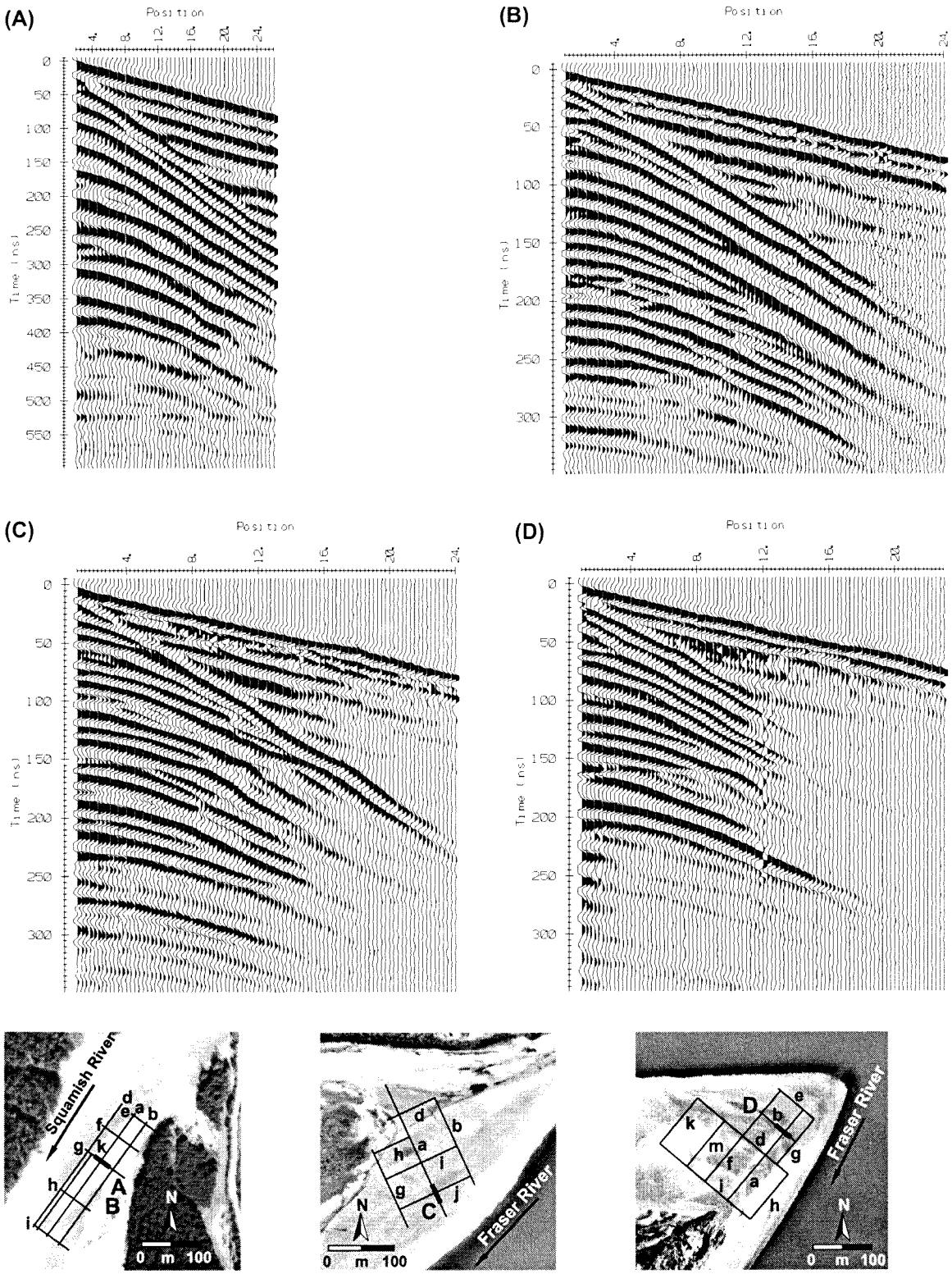


**Fig. 2.2** CMP gathers analyzed in Fig. 2.5 collected on TFLENT Bar in Squamish River, and Calamity and Wellington Bars in Fraser River. **(A)** 50 MHz, and **(B)** 100 MHz CMPs, TFLENT Bar. **(C)** 100 MHz CMP, Calamity Bar. **(D)** 100 MHz CMP, Wellington Bar. The thicker line segments in the photographs show the extent and location of the CMPs.

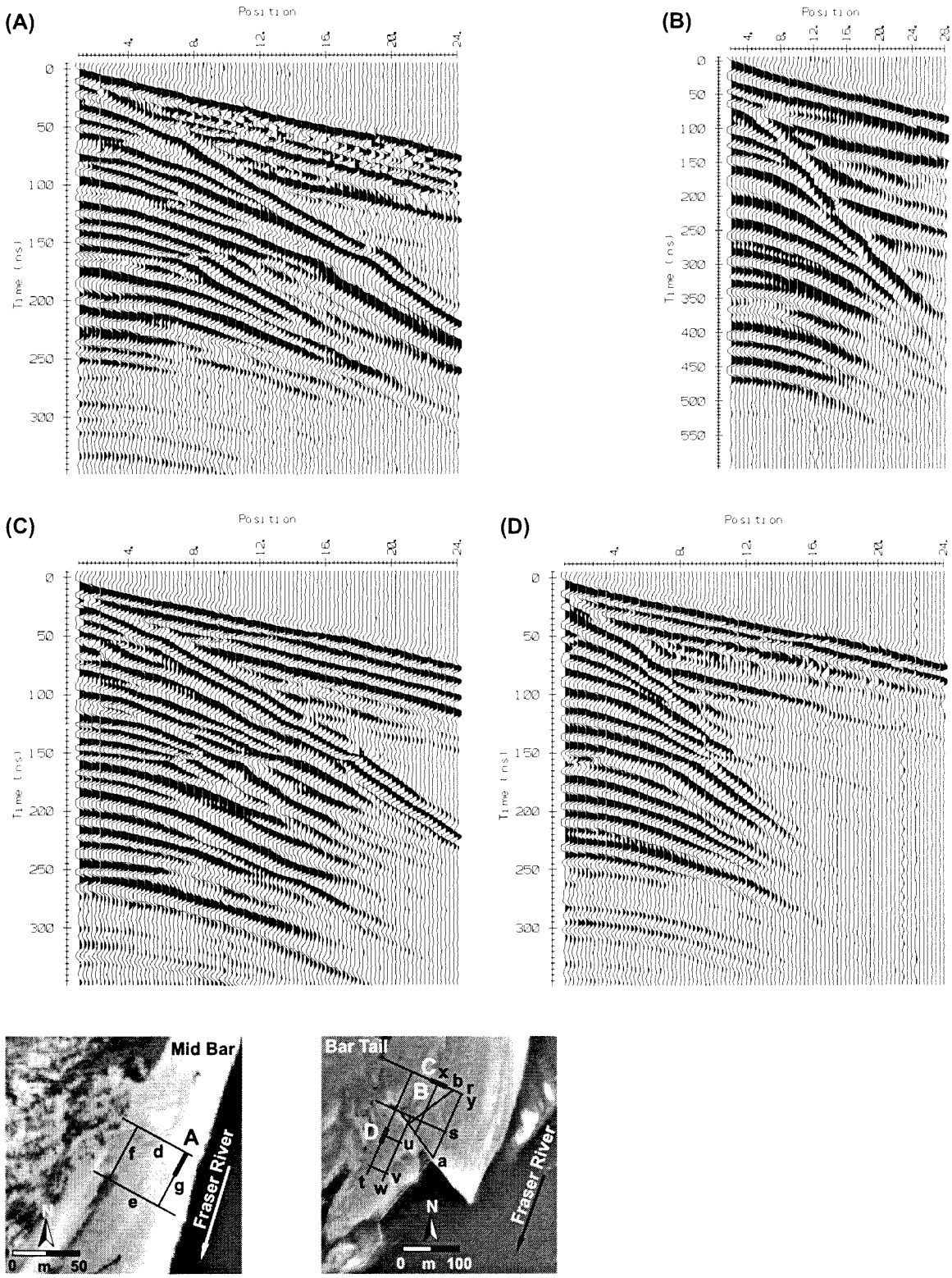


**Fig. 2.3** CMP gathers analyzed in Fig. 2.5 collected on Queens Bar, Fraser River. **(A)** 100 MHz mid bar CMP, Mid Bar site. **(B)** 50 MHz, and **(C)** 100 MHz bar end CMPs, Bar Tail site. **(D)** 100 MHz bar tail CMP, Bar Tail site. The thicker line segments in the photographs show the extent and location of the CMPs.

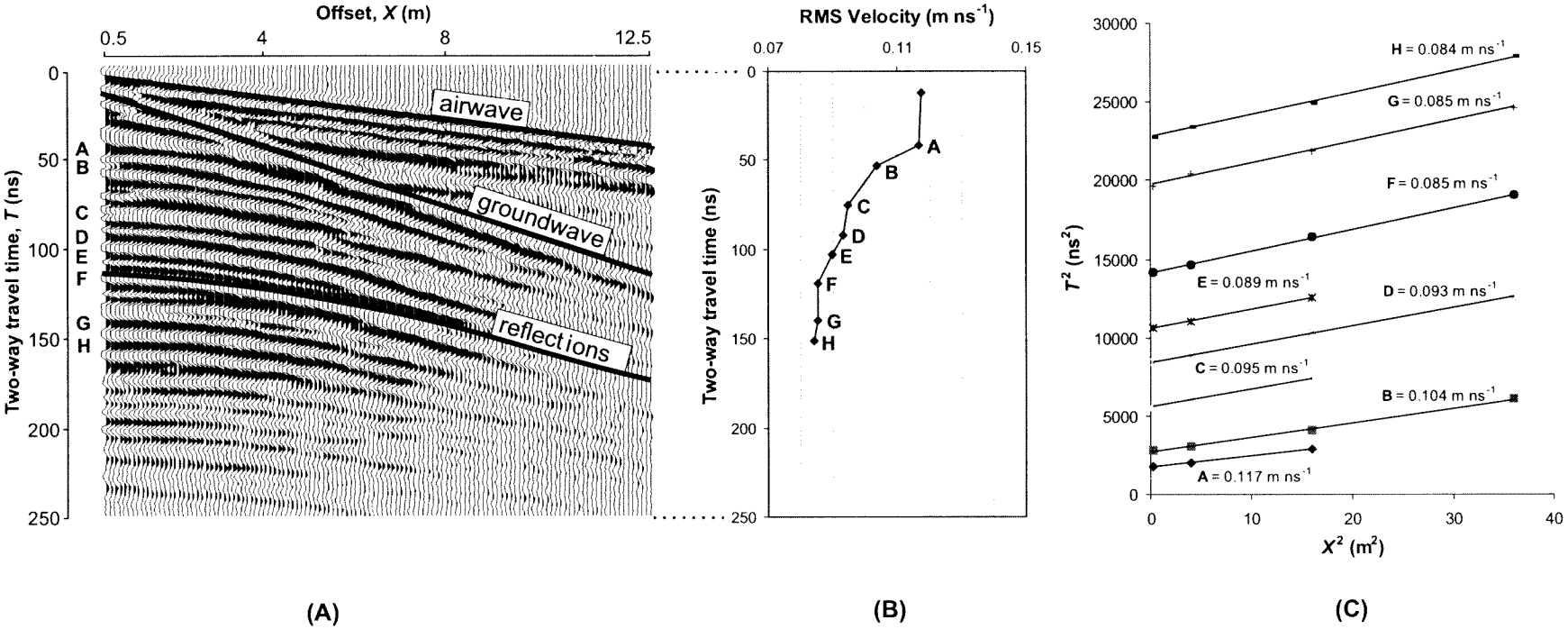


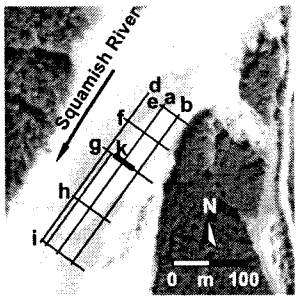


**Fig. 2.4** Velocity analysis of 200 MHz CMP, TFLENT Bar, Squamish River. **(A)** CMP gather. Airwave velocity is 0.307 m ns$^{-1}$. Groundwave velocity is 0.118 m ns$^{-1}$. Reflected waves plot as hyperbolic forms. **(B)** Subsurface velocity profile shows changes in RMS (Root Mean Square) velocity with increasing travel time. **(C)** Individual reflectors plot as straight lines on $T^2$-$X^2$ plots. RMS velocities of individual lettered reflectors are calculated from $T^2/X^2 = [1/V]^{0.5}$. The thicker line segment in the photograph shows the extent and location of the CMP.

Waves penetrating the subsurface are reflected back to the surface and plot as hyperbolic signatures on $T$-$X$ graphs. Squaring the two-way travel time ($T^2$) and offset ($X^2$) of individual reflections yields $T^2$-$X^2$ plots in which hyperbolas plot as straight lines whose velocity is the square root of the inverse of the slope of the line ($T^2/X^2 = [1/V]^{0.5}$) (Fig. 2.4C).

### 2.6.1 RMS Velocities

The velocity calculated for each reflection is the RMS (root mean square) velocity ($V_{RMS}$), not the true velocity of the strata. RMS velocities give the effective velocity of reflections as they are time-averaged velocities over the interval from zero-time to the time of the reflection of interest. RMS velocities then integrate the properties of the overlying strata into the velocity.

Figure 2.4B plots the RMS velocities of individual reflections against two-way travel time and shows distinctly faster velocities in the upper sediments than at long travel times. The velocity contrast is a result of the CMPs profiling unsaturated near-surface sediment and saturated deeper sediments because the CMPs were shot 1 to 2 m above river level. Water is conductive and attenuates the propagation of radiowaves slowing their velocity. Figure 2.4B shows clearly that the standard practice of using the groundwave velocity (the first data point) to characterize saturated sites is inappropriate for the deeper sections and its fast velocity would overestimate the thickness of the sediment pile. The depth ($d$) to a reflection is given by $d = (VT)/2$, where $T$ is the two-way travel time.

### 2.6.2 Interval Velocities

To determine a geologically more meaningful velocity (the velocity of individual strata) the interval velocity ($V_{int}$) must be calculated from Dix's equation developed for seismic velocity analysis:

$$V_{\text{int}} = \left[ \frac{\left(V_{\text{RMS}.n}\right)^2 T_n - \left(V_{\text{RMS}.n-1}\right)^2 T_{n-1}}{\left(T_n - T_{n-1}\right)} \right]^{0.5} \qquad (3)$$

where $V_{RMS.n}$, $T_n$, and $V_{RMS.n-1}$, $T_{n-1}$ are the RMS velocity and reflected two-way travel times to the $n$th and ($n$-1)th reflections respectively (Dix, 1955).

Interval velocities were calculated for some of the CMPs. The resultant velocities ranged from very large to very small values (0.2 m ns$^{-1}$ to 0.01 m ns$^{-1}$). Neither of these values are physical representations of subsurface velocities. Short travel times (*e.g.*, 6 ns), and large changes in RMS velocities (*e.g.*, 0.01 m ns$^{-1}$) between reflections led to the propagation of large errors in computing interval velocities. Rust and Russell (2001) reduced their $V_{int}$ errors by using a smoothing function to resample their RMS velocities in order to derive reasonable interval velocities. Tillard and Dubois (1995), however, also found the computation of interval velocities to be problematic and concluded that velocity analysis using Dix's formula was not an advantageous process. They further concluded that a velocity profile similar to that derived from the RMS values was enough to establish a representative velocity versus depth profile provided that the antenna offsets were small in comparison to reflection depths. For these reasons, interval velocities were not used in the velocity analysis. Instead, RMS velocities were used to characterize the subsurface.

### 2.6.3 Velocity Results

Velocity analysis of the CMP data yielded RMS velocities ranging from ~0.08 to ~0.13 m $ns^{-1}$ (Figs. 2.5A-C). The near-surface sediment (typically 1 to 2 m above river level) produced the fastest velocities (*i.e.*, the groundwave), and the deeper saturated sediment gave the slowest velocities. The large spread in groundwave and near-surface velocities (0.10 to 0.135 m $ns^{-1}$) is attributable to differences in grain-size and the degree of saturation in the near-surface sediment. At long travel times the velocity of the thicker saturated strata overprints, but still incorporates, the unsaturated velocities of the near-surface sediment. Overall, the results show that RMS velocities typically converge on a velocity of 0.085 m $ns^{-1}$. Comparison with typical velocities (in m $ns^{-1}$) for unconsolidated sediments shows that the data fall within the expected velocity range: 0.06 for clay, 0.07 for silt, 0.06 to 0.07 for wet sand, 0.08 for wet gravel, 0.12 to 0.15 for both dry sand and dry gravel (Sensors and Software, 1996). Depths plotted on the radar profiles are based on a velocity of 0.085 m $ns^{-1}$. This was adopted as the constant velocity, meaning that a two-way travel time of 600 ns corresponds to an approximate depth of 25.5 m.

### 2.6.4 Velocity Discussion

Figure 2.5A shows three velocity soundings superimposed upon each other from 200, 100 and 50 MHz CMP gathers profiling the same sediment pile on the Squamish River. The soundings exhibit consistent velocity trends with time suggesting that the use of any of the three antenna frequencies is adequate to determine subsurface velocities. There are differences between individual soundings caused by errors associated in RMS velocity picks, or by the fact that each antenna frequency averages different volumes of sediment whose velocity characteristics differ. This is illustrated in Fig. 2.5B where 50 and 100 MHz antennas shot over the same bar end area on Queens Bar show different groundwave (first data point) and near-surface velocities (~0.085 versus ~0.115 m $ns^{-1}$, respectively). This is likely the result of the 50 MHz antennas capturing slow velocity, saturated sediments as the water table was about 1 m below the surface. In contrast, the 100 MHz antennas did not penetrate as deeply and imaged shallower, faster velocity, dry sediments.

Figure 2.5B shows three 100 MHz velocity profiles from mid bar, bar end, and bar tail positions on Queens Bar, Fraser River. Saturated velocities at long travel times converge between 0.08 and 0.09 m $ns^{-1}$, but the near-surface velocities between the three sites show a trend down the bar. Larger surface grain-sizes (cobbles) and higher elevations (2.5 m above river level) at the mid bar site result in higher velocities. The velocities decline down the bar to the bar tail site where elevation drops to river level and surface grains are sand and fine gravel. The fact that velocity trends mirror physical trends supports the theory driving radar imaging, in that physical and electric properties can be correlated.

Three 100 MHz velocity profiles from Calamity, Queens, and Wellington Bars in Fraser River (Fig. 2.5C) show similar velocity trends with time suggesting that the sedimentology of the bars is not that dissimilar. For instance, if one of the bars were merely a thin fluvial cap on top of bedrock (0.10 to 0.12 m $ns^{-1}$), its velocity profile would increase with time rather than decline. On the other hand, if a bar were underlain by silt, it would display a velocity profile with slower velocities (0.06 to 0.07 m $ns^{-1}$).

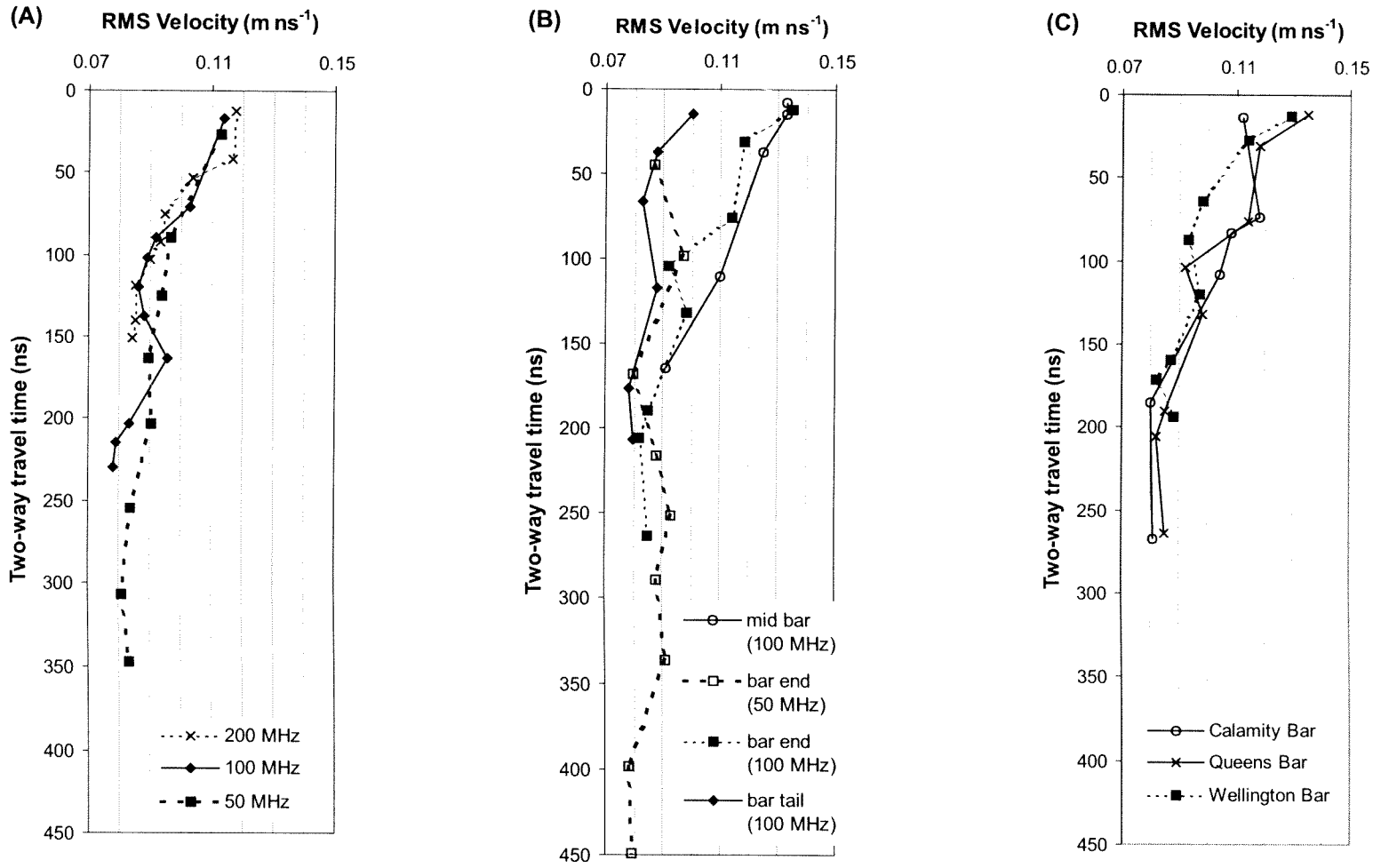


**Fig. 2.5** GPR velocity analysis. **(A)** Comparison of RMS (Root Mean Square) velocity profiles gathered with 200, 100, and 50 MHz antenna frequencies from the same location on TFLENT Bar, Squamish River (shown in Fig. 2.2). **(B)** Comparison of RMS velocity profiles gathered from sites positioned in a downstream succession on Queens Bar, Fraser River. The mid bar CMP (Mid Bar site) is the furthest upstream, and the bar tail CMP (Bar Tail site) is the furthest downstream (locations are shown in Fig. 2.3). **(C)** Comparison of RMS velocity profiles gathered with 100 MHz antenna on Calamity, Queens, and Wellington Bars, Fraser River (locations are shown in Figs. 2.2 and 2.3).

## 2.7 GPR Processing

The radar profiles were processed to improve the quality of the GPR data. This improved visualization and interpretation of the profiles. Some profiles were migrated in an attempt to remove diffractions, and in some cases migration was very successful. Yet, in most cases migration was incapable of removing diffractions without producing other artifacts such as 'smiles' due to velocity contrasts in the sediment pile. As a result of this outcome, radar data processing was kept to a minimum and included: (1) time-zero adjustment, (2) topographic corrections, (3) dewow, (4) 7-point down-trace and 2 trace-to-trace averaging, and (5) automatic gain control (AGC). These steps were necessary to (1 and 2) correctly reposition reflections, (3) correct for signal saturation, (4) improve the signal-to-noise ratio, and (5) compensate for signal attenuation with depth.

**(1) Time-zero:** The first arrival at the receiver was designated time-zero, and should have been at an equivalent travel time on each trace. A time-zero correction was applied to correct any traces that drifted from time-zero.

**(2) Topography:** Elevation data were applied to the radar profiles to correctly position reflections in the subsurface.

**(3) Dewow:** The radar data were corrected for signal saturation effects by applying the dewow filter. The airwave, groundwave, and near-surface reflections overwhelm and saturate the receiver with a large energy signature. This signature takes the form of a slowly decaying 'wow' of very low frequency that is superimposed on each trace. The dewow filter was an optimal high pass filter determined by Sensors and Software that preserved the high frequency reflections.

**(4) Filters:** Applying a low pass temporal filter reduced random and high frequency noise. A 7-point running time average was applied along each trace to remove the high frequency noise. Additionally, a 2-trace running spatial average was applied to improve reflection continuity and amplitude. In order to evaluate the effects of filters, two profiles are compared. Figure 2.6A shows a profile without any filters applied to it, and Fig. 2.6B shows the same profile with the filters applied to it. It can be seen that weak amplitude reflections were muted, but no noteworthy spatial artifacts were created.

**(5) Gains:** The gain function was the final stage in the signal processing as it physically changed the data set, whereas the filtering simply pulled selected information from the data set. Later arrivals on a signal trace show noticeably lower amplitudes than earlier arrivals as a result of energy losses and signal attenuation. Energy is lost (1) at each reflection/transmission interface, (2) due to the geometrical spreading of the radar beam as it travels into the ground, (3) when radiowaves are scattered by objects having similar dimensions as the wavelength, and (4) when the signal attenuates because of complex interactions between the dielectric ($\varepsilon_r$) and electric ($\sigma$) properties of the sediment, and the frequency of the radar beam. A time varying gain function (automatic gain control, AGC) was applied to increase the amplitude of deep reflections; the maximum gain cut-off was 3000.

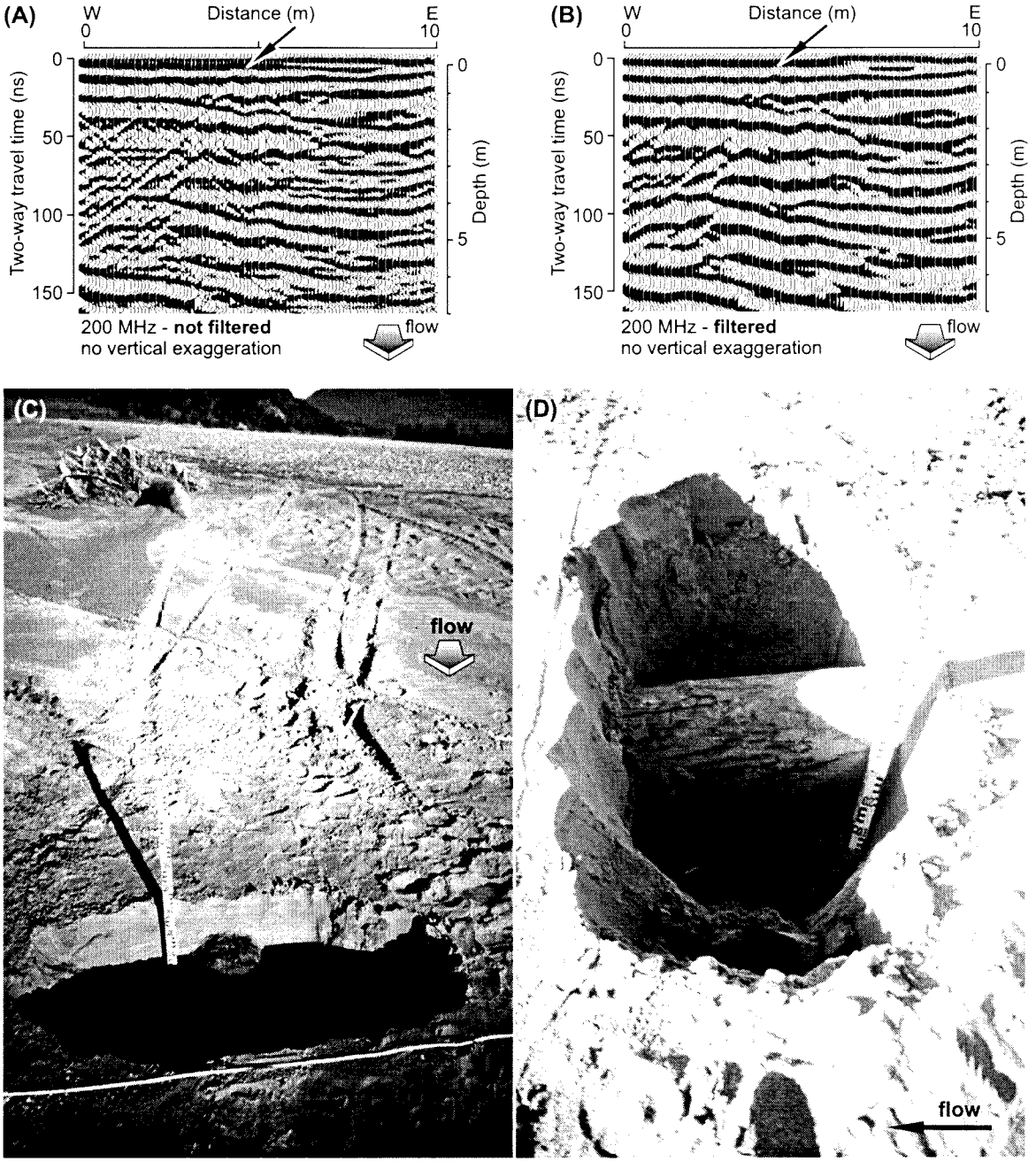


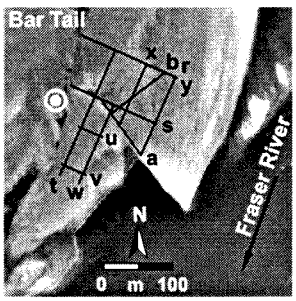


**Fig. 2.6** GPR profiles across a buried log and photographs of the excavated log, Queens Bar, Bar Tail site, Fraser River. **(A)** 200 MHz profile without any temporal or spatial filters. **(B)** 200 MHz profile with 7 point running time average filter and a 2 trace running spatial average filter applied. Arrows point to diffraction patterns 0.18 m below the surface of the bar. **(C)** Upstream view of the buried log and exposed rootwad. The radar was shot along the tape, before the log was excavated. **(D)** Excavated view of the 0.35 m diameter log, 0.17 m below the bar surface. The water table is 0.8 m below the bar surface. The bulls eye in the aerial photograph of the Bar Tail site shows the location of the log.

## 2.8 GPR Diffractions

Hyperbolic reflections (diffractions) are caused by point sources reflecting EM energy, and are likely caused by boulders or buried logs (Figs. 2.6A and 2.6B). To resolve the nature of the diffraction targets, an examination of reflection polarity and velocity characteristics of the diffractions was performed. Additionally, a field experiment over a buried log was conducted. Examination of reflection polarity allows the dielectric constant ($k$) of the diffraction targets to be determined relative to the bar sediments. Diffraction patterns consistently show - + - polarity meaning that the targets within the bar have opposing polarity to bar sediments indicating that they have a lower dielectric constant than bar sediments. (Fig. 2.1C(2) shows a single radar trace and graphically defines signal polarity.)

Logs ($k$ ~12) and boulders ($k$ ~5 to ~8) are both expected to generate reflections with - + - polarity as they have lower dielectric constants than wet sand ($k$ ~25 to ~30) or gravel ($k$ ~21) (Huggenberger, 1993). To differentiate logs from boulders, the velocity of the diffractions ($V$) is calculated from

$$V = \left[ \frac{x^2}{t^2 - t_o^2} \right]^{0.5} \qquad (4)$$

where $x$ is the distance from the apex of the diffraction, at one-way travel time $t_o$, to a point on the diffraction tail, at one-way travel time $t$ (Reynolds, 1997). Calculated diffraction velocities are about 0.055 m $ns^{-1}$, which is a bit slower than velocities associated with organic material (~0.086 m $ns^{-1}$) and much slower than boulders (0.10 to 0.12 m $ns^{-1}$) (Reynolds, 1997). These results suggest that isolated, buried logs cause singular diffractions, whereas clusters of overlapping diffractions are imaging buried logjams. Logs on the surface cause arcuate and chaotic reflections at depth (Bano *et al.*, 2000).

Figures 2.6A-D present the results of a field experiment attempting to capture the diffraction pattern of a partially buried log on Queens Bar, Bar Tail site, Fraser River. Arrows in Figs. 2.6A and 2.6B point to the top of the diffraction pattern ~0.18 m below the surface of the bar, which corresponds to the excavated 0.17 m depth to the top of the 0.35 m diameter log. The diffraction pattern is not very well defined because the shallow depth of the log is being imaged by the groundwave. Further, the diffraction pattern has two peaks, which *appears* to record the presence of two logs in the subsurface. Yet, there are only two diffraction tails (one on each side of the log), revealing the singular nature of the point source. The spread between the diffraction tails, and the multi-peaked character of the diffraction also give an indication of the large diameter of the log, relative to the resolution of the 200 MHz antennas. The experiment shows diffractions contain a wealth of information about buried objects, and confirms that diffractions likely signify buried logs in bar sediments.

## 2.9 Interpreting Radar Stratigraphy

Radar signatures are partial reflections of high frequency EM radiowaves transmitted through the ground. The reflections are caused by changes in the relative dielectric of adjacent geologic materials and typically occur at physical boundaries such as geologic interfaces, the water table, and stratal

contacts. Leclerc and Hickin (1997) and Van Dam and Schlager (2000) warn that radar reflections do not always represent sedimentological boundaries as changes in grain-size, porosity, organic matter, and fluid content effect relative dielectric differences between materials (Davis and Annan, 1989; van Dam, 2001). Leclerc (1995) profiled two gravel pit walls and found that not all GPR reflections could be correlated to bedding or erosional surfaces apparent in the sedimentary deposits. Instead, he found good correspondence between patterns of radar reflections and large-scale stratal trends (>10 m), but not direct correlation. Yet, others such as Stephens (1994) correlated and extended major sedimentary bounding surfaces observed in outcrop with radar reflections showing similar geometries and depths. Moreover, Bridge *et al.* (1998) found sedimentary cross-set thickness to be similar to the GPR profiled thickness suggesting that reflections may correspond to changes in grain-size and proportion of drifted plant material at the bases of medium-scale cross-sets.

### 2.9.1 Radar Stratigraphy

To overcome the difficulty of interpreting the exact nature of the subsurface expression being profiled, profiles are interpreted using the principles of radar stratigraphy (Beres and Haeni, 1991; Jol and Smith, 1991). Its principles are derived from the technique of seismic stratigraphy (Mitchum *et al.*, 1977). Radar stratigraphy systematically defines the stratigraphy and depositional facies from radar signatures in which facies geometry and associations can be determined. Radar stratigraphy can be interpreted at three scales of hierarchical ordering, and is analogous to Jackson's (1975) ordering of alluvial bedforms [stated in square brackets]: radar sequences and boundaries [macroforms], radar elements and facies [mesoforms], and radar reflections [microforms].

### 2.9.2 Radar Boundaries

Delineating storeys (and to some extent facies and elements) in radar stratigraphy requires the explicit identification of bounding surfaces, which express the geometrical and constructional patterns of sedimentary bodies. The delineation of bounding surfaces is based on cross-cutting relationships and the principle of superposition, which assume that primary/depositional strata records a stratigraphy where:

(1) each surface is unique and laterally continuous until truncated or deemed indiscernible,
(2) a surface may truncate another, but surfaces may not cross,
(3) though surfaces may be diachronous, any location on a surface must be younger than the sediments/surfaces it cuts and older than the sediments/surfaces it binds (Holbrook, 2001).

Bounding surfaces can be hierarchically ordered using the numeric scale of Allen (1983) and Miall (1985), or the relative scale of strata (Bridge, 1993a). Neither method is capable of adequately ordering gravelly strata or radar stratigraphies. This is due, in part, to the 'cryptic nature' of gravelly stratification, which tends to be more ambiguous than sandy fluvial deposits (Smith, 1990). Consequently, different styles of stratification and their associated hierarchical bounding surfaces may be difficult to recognize and trace confidently in stratigraphic sections.

The scale of radar strata is dependent on the resolution of the antennas meaning that bounding surfaces delineated on 200 MHz profiles might not be resolvable on 50 MHz profiles. This defies an absolute hierarchy of surfaces and does not allow profiles (imaged at different scales) to be readily compared. Instead, radar boundaries are delineated by systematic reflection terminations (onlap,

downlap, toplap, and erosional truncation) that mark erosional discontinuities, non-erosional, conformable, or discordant contacts (Bristow, 1995).

Bounding surfaces enclose packages (storeys in this study; Gawthorpe *et al.* (1993) radar sequences) of radar reflections (radar facies and elements) that record the accretionary style of bar development (Fig. 2.7).

### 2.9.3 Radar Elements

Radar elements are characterized by a distinctive facies assemblage, internal geometry, and external form. Radar elements combine closely related facies into facies associations, but elements emphasize the 3D geometry and architecture of the associations. The 3D geometrical form of sedimentary bodies also aids in determinations of depositional processes from subsurface geophysical profiles. Sediments with similar geometric forms are identified as architectural elements (Allen, 1983) and it is inferred that similar processes deposited them. The concept of elements is premised on the notion that alluvial sedimentary bodies can be divided into a number of discrete and unique elements that confer particular depositional styles (*e.g.*, lateral accretion), regardless of fluvial style (*e.g.*, braiding, meandering) (Miall, 1988, 1996). Ultimately, it is the spatial assemblage of elements that provides insights into river style rather than vertical facies successions. Facies successions are not particularly diagnostic of river style, as they merely record variations in flow conditions.

### 2.9.4 Radar Facies

Radar facies are mappable, three-dimensional units composed of reflections whose internal reflection configuration (*e.g.*, shape and orientation), continuity, amplitude, polarity, spacing, interval velocity, and external 3D geometry differ from adjacent units (Mitchum *et al.*, 1977). Facies are internally consistent forms recording specific depositional processes. In order to characterize the large-scale subsurface architecture of channel bars, the identification of discrete radar facies is limited to reflection geometries >10 m in length and >1 m thick. Figures 2.8A-D show characteristic reflection configurations and their depositional interpretations.

### 2.9.5 Radar Reflections

Radar reflections are individual reflections that are largely defined by reflection attributes (*i.e.*, reflection configuration) and facies associations.

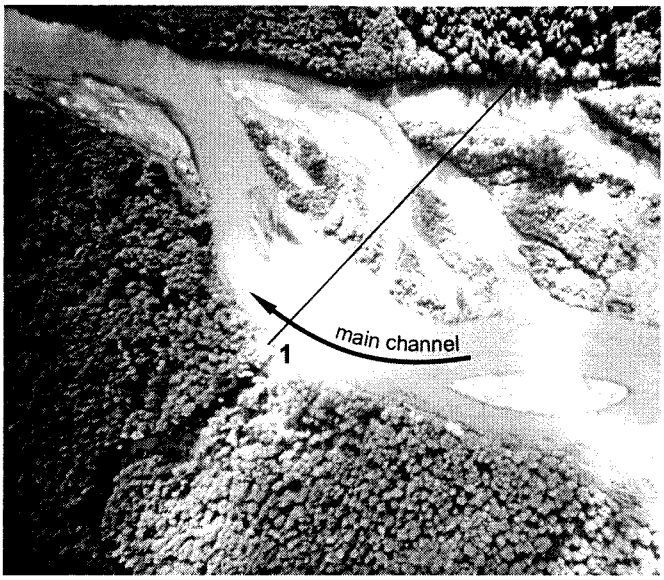


**Alluvial Architecture**
the geometry, proportion, and spatial distribution of fluvial deposits in a sedimentary basin

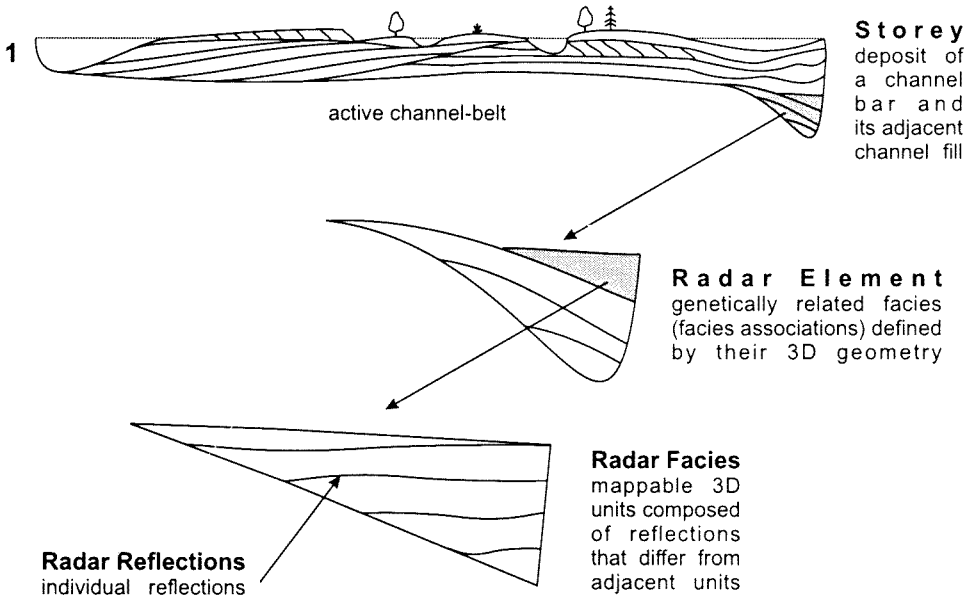


**Fig. 2.7** Hierarchical ordering within alluvial architecture. The cross-section along 1 delineates the extent of the active channel-belt.

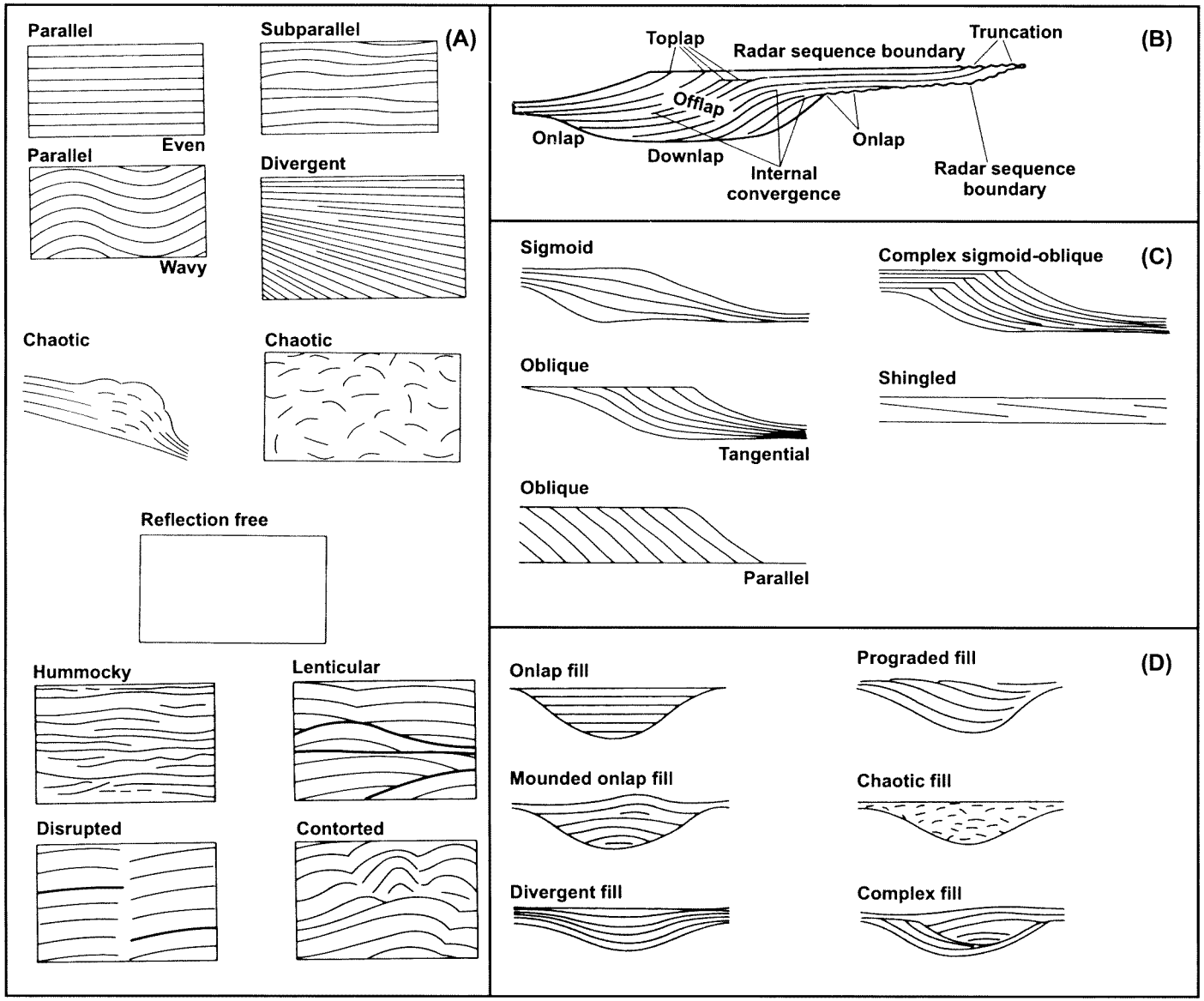


**Fig. 2.8** Common types of radar reflection patterns. **(A)** Reflection configurations. **(B)** Stratigraphic terminations. **(C)** Prograding clinoforms. **(D)** Fill configurations. The reflection patterns are not scale dependent (modified from Mitchum *et al.*, 1977).

# 3 TFLENT Bar, Squamish River

## 3.0 Results

The results of the channel mapping, bathymetry, and GPR surveys are discussed and interpreted for each bar largely independent of the other bars. Select 200, 100, and 50 MHz radar profiles are presented (both in original and interpreted form) that show characteristic radar facies and stratigraphic relationships found in Squamish and Fraser River bars. Six radar facies and two radar elements were identified and interpreted from the complete set of radar profiles. Although each facies and element is uniquely numbered, thus conferring a specific genetic interpretation, the description of facies properties (*e.g.*, thickness) is specific to individual bars. Reflection orientations are stated in reference to mean flow directions, which are given with respect to the orientation of the channel-belt (river-scale flow, not local flow). All dip angles reported are apparent dip angles. Consolidated facies descriptions are presented in the final chapter.

The upper radar stratigraphy (storey 2) is generally interpreted in relation to the photographic and bathymetric records. Comparison with these independent data sources enables conclusions to be drawn about the timing of sedimentation, scour depths, and locations of former bar positions documented in the radar stratigraphy. Although mention is made of the deeper stratigraphy (storey 1), interpretations are largely speculative.

Storey and facies boundaries differ between profiles depending on the antenna frequency plotted. 200 and 100 MHz profiles spatially average less of the subsurface providing better definition of stratal thicknesses and configurations than the 50 MHz antennas. The 50 MHz antennas give a view of the overarching architecture of a section. Subtle changes in reflection geometry and amplitude indicate the presence of smaller-scale structures than can be imaged by the 200 and 100 MHz antennas.

In general, mean signal penetration was 10, 15, and 25 m depth for 200, 100, and 50 MHz antennas, respectively; maximum penetration was 35 m. The profiles show distinct, high-amplitude reflection patterns with little evidence of signal attenuation suggesting that bar sediments are largely gravel and sand with minor silt. The lack of penetration in this resistive environment is likely due to the saturated nature of the sediments attenuating and dissipating EM energy.

## 3.1 TFLENT Bar Morphology

The bank-attached macroform, TFLENT (Tree Farm License Entrance) Bar, is located 450 m downstream of the Squamish-Ashlu Bridge and 2.1 km upstream of the Ashlu River confluence at 34 to 35 m elevation (Fig. 3.1). The compound bar is about 1.1 km long with a maximum width of 400 m and is dissected by multiple chute channels that are active at high-stage flows. The inner portions of the bar support mature cottonwoods, whereas the outer portions are unvegetated channel sands and gravels. Brierley (1989a, 1989b, 1991a, 1991b; Brierley and Hickin, 1991) characterized the sedimentology of the mid and lower portions of TFLENT Bar by digging pits through sands down to the framework gravel. Radar could not be shot over Brierley's sites due to the numerous logs that have since covered his area of investigation (Figs. 1.2C and 1.2D); instead radar was shot at the barhead directly over framework gravel and thin sand sheets (Fig. 3.2A).

The barhead at moderate-stage flows appears as an elongate lobe (unit bar) attached at an angle of 35 to 40° to the older vegetated bar (Fig. 3.1). The angle of attachment causes the bar to resemble a 'gravel wave' attached at its tip, but detached at its tail from the older island. Topographically, the bartop is a ridge with a chute (swale) separating the older island from the ridge (Fig. 3.2B). The detachment is probably maintained and caused by secondary currents acting in a fashion similar to the development of ridge and swale topography in meandering rivers. The chute and ridge are also maintained by flow divergence around, and sediment deposition downstream of, a large logjam (~50 m long x ~50 m wide x ~4 m thick, of which 2 m is buried below the surface of the bar). The logjam (Fig. 3.2C) is located immediately upstream of the ridge and GPR profiled bar surface, and is the topographic high of the bar, away from which the bar surface dips <1° upstream and downstream. Flow around the western edge of the logjam has eroded a steep, 2.5 m high bar-margin (Fig. 3.2D). Lighter colored sediment overriding older, darker colored gravel at the tail of the site provides evidence of recent sediment transport (Fig. 3.2E). The site has a surface median diameter ($D_{50}$) grain-size of 55 mm and $D_{95}$ of 123 mm (Fig. 3.2F) (Brierley, 1984; Brierley and Hickin, 1985).

## 3.2 TFLENT Bar Evolution

TFLENT Bar evolved from a collection of mid-channel islands and bars in a multiple channeled planform in 1951 to a large bank-attached compound bar in a single thread channel (with subordinate sloughs) by the 1970s (Fig. 3.3). Perhaps the most obvious changes through time are the increased bar area and vegetation cover within the channel-belt. This suggests a change in the style of river instability with frequent channel shifts and reoccupation of existing channels prior to the 1970s, followed by directionally consistent lateral and longitudinal bar growth. Mapping flow directions through time shows flow was largely parallel to the channel-belt (and oblique to the 1996 barform) from 1951 to 1967, coincident with the multiple channeled planform. After 1976 bar tail sediments were deposited (prior to this time the western edge of the floodplain occupied this position) and bar-parallel flow patterns commenced.

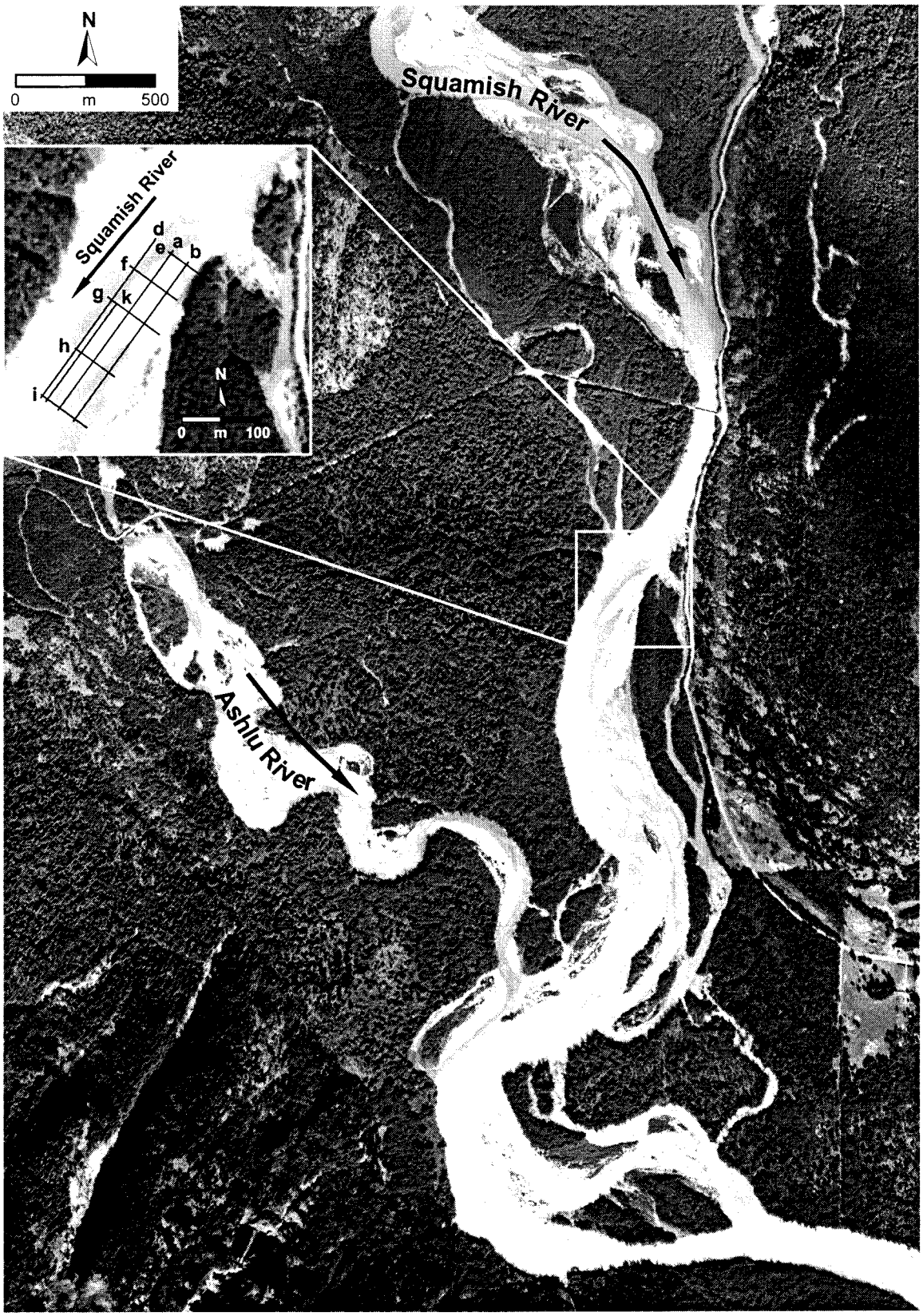


**Fig. 3.1** Bank-attached TFLENT Bar, Squamish River. Inset shows GPR transects shot with 200, 100, and 50 MHz antenna frequencies. Photograph taken 8 August 1996, $Q = 364\ m^3\ s^{-1}$ (BCB96036: 19).

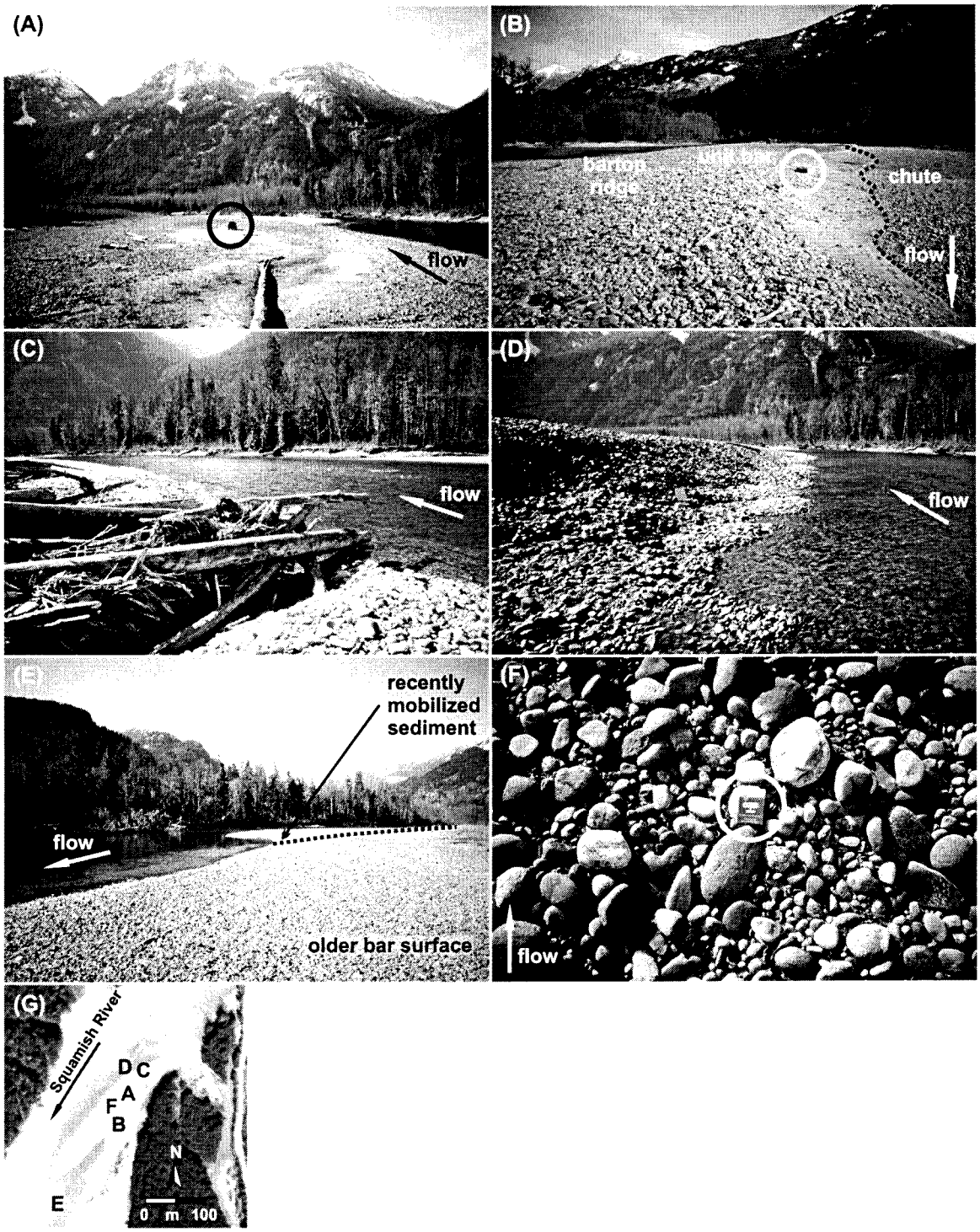


**Fig. 3.2** Surficial morphology of TFLENT Bar, Squamish River. **(A)** Downstream view of the bar (truck for scale). **(B)** Upstream view of a unit bar prograding into a chute. Bartop is 0.6 m above chute (abandoned car tire for scale). **(C)** Downstream view of a 4 m thick logjam, 2 m of which is buried. **(D)** Downstream view of a 2.5 m high bar edge. **(E)** Recently mobilized lighter colored gravel in the background is prograding over older, darker colored gravel. The channel is ~75 m wide in the foreground. **(F)** Surface grain-size texture (cigarette pack for scale is 10 cm on each side). **(G)** Photograph locations.

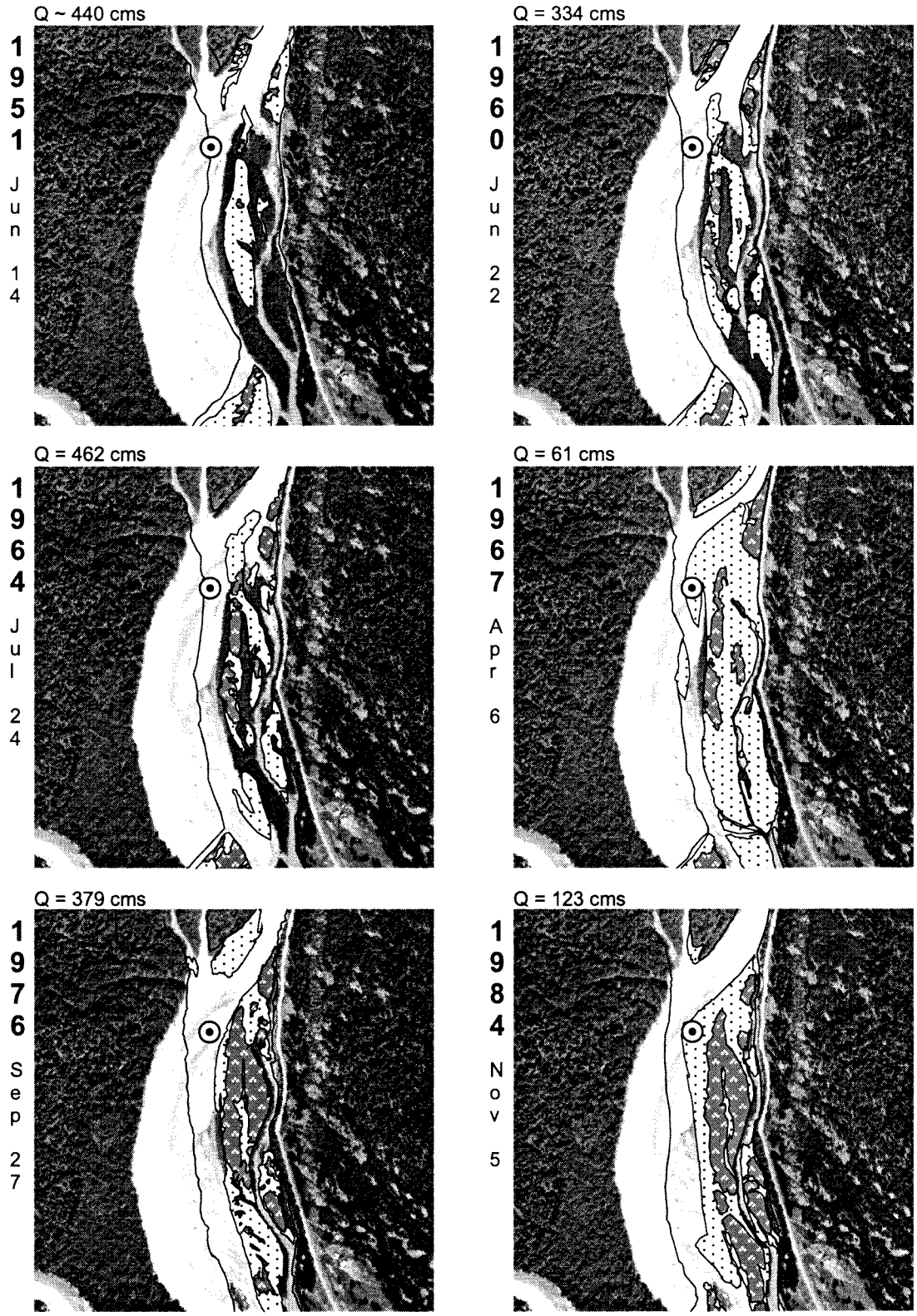


**Fig. 3.3** Morphological evolution (1951 to 1996) of TFLENT Bar, Squamish River. Successive changes in channel position and bar morphology mapped from aerial photographs and superimposed on 1996 photograph in background. The bulls eye marks the center of the GPR grid. 1996 photograph taken 8 Aug 1996, discharge (Q) = 364 cms. Flow is to bottom of page.

The flood of record in 1984 eroded islands in the Squamish-Ashlu Bend Reach and knocked down the Squamish-Ashlu Bridge upstream of TFLENT (visible in Fig. 3.1; Sichingabula, 1985; Hickin and Sichingabula, 1986). The flood locally deposited gravel onto the TFLENT barhead, but produced few immediate planform changes. Subsequently the enlarged barhead forced the thalweg against the western bank instigating bank retreat over the next decade. During this time two large gravel bars (unit bars) became attached to the barhead. The larger downstream bar was built by 1994 and a dense cover of 3 m high willow in 2000 indicates that the bar had not been remobilized since 1996 (Fig. 3.1). Between 1994 and 1996 the smaller upstream bar aggraded vertically to become a prominent barform (Fig. 3.1 inset). Its development effectively buffered the larger downstream bar from formative flows.

At the barhead site the logjam shown in Fig. 3.2C developed after 1996. The barform was already established, but the logjam undoubtedly influenced the style of deposition in the upper 2 m of sediment immediately upstream and downstream of the logjam as flow was forced to bifurcate around the logjam. By 2000 the bartop was relatively stable and willow was beginning to colonize its surface. A flow of ~1100 $m^3s^{-1}$ on 28 July 2000 deposited fine sand and silt over the bartop, but did not transport gravel due to the height of the bar surface. In contrast, flow convergence at the entrance to a slough adjacent to the valley wall (evident at the eastern edge of the Fig. 3.1 inset) mobilized the gravel floor and caused moderate bank erosion transporting sand and gravel, as well as ~1 m diameter trees.

## 3.3 TFLENT Bar Bathymetry

Figures 3.4A-C are bathymetric soundings across TFLENT Bar showing channel cross-sections along a riffle-pool sequence. A channel centerline sounding (Fig. 3.4D) was conducted to determine the bed geometry into a 4 m deep scour hollow. The downstream end of the centerline sounding (Fig. 3.4D) abutted against a 6 m diameter root wad oriented normal to flow (half of which was above water level). The root wad of a 74 m long Spruce tree (lying parallel to flow) was anchored to the bed of the channel. The riffle is located in a straight reach of channel and its geometry is generally planar with 0.8 m mean depth (Fig. 3.4A). Downstream of the riffle, flow deepens and enters a bend at which point the bed shows some topography (0.7 m bed relief) and slight asymmetry (Fig. 3.4B). The bed dips steeply into (19°; Fig. 3.4D) and steeply across (10 to 13.5°; Fig. 3.4C) the scour hollow highlighting the fully pronounced bed asymmetry at the apex of the bend.

The bathymetric soundings indicate a range of bed elevations and varied bed topography in-channel suggesting that the radar stratigraphy of the bar sediments may also display a similar diversity of scour and depositional surfaces. This is suggested because the bar has hosted the main channel and a variety of barforms (*i.e.*, small mid-channel bars) throughout the photographic record. It is assumed that some of those relict features might be preserved in the radar stratigraphy.

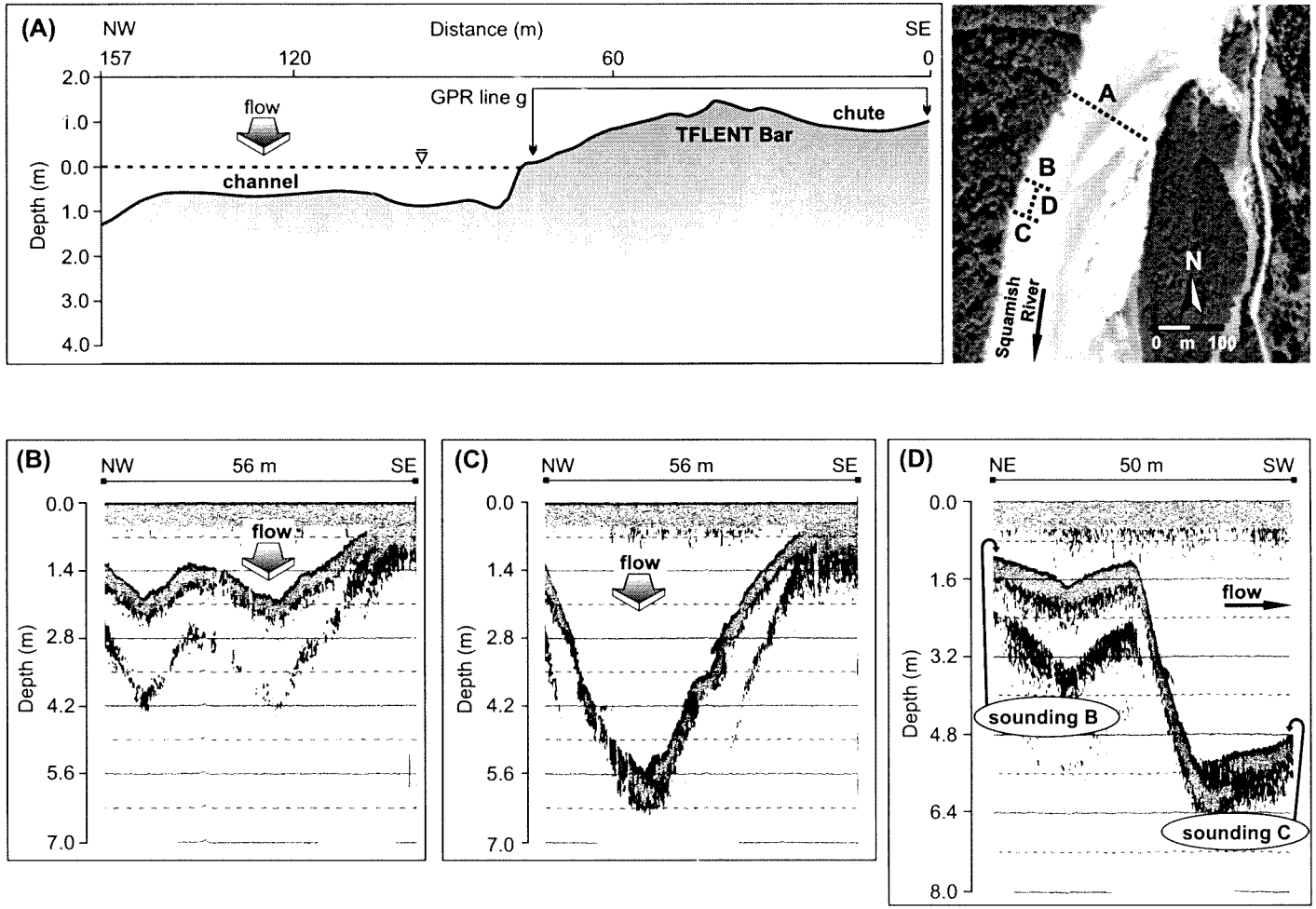


**Fig. 3.4** Bathymetry soundings across TFLENT Bar, Squamish River. **(A)** Cross-sectional sounding across riffle and along radar line g. **(B)** Cross-channel sounding 160 m downstream of sounding A opposite radar line i. **(C)** Cross-channel sounding 50 m downstream of sounding B. **(D)** Channel-centerline sounding between sounding B and sounding C. 0.0 m is water level ( $\bar{\nabla}$ ) at low-stage flow, $Q \sim 50\ m^3 s^{-1}$. Sounding locations are shown (••••) in the photograph.

## 3.4 TFLENT Bar Radar Facies and Elements

Figure 3.1 inset shows the grid profiled on TFLENT Bar with GPR.

### 3.4.1 Radar Facies 1: subhorizontal, continuous, subparallel reflections

Radar facies 1 is characterized by stacked (1 to 3 m thick), horizontal to subhorizontal, continuous (20 to 80 m long), parallel to subparallel reflections (Figs. 3.5A, 3.6A, 3.7A, and 3.8A). The facies occurs in all stratigraphic positions and has a large spatial coverage across the bar. Due to its ubiquitous extent it grades into and out of most of the other facies. Some reflections can be traced in both flow-normal (Fig. 3.6A) and flow-parallel (Fig. 3.7A) GPR profiles where their expressions are equivalently subhorizontal, continuous, subparallel reflections.

*3.4.1.1 Interpretation: vertical accretion deposits (stratified bedload sheets)*

The radar signature is interpreted as stacks of vertically accreted gravel sheets deposited from bedload sheets migrating across bar surfaces and channel floors (Figs. 3.5B, 3.6B, 3.7B, and 3.8B). Individual sheets may be imaged in the 200 MHz profiles (Fig. 3.6B), as their thickness is roughly equivalent to the vertical resolution of the reflections (~0.2 m). The facies occurs at all stratigraphic levels because it is the dominant mechanism of sediment transport in gravel-bed rivers. Bedload sheets are low amplitude, relatively planar features, up to 0.2 m thick, composed of normally loose sediment with angle of repose sheet-margins. The sandy matrix and normally loose texture of the sheets presents an obvious contrast to the older imbricated, cobble armored surfaces they are overriding. Sheets are commonly preserved on bartop surfaces because as stage declines below the threshold of motion, flow is not competent enough to rework the sediments stranding the sheets in mid-transport across bars. The subparallel nature of the radar signature is probably due to the intermittent nature of bedload transport whereby bedload sheets overtake and bury other stalled sheets creating subdued topographic relief.

### 3.4.2 Radar Facies 3: low-angle (3 to 5°), downstream dipping, subparallel reflections

Radar facies 3 is characterized by low-angle (3 to 5°), divergent to subparallel reflections (1 to 4 m thick and 25 to 60 m long) that dip downflow (Figs. 3.5A, 3.7A, and 3.8A). The steeply inclined reflections of radar facies 5 typically grade into this lower-angled facies, which primarily occurs in the upper bar stratigraphy and is well developed in downstream portions of the bar. The flow-normal signature is composed of subhorizontal and hummocky reflections (Fig. 3.6A).

*3.4.2.1 Interpretation: downstream accretion deposits (stratified bedload sheets)*

The flow-parallel radar signature is interpreted as stratified bedload sheets deposited on the former and current downstream margins of the bar (Fig. 3.5B, 3.7B, 3.8B). It is likely that sediment accumulates by gravelly sheets migrating over the bartop or being driven along the channel floor onto the downstream periphery of the bar. The hummocky flow-normal signatures image the topography associated with overlapping and juxtaposed sheets migrating across the bar (Fig. 3.6B). Sediment accumulation extends the bar downstream, and by implication, vertically as well.

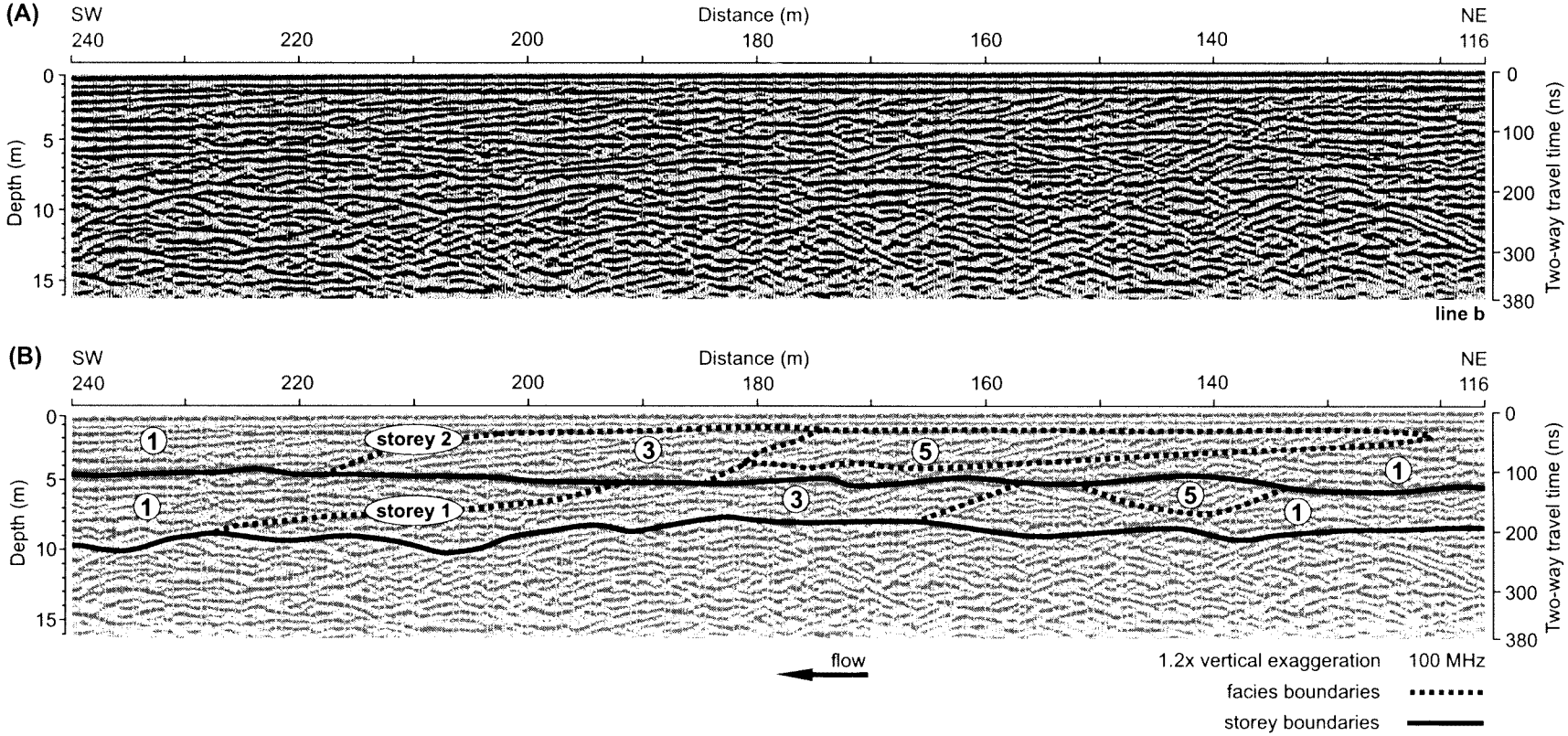


**Fig. 3.5** GPR profile b (100 MHz), TFLENT Bar, Squamish River. **(A)** Flow-parallel profile along line b. **(B)** Interpreted line b profile. Radar facies 1 (vertical accretion), 3 (downstream accretion), and 5 (slipface accretion) are delineated. Storeys 1 and 2 record the thickness of Holocene alluvial sedimentation. The thicker line segment in the photograph shows the extent and location of the profile.

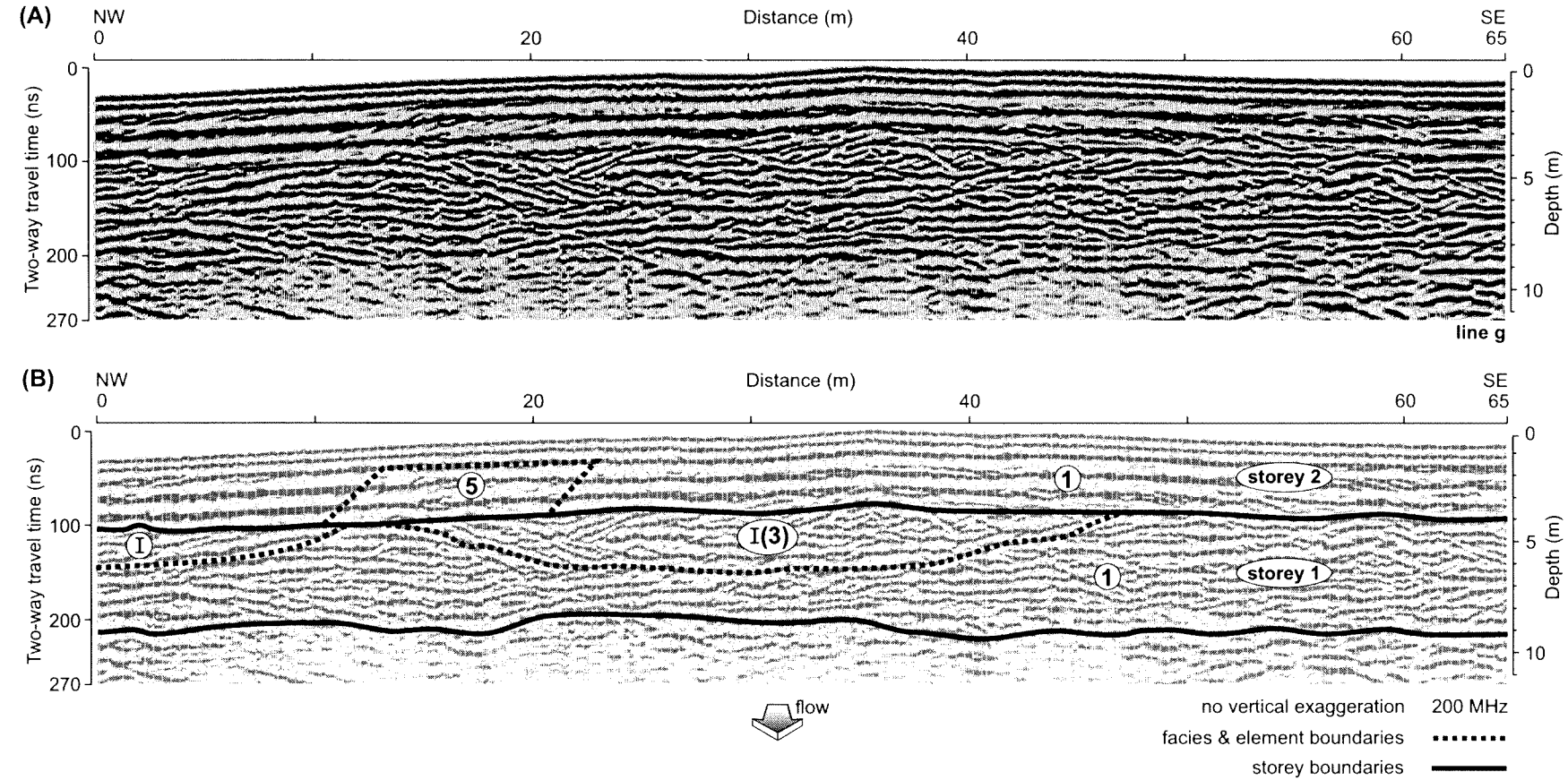


**Fig. 3.6** GPR profile g (200 MHz), TFLENT Bar, Squamish River. **(A)** Flow-normal profile along line g. **(B)** Interpreted line g profile. Radar facies 1 (vertical accretion), 5 (slipface accretion), and element I (chute deposits filled with downstream accretion strata) are delineated. Storeys 1 and 2 record the thickness of Holocene alluvial sedimentation. The thicker line segment in the photograph shows the extent and location of the profile.

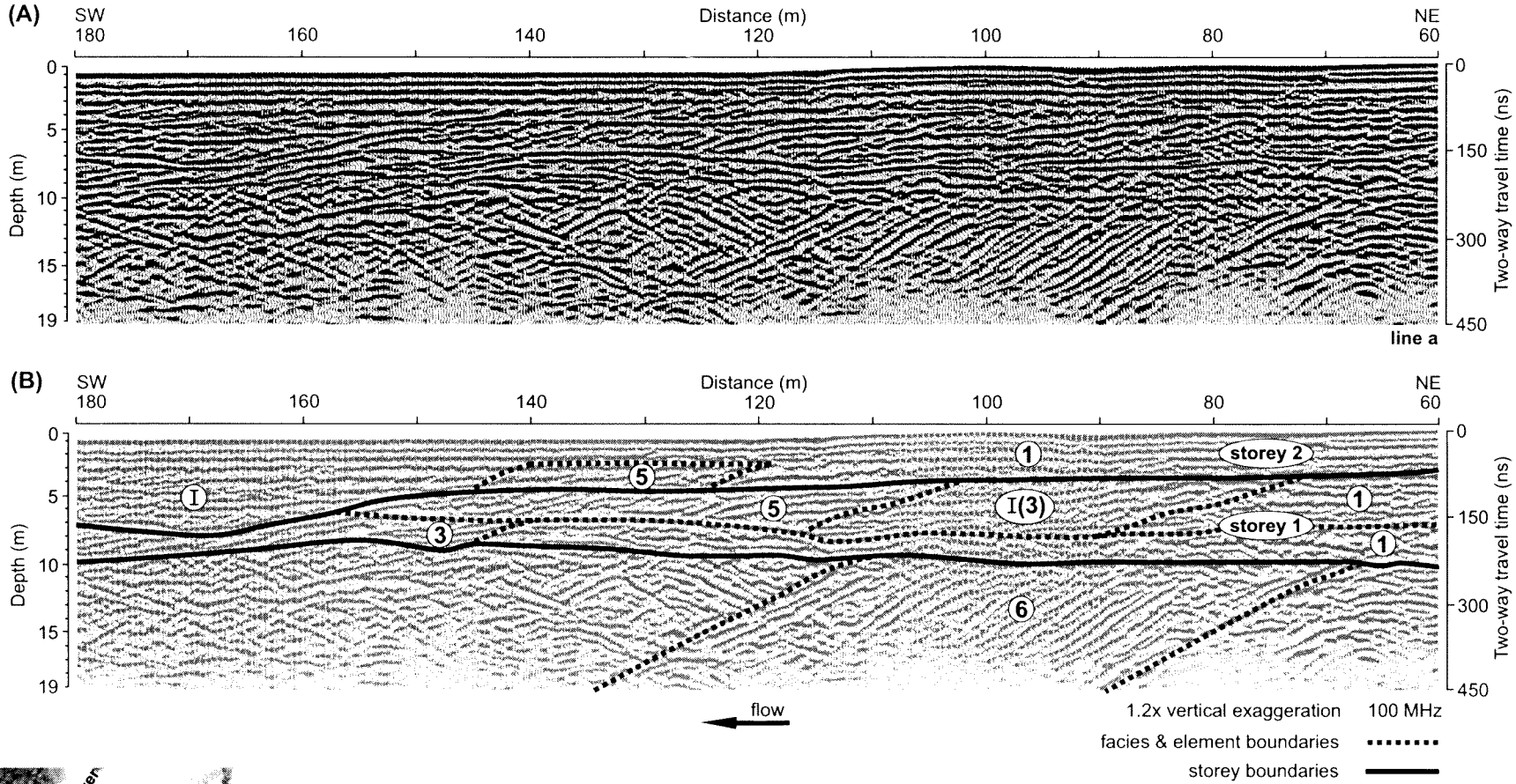


**Fig. 3.7** GPR profile a (100 MHz), TFLENT Bar, Squamish River. **(A)** Flow-parallel profile along line a. **(B)** Interpreted line a profile. Radar facies 1 (vertical accretion), 3 (downstream accretion), 5 (slipface accretion), 6 (delta foresets and topsets), and element I (channel deposits and chute forms filled with downstream accretion strata) are delineated. Storeys 1 and 2 record the thickness of Holocene alluvial sedimentation. The thicker line segment in the photograph shows the extent and location of the profile.

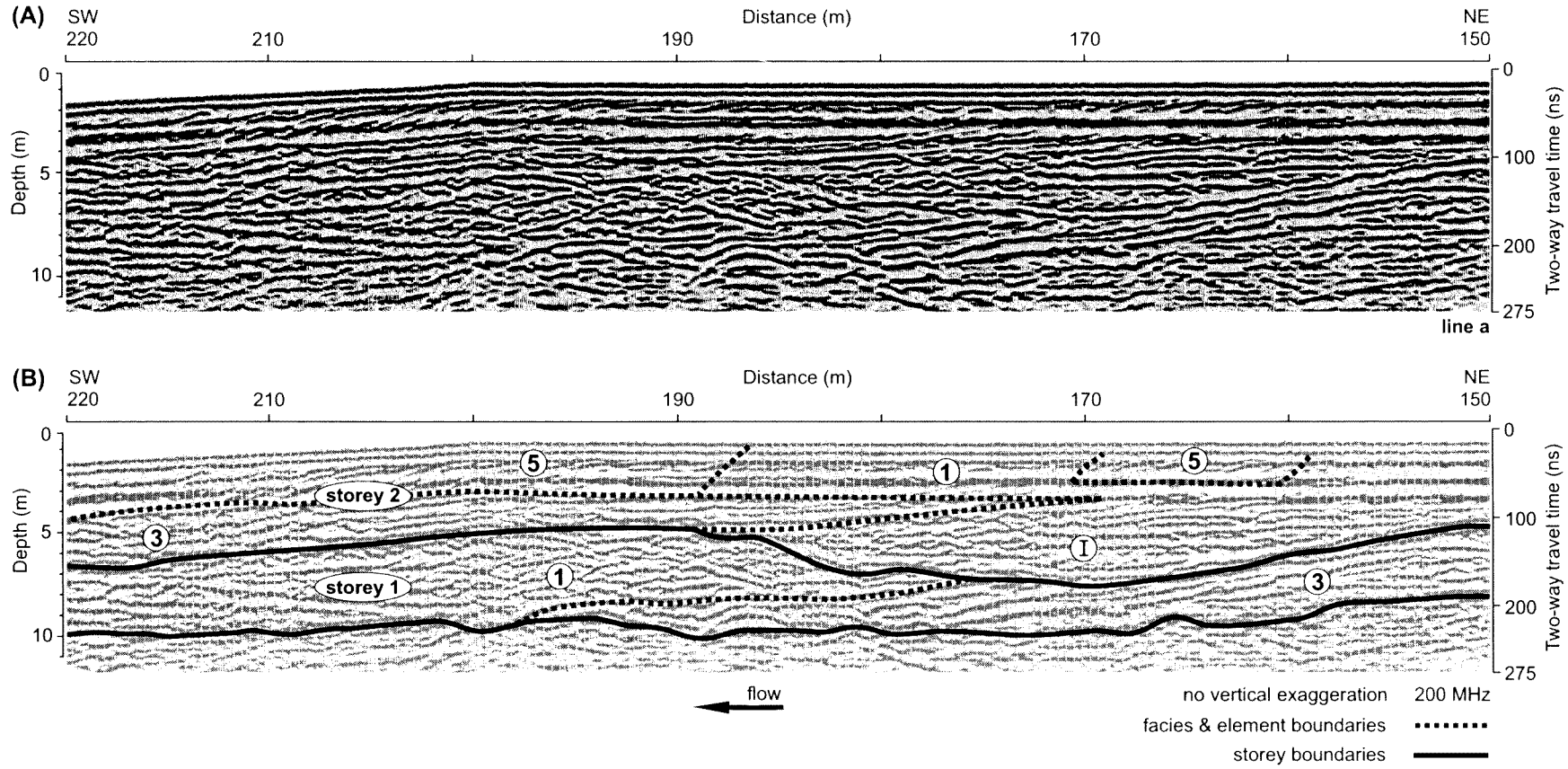


**Fig. 3.8** GPR profile a (200 MHz), TFLENT Bar, Squamish River. **(A)** Flow-parallel profile along line a. **(B)** Interpreted line a profile. Radar facies 1 (vertical accretion), 3 (downstream accretion), 5 (slipface accretion), and element I (channel deposits) are delineated. Storeys 1 and 2 record the thickness of Holocene alluvial sedimentation. The thicker line segment in the photograph shows the extent and location of the profile.

### 3.4.3 Radar Facies 5: small- to medium-scale (0.5 to 2.5 m), steeply inclined (13 to 26°), oblique reflections

Radar facies 5 is characterized by continuous sets (10 to 60 m long) of small- to medium-scale (0.5 to 2.5 m thick), roughly parallel, steeply inclined (13 to 26°), oblique reflections that dip downflow (Figs. 3.5A, 3.7A, and 3.8A) and normal to flow (Fig. 3.6A). They are typically found as discrete packages that occasionally thicken downflow and in most instances are externally bound above and below by continuous, subhorizontal reflections. The facies is found at all stratigraphic levels in the upper stratigraphy (above 10 m depth).

#### *3.4.3.1 Interpretation: bar-margin slipface accretion deposits*

The radar signature is interpreted as bar-margin slipface sediments indicative of sediments avalanching over high relief bar-margins into deeper water (Figs. 3.5B, 3.6B, 3.7B, and 3.8B). High relief bar-margins are typically oriented downflow, but can also dip steeply normal to flow causing bar edges to prograde both normal to flow and downflow. The strata are likely deposited from bedload sheets periodically passing over the bar-margin at high-stage flow. When the discharge falls below the threshold of motion for gravel, sand is deposited on the slipface and at its toe reducing the dip angle of face (it is likely that gravel rolling to the bottom of the face also contributes to the reduction in dip angle). Hence, sets of steeply inclined reflections commonly decrease in dip angle downstream and grade into lower-angled downstream accretion strata (radar facies 3). This interpretation is supported from observations of TFLENT and other Squamish River bar-margins, which exhibit similar geometries (heights and dip angles) and surface morphologies (steep bar-margins grading laterally and downstream into gently inclined channel floors). There is little indication of bar-margin reactivation surfaces evident in the radar profiles even though some Squamish River bar-margins do show reactivation surfaces.

### 3.4.4 Radar Facies 6: large-scale (4 to 7 m), steeply inclined (25 to 28°), oblique reflections

Radar facies 6 is characterized by large-scale (4 to 7 m), parallel, steeply inclined (25 to 28°), oblique reflections that dip downvalley and in some cases can be traced up-dip into horizontal reflections (Fig. 3.7A). The lower boundary is indistinct with dipping reflections terminating abruptly in undulating subhorizontal reflections. The facies extends at least 200m across the valley (it was also profiled adjacent to the bedrock valley wall), but it only persists for some 45 m down the valley. The stratigraphic thickness of the facies varies from 4 to 7 m, but the top of the facies always occurs at ~200 ns (~8.5 m depth).

#### *3.4.4.1 Interpretation: delta foreset (and topset) deposits*

There are three possible sedimentary interpretations of the radar signature (Fig. 3.7B): (1) delta foresets, (2) gravel dunes, or (3) scour hollows.

(1) The deltaic interpretation is favored (a) because the dip angle is close to the 25° angle of repose of gravel found on gravelly delta fronts (Smith, 1991), (b) the stratigraphic thickness can be accommodated by increased water depths associated with marine flooding, (c) delta fronts are laterally extensive features, (d) the consistent depth to the top of the inclined reflections suggests progradation into a standing body of water, and (e) some of the steeply dipping reflections can be traced up-dip into horizontal reflections suggestive of a depositional topset facies. The limited downvalley extent of the

facies is somewhat problematic and can be explained by inferring discontinuous lobe-like delta progradation associated with fluctuating sediment loads and/or sea level. Alternatively, channel switching across the ancestral delta may have excavated and removed any trace of deltaic sediments, or sediment supply to one portion of the delta front may have been shut off halting delta progradation and deltaic sedimentation.

(2) The facies is reminiscent of large-scale gravel dunes such as those deposited by outburst floods, which are up to 16 m high, with decimeter thick, steeply dipping (12-27°), planar cross-strata (Carling, 1996). The formation of large-scale gravel dunes requires high water discharges that typically can only be generated from the instantaneous release of large volumes of ponded water impounded by, in the case of the Squamish Valley, either debris avalanche deposits or glacial ice. The Squamish River has been impounded temporarily by 7 or 8 Holocene debris avalanches from Mount Cayley, the largest of which ~4800 BP was on the order of $9x10^7$ $m^3$ (Brooks and Hickin, 1991). The volume of impounded water is great enough to generate duneforms, if released instantaneously. Brooks and Hickin (1991) note however, that the dam was probably rapidly incised into, rather than catastrophically overtopped and that drainage was more than likely arrested by the development of outlet channel armoring. Alternatively, glacial damming and ponding has not been documented in the Squamish Valley, although presumably large volumes of meltwater were discharged during deglaciation. If sea level was much higher than its present level during deglaciation, the river-bed would have been decoupled from the generating flows and it is unlikely discharges could have deposited duneforms at the TFLENT site. On the other hand, if sea level was much lower, then perhaps high discharge events could have deposited dunes. Yet, the internal architecture of the radar signature is incongruent with duneform structure. The juxtaposition of subhorizontal reflections upvalley of the steeply inclined reflections is not expected of duneform structures and it is unlikely that the subhorizontal reflections record alluvial deposition infilling dune troughs without reworking most of the duneform.

(3) High discharge meltwater flows, if coupled to the river-bed, could have eroded a large scour hollow that progressively infilled by sediment avalanching over the upstream-margin of the hollow. This scenario is not favored because the basal form of the reflection configuration is not defined by a continuous, high-amplitude, 3D, scallop-shaped reflection as is evident on scour elements in the Fraser River. Also, the consistent internal structure of the fill favors deposition into standing water rather than sedimentation into a flowing current, which would show a more variable fill configuration.

### 3.4.5 Radar Element I: 2D, basal, concave-up reflections

Radar element I is distinguished by 2D, basal, concave-up reflections that truncate adjacent reflection patterns and is typically infilled with subhorizontal and steeply inclined reflections (Figs. 3.6A, 3.7A, and 3.8A). The element extends 30 to 45 m laterally, with depths approaching 3 to 4 m, and the concave-up edges dip into the center of the form with apparent dips between 6° and 10°. There are few preserved forms and it is stratigraphically restricted to the middle portions of the succession.

#### *3.4.5.1 Interpretation: channel and chute deposits*

The radar signature is interpreted as an element in which the 2D, concave-up geometry of the basal reflection identifies the scour of channels and chutes (Figs. 3.6B, 3.7B, and 3.8B). The basal reflection is associated with (and infilled by) a variety of reflections that make up the channel fill.

Additionally, the dimensions of the element scale to channels and chutes found in the Squamish River. Further, the paleochannel imaged in Figs. 3.7B and 3.8B records a flow direction cutting across the bar, normal to the present course of the river. This matches flow directions across the site prior to 1976 (Fig. 3.3). Subsequent channel shifting, bank erosion, and bar deposition displaced the channel further westward forcing flow away from the site. The geometry of the fills is deciphered from their 3D expressions. For example, the chute form imaged in Fig. 3.6B is infilled with downstream accretion strata (radar facies 3) imaged in Fig. 3.7B. The lack of preserved chute and channel forms would seem to indicate a high degree of channel reworking within a rather thin sediment pile.

## 3.5 TFLENT Bar Radar Stratigraphy

A prominent subhorizontal reflection about 10 m below the surface of the bar separates the TFLENT Bar stratigraphic succession into two distinct packages of radar signatures. The deeper stratigraphy shows large-scale, steeply inclined reflections that dip downvalley and are overlain by subhorizontal reflections interpreted to be delta foresets and topsets, respectively. The sediments trace delta front progradation into a flooded Squamish River valley in the late Pleistocene/early Holocene deglacial period, after which relative sea level dropped and alluvial sedimentation commenced.

The upper 10 m of TFLENT Bar architecture is complex and diverse with three discrete and intertonguing alluvial radar facies and one element building the sediment pile. Architecturally, downstream accretion, channel and chute elements, and slipface accretion are local features abutting the widely distributed vertical accretion deposits, which are found in all stratigraphic positions. The style of bar construction is dependent on its barhead position and the size of the river channel. The juxtaposition of multiple radar facies and one element is a function of flow cutting across, converging, and diverging around the barhead forming a topographically intricate bar configuration. The facies and element scale to the moderate size (width and depth) of the Squamish River.

It is difficult to isolate individual storeys in the complex stratigraphy because the river can achieve scour depths between 3 and >8 m below the bar surface (Figs. 3.4A-D). The >8 m scour depth is calculated by adding 5.5 m scour depths (from bathymetry data in Fig. 3.4D) to 2.5 m bar heights above the water surface. Scour is deeper than 8 m because the bathymetry was collected at very low-stage flow ($Q \approx 50\ m^3s^{-1}$) when the boundary was not mobile. In contrast, high-stage freshet flows actively scour and over-deepen the channel-bed. Paige and Hickin's (2000) data from the gravel-bed meandering reach of the Squamish River (15 km downstream) shows active scour can over-deepen the channel by up to 2 m. This represents the maximum limit of scour in the wandering reach, as its multiple channeled planform probably does not concentrate flow to the same degree as in the single thread meandering channel. This scour depth corresponds closely to the GPR-imaged scour depths of about 10 m (coincident with the base of the alluvial fill).

Thus it is possible that the 10 m thick alluvial radar stratigraphy is one storey and records bar formation since 1951 (the beginning of the photographic record). This interpretation is somewhat problematic, as it requires the entire site to have been scoured to the absolute maximum scour depth calculated. Instead, it is more likely that scouring to this depth occurred locally, such as when bar growth constricted the channel after the flood of 1984. The channel form ~7 m below the surface of the bar

(Figs. 3.7B and 3.8B) is probably the subsurface expression of the channel scouring against, and forcing the retreat of, the western bank. Based on the juxtaposition of this element, the stratigraphy is interpreted to show two storeys. Further evidence is drawn from the coincidence between the depositional style imaged in the uppermost strata (storey 2), and the depositional history traced in the photographic record. For instance, the facies succession interpreted in Fig. 3.5B probably corresponds to the downstream extension of the bar between 1984 and 2000. The succession shows steeply inclined slipface accretion strata (radar facies 5) grading downbar into low-angle, downstream accretion strata (radar facies 3), and subhorizontal, vertical accretion deposits (radar facies 1). The lack of distinct lateral accretion deposits reflects the low sinuosity of the channel indicating that most bar growth is directed downflow rather than normal to flow.

Both storeys record similar styles of bar accretion, which may indicate that the style of sedimentation during the last few hundred years has remained unchanged. Yet, sediment supply rates have declined throughout the current non-glacial period suggesting that the river may have experienced a shift in stability regimes from a rapidly shifting, braiding system characterized by high bedload transport rates to its current wandering style. There is little stratigraphic evidence of this shift in stability regimes. Rather, the presence of medium-scale, steeply inclined reflections points to high relief barforms, rather than shallow flow bifurcating around low relief barforms characteristic of braiding regimes. In this respect, the greater scour depths associated with wandering systems have probably eliminated previous stratigraphic evidence of former channel patterns as the river continually reworks its channel-belt.

# 4 Calamity Bar, Fraser River

## 4.1 Calamity Bar Morphology

Calamity Bar is a bank-attached macroform approximately 1 km long and 400 m across situated 1.3 km downstream of the Harrison River confluence at 8 to 9 m elevation (Fig. 4.1). The bar is separated from the bank (bedrock) by a long-lived chute (>58 years old) that lies along its northern margin (4.2A). The chute has a concave-up, cross-flow form, which is roughly 30 m wide and upwards of 1 m deep. The upstream portion of the chute (at the bar tip) abuts bedrock and is floored by gravel, bedrock protuberances, and buried logs. Sands become more prevalent in the distal portion of the chute, which ends abruptly at a steeply dipping (angle of repose), sandy bar-margin prograding into deep water. The upstream end of the chute is flanked to the south by a low relief, armored, gravelly surface that dips into the chute. Willows and cottonwoods (~7 years old) are colonizing the central portion of the bar adjacent to the downstream portion of the chute. Curiously, the vegetated area is not the topographic high of the bar. Instead, the topographic high is coincident with the top of a prominent unit bar that had become attached to the southern margin of the bar by 1999 (Figs. 4.2A and 4.2B). The older, vegetated surfaces are being overridden by the unit bar, with a slipface (up to 1.5 m high) that extends along the (flow-parallel) length of the bar. The curviplanar surface of the unit bar is composed of normally loose gravel and sand that is roughly horizontal at its crest and increases in dip angle (up to 3°) into the channel along its southern margin. The gravelly bar surface (Fig. 4.2C) also dips (<1°) upstream and downstream from roughly the middle of the bar causing it to have a dome-like form.

## 4.2 Calamity Bar Evolution

Calamity Bar in the last 58 years has maintained its bank-attached form and evolved from a small bank-attached bar in 1943 to a much larger bank-attached bar in 2001 (Fig. 4.3). Its increased size is related to channel switching and deflection of the thalweg away from the bar. From 1943 to 1971 the main channel flowed west across Harrison Bar and impinged directly onto the bar. Bar growth was rather limited during this time as the bar was subject to intermittent deposition and erosion until the main channel abandoned its course across Harrison Bar after 1971. The main channel then switched to a more northerly position flowing around the tip of Harrison Bar. This major realignment recast Harrison Bar as a single, large (5.4 km long), mid-channel bar formed by islands accreting to its northern margin and sediment infilling the former channel across the bar, opposite Calamity Bar. Figures 4.4B and 4.4C document the channel realignment between 1952 and 1999 (Calamity Bar is not evident in 1952 due to high-stage flow drowning the entire bar).

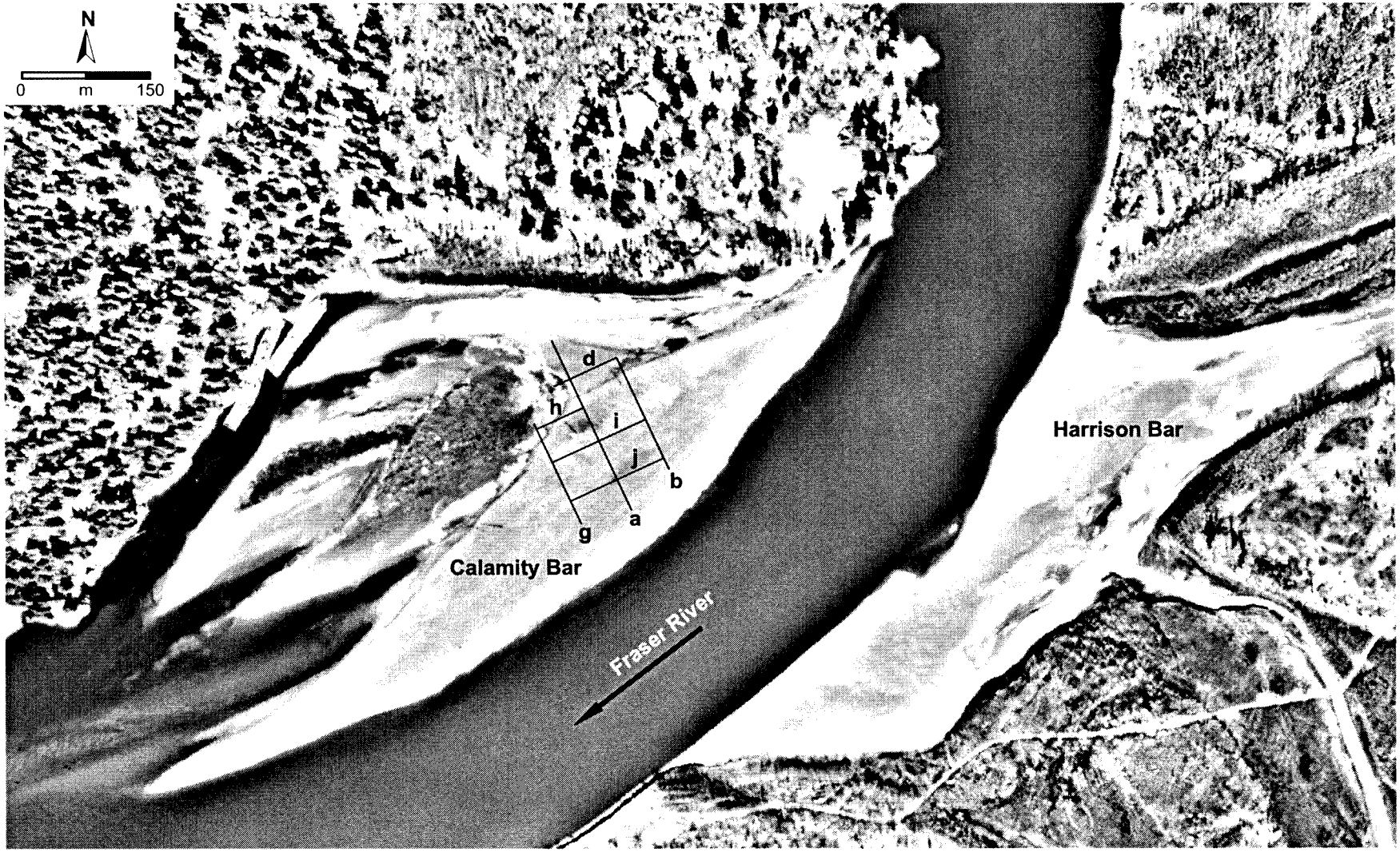


**Fig. 4.1** Bank-attached Calamity Bar, Fraser River. Lettered lines are GPR transects shot with 200, 100, and 50 MHz frequency antennas. Photograph taken 7 March 2001, $Q$ = 485 $m^3s^{-1}$ (SRS6348: 63).

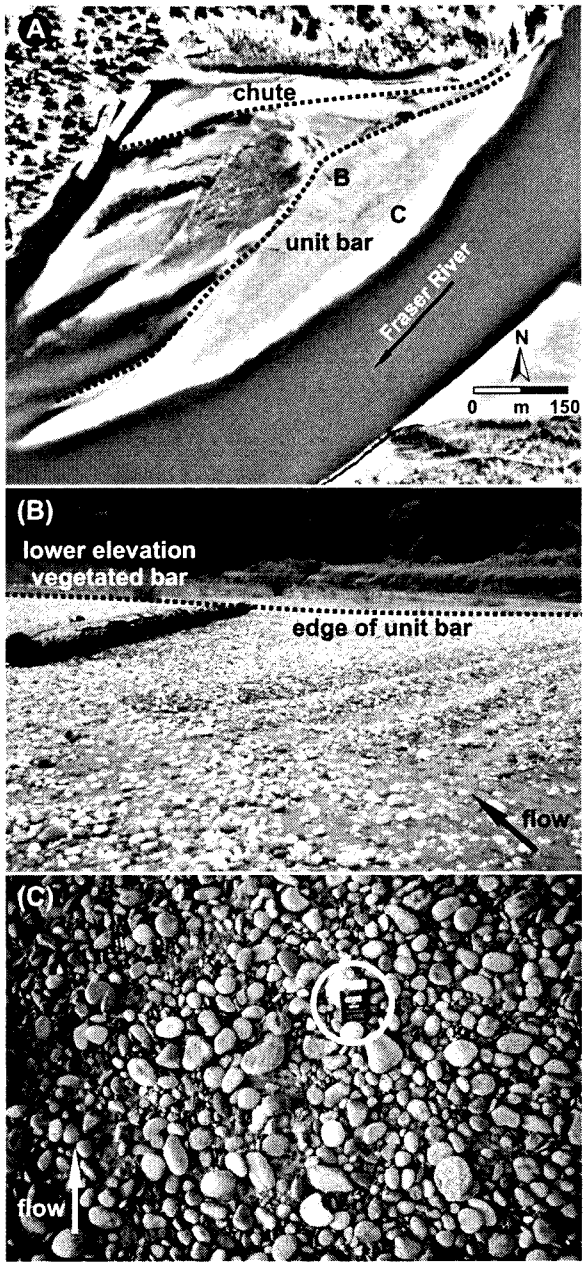


**Fig. 4.2** Surfical morphology of Calamity Bar, Fraser River. **(A)** Extent of chute and unit bar. The slipface of the unit bar is dashed. Photograph locations also shown (SRS6348: 63). **(B)** Recently attached unit bar prograding over lower elevation, older, vegetated portion of bar. Log is 20 m long. Photograph courtesy of T.F. Johnsen. **(C)** Surface grain-size texture. (cigarette pack for scale is 10 cm on each side).

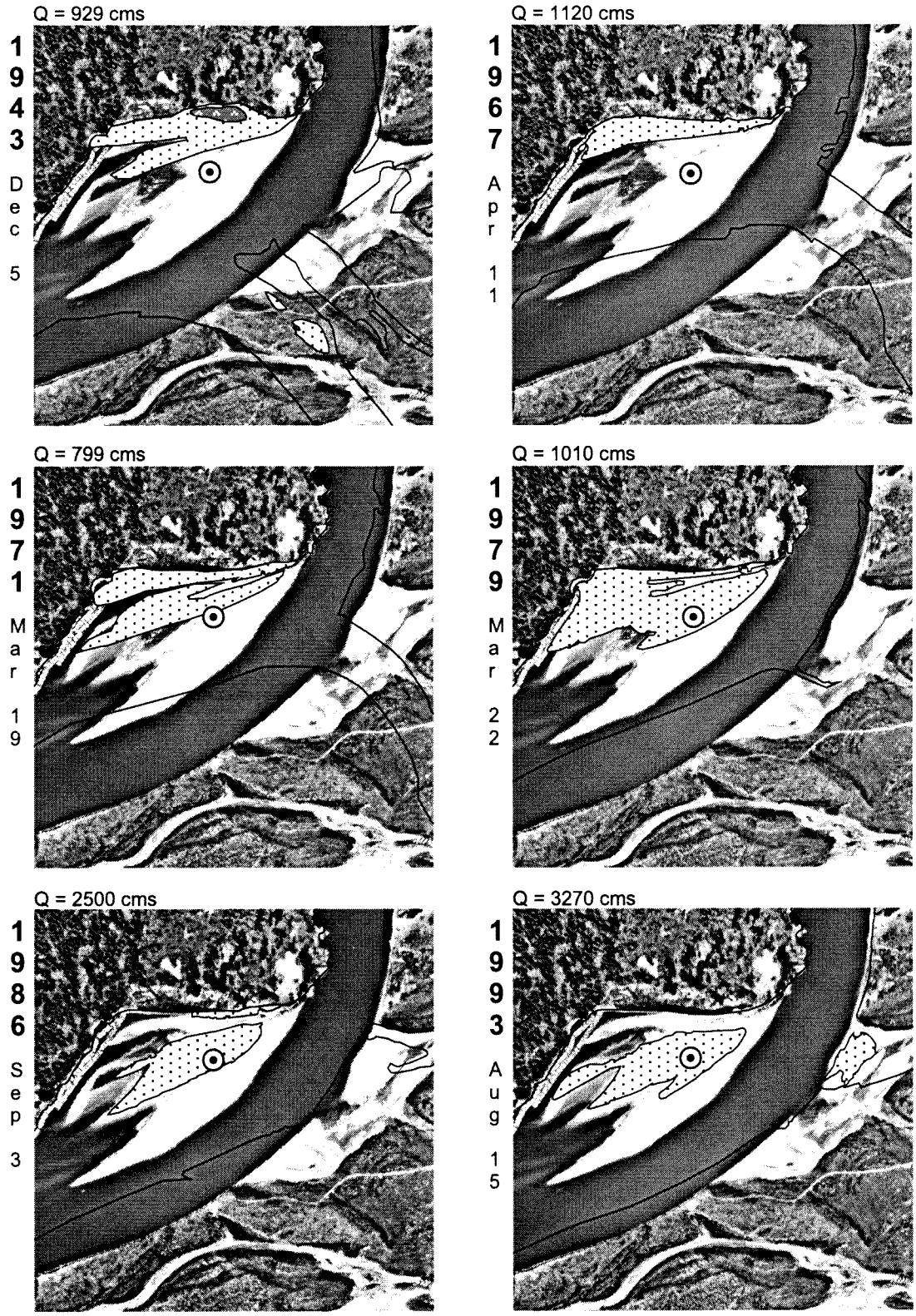


**Fig. 4.3** Morphological evolution (1943 to 2000) of Calamity Bar, Fraser River. Successive changes in channel position and bar morphology mapped from aerial photographs and superimposed on 2000 photograph in background. The bulls eye marks the center of the GPR grid. 2000 photograph taken 10 March 2000, discharge (Q) = 677 cms. Flow is from top right to bottom left.

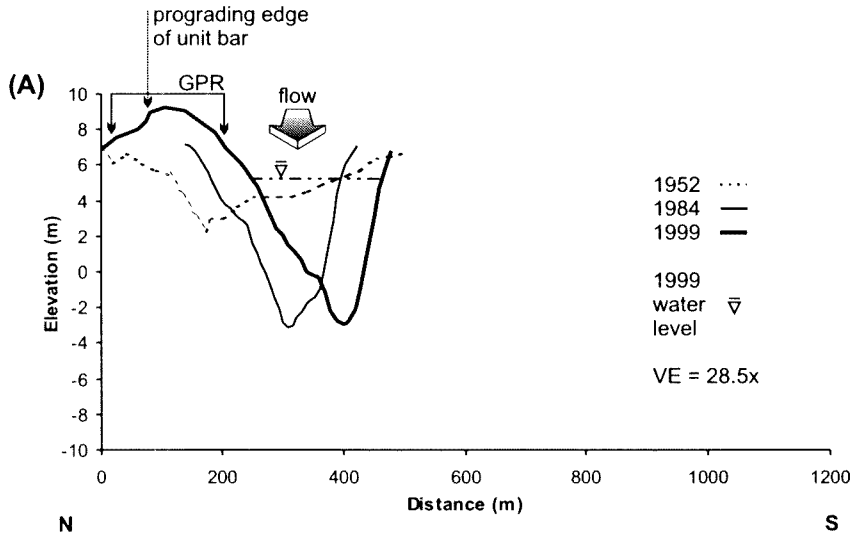


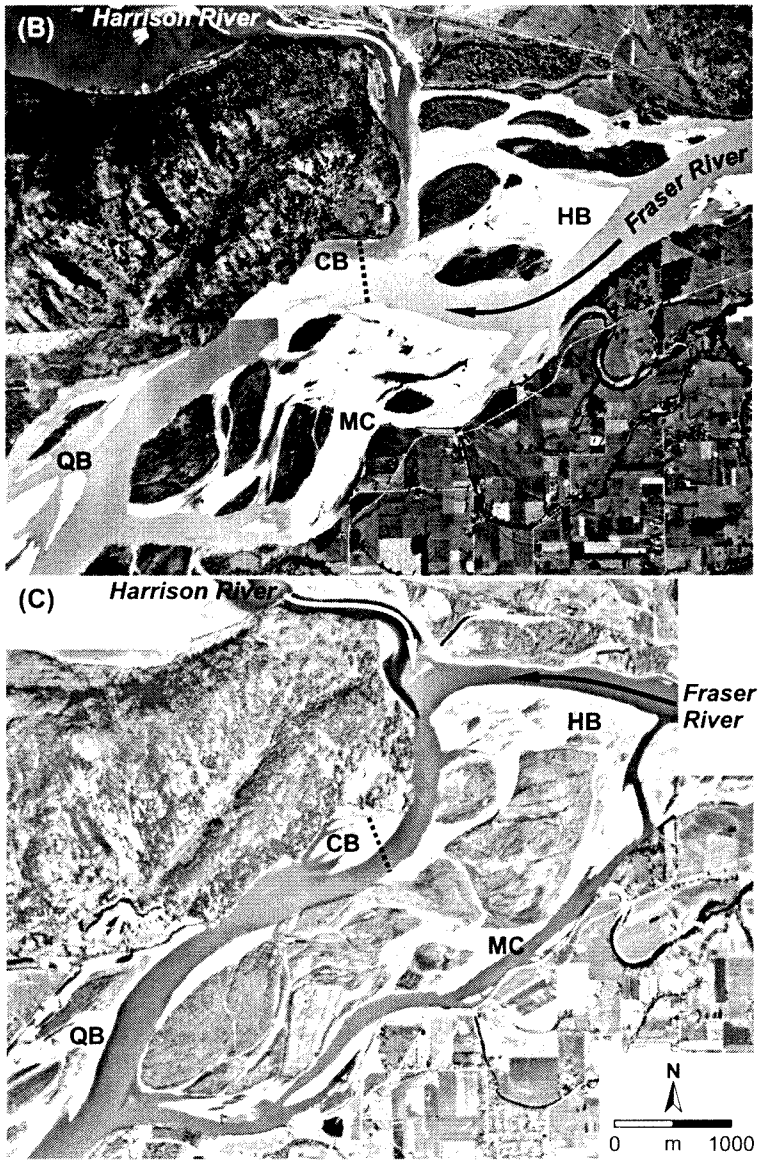


**Fig. 4.4** Bathymetry soundings across Calamity Bar, Fraser River. **(A)** 1999, 1984, and 1952 cross-stream channel geometry. 0 m elevation is mean sea level. Water level is at low-stage flow, $Q$ = 677 $m^3s^{-1}$. Extent of bar surface profiled with GPR is also shown. Bathymetry data courtesy of the Department of Geography, UBC. **(B)** 1952, and **(C)** 1999 sounding locations (•••••). Photographs taken 2 October 1952, $Q$ = 2350 $m^3s^{-1}$ (BC1622: 24, 68), and 20 March 1999, $Q$ = 701 $m^3s^{-1}$ (15BCB99001: 22). Calamity Bar (CB), Queens Bar (QB), Harrison Bar (HB), and Minto Channel (MC).

After 1971 the main channel flowed around Harrison Bar in a more southerly direction, roughly parallel to the long axis of Calamity Bar. The bar began accreting laterally and downstream into the channel, as sediment was deposited onto the bar and not reworked by subsequent flows. Evidence of vertical and downstream growth comes from high-stage 1993 photographs (3250 $m^3 s^{-1}$) in which more bar area was exposed than in 1986, a lower stage year (2500 $m^3 s^{-1}$) (Fig. 4.3). Plant colonization in the middle of the bar began after 1993, thus altering the style of vertical accretion by enhancing the deposition of sand across the vegetated bar area forming an incipient fining (gravel to sand) island stratigraphy. The shape of the bar changed little in 1999 (Fig. 4.4C), 2000 (Fig. 4.3), or 2001 (Fig. 4.1), although it continued to expand (on the scale of meters) laterally and downstream during this time.

## 4.3 Calamity Bar Bathymetry

Figure 4.4A displays three bathymetric soundings across Calamity Bar and the main channel completed in 1952, 1984, and 1999 (Figs. 4.4B and 4.4C show their locations). Harrison Bar and Minto Channel extend the active channel-belt another 1.2 km south to the edge of the Fraser River floodplain. The 1952 bathymetry shows Calamity Bar to be a small barform (lying between 0 and 100 m distance) attached to the northern channel-margin (at 0 m distance). By 1984 the bar had laterally extended southward into the channel as a consequence of the channel realignment. The much deeper, fully asymmetrical channel evident in the 1984 sounding indicates that flow was deflected away from Calamity Bar and impinged on Harrison Bar. This in stark contrast to the shallow, symmetrical channel profiled in the 1952 sounding, in which flow impinged directly onto, and undoubtedly reworked, Calamity Bar sediments. By 1999, flow had further scoured Harrison Bar commensurate with Calamity Bar continuing to expand laterally into the channel. The channel geometry was nearly identical between 1984 and 1999, with comparable channel depths and bar-margin dip angles suggesting a consistent style of bar development. Indeed, the dip angles (~3°) along the southern margin of Calamity Bar in 1952, 1984, and 1999 also show a remarkable similarity. This indicates that sediments deposited on the bar-margin, after the channel realignment in 1971, record a largely depositional succession of strata with little reactivation.

The 1999 sounding also captures the convex-up form of the bartop, including the small-scale angular form of the unit bar slipface and the topographically low chute adjacent to the northern edge of the sounding (Fig. 4.4A).

## 4.4 Calamity Bar Radar Facies and Elements

Figure 4.1 shows the grid profiled on Calamity Bar with GPR.

### 4.4.1 Radar Facies 1: subhorizontal, continuous, subparallel reflections

Radar facies 1 is characterized by stacked (3 to 5 m thick), horizontal to subhorizontal, continuous (50 to 150 m long), parallel to subparallel reflections (Fig. 4.5A). The 3D perspective in Fig. 4.6A shows that some reflections can be traced in both flow-parallel and flow-normal GPR profiles, as they retain their subhorizontal, subparallel character. The facies is limited to deeper stratigraphic positions. It occurs as discrete packages and also grades into or out of the other facies.

#### *4.4.1.1 Interpretation: vertical accretion deposits (stratified bedload sheets)*

The radar signature is interpreted as stacks of vertically accreted gravel sheets deposited from bedload sheets migrating across bar surfaces and channel floors (Figs. 4.5B and 4.6B). The subparallel nature of the radar signature is probably due to the intermittent nature of bedload transport whereby bedload sheets overtake and bury other stalled sheets creating subdued topographic relief.

### 4.4.2 Radar Facies 2: low-angle (3 to 5°), cross-stream dipping, subparallel reflections

Radar facies 2 is characterized by stacked (3 to 8 m thick), continuous (>150 m long), gently inclined (3 to 5°), subparallel to parallel reflections that dip normal to flow (Fig. 4.5A). The facies dominates the entire stratigraphic thickness of the southern portion of the bar and onlaps a prominent reflection dipping to the south-southeast. Some reflections can be traced along strike and their flow-parallel expression is largely as continuous, parallel, subhorizontal reflections (Fig. 4.6A).

#### *4.4.2.1 Interpretation: lateral accretion deposits (stratified bedload sheets)*

The flow-normal radar signature is interpreted as lateral accretion deposits (Figs. 4.5B and 4.6B). The interpretation is supported by the flow-normal apparent dip of the reflections roughly paralleling the ~3° dip of the bar surface. The bar surface slopes into the channel suggesting that bedload sheets migrate onto its surface causing the bar to accrete laterally. The flow-parallel, subhorizontal reflections also support this inference and speak to the continuous nature of sheet-like sedimentation. There is little evidence of reactivation surfaces suggesting a relatively conformable depositional succession that has both vertically and laterally extended the bar.

### 4.4.3 Radar Facies 5: small- to medium-scale (0.5 to 3 m), steeply inclined (16 to 25°), oblique reflections

Radar facies 5 is characterized by continuous sets (40 to 60 m long) of small- to medium-scale (0.5 to 3 m thick), parallel to subparallel, steeply inclined (16 to 25°), oblique reflections that dip normal to flow (Fig. 4.5A) and downflow (Fig. 4.6A). The facies is found as discrete packages that occasionally thicken downflow and are externally bound above and below by continuous, subhorizontal reflections. The facies is restricted to the northern half of the bar, and is stratigraphically confined to the middle and deeper portions of the succession.

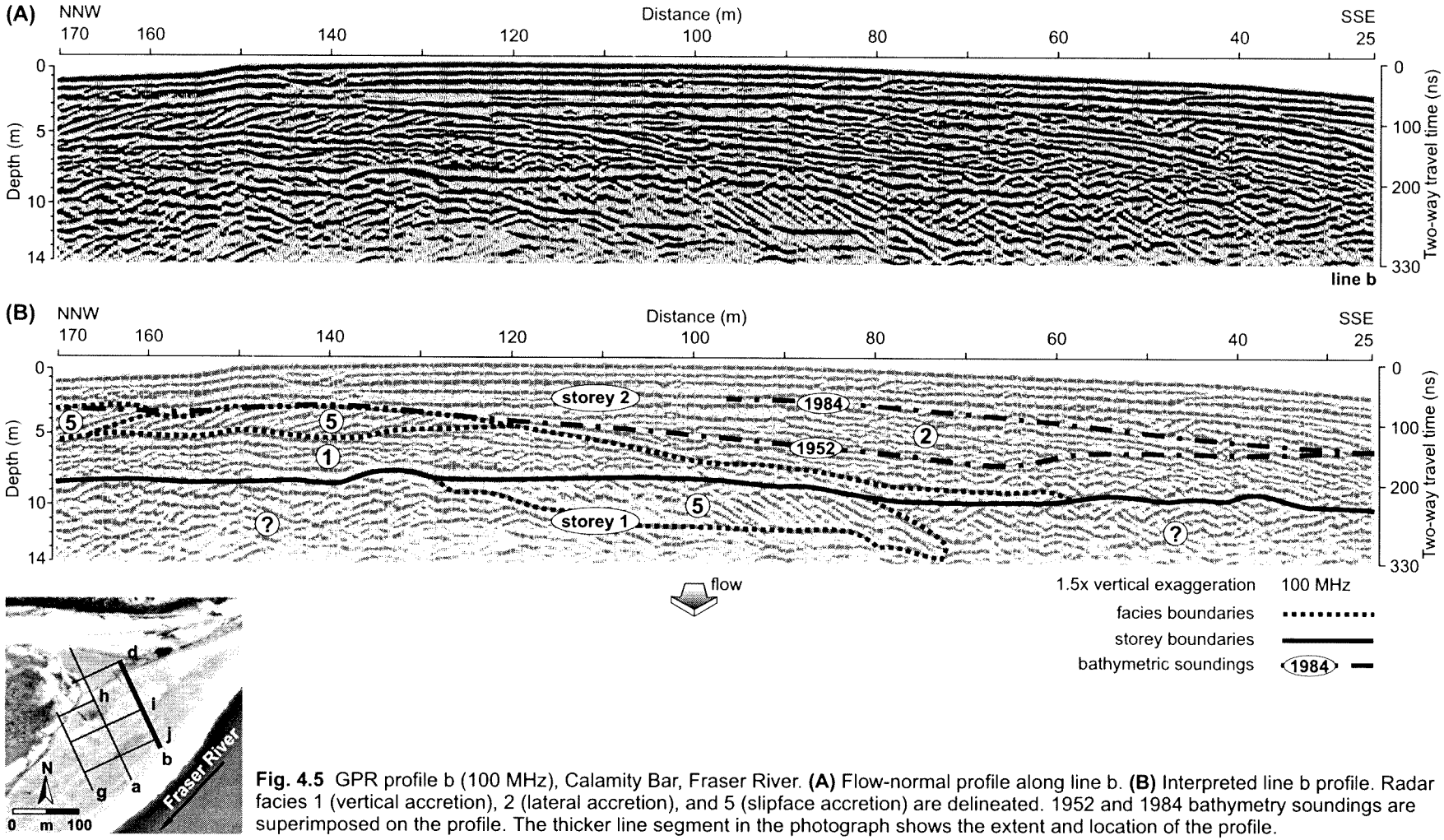


**Fig. 4.5** GPR profile b (100 MHz), Calamity Bar, Fraser River. **(A)** Flow-normal profile along line b. **(B)** Interpreted line b profile. Radar facies 1 (vertical accretion), 2 (lateral accretion), and 5 (slipface accretion) are delineated. 1952 and 1984 bathymetry soundings are superimposed on the profile. The thicker line segment in the photograph shows the extent and location of the profile.

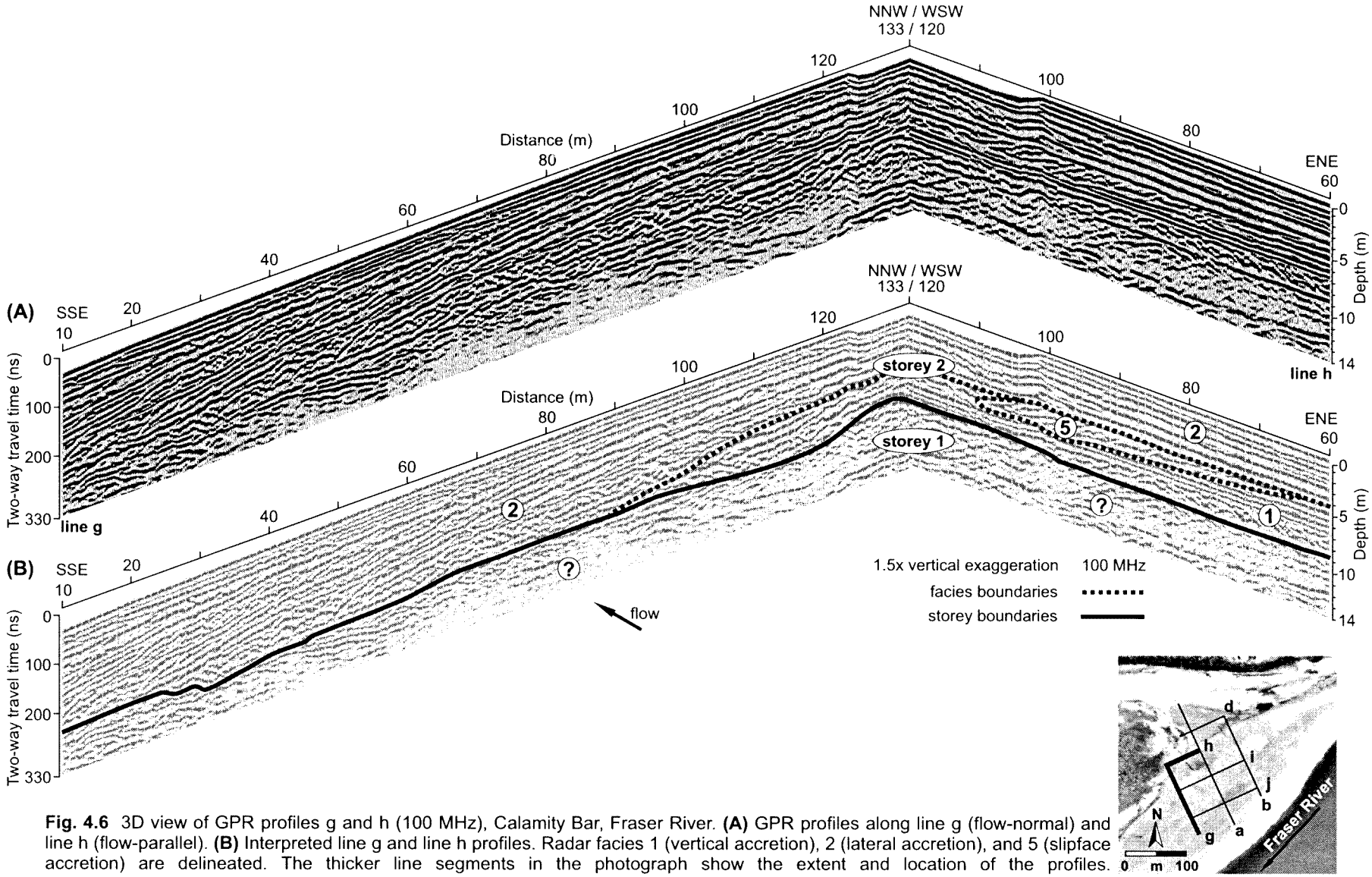


**Fig. 4.6** 3D view of GPR profiles g and h (100 MHz), Calamity Bar, Fraser River. **(A)** GPR profiles along line g (flow-normal) and line h (flow-parallel). **(B)** Interpreted line g and line h profiles. Radar facies 1 (vertical accretion), 2 (lateral accretion), and 5 (slipface accretion) are delineated. The thicker line segments in the photograph show the extent and location of the profiles.

#### 4.4.3.1 *Interpretation: bar-margin slipface accretion deposits*

The radar signature is interpreted as bar-margin slipface sediments indicative of sediments avalanching over high relief bar-margins into deeper water (Figs. 4.5B and 4.6B). The facies occurs in both flow-parallel and flow-normal orientations causing bar edges to prograde in both directions. The strata were likely deposited from bedload sheets periodically passing over bar-margins at high-stage flow. The flow-parallel strata thicken downflow indicating sediments prograded over a gently inclined downstream bar-margin. The spatially limited nature of the facies in Fig. 4.6B and its lack of internal reactivation surfaces suggest that the strata may have been deposited as a continuous slug of sediment during one freshet.

## 4.5 Calamity Bar Radar Stratigraphy

The Calamity Bar radar stratigraphy is split by a prominent, subhorizontal reflection about 8 m below the bar surface. The bounding surface is inferred to represent the depth of scour in the most recent phase of deposition since 1943 (Figs. 4.5B and 4.6B). The radar images of the deeper sediments (below 8 m depth in storey 1) are not well defined, especially in Fig. 4.6B. Hummocky reflections surround a set of steeply inclined reflections dipping to the south-southeast (radar facies 5). The hummocks may represent intertonguing gravelly lobes, and in some cases diffraction tails are obscuring the sedimentary structures. In either case, the genetic character of the hummocky reflections is ambiguous and because of this the reflection configuration is not interpreted. The stratigraphy is interpreted as storey 1 because a bounding surface separates the distinct set of inclined reflections (radar facies 5) from the upper sediment pile (Fig. 4.5B). Further, the direction of sediment transport is reversed between the two storeys implying that sediment avalanched over a southerly prograding bar-margin in a direction opposite to what is seen in the upper stratigraphy (storey 2).

The upper stratigraphy (storey 2) is dominated by extensive, low-angle, southerly dipping reflections (radar facies 2) that are characteristic of lateral accretion and point bar sedimentation. The lateral accretion sediments are separated from the slipface deposits (radar facies 5) by an inclined bounding surface, indicating that there is no genetic affinity between the two facies. The bathymetry data shows that the 1952 sounding roughly coincides with the upper bounding surface of the discrete set of steeply dipping reflections prograding toward the northern channel margin (Fig. 4.5B). This suggests that the facies was likely deposited prior to 1952 when the thalweg impinged directly onto the bar (Fig. 4.3). Of course it is possible that the facies was deposited after 1952, in which scour mobilized the 1952 bar surface and another wave of sediment was transported onto the site.

The shift in the style of deposition (from slipface to lateral accretion) within the storey was due to a change in flow directions across the bar after 1971. By this time flow was directed away from the bar, rather than directly onto it, thus impeding the ability of the channel to scour and rework Calamity Bar sediments. The new style of sedimentation saw bedload sheets onlapping the slipface deposits causing the unsteady lateral and downstream growth of the bar. This style of deposition is recorded by the 1984 bathymetric surface, which is positioned in the midst of the lateral accretion deposits (Fig. 4.5B). The scale of the lateral accretion deposits speaks to the nature of barform sedimentation, as the facies is

comparable to the depth of the channel in which it formed. There are few reactivation and truncation surfaces suggesting little scour of previous surfaces during the deposition of onlapping sheets.

The lack of diffractions suggests that there are few buried logs in the sediment pile reducing flow complexity over the bar surface. Altogether, the lack of stratigraphic complexity within the lateral accretion strata, and the limited number of depositional facies in the stratigraphy indicates a relatively uniform and consistent style of sedimentation across the bar since 1971. Thus, the stratigraphic record is entirely consistent with the morphologic evolution shown in the photographic record (Fig. 4.3).

The nature of point bar sedimentation, being largely depositional and unidirectional, allows aggradation rates to be calculated from bathymetric differencing of surfaces (Table 4.1). Coincidence between the bathymetry soundings and stratal configurations suggests that inferred former bar positions are correct, increasing the level of confidence in the derived rates. The table shows that sedimentation increased after 1984, but the rates hide the incremental and unsteady nature of sediment transport. Rather, they only provide a picture of long term sedimentation rates, and do not give expected annual rates of bar growth.

**Table 4.1** Calamity Bar vertical aggradation and lateral accretion rates determined from bathymetry data.

| Bathymetric Differencing | Vertical Aggradation ($m\ a^{-1}$) | Lateral Accretion ($m\ a^{-1}$) |
|---|---|---|
| 1952 to 1984 | 0.10 | 1.56 |
| 1984 to 1999 | 0.15 | 3.67 |
| 1952 to 1999 | 0.12 | 2.23 |

# 5 Queens Bar, Fraser River

## 5.1 Queens Bar Morphology

Queens Bar is a partially bank-attached macroform about 800 m wide and 3.2 km long located 3 km downstream of the Harrison River confluence at 6 to 7 m elevation (Fig. 5.1). The compound bar is crossed by a number of chutes and partially infilled channels that are bounded by vegetation of differing ages. Discussion of Queens Bar morphology and evolution will focus on the three sites profiled with GPR: Inner Channel, Mid Bar, and Bar Tail shown in the Fig. 5.1 insets.

The Inner Channel site is a partially filled secondary channel that a series of bedload sheets (Fig. 5.2A) and unit bars (Fig. 5.2B) have migrated down. The unit bars terminate in 0.5 to 2.5 m high slipfaces that are posed beside, and on top of, each other. Their juxtaposition presumably reflects different stages of flow transporting sediment (Fig. 5.2B). Over 5 m of relief across the former channel reflects the occurrence of varied bar features such as erosional banks (>3 m high), scours (>1 m deep), and depositional unit bars (>2 m high). The varied topography is due to complex interactions between the confined boundary of the secondary channel and flow conveyance through the channel. This creates zones of scour and deposition that vary with flow stage leading to differential, and directionally variable patterns of sedimentation.

The Mid Bar and Bar Tail sites occupy upstream and downstream portions, respectively, of a large (~250 m wide x ~750 m long) unit bar. The western edge of the unit bar terminates in ~1.5 m high slipface at the Mid Bar site that is overriding older, vegetated bar sediments (Fig. 5.2C). Downstream (at Bar Tail site), the western edge of the unit bar also terminates in a ~2 m high slipface that is prograding across an older, exposed gravel bar surface (Fig. 5.2D). In both cases local flow directions are largely normal to the channel-belt and mean flow directions.

The geometry of the laterally attached unit bar bears close resemblance to the unit bar attachment at TFLENT Bar, Squamish River (Fig. 3.1). In both cases the downstream tail of the bars appear to be detached and separated from the older bars at moderate-stage flows. Sediment transport onto the older bar surfaces is likely inhibited by the development of secondary flow cells in chute-like features that separate the bar-margin slipfaces from the older bars (Fig. 5.2D).

The downstream terminus (southern edge) of the unit bar is morphologically complex as one half of the bar terminates in a slipface (up to 3 m high; Fig. 5.2E) and the other half grades into sandy channel sediments. These surfaces with differential elevations make reconstructing flow patterns and their associated deposits problematic. For instance, a large sandy deposit in the lee of the slipface seems to be deposited, not by flow-separation over the bartop at high-stage flow, but rather by lower stage flow bypassing and curving around the crest of the slipface.

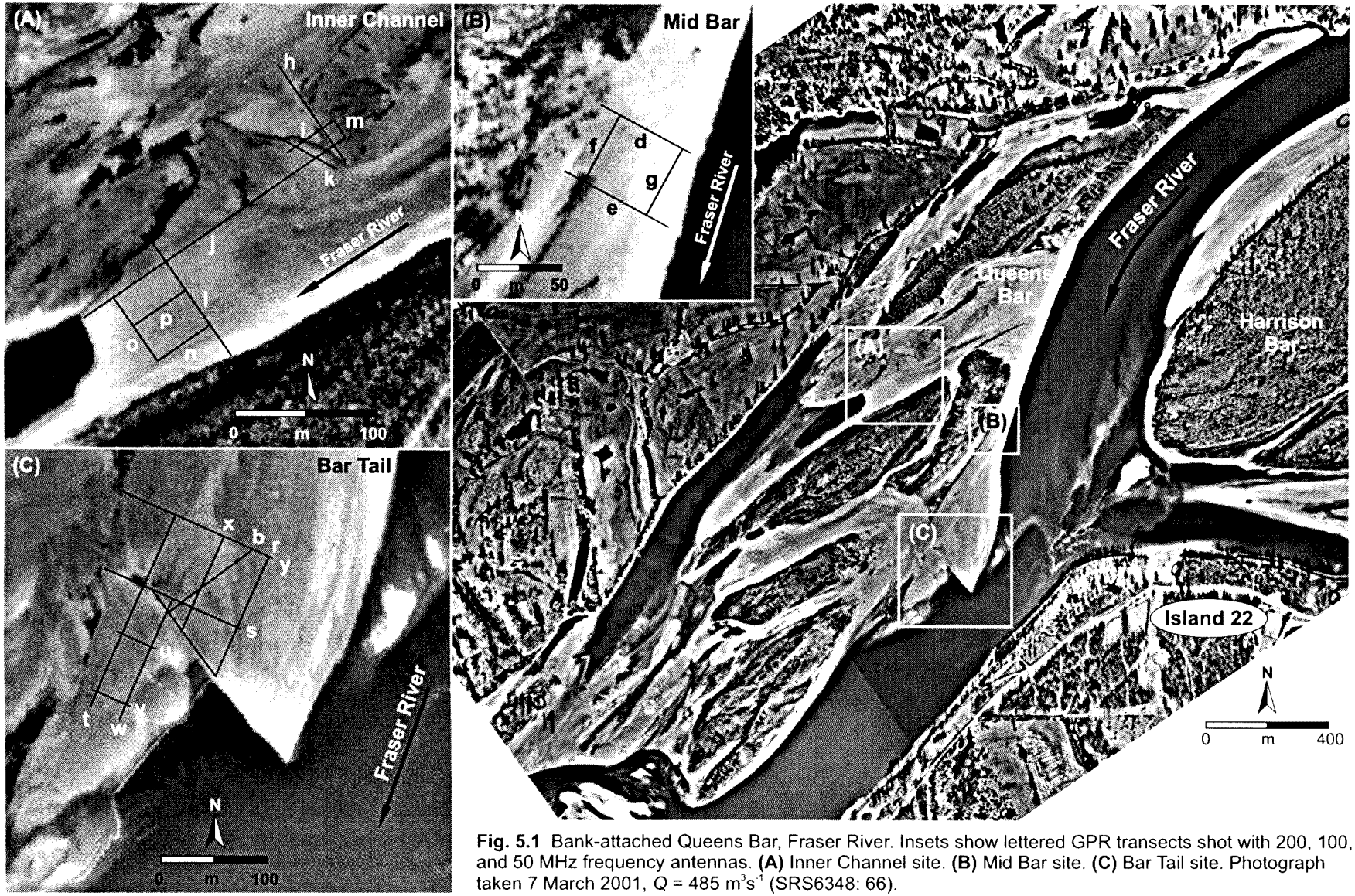


**Fig. 5.1** Bank-attached Queens Bar, Fraser River. Insets show lettered GPR transects shot with 200, 100, and 50 MHz frequency antennas. **(A)** Inner Channel site. **(B)** Mid Bar site. **(C)** Bar Tail site. Photograph taken 7 March 2001, $Q$ = 485 $m^3s^{-1}$ (SRS6348: 66).

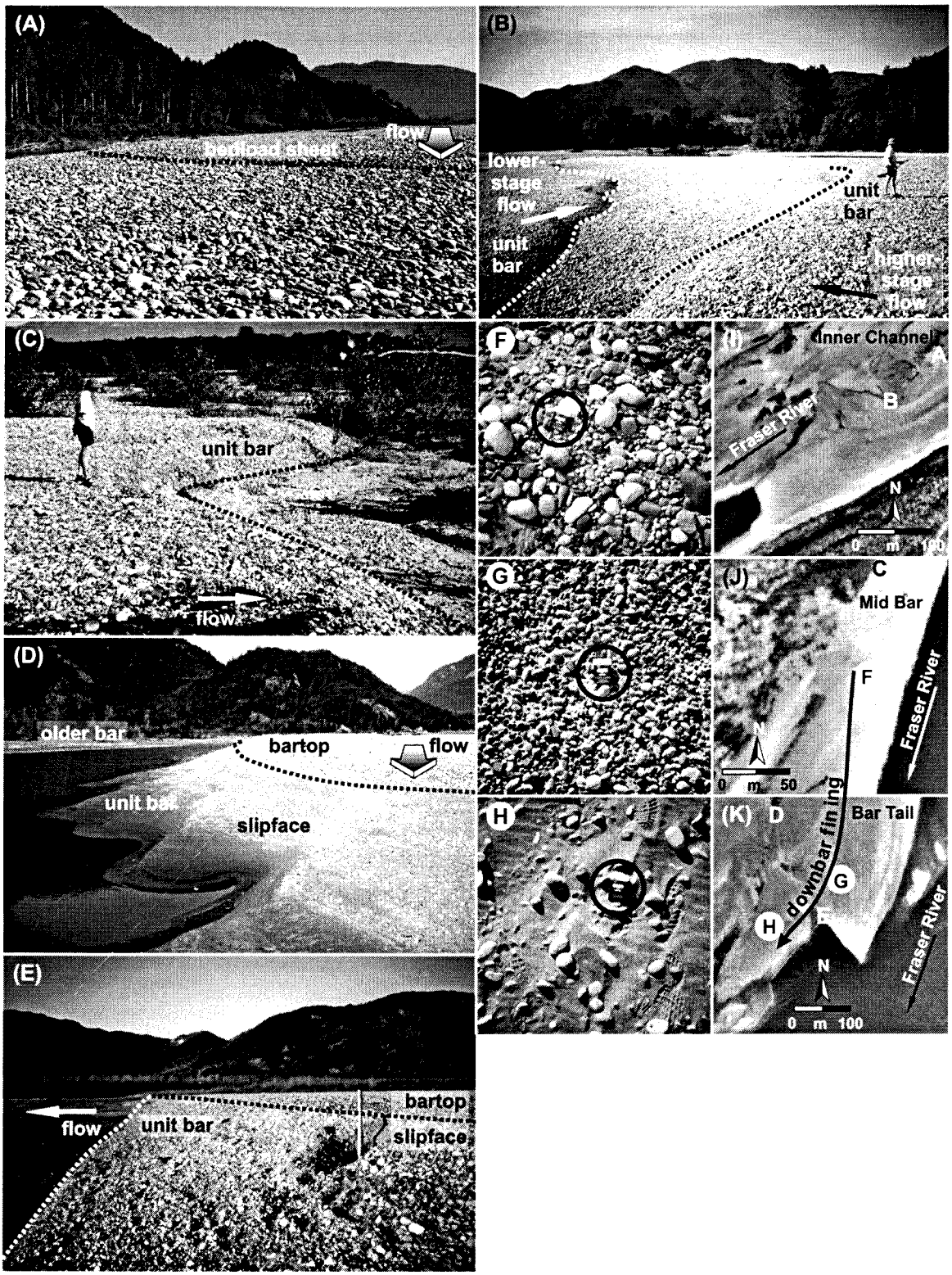


**Fig. 5.2** Surficial morphology of Queens Bar, Fraser River. **(A)** Bedload sheet (0.10 to 0.15 m thick) prograding down Inner Channel site. Photograph courtesy of D.G. Ham. **(B)** Juxtaposition of two unit bars building at different stages of flow, Inner Channel site (person for scale). **(C)** Unit bar burying established vegetation, Mid Bar site (person for scale). **(D)** Unit bar building onto, but separated from older bar in background, Bar Tail site. Bartop is 1.5 m above water surface. **(E)** 3 m high slipface, of which 2 m is exposed above water surface, Bar Tail site. **(F)** Surface grain-size texture fining downbar from Mid Bar site, to **(G)** elevated Bar Tail site, to **(H)** lower-elevation Bar Tail site (cigarette pack for scale is 10 cm on each side). **(I)** Photograph locations at Inner Channel, **(J)** Mid Bar, and **(K)** Bar Tail sites.

In contrast to the steeply dipping slipfaces, the eastern edge of the unit bar grades moderately (~8°) into (and is being eroded by) the channel at the Mid Bar site and more gently (~1°) at the Bar Tail site. A few logs drape the rather planar bar surface and are also present at the Inner Channel site. Surface grain-size fines downstream along the unit bar, from cobbles (Mid Bar site; Fig. 5.2F) to pebbles (elevated Bar Tail site; Fig. 5.2G) to sandy gravel (low elevation Bar Tail site; Fig. 5.2H).

## 5.2 Queens Bar Evolution

Queens Bar has evolved from a collection of mid-channel islands and bars in 1943 to a large, partially bank-attached bar in 1967 (Fig. 5.3). This evolution occurred by way of the progressive infilling of chutes, secondary channels, and vegetation colonization of bar surfaces.

The Inner Channel site was a secondary channel that became disconnected from the main channel by 1967 when a unit bar became attached to the eastern margin of the bar and began prograding down the former channel (Fig. 5.3). The site's low elevation enabled high-stage flow to deposit and erode sediment in the channel causing it to infill intermittently through the 1970s. More recently, unit bars have prograded 10 and 60 m a year along the former channel causing it to progressively infill.

The Mid Bar site was the floor of the main channel in 1943, but had become a mid-channel bar by 1952 (Fig. 5.3). The bar had coalesced with other mid-channel bars by 1967 to form the larger singular Queens Bar, but always remained near the southeastern margin of the bar adjacent to the main channel. Historic bathymetry soundings show similar bar heights in 1952 and 1999 (~2.5 m above river level at ~6.5 m elevation), but 1984 heights are 2 m lower indicating a period of erosion prior to 1984. After 1984, deposition did not commence until 1998 when a unit bar became attached to Queens Bar at the Mid Bar and Bar Tail sites.

The Bar Tail site in 1943 was also the floor of the main channel, but by 1952 a mid-channel bar had migrated onto the northwest corner of the site (Fig. 5.3). The bar was subsequently eroded and the main channel reoccupied the site until 1998 when a unit bar (~500 m long x ~130 m wide) became attached to the bar-margin. In 1999 a second bar attached to the first bar (doubling the width of the unit bars) and prograded ~250 m downstream. In 2000 the bars had prograded ~125 m further downstream and they terminated in a 3 m high slipface.

## 5.3 Queens Bar Bathymetry

Three bathymetric soundings across (and downstream of) the eastern half of Queens Bar and the main channel completed in 1952, 1984, and 1999 are shown in Figs. 5.4A and 5.4B, respectively (Figs. 5.4C and 5.4D show their locations). Queens Bar extends northwest another 500 m to the edge of the channel-belt from the end of the bathymetry soundings (0 m distance) in Fig. 5.4A. The 1952 bathymetry shows a prominent small, mid-channel barform (at ~300 m distance) with a relatively shallow multiple channeled network and little relief (~7 m) across the sounding. By 1984 several mid-channel bars had coalesced and secondary channels had started to infill spilling only high-stage flows across the bar. This reduced the amount of secondary channel area transmitting flow through the channel, and ultimately caused the main channel to deepen and become channelized in order to convey flow through the reach.

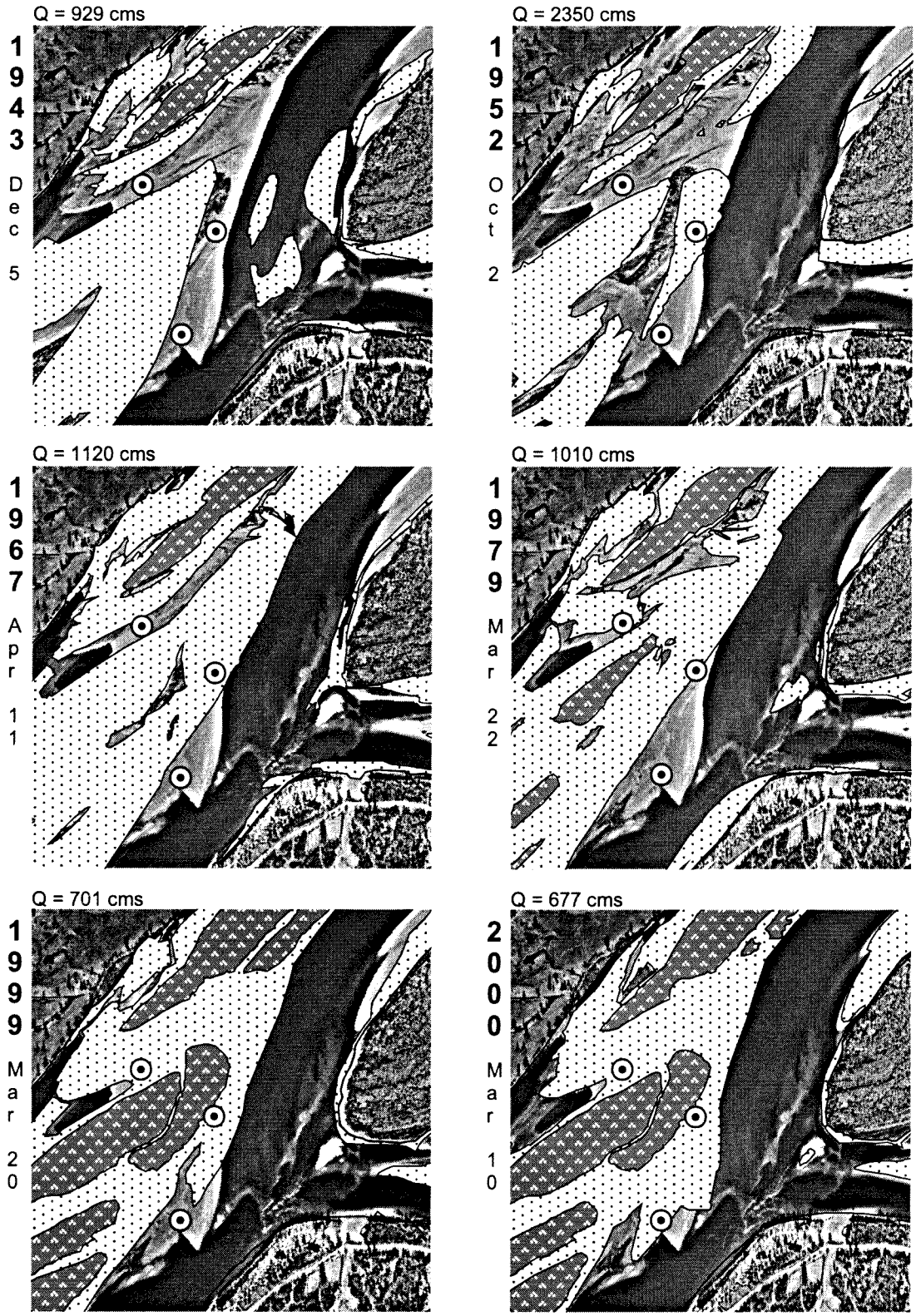


**Fig. 5.3** Morphological evolution (1943 to 2001) of Queens Bar, Fraser River. Successive changes in channel position and bar morphology mapped from aerial photographs and superimposed on 2001 photograph in background. The bulls eyes mark the center of the GPR grids. 2001 photograph taken 7 March 2001, discharge (Q) = 485 cms. Flow is from top right to bottom left.

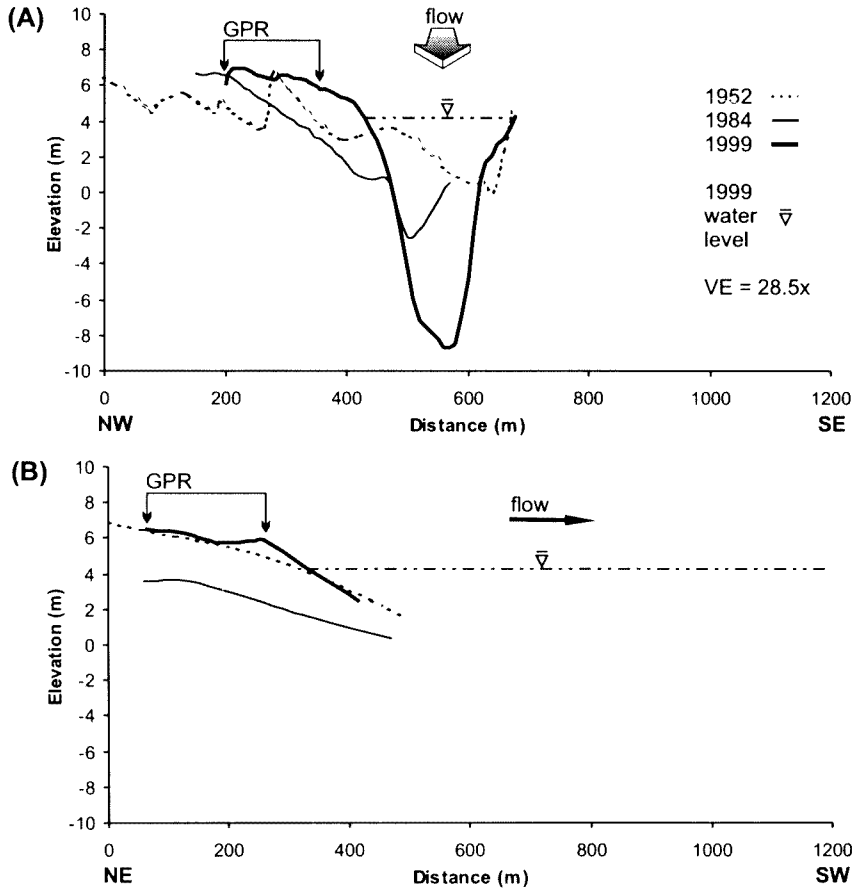


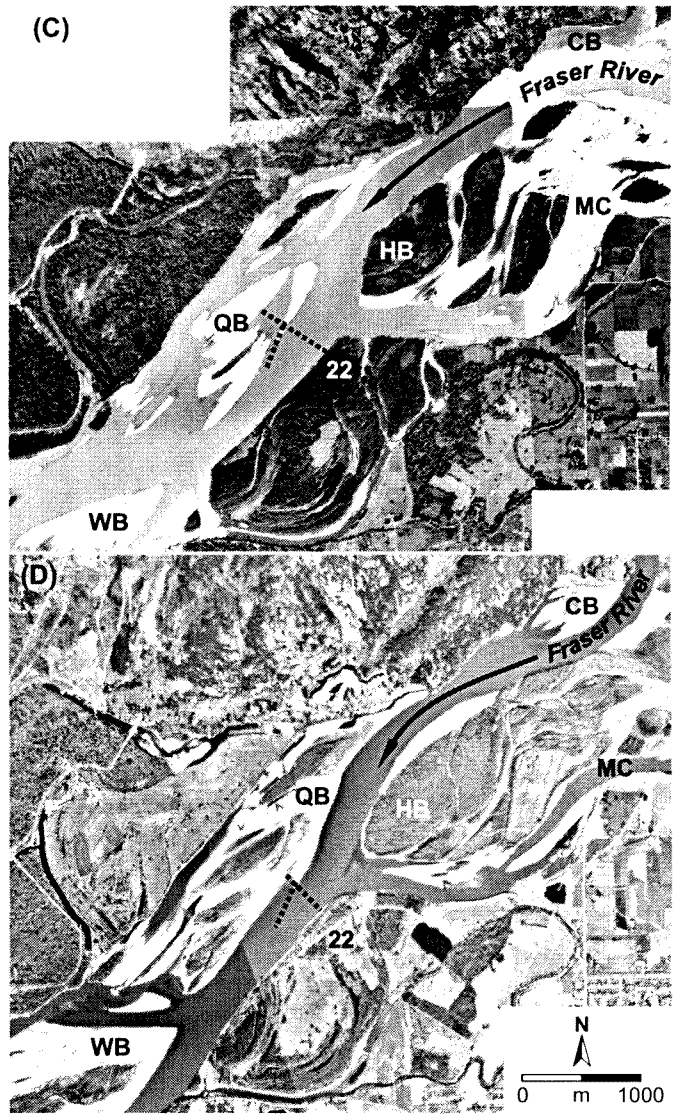


**Fig. 5.4** Bathymetry soundings across Queens Bar, Fraser River. **(A)** 1999, 1984, and 1952 cross-stream, and **(B)** downstream channel geometries. 0 m elevation is mean sea level. Water level is at low-stage flow, $Q = 677\ m^3s^{-1}$. Extent of bar surface profiled with GPR is also shown. Bathymetry data courtesy of the Department of Geography, UBC. **(C)** 1952, and **(D)** 1999 sounding locations (•••••). Photographs taken 2 October 1952, $Q = 2350\ m^3s^{-1}$ (BC1622: 24, 68), and 20 March 1999, $Q = 701\ m^3s^{-1}$ (15BCB99001: 22, 29). Queens Bar (QB), Wellington Bar (WB), Calamity Bar (CB), Harrison Bar (HB), Island 22 (22), and Minto Channel (MC).

By 1999, a large (>200 m wide) unit bar had been deposited on the southeast edge of Queens Bar. The rapid building of the bar constricted the channel and caused it to scour deeply at the site because bank retreat along the edge of Island 22 was limited. Revetment placed along Island 22 undoubtedly served to restrict erosion and bank retreat, but bank retreat in natural systems typically lags behind bar forming events (*cf.* Squamish River, Fig. 3.3).

The bathymetric evolution of Queens Bar captures the full range of channel forms found in wandering gravel-bed rivers from shallow, multiple channels forcing flow around mid-channel bars to a deep, singular channel channeling flow around large bank-attached bars (Fig. 5.4A). From 1952 to 1999 the depth of scour below the bartop more than doubled from ~7 to ~16 m. This shows that subsurface structures profiled with GPR to a depth of at least 16 m are sediments that could have been deposited by the present-day river. In this regard, they represent deposits associated with a wandering fluvial style.

The downstream bathymetric soundings (Fig. 5.4B) illustrate that at least 3 m of sediment were eroded between 1952 and 1984 and ~3 m deposited between 1984 and 1999. It is interesting to note that although the dip angle of each surface largely mirrors the other, the barform and adjacent channel have changed considerably in the 47 year period from 1952 to 1999.

## 5.4 Queens Bar Radar Facies and Elements

Figure 5.1 insets show the three grids profiled on Queens Bar with GPR.

### 5.4.1 Radar Facies 1: subhorizontal, continuous, subparallel reflections

Radar facies 1 is characterized by stacked (3 to 4 m thick), horizontal to subhorizontal, continuous (30 to 100 m long), parallel to subparallel reflections (Figs. 5.5A, 5.6A, 5.7A, 5.8A, 5.9A, 5.10A, and 5.11A). The facies occurs in all stratigraphic positions, but does not dominate the succession. Rather it is a minor facies that has a patchy spatial distribution across the bar.

#### *5.4.1.1 Interpretation: vertical accretion deposits (stratified bedload sheets)*

The radar signature is interpreted as stacks of vertically accreted gravelly sheets deposited from bedload sheets migrating across bar surfaces (Figs. 5.5B, 5.6B, 5.7B, 5.8B, 5.9B, 5.10B, and 5.11B). Sheet-like deposition dominates topographically low bar areas that grade into channel floors. The facies occurs more sporadically where it adjoins steeply dipping reflections.

### 5.4.2 Radar Facies 2: low-angle (5 to 6°), cross-stream dipping, subparallel reflections

Radar facies 2 is characterized by continuous sets (>55 m long) of stacked (1 to 5 m thick), low-angle (5 to 6°), parallel to subparallel reflections that dip normal to flow (Figs. 5.5A and 5.6A). Its dip angle, typically 5 to 6°, does range up to 14° occasionally, although the steeper dipping reflections decline in dip angle cross-stream and become more tangential and less oblique. The facies occurs throughout all stratigraphic positions and has a limited extent at the Inner Channel site. The facies flow-parallel character displays horizontal to subhorizontal reflections (Fig. 5.7A).

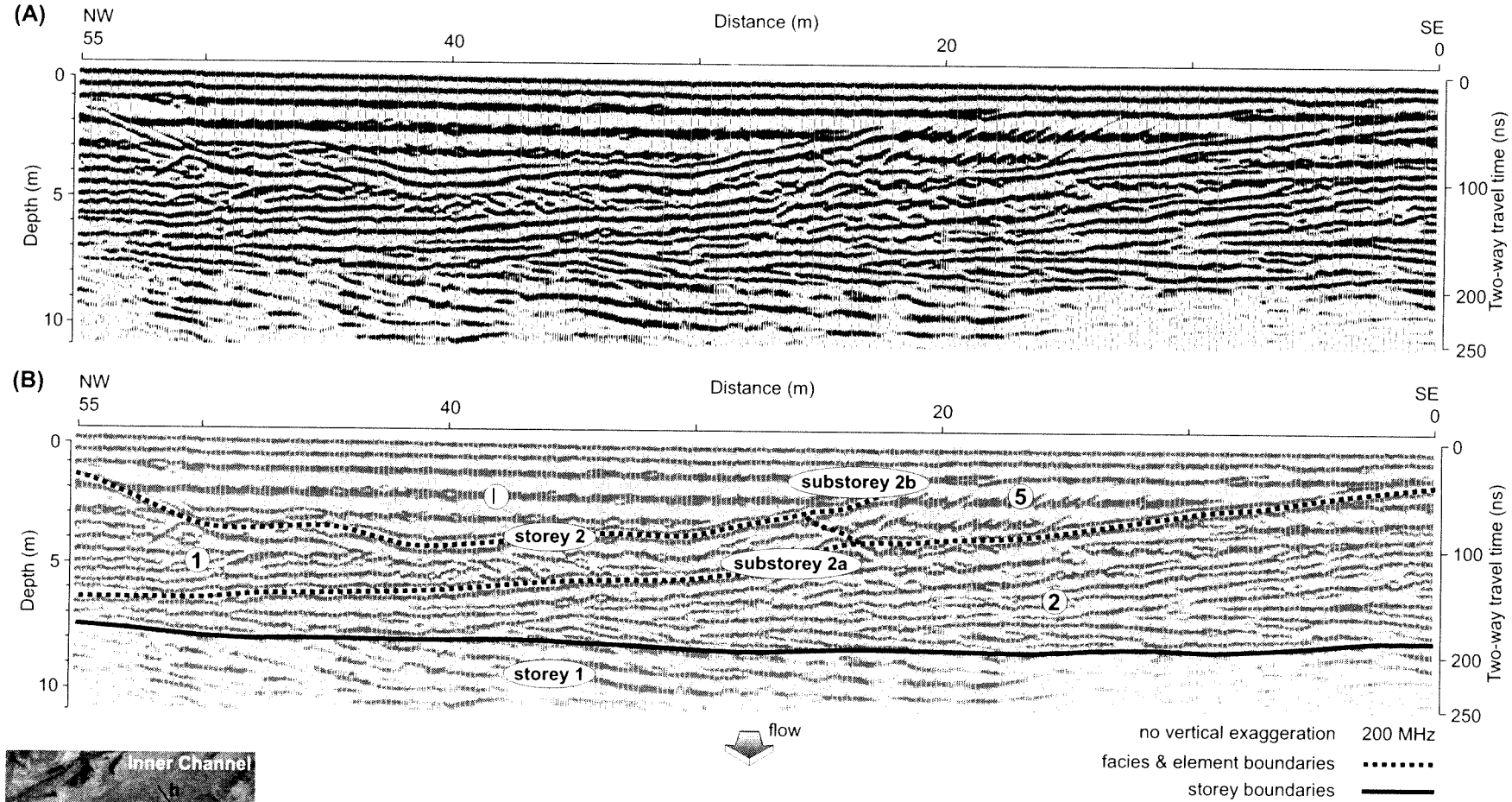


**Fig. 5.5** GPR profile o (200 MHz), Queens Bar, Inner Channel site, Fraser River. **(A)** Flow-normal profile along line o. **(B)** Interpreted line o profile. Radar facies 1 (vertical accretion), 2 (lateral accretion), 5 (slipface accretion), and element I (channel deposits) are delineated. The thicker line segment in the photograph shows the extent and location of the profile.

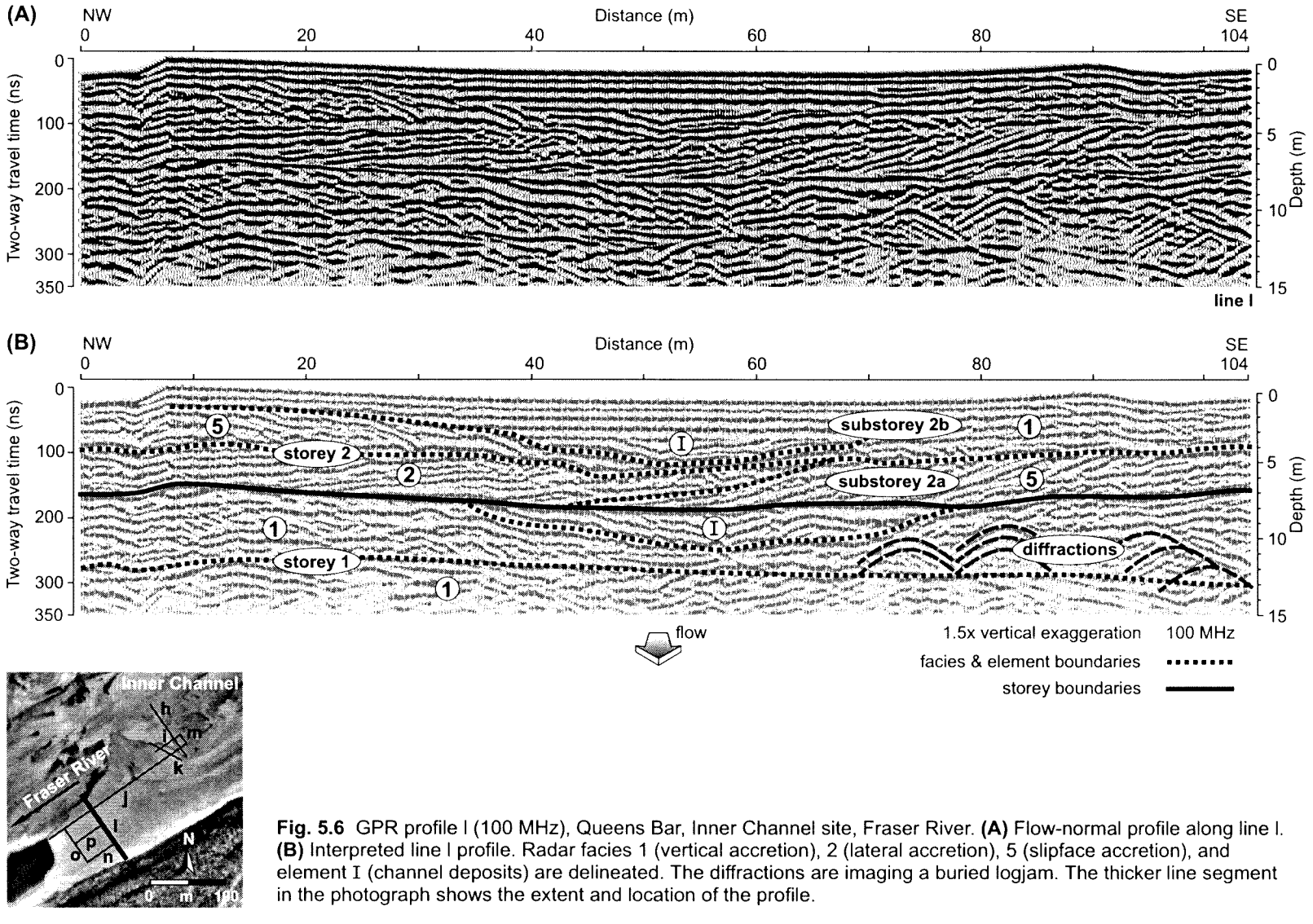


**Fig. 5.6** GPR profile I (100 MHz), Queens Bar, Inner Channel site, Fraser River. **(A)** Flow-normal profile along line I. **(B)** Interpreted line I profile. Radar facies 1 (vertical accretion), 2 (lateral accretion), 5 (slipface accretion), and element I (channel deposits) are delineated. The diffractions are imaging a buried logjam. The thicker line segment in the photograph shows the extent and location of the profile.

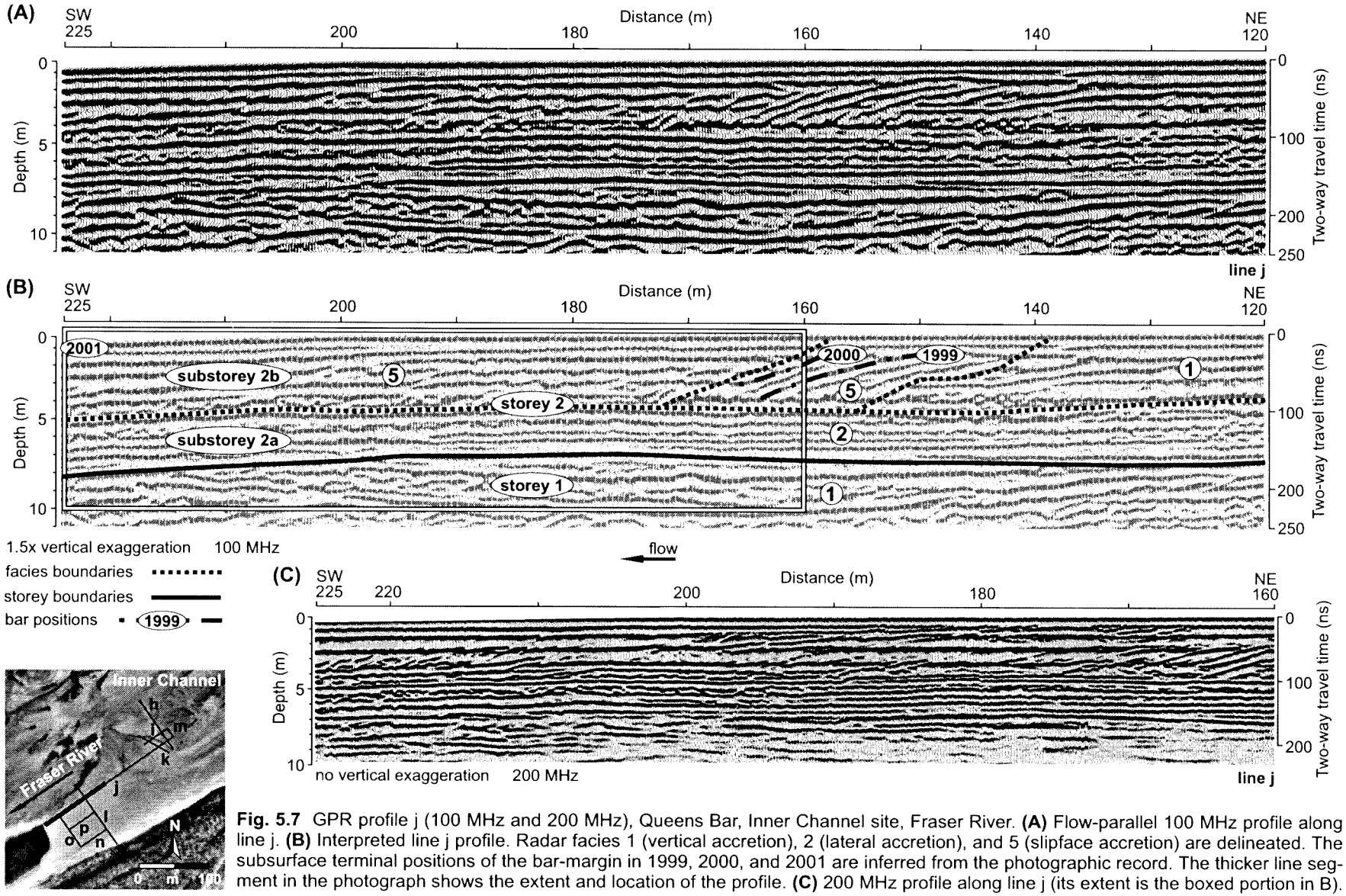


**Fig. 5.7** GPR profile j (100 MHz and 200 MHz), Queens Bar, Inner Channel site, Fraser River. **(A)** Flow-parallel 100 MHz profile along line j. **(B)** Interpreted line j profile. Radar facies 1 (vertical accretion), 2 (lateral accretion), and 5 (slipface accretion) are delineated. The subsurface terminal positions of the bar-margin in 1999, 2000, and 2001 are inferred from the photographic record. The thicker line segment in the photograph shows the extent and location of the profile. **(C)** 200 MHz profile along line j (its extent is the boxed portion in B).

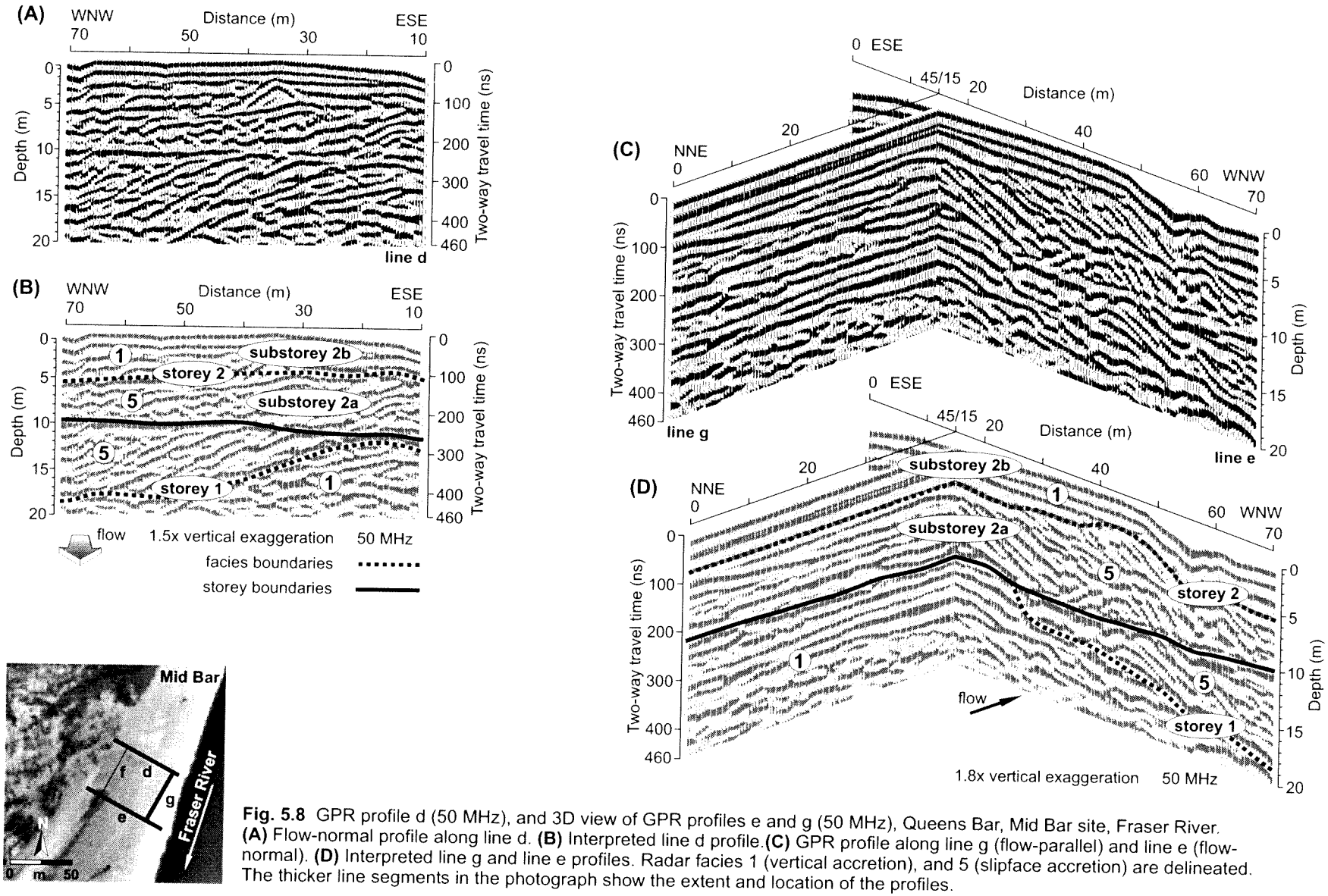


**Fig. 5.8** GPR profile d (50 MHz), and 3D view of GPR profiles e and g (50 MHz), Queens Bar, Mid Bar site, Fraser River. **(A)** Flow-normal profile along line d. **(B)** Interpreted line d profile.**(C)** GPR profile along line g (flow-parallel) and line e (flow-normal). **(D)** Interpreted line g and line e profiles. Radar facies 1 (vertical accretion), and 5 (slipface accretion) are delineated. The thicker line segments in the photograph show the extent and location of the profiles.

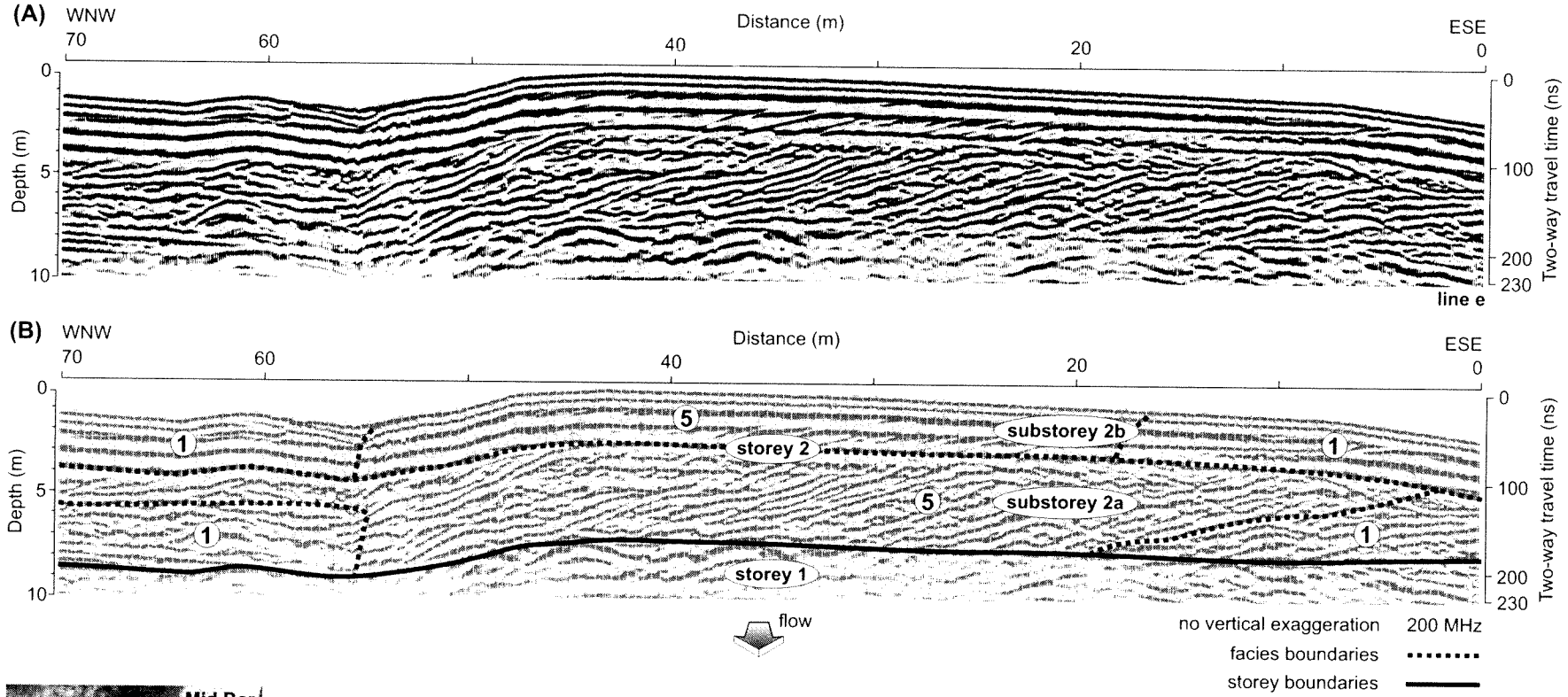


**Fig. 5.9** GPR profile e (200 MHz), Queens Bar, Mid Bar site, Fraser River. **(A)** Flow-normal profile along line e. **(B)** Interpreted line e profile. Radar facies 1 (vertical accretion), and 5 (slipface accretion) are delineated. The thicker line segment in the photograph shows the extent and location of the profile.

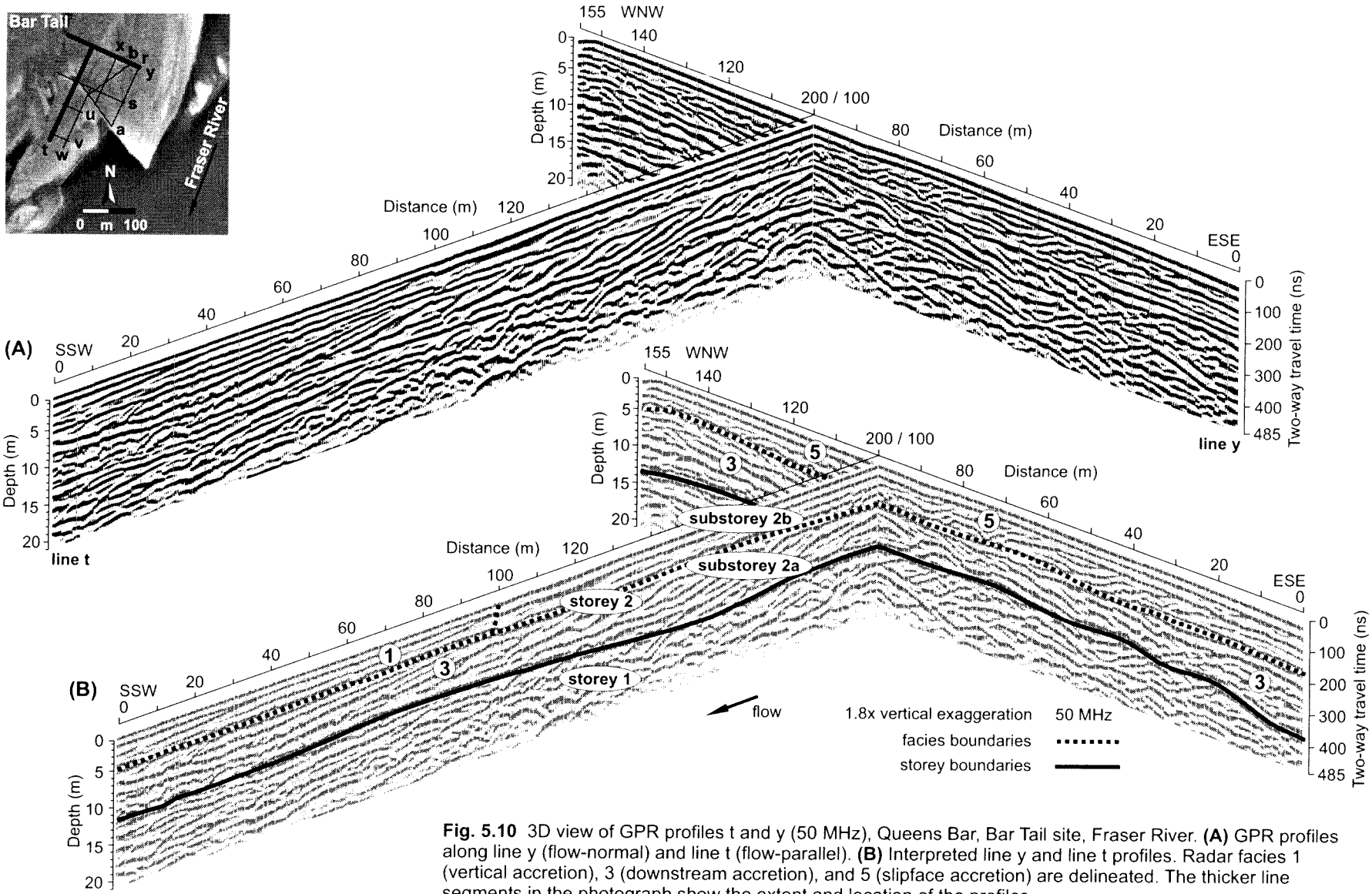


**Fig. 5.10** 3D view of GPR profiles t and y (50 MHz), Queens Bar, Bar Tail site, Fraser River. **(A)** GPR profiles along line y (flow-normal) and line t (flow-parallel). **(B)** Interpreted line y and line t profiles. Radar facies 1 (vertical accretion), 3 (downstream accretion), and 5 (slipface accretion) are delineated. The thicker line segments in the photograph show the extent and location of the profiles.

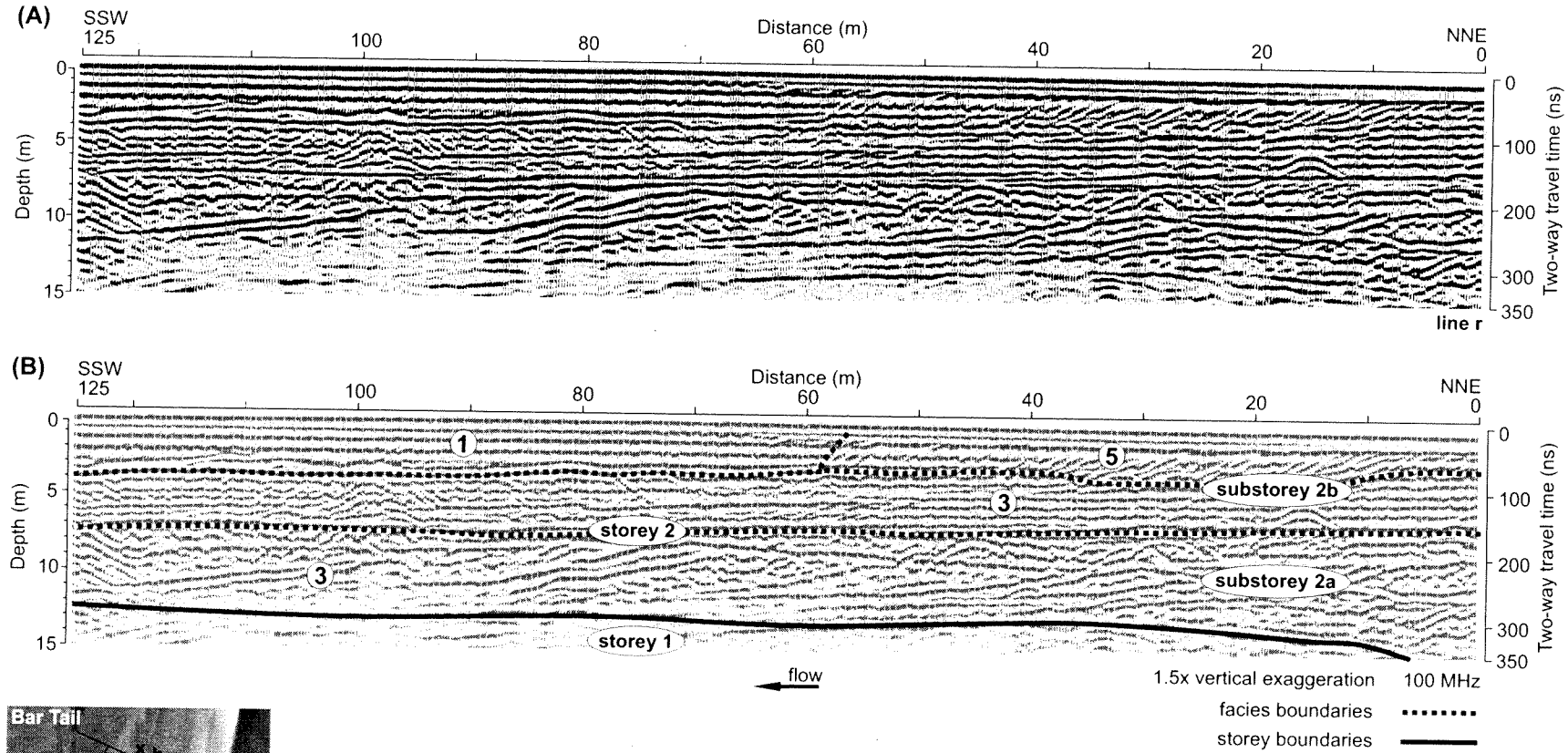


**Fig. 5.11** GPR profile r (100 MHz), Queens Bar, Bar Tail site, Fraser River. **(A)** Flow-parallel profile along line r. **(B)** Interpreted line r profile. Radar facies 1 (vertical accretion), 3 (downstream accretion), and 5 (slipface accretion) are delineated. The thicker line segment in the photograph shows the extent and location of the profile.

*5.4.2.1 Interpretation: lateral accretion deposits (stratified bedload sheets)*

The flow-normal radar signature is interpreted as lateral accretion deposits (Figs. 5.5B and 5.6B). The facies traces the lateral extension of barforms and the reduction in dip angle of the reflections records the transition from sediment avalanching over steep bar-margin slipfaces to bedload sheets migrating along lower angled surfaces. The steeper dipping reflections indicate bar proximal sediments, which reduce in dip angle as the bar progrades over the adjacent channel floor. The subhorizontal (flow-parallel) signature remains largely unchanged regardless of changing flow-normal dip angles (Fig. 5.7B).

### 5.4.3 Radar Facies 3: low-angle (4 to 8°), downstream dipping, subparallel reflections

Radar facies 3 is characterized by low-angle (4 to 8°), divergent to subparallel reflections (5 to 7 m thick) that dip downflow (Figs. 5.10A and 5.11A). Extensive sets of downlapping tangential reflections (>200 m long) stratigraphically dominate the middle portions of the Bar Tail site succession between 5 and 10 m depth. The flow-normal signature is composed of subhorizontal and hummocky reflections (Fig. 5.12A).

*5.4.3.1 Interpretation: downstream accretion deposits (stratified bedload sheets)*

The flow-parallel radar signature is interpreted as downstream accretion deposits (Figs. 5.10B and 5.11B). The facies documents the migration of gravelly bedload sheets over the bartop onto the downstream margin of the bar causing the barform to vertically aggrade and translate downstream. The geometry of the facies tends to decline in dip angle downstream because reflections diverge from each other as the barform extends into the channel. The subhorizontal and hummocky flow-normal signatures indicate that sedimentation is influenced by mean flow conditions depositing extensive sheet-like strata, as well as by more variable local flow depositing smaller lobe-like features (Fig. 5.12B).

### 5.4.4 Radar Facies 5: small- to medium-scale (0.5 to 3 m), steeply inclined (16 to 26°), oblique reflections

Radar facies 5 is characterized by continuous sets (10 to 90 m long) of small- to medium-scale (0.5 to 3 m thick), parallel to subparallel, steeply inclined (16 to 26°), oblique reflections that dip downflow (Figs. 5.7A and 5.11A) and normal to flow (Figs. 5.5A, 5.6A, 5.8A, 5.9A, 5.10A, and 5.12A). The facies is common to all three Queens Bar sites and it dominates the entire thickness of the depositional succession across the Mid Bar site. At the other sites it occurs as discrete packages, commonly surrounded by continuous, subhorizontal reflections.

*5.4.4.1 Interpretation: bar-margin slipface accretion deposits*

The radar signature is interpreted as bar-margin slipface deposits indicative of sediments avalanching over high relief bar-margins into deeper water (5.5B, 5.6B, 5.7B, 5.8B, and 5.9B). At the Bar Tail site, flow-parallel (Fig. 5.11B) and flow-normal reflections (Figs. 5.10B and 5.12B) occur at the same stratigraphic level showing that flow diverged across the bartop and deposited sediment over the bar-margins causing the barform to prograde both downstream and cross-flow. The medium-scale inclined reflections are better defined (more clearly imaged) than the smaller-scale reflections, which tend to appear as faint ghosts in the profiles. The small-scale reflections are likely the depositional signature of unit bars (a few bedload sheets thick) migrating across bar surfaces.

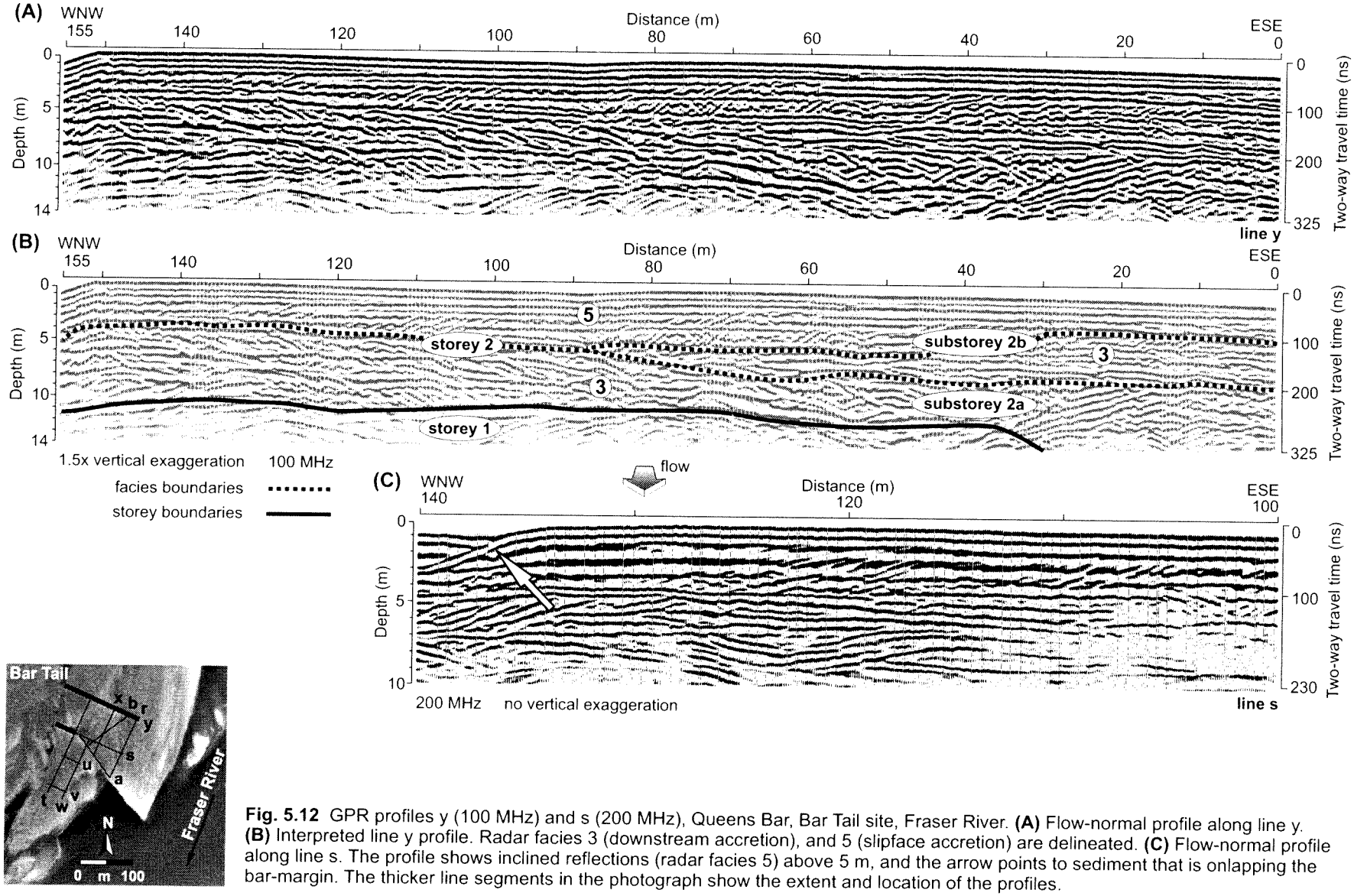


**Fig. 5.12** GPR profiles y (100 MHz) and s (200 MHz), Queens Bar, Bar Tail site, Fraser River. **(A)** Flow-normal profile along line y. **(B)** Interpreted line y profile. Radar facies 3 (downstream accretion), and 5 (slipface accretion) are delineated. **(C)** Flow-normal profile along line s. The profile shows inclined reflections (radar facies 5) above 5 m, and the arrow points to sediment that is onlapping the bar-margin. The thicker line segments in the photograph show the extent and location of the profiles.

### 5.4.5 Radar Element I: 2D, basal, concave-up reflections

Radar element I is distinguished by 2D, basal, concave-up reflections that truncate adjacent reflections and is typically filled with subhorizontal and concave-up reflections (Figs. 5.5A and 5.6A). The element extends 35 to 45 m laterally with depths between 2 and 2.5 m. The concave-up edges dip into the center of the form with an apparent dip of ~11°. There are few preserved forms and it is stratigraphically restricted to the middle and upper portions of the Inner Channel site succession.

*5.4.5.1 Interpretation: channel and chute deposits*

The radar signature is interpreted as an element in which the 2D, concave-up geometry of the basal reflection identifies the scour of secondary channels and chutes (Figs. 5.5B and 5.6B). The basal reflection is associated with (and infilled by) a variety of reflections that make up the channel fill. The element is only found at the Inner Channel site and does not extend across the full width of the former (morphological) channel indicating that the scale of the element corresponds to the local scouring and infilling of portions of the former channel.

## 5.5 Queens Bar Radar Stratigraphy

### 5.5.1 Inner Channel Site

The radar stratigraphy at the Inner Channel site (Figs. 5.5B, 5.6B, and 5.7B) records the serial nature of channel infilling. The architecture is divided into two sedimentary packages (storeys 1 and 2) by a subhorizontal reflection about 7 m below the surface of the bar.

Storey 1 shows concave-up forms (radar element I) truncating subhorizontal reflections (radar facies 1), which likely indicates the development of a chute at the site (Fig. 5.6B). The chute was probably scoured into stacked, sheet-like deposits and filled by successive sheets. The sheets contour the geometry of the chute suggesting that the chute aggraded in-place as it actively conveyed sediment. The diffractions in the southeastern half of the storey are likely caused by a buried logjam. The stratigraphic interval is interpreted as a storey because of the depth of the sediments and the laterally continuous nature of the bounding surface.

Storey 2 shows two styles of sedimentation interpreted to be growth increments (substoreys 2a and 2b) in the infill of the channel. The lowermost growth interval (substorey 2a) documents steeply inclined reflections (radar facies 5) grading into lower angled reflections (radar facies 2) (Fig. 5.6B). The stratal configuration probably traces sediment avalanching northwest over high relief bar-margins, and then traction transport over a lower-angled margin. The decline in dip angle could be related to deposition during waning flow conditions or sedimentation further in-channel, away from the bar edge. This seems to be the case further downstream where steeply inclined reflections are absent (Fig. 5.5B). The distinct terminations of the lower-angled, downlapping reflections imply that the strata were deposited by flow-normal directed sediment transport continuing to pass over the bar crest.

The upper growth interval (substorey 2b) shows very similar reflection configurations and facies juxtapositions as those found in storey 1. The depositional history is proposed to be nearly equivalent to the lower storey, except the style of chute infilling is different. Instead of concave-up (parallel to form) reflections, the chute is infilled with subhorizontal reflections. This indicates that sediment transport was

not confined within the chute, but rather bedload sheets buried the chute and were transported downflow independent of the previous concave-up geometry.

The architecture in substorey 2b is largely coincident with the recent photographic record in which a slug of sediment is seen to be migrating down the former channel and terminating in a 2.5 m high slipface. Figure 5.7B shows the flow-parallel stratigraphy composed of downflow dipping reflections and the position of the bar-margin in 1999, 2000, and 2001. The pronounced medium-scale, steeply inclined reflections (radar facies 5) appear to have been deposited when the bar-margin stalled. The barfront only moved ~9 m between 1999 and 2000. Conversely, small-scale, steeply inclined reflections were deposited when the bar prograded 10s of meters, such as in 2001 when it moved ~65 m downflow. Although there are some dipping reflections evident in the 200 MHz profile (Fig. 5.7C), they do not dominate the profile as expected of slipface accretion. This may be due to a lack of grain-size partitioning (and pore water contrasts between strata) in rapidly migrating, avalanching sediments. Together, these effects inhibit the ability of GPR to discern sedimentary structures.

The multistorey nature of the stratigraphy (with multiple internal scour surfaces) supports morphological observations that former channels do not fill in a coherent pattern of sedimentation. Rather, they are unsteadily filled by successive sediment waves prograding through the former channel.

### 5.5.2 Mid Bar Site

The radar stratigraphy at the Mid Bar site (Figs. 5.8B, 5.8D, and 5.9B) records the former position of a series of bar-margin slipfaces. The simple architecture is characterized by only two radar facies that repeat in the vertical successions above and below a distinct, subhorizontal reflection (~10 m below the surface of the bar). Although the style of sedimentation appears to be similar throughout the radar stratigraphy, the facies terminate at the bounding reflection, thus defining two genetically unrelated sediment bodies (storeys 1 and 2).

Storey 1 shows steeply inclined reflections (radar facies 5) offlapping subhorizontal reflections (radar facies 1). This facies association probably marks the advancement of a high relief bar-margin over a lower angled bar surface.

Storey 2 is dominated by two sets (substoreys 2a and 2b) of steeply inclined reflections (radar facies 5) that also dip westward and trace the position of former barfronts as they accreted. Figure 5.9B details scale differences between the two sets of slipfaces in the substoreys. The differences are likely due to different autogenic processes depositing sediment in-channel (substorey 2a) and on bartops (substorey 2b). In both cases they interfinger with, and are juxtaposed beside, subhorizontal reflections (radar facies 1). Bathymetric soundings indicate ~2 m of deposition at the site since 1952. This is roughly equivalent to the thickness of the sediments in the substorey 2b interval. The style of deposition closely matches the unit bar morphology at the site, and the photographic record also shows bar sediments at the site from 1952 onwards. Thus it would seem that the sediments record the migration of a unit bar onto the site.

Prior to 1952 the site was occupied by the main channel and the maximum depth of scour in the multiple channeled planform was likely similar to the ~8 m scour depths observed in the 1952 bathymetry. It is tempting to suggest that the bounding surface below storey 2 was scoured during the 1948 flood and subsequent channel shifting deposited the larger set of steeply inclined reflections in substorey 2a.

Although this interpretation is speculative, the geometry of the adjacent barforms in 1943 is suggestive of this scenario meaning that storey 1 was deposited prior to 1943.

### 5.5.3 Bar Tail Site

The near-surface radar stratigraphy at the Bar Tail site (Figs. 5.10B, 5.11B, and 5.12B) highlights internally consistent packages of reflections associated with unit bar deposition (substorey 2b). In contrast, the deeper stratigraphy (storey 1) is composed of reflections that cannot be traced laterally in three-dimensions, and their altogether different character separates them from the upper stratigraphy (storey 2). Storey 1 is delineated because of its position beneath storey 2, but facies are not interpreted in storey 1 because reflection geometries could not be determined confidently.

Storey 2 is divided into two distinct sedimentary bodies that are separated by a subhorizontal bounding surface about 5 m below the bar surface. The lower interval (substorey 2a) is entirely dominated by flow-parallel, downstream dipping, low-angle reflections (radar facies 3) whose dip angle declines downflow. Where its flow-parallel pattern of downstream dipping reflections is coherent and internally consistent, its flow-normal signature is somewhat undulatory. The configuration appears to document the migration of a number of gravelly sheets descending over the distal margin of a bar onto the channel floor. The depth and scale of the downstream accretion facies (5 to 7 m thick) in substorey 2a approaches the depth of flow and likely indicates sedimentation in the basal portion of a bar. In contrast, the shallow depths and smaller scale reflections (0.5 to 3 m) in substorey 2b probably point to, and are characteristic of, bartop sedimentation.

The bounding surface between substoreys 2a and 2b was likely scoured between 1984 and 1952 because the photographic record shows that a small barform occupied a portion of the site in 1952, but was subsequently eroded by 1967. Between 1984 and 1999, the bathymetry soundings indicate that at least 3 m of sediments were deposited, nearly filling the remainder of substorey 2b (Fig. 5.4B).

Substorey 2b is composed of sets of steeply inclined reflections (radar facies 5) that grade into and out of subhorizontal reflections (radar facies 1). The inclined reflections dip both downflow (Fig. 5.11B) and cross-flow (Fig. 5.12B) indicating flow divergence across the bartop enabling the barform to migrate in both directions. This style of deposition is consistent with the twin slipfaces evident on the contemporary unit bar (Figs. 5.2D and 5.2E) and matches the morphologic evolution of the site since 1998 (Fig. 5.3). The radar stratigraphy of substorey 2b at the western edge of the site (Fig. 5.12B) is probably equal to the thickness of sediment deposited between 1998 and 2000 when the unit bar overrode the site. This implies that the radar profiles image the complete stratigraphy of a unit bar.

The relative timing of sedimentation along the western edge of the unit bar (and in the chute-like feature separating the unit bar from the older Queens Bar; Fig. 5.2D) can also be deciphered from the radar profiles. The northwest edge of Fig. 5.12C shows horizontal reflections onlapping onto the edge of the bar. This clearly indicates that the chute-like feature filled with sand after barfront sedimentation had ceased.

# 6 Wellington Bar, Fraser River

## 6.1 Wellington Bar Morphology

Wellington Bar is a mid-channel macroform about 1.1 km wide and 3.2 km long, positioned 6.6 km downstream of the Harrison River confluence at 7 to 8 m elevation (Fig. 6.1). The barhead is a curviplanar, extensive gravelly surface with little relief and low dip angles (Figs. 6.2A and 6.2B). Its surface dips ~2° into the southeast channel, <1° upstream, and <1° into the northwest channel. The barhead is part of a laterally extensive (~1 km wide) gravelly unit bar that is prograding (Fig. 6.2C) onto the topographically higher, sandy, vegetated inner bar (Fig. 6.2D). Gravelly tongues projecting downflow from the slipface margin of unit bars give the bar edge a fingered appearance (Fig. 6.2C). The tongues are deposited during falling stage flow, due to flow convergence at the edge of the bars scouring sediment from the planar bartop (Fig. 6.2D). The tongues are preserved because declining flow velocities are not able to erode and remobilize the gravelly sediment.

Other bartop features include stalled bedload sheets and scour hollows. Scour hollows with ~1 m of relief occur in the immediate vicinity, and upstream, of a large Cottonwood tree lying parallel to flow (Fig. 6.2E).

## 6.2 Wellington Bar Evolution

Wellington Bar developed from a large, bank-attached, unvegetated bar in 1943 to a mid-channel bar by 1952 (Fig. 6.3). Bar development after 1952 has seen the bar become larger and thickly vegetated. The flood of 1948 initiated the dramatic change in channel position between 1943 and 1952. The flood removed a portion of the barhead and eroded a small, shallow chute across the barhead adjacent to the southeastern channel margin (visible in 1949 photographs). By 1952 the chute had incised into the bar and detached it from the bank. During the next decade, high-stage flows divided around the barform and had enlarged the incipient channel to its current width by 1967. The sequence of events clearly shows that large floods do not produce immediate large-scale channel changes. Rather, large floods initially deflect the thalweg producing small-scale channel changes that are amplified by high-stage flows in successive years. It is the later flows that ultimately produce large-scale channel changes. This style of channel development is characteristic of (and perhaps unique to) wandering gravel-bed rivers. It is unlike other fluvial styles where large floods cause pronounced and immediate channel changes.

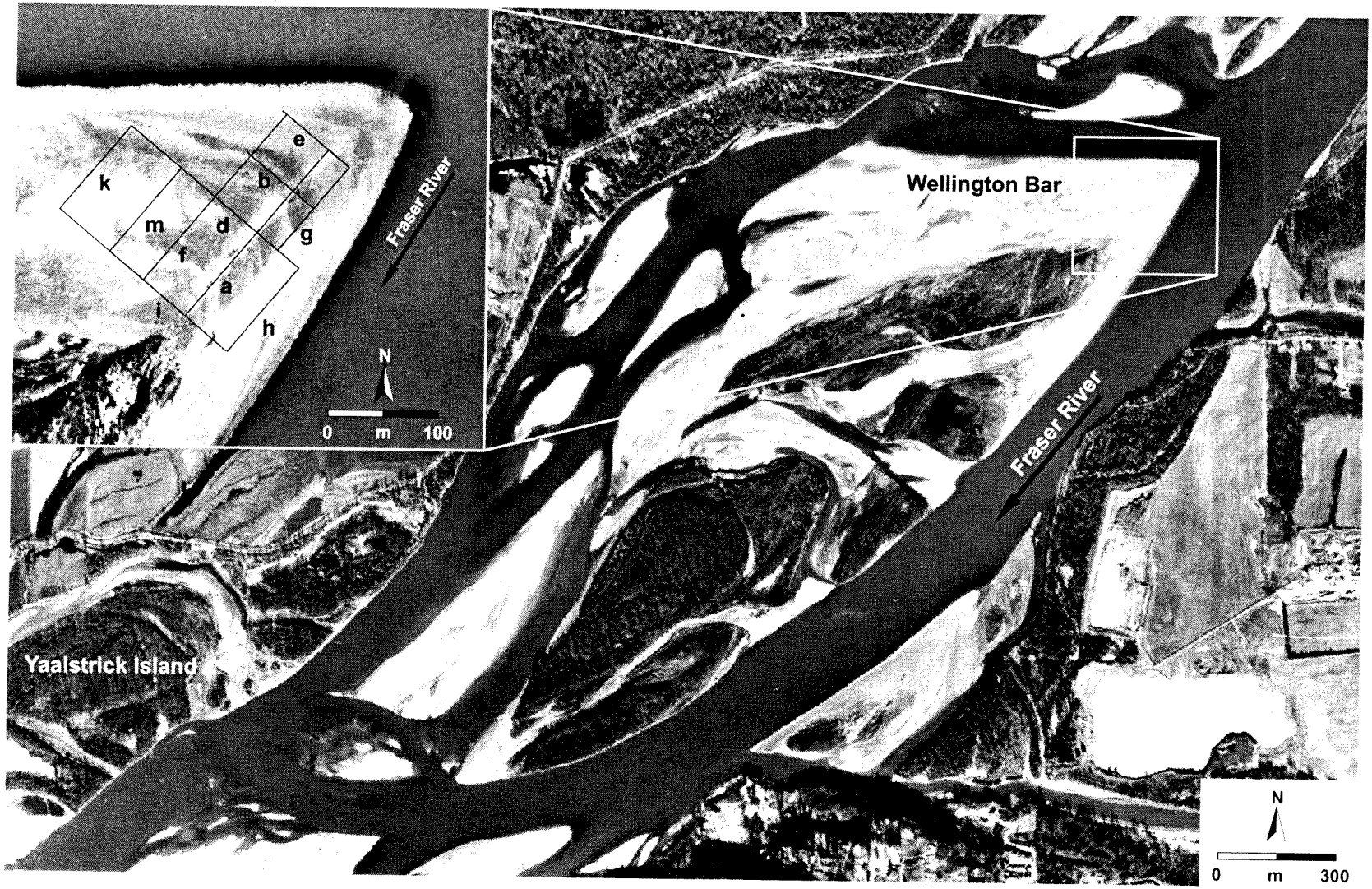


**Fig. 6.1** Mid-channel Wellington Bar, Fraser River. Photograph taken 20 March 1999, $Q$ = 701 $m^3s^{-1}$ (BCB99001: 29). Inset shows lettered GPR transects shot with 200, 100, and 50 MHz frequency antennas. Lines k, m, and the western half of lines d and i were only profiled with 50 MHz antennas. Photograph taken 10 March 2000, $Q$ = 677 $m^3s^{-1}$ (SRS6164: 90).


**Fig. 6.2** Surficial morphology of Wellington Bar, Fraser River. **(A)** Planar bar surface (case for scale is 0.5 m wide). **(B)** Surface grain-size texture (cigarette pack for scale is 10 cm on each side). **(C)** Slipface margin of a kilometer-scale unit bar (person for scale). **(D)** Downstream view of the prograding unit bar in C (person for scale). **(E)** Bartop scour hollows (person for scale). **(F)** Photograph locations.

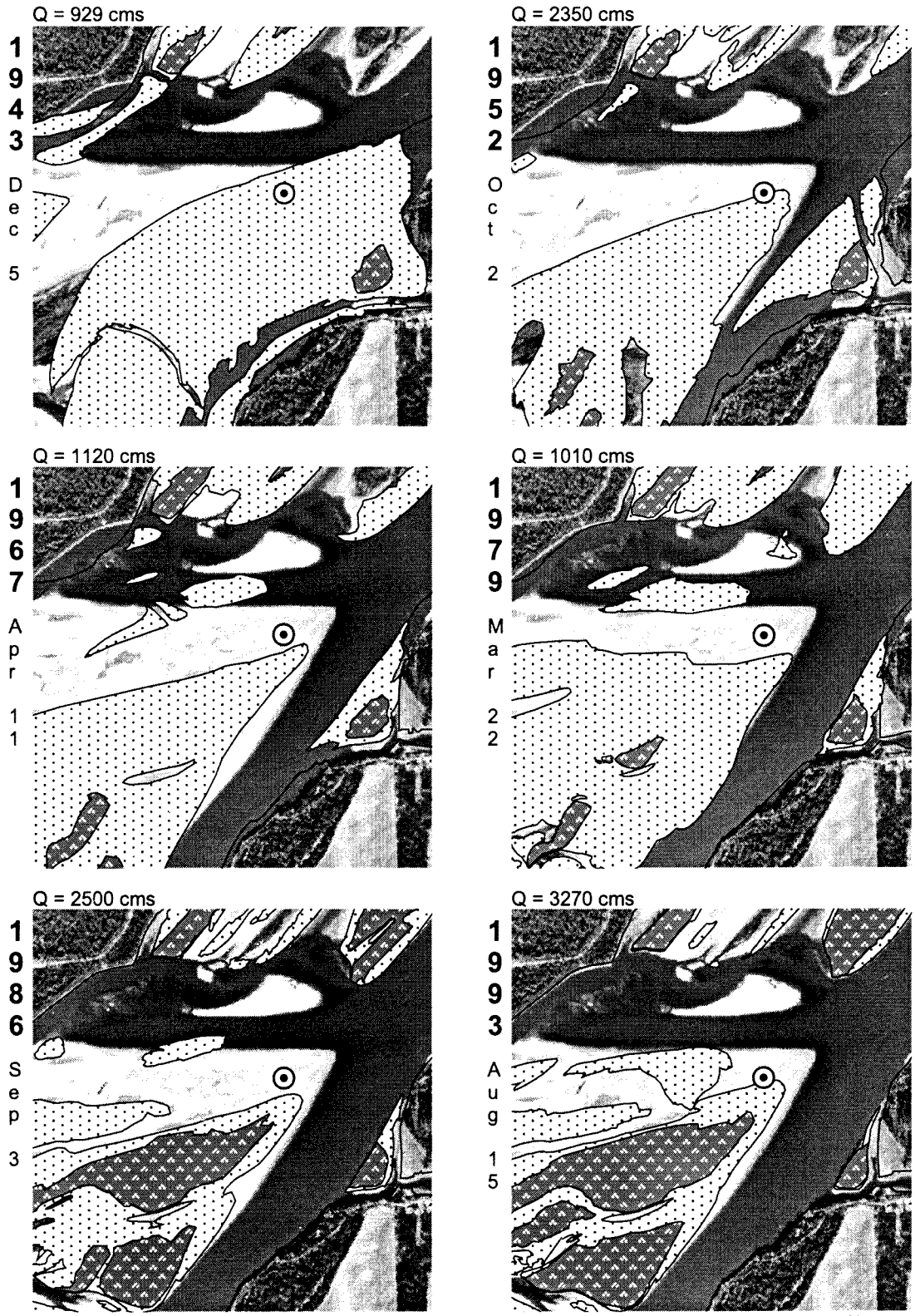


**Fig. 6.3** Morphological evolution (1943 to 1999) of Wellington Bar, Fraser River. Successive changes in channel position and bar morphology mapped from aerial photographs and superimposed on 1999 photograph in background. The bulls eye marks the center of the GPR grid. 1999 photograph taken 20 March 1999, discharge (Q) = 701 cms. Flow is from top right to bottom left.

By 1967 small, individual mid-channel gravel bars had developed in the northwest channel (the former thalweg) and sediment began accreting to the northwest margin of Wellington Bar by 1979. By 1986 further accretion saw the bar enlarge to a point whereby the inner portions of the bar were stable enough for vegetation to take root and steadily colonize the inner bar. Accretion along the northwest margin of the barhead between 1967 and 1993 saw it enlarge from a very narrow, sliver of sediment to more of a broad-tipped barhead. The barhead migrated upstream until 1999, where it has remained relatively unchanged through 2001 (Figs. 6.1 and 6.1 inset). The style of bar evolution (and by consequence depositional style) has differed across the barhead in response to the thalweg being redirected from the northwest channel to the southeast channel. The width and shape of the high velocity southeast channel have remained relatively constant since 1967, implying that local scour and fill events probably characterize its depositional style. In contrast, the width and shape of the low velocity northwest channel have varied considerably as sediment has been intermittently deposited and eroded in the channel as it progressively infills.

## 6.3 Wellington Bar Bathymetry

Figure 6.4A displays three bathymetric soundings across Wellington Bar and the entire ~1.1 km width of the active channel-belt completed in 1952, 1984, and 1999 (Figs. 6.4B and 6.4C show their locations). The bathymetry gives a vivid perspective of typical wandering style defined by multiple shallow channels bifurcating around small and large mid-channel bars. The bathymetry is quite unlike the entrenched channel geometries evident at the bank-attached Calamity and Queens Bars (Figs. 4.4A and 5.4A, respectively). The difference in scour depths between the three bars is primarily due to the mid-channel position of Wellington Bar and the unconfined nature of the channel-belt in the valley (the river is not impinging on hard points). Bathymetric differencing between 1952 and 1999 reveals the depth of scour at Wellington Bar to be ~8 m. It is possible that fluvial depositional patterns have always been unconfined at the site, implying that the depth of scour has also been rather limited. This circumstance may allow for the preservation of deeper strata and a more complete ancient stratigraphy.

The 1952 bathymetric sounding documents the incipient incision across the bank-attached bar as a small, shallow chute is evident at the southeast edge of the sounding (~950 m distance). The northwest margin of the bar dipped steeply into the broad channel across which there was some relief as a subaqueous mid-channel ridge occupied the middle of the channel similar to a sounding across the Squamish River (Fig. 3.4B). The 1984 and 1999 soundings show that the southeastern margin of the bar remained relatively unchanged in the 15 year period as it dipped steeply into the recently developed channel with similar angles and bar positions. In contrast, the northwest channel shows spatially variable patterns of filling. During the same period, the barhead experienced ~2 m of vertical aggradation as the tip of the bar migrated upstream into the channel.

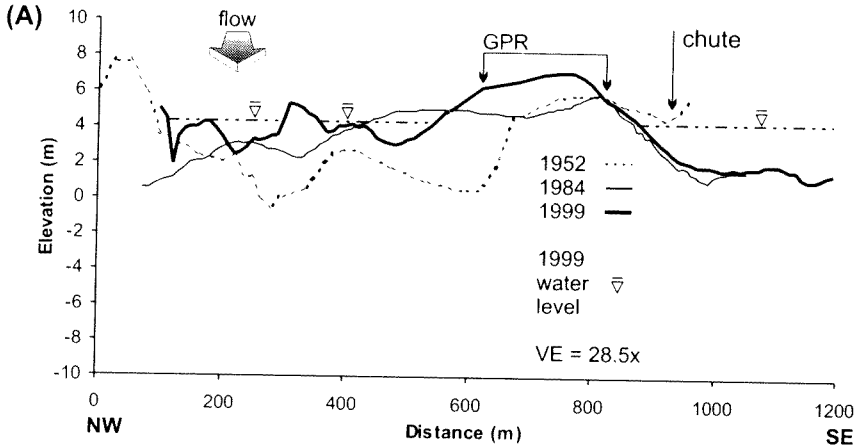


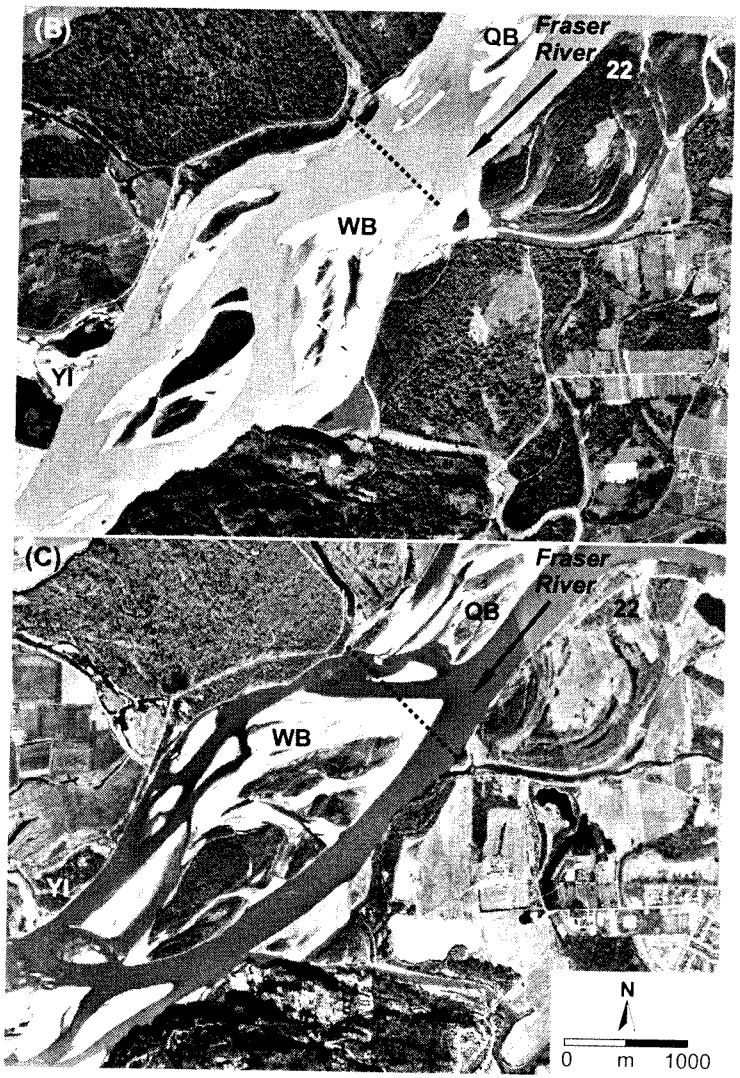


**Fig. 6.4** Bathymetry soundings across Wellington Bar, Fraser River. **(A)** 1999, 1984, and 1952 cross-stream channel geometry. 0 m elevation is mean sea level. Water level is at low-stage flow, $Q$ = 677 $m^3s^{-1}$. Extent of bar surface profiled with GPR is also shown. Bathymetry data courtesy of the Department of Geography, UBC. **(C)** 1952, and **(D)** 1999 sounding locations (·····). Photographs taken 2 October 1952, $Q$ = 2350 $m^3s^{-1}$ (BC1622: 24), and 20 March 1999, $Q$ = 701 $m^3s^{-1}$ (15BCB99001: 22, 29). Island 22 (22), Wellington Bar (WB), Queens Bar (QB), and Yaalstrick Island (YI).

## 6.4 Wellington Bar Radar Facies and Elements

Figure 6.1 inset shows the grid profiled on Wellington Bar with GPR.

### 6.4.1 Radar Facies 1: subhorizontal, continuous, subparallel reflections

Radar facies 1 is characterized by stacked (2 to 5 m thick), horizontal to subhorizontal, continuous (>50 m long), parallel to subparallel reflections (Figs. 6.5A, 6.6A, and 6.7A). Some reflections can be traced in flow-parallel and flow-normal GPR profiles (Fig. 6.7A) as they retain their subhorizontal, subparallel character in three dimensions. The facies occurs at all stratigraphic levels, but has a limited spatial coverage across the bar and tends not to grade into or out of the other facies.

*6.4.1.1 Interpretation: vertical accretion deposits (stratified bedload sheets)*

The radar signature is interpreted as stacks of vertically accreted gravel sheets deposited from bedload sheets migrating across bar surfaces and channel floors (Figs. 6.5B, 6.6B, and 6.7B). The subparallel nature of the radar signature is probably due to the intermittent nature of bedload transport whereby bedload sheets overtake and bury other stalled sheets creating subdued topographic relief.

### 6.4.2 Radar Facies 2: low-angle (<1°), cross-stream dipping, parallel reflections

Radar facies 2 is characterized by stacked (1 to 5 m thick), continuous (>130 m long), low-angle (~0.8°), parallel reflections that dip normal to flow (Fig. 6.5A). The facies covers the northwest half of the bar, but is stratigraphically limited to the upper portion of the succession. The facies thins toward the middle (crest) of the bar because the reflections onlap a cross-stream dipping lower bounding surface. The flow-normal signature is composed of subhorizontal reflections (Fig. 6.7A).

*6.4.2.1 Interpretation: lateral accretion deposits (stratified bedload sheets)*

The flow-normal radar signature is interpreted as lateral accretion deposits that record the progressive onlap of gravelly bedload sheets onto the gently inclined northwest bar-margin (Fig. 6.5B). Evidence of this depositional style comes from the coincidence between the apparent dip angle of the deposits and the <1° dip angle of the bar surface. The flow-parallel signature confirms the sheet-like style of sedimentation (Fig. 6.7B).

### 6.4.3 Radar Facies 3: low-angle (2 to 3°), downstream dipping, subparallel reflections

Radar facies 3 is characterized by low-angle (2 to 3°), divergent to subparallel reflections (2 to 6 m thick) that dip downflow (Fig. 6.6A). Sets of downlapping tangential reflections (>60 m long) occur in the middle of the stratigraphy between 7 and 13 m depth.

*6.4.3.1 Interpretation: downstream accretion deposits (stratified bedload sheets)*

The flow-parallel radar signature is interpreted as downstream accretion deposits (Fig. 6.6B). The facies documents the migration of gravelly bedload sheets over the bar onto its downstream margin causing the barform to vertically aggrade and translate downstream. The relatively consistent bar-margin geometry recorded by the tangential reflections shows that a coherent style of sedimentation was maintained throughout the growth of the barform down the channel.

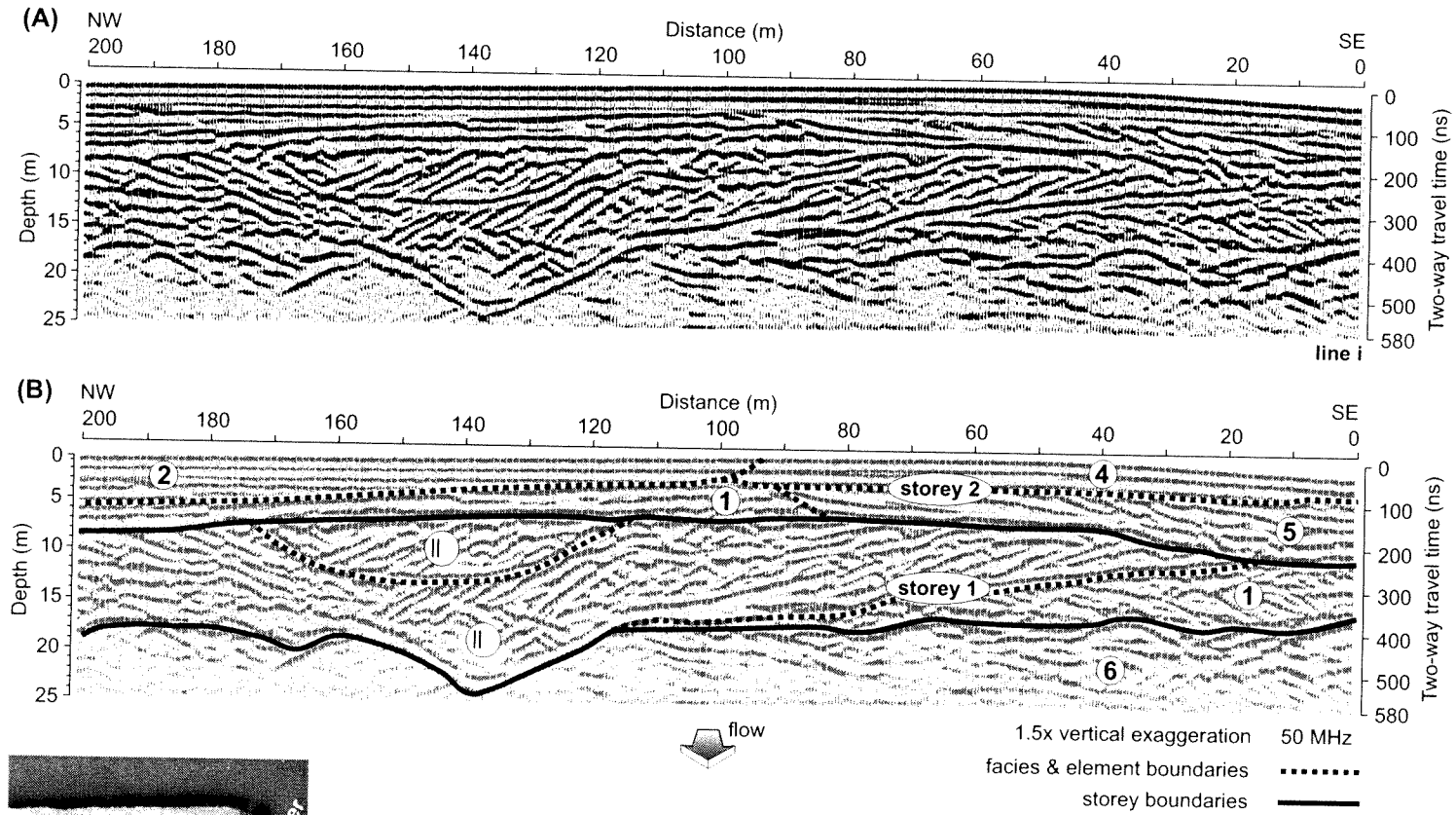


**Fig. 6.5** GPR profile i (50 MHz), Wellington Bar, Fraser River. **(A)** Flow-normal profile along line i. **(B)** Interpreted line i profile. Radar facies 1 (vertical accretion), 2 (lateral accretion), 4 (upstream accretion), 5 (slipface accretion), 6 (delta foresets), and element II (scour hollows) are delineated. Stories 1 and 2 record the thickness of Holocene alluvial sedimentation. The thicker line segment in the photograph shows the extent and location of the profile.

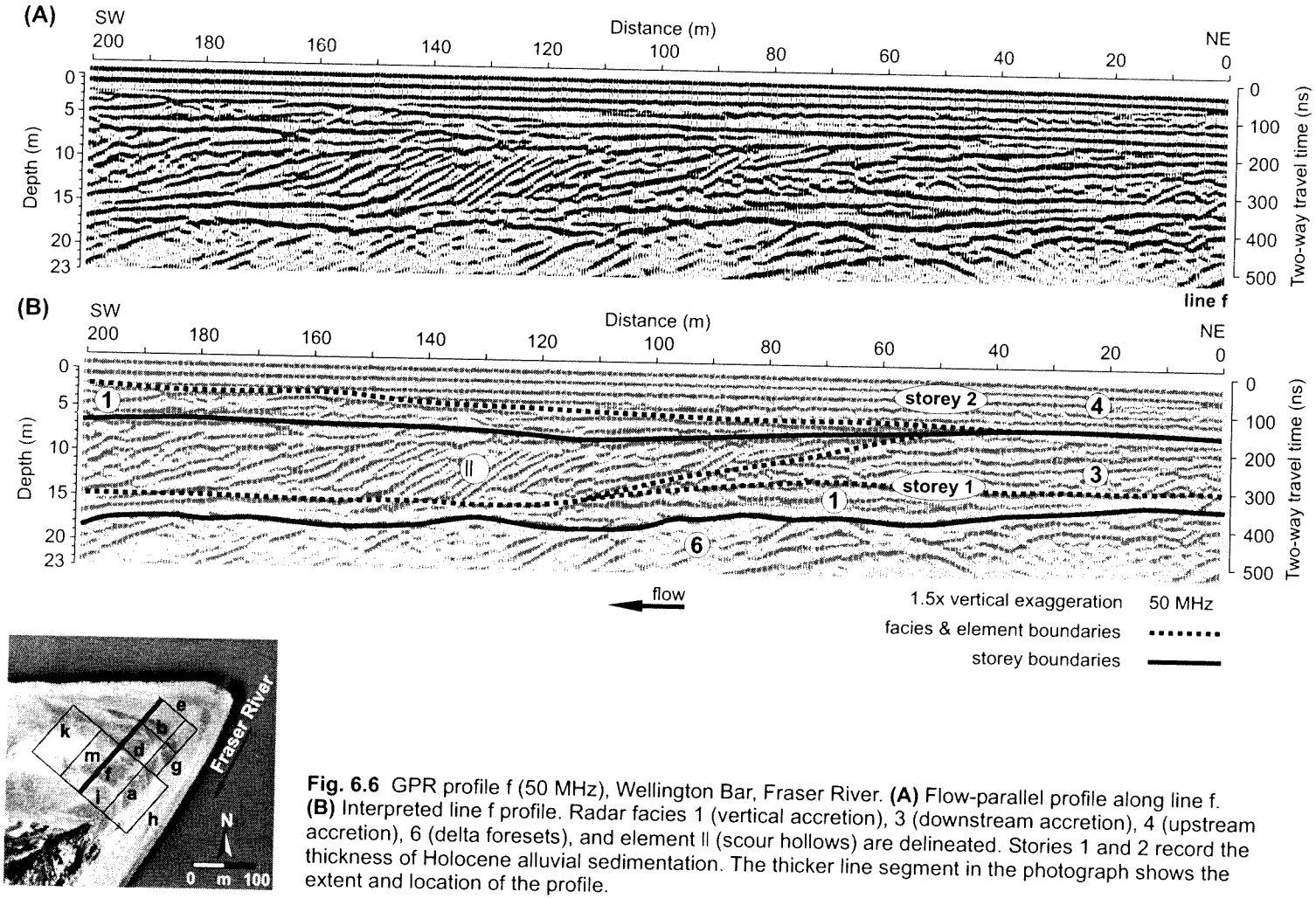


**Fig. 6.6** GPR profile f (50 MHz), Wellington Bar, Fraser River. **(A)** Flow-parallel profile along line f. **(B)** Interpreted line f profile. Radar facies 1 (vertical accretion), 3 (downstream accretion), 4 (upstream accretion), 6 (delta foresets), and element II (scour hollows) are delineated. Stories 1 and 2 record the thickness of Holocene alluvial sedimentation. The thicker line segment in the photograph shows the extent and location of the profile.

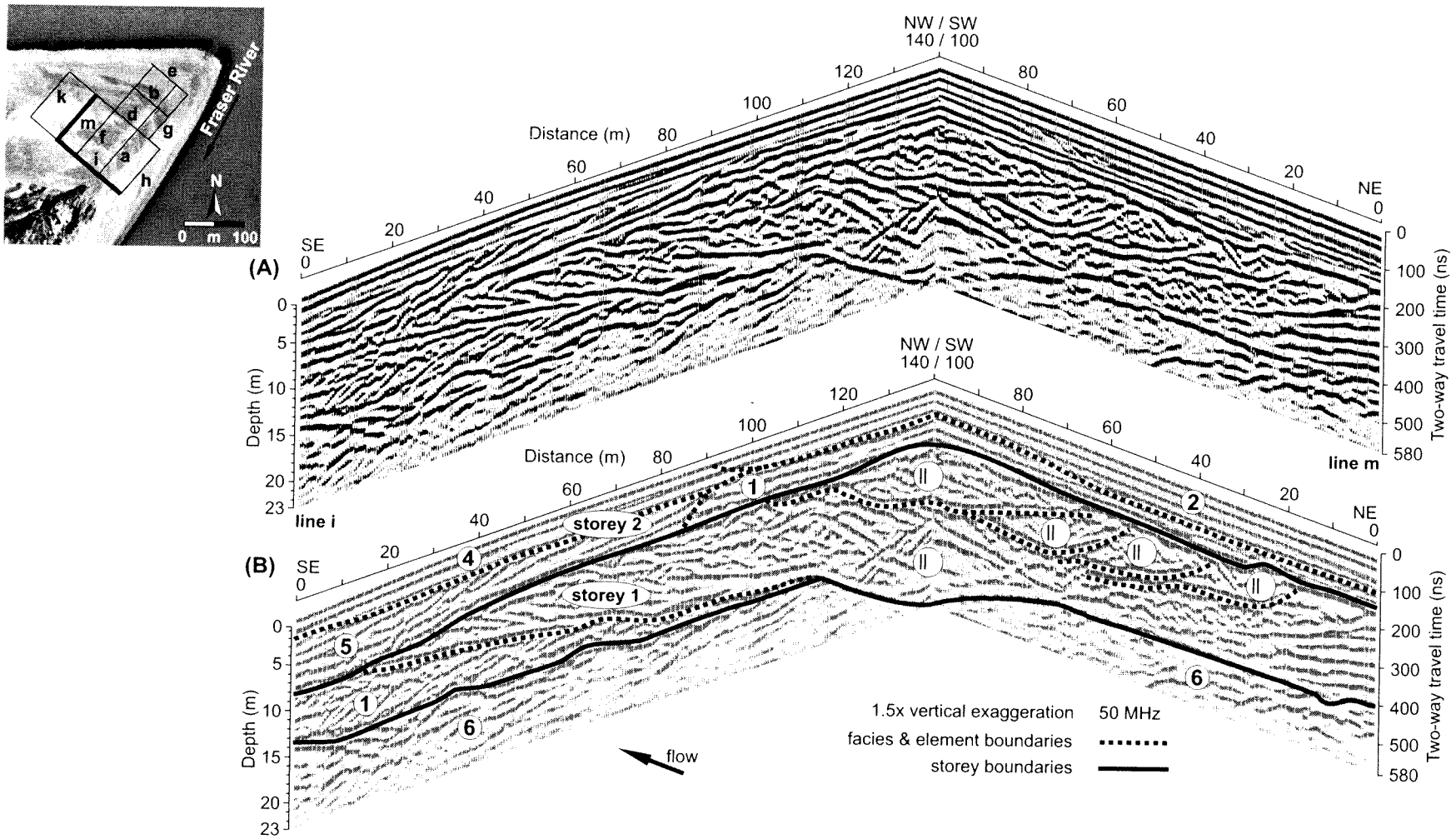


**Fig. 6.7** 3D view of GPR profiles i and m (50 MHz), Wellington Bar, Fraser River. **(A)** GPR profiles along line i (flow-normal) and line m (flow-parallel). **(B)** Interpreted line i and line m profiles. Radar facies 1 (vertical accretion), 2 (lateral accretion), 4 (upstream accretion), 5 (slipface accretion), 6 (delta foresets), and element II (scour hollows) are delineated. Stories 1 and 2 record the thickness of Holocene alluvial sedimentation. The thicker line segments in the photograph show the extent and location of the profiles.

### 6.4.4 Radar Facies 4: low-angle (<1°), upstream dipping, parallel reflections

Radar facies 4 is characterized by stacked (>6 m thick), continuous (>200 m long), low-angle (~0.5°), parallel reflections that dip upstream (Fig. 6.6A). The facies is areally extensive across the bar, but is stratigraphically limited to the upper portion of the succession. The reflections onlap an upstream dipping lower bounding surface and hence the thickness of the facies thickens upflow. The flow-normal signature is composed of subhorizontal reflections (Figs. 6.5A and 6.7A).

*6.4.4.1 Interpretation: upstream accretion deposits (stratified bedload sheets)*

The flow-parallel radar signature is interpreted as upstream accretion deposits (Fig. 6.6B). Sediment is accreted to the bar in much the same fashion as vertical, downstream, and lateral accretion sediments are deposited, by the migration of gravelly bedload sheets onto the bar surface. Yet in this case, the strata dip in the upstream direction. This interpretation is supported by evidence of stalled bedload sheets on the surface of the bar and because the apparent dip angle of the reflections is coincident with the <1° upstream dip of the bar surface. The flow-normal signature confirms the sheet-like style of sedimentation (Figs. 6.5B and 6.7B).

### 6.4.5 Radar Facies 5: medium-scale (1.5 to 2.5 m), steeply inclined (14 to 20°), oblique reflections

Radar facies 5 is characterized by medium-scale (1.5 to 2.5 m thick), parallel to subparallel, steeply inclined (14 to 20°), oblique reflections that dip normal to flow (Figs. 6.5A and 6.7A). The steeply dipping reflections occur as a discrete package (>90 m long) of reflections which downlap onto a continuous, subhorizontal bounding surface. The facies is stratigraphically restricted to the upper portion of the southeastern half of the barhead sediments.

*6.4.5.1 Interpretation: bar-margin slipface accretion deposits*

The flow-normal radar signature is interpreted as bar-margin slipface deposits indicative of sediments avalanching over a high relief southeastern bar-margin into the deeper main channel (Figs. 6.5B and 6.7B). The thickness and stratigraphic position of the facies suggest that the deposit traces the progradation of the bar into the recently formed main channel after 1952. Sedimentation began after the bar had been dissected and was probably complete by 1967 when the incipient channel had reached its current width.

### 6.4.6 Radar Facies 6: large-scale (>6.5 m), steeply inclined (11 to 18°), oblique reflections

Radar facies 6 is distinguished by low-amplitude, large-scale (>6.5 m thick), steeply dipping (11 to 18°), oblique reflections that dip downvalley (Figs. 6.6A and 6.7A). The flow-normal signature is composed of subhorizontal reflections (Fig. 6.5A). The facies is only found below 16 m depth (-9 m elevation) and its upper surface is bound by a high-amplitude, subhorizontal, wavy reflection. The complete thickness of the inclined reflections was not imaged, as the reflections appear to extend beneath the imaged sediment pile (due to the length of the time window used to shoot the profiles). Individual flow-parallel reflections are up to 30 m long and the facies is found beneath the entire profiled area (200 m x 200 m).

#### 6.4.6.1 *Interpretation: delta foreset deposits*

The flow-parallel radar signature is interpreted as delta foresets (Figs. 6.6B and 6.7B). The flow-normal signature reveals the planar stratal geometry along the strike of the sedimentary body (Fig. 6.5B). The large-scale character of the deposit, both its thickness and widespread areal extent, suggests that it was not generated by local channel scouring mechanisms, but rather probably indicates sedimentation into a standing body of water due to marine flooding during deglaciation in the late Pleistocene. Further, the dip angle of the sediments and the geophysical character of the reflections support this interpretation. The dip angles of the foresets are similar to other modern (Kostaschuk and McCann, 1983) and ancient (*e.g.* Britannia Creek delta; Fig. 6.8D) sand and gravel marine deltas subject to tide or wave influence. The low-amplitude character of the reflections is unlike the high-amplitude reflections of the alluvial strata and could be a result of sand-dominated sediments, or alternatively may be due to connate saltwater, both of which attenuate signal returns. The sand-dominated late Pleistocene Britannia Creek delta (Figs. 6.8A-D) is a likely analog for the ancestral Fraser River delta because its sediments are sandy, and are saltwater saturated. Yet its high-amplitude reflections do not exhibit the attenuation seen in the Fraser River deltaic sediments. This may signify that the gravelly strata above the Fraser River deltaic sediments are returning most of the GPR signal.

The wavy upper bounding surface of the deltaic sediments appears to truncate the foresets, suggesting that fluvial processes eroded the deposit after it had been deposited. Although the delta foresets were eroded, they were likely preserved due to their mid-valley position where river scour depths are limited.

### 6.4.7 Radar Element II: 3D, basal, steep-sided (5 to 19°), scallop-shaped reflections

Radar element II is characterized by 3D, basal, large-scale (up to 16 m deep, >150 m long [flow-parallel; Figs. 6.6A and 6.7A]), and >180 m wide [flow-normal; Fig. 6.5A]), steep-sided, scallop-shaped reflections. The stratigraphy records two sets of large-scale reflections with a smaller collection of reflections (up to 6.5 m deep, 30 m long [flow-parallel], and 50 m wide [flow-normal]) entrenched within the larger reflection configuration, whose dimensions are stated above.

The smaller set of reflections shows flow-parallel, scallop-shaped reflections truncating each other in a downstream direction with similar depths (~13.5 m below bar surface; Fig. 6.7A). The flow-parallel, external, basal geometry of the scallops shows curvatures dipping downstream between 13 and 19°. The scalloped-shaped reflections are filled with variable patterns of dipping reflections (Fig. 6.7A). In contrast, flow-normal profiles exhibit symmetrical, trough-shaped, basal reflections dipping (~18°) into the center of the element (Fig.6.5A). The fill within these reflections shows a coherent set of steeply dipping reflections. The total 3D configuration of the external reflections and internal fill reveals a discrete reflection pattern bounded above by subhorizontal reflections (Fig. 6.7A). The pattern is a local feature as it is stratigraphically limited (between 7 and 13.5 m depth below bar surface) and its bounding edges are evident in the profiles.

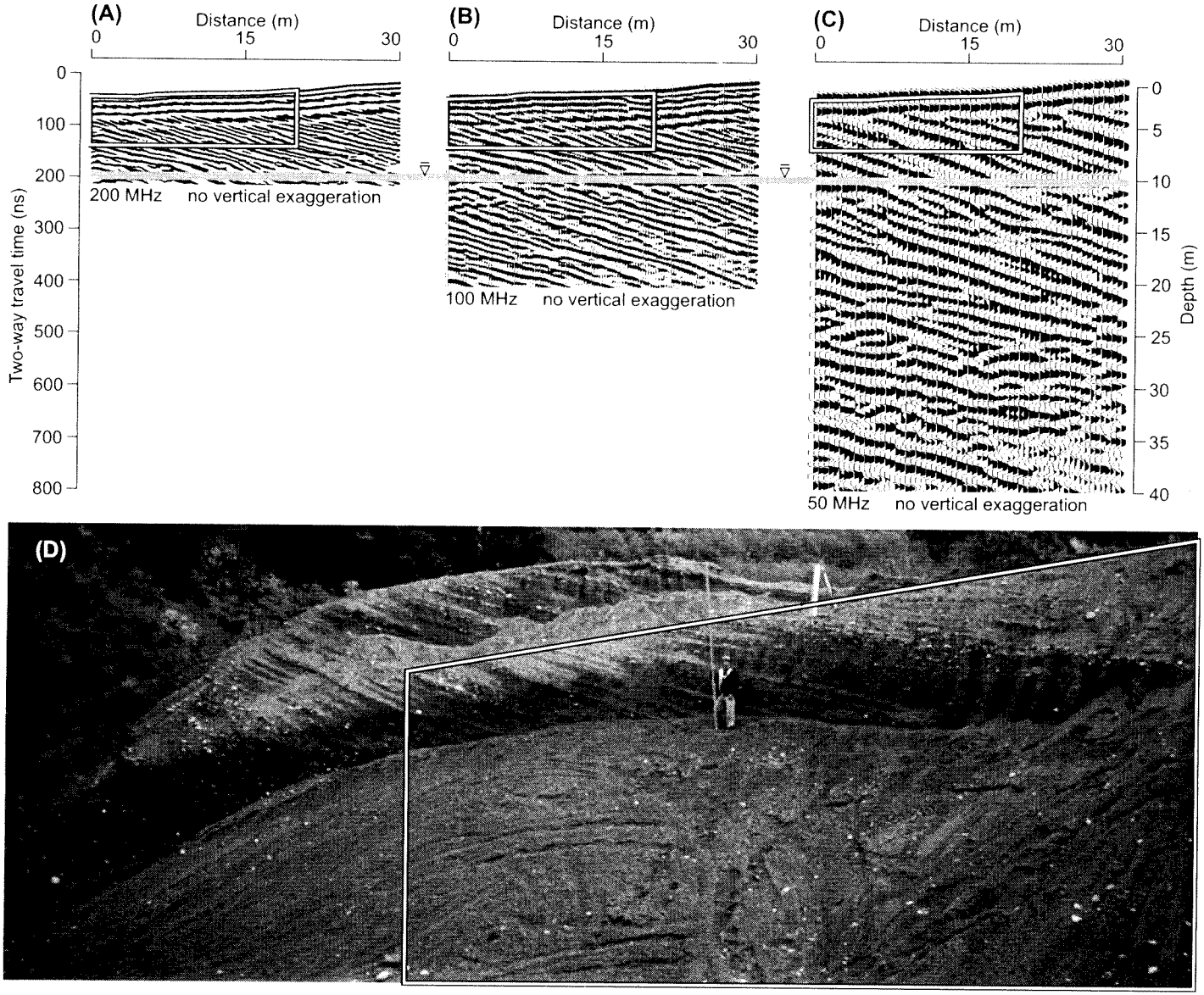


**Fig. 6.8** Britannia Creek delta, GPR profiles and outcrop. **(A)** 200 MHz profile. **(B)** 100 MHz profile. **(C)** 50 MHz profile. **(D)** Photograph of exposed delta foresets. Boxed portion on the profiles corresponds to the boxed portion on the photograph. The water table ( $\bar{\nabla}$ ) is sea level.

The larger-scale reflection pattern is also scallop-shaped, but is demarcated by a singular basal reflection (rather than a series of reflections) dipping ~7° downstream and cross-stream into the center of the element between 5 and 18° (Figs. 6.5A, 6.6A, and 6.7A). Its fill is made up of downflow and cross-flow dipping reflections that are inclined up to 26°. The element dominates the lower portion of the profiled alluvial succession and is bound above by subhorizontal continuous reflections.

*6.4.7.1 Interpretation: scour hollow deposits*

The radar element is interpreted as scour fill structures (Figs. 6.5B, 6.6B, and 6.7B). The element is defined by the architectural arrangement of basal, scoop-shaped reflections (erosional scour forms) in association with, and infilled by, a variety of reflection patterns (the fill). The interpretation is contingent on the three-dimensional scallop-shaped external form of the element (Fig. 6.7B), because in two-dimensions the troughs appear as channel forms (Fig. 6.5B). The interpretation is corroborated by bathymetric soundings which show localized scours generally ~50 m wide (normal to flow) and 6 m deep, indicating that both scales of reflections are local, constrained features that have over-deepened the succession. Further evidence of the genesis of the element is inferred from the continuous, high-amplitude, basal reflections, which clearly truncate strata beneath the scours. The series of smaller-scale elements (with equivalent scour depths) indicate that the scour hollow migrated downstream, perhaps in conjunction with the downstream translation of a channel constriction or confluence between two bars. The internal geometry of the fill is directionally variable, a consequence of sediment avalanching into the scours from both the upstream edge and sides of the scours.

## 6.5 Wellington Bar Radar Stratigraphy

A wavy reflection about 17 m below the surface of the bar separates deep, low-amplitude radar signatures from high-amplitude reflections in the Wellington Bar stratigraphy. The deeper stratigraphy shows large-scale, steeply inclined reflections that dip downvalley and are interpreted to be delta foresets. The sediments likely trace the progradation of a delta front into a flooded Fraser Lowland in the late Pleistocene deglacial period, followed by alluvial sedimentation throughout the Holocene.

The upper 17 m of Wellington Bar architecture is split into two distinct packages of alluvial strata (storeys 1 and 2) by a subhorizontal bounding surface about 8 m below the bar surface. The discrete appearance of each stratigraphic package suggests that each is a complete storey. This is further supported by the altogether contrasting alluvial styles recorded in each storey. Also, it is unlikely that the river scours to 24 m depth at the site given its mid-channel position. This indicates that storey 1 represents a previous stage of river development, rather than it merely representing a growth element in the development of the contemporary barform.

Storey 1 images two sets of steeply dipping downstream and cross-stream strata (radar element II) interpreted to be nested scour hollows. The smaller scour elements are locally entrenched into the steeply dipping fill of the larger scour deposit. The scale differences between the two scour elements may reflect a decrease in river size due to allogenic forcing, or are simply the product of autogenic mechanisms acting on the site. For instance, the shallow scours may have been formed in response to barforms migrating through and constricting a secondary channel causing it to locally over-deepen. In

contrast, the larger scours undoubtedly record the constriction of the main channel. This autogenic interpretation is favored because the larger scours scale to contemporary scours in the main channel (which also show up to 16 m of bed relief and occupy most of the width of the channel).

The bounding surface separating storeys 1 and 2 (~8 m below the surface of the bar) corresponds very closely to the elevation of the channel floor captured by the 1952 bathymetry soundings (and the 1984 and 1999 soundings; Fig. 6.4A). This suggests that the radar stratigraphy in storey 2 (above 8 m depth) should match the evolution of the bar recorded in the photographic record (Fig. 6.3). The bounding surface dips upstream and cross-stream away from the inner portions of the bar indicating that the river scoured more deeply at the tip of the bar as flow eroded a new channel at its southeast margin. This caused the bar to shift from its previous bank-attached position to its current mid-channel location.

The shift was accompanied by sedimentation across the newly eroded surface. Low-angle, cross-stream (radar facies 2) and upstream (radar facies 4) dipping reflections likely record the onlap of gravelly bedload sheets onto the lateral and upstream margins of the low-angled bar surface in response to flow divergence across the mid-channel barhead. These sediments are juxtaposed beside a limited set of steeply dipping reflections (radar facies 5) that trace the progradation of sediment over a high relief bar-margin into the recently formed main channel. Subsequent sheet-like deposition unsteadily built the barform upstream and laterally, overriding the steeply dipping reflections to form a smooth curviplanar bar surface.

The lack of correspondence between the radar stratigraphy and the bank-attached form evident in the 1943 photography indicates that the sediments above ~8 m are truly a storey. Indeed, there is no stratigraphic evidence of the former 1943 barform indicating that the deeper facies and elements are part of a separate storey. The architecture shows the difficulty (impossibility) of trying to reconstruct the bar's transition from a bank-attached position to a mid-channel position. It shows that bar reconstructions merely recapture a brief moment in the evolutionary history of a sedimentary body. The stratigraphy also points to the limited preservation potential of mid-channel and bank-attached channel forms, unlike scour elements, which over-deepen the stratigraphy and are readily preserved.

# 7 Discussion and Conclusions

## 7.1 Storey Architecture

### 7.1.1 Deciphering Gravelly Multistorey Architecture

Multistorey alluvial deposits reveal patterns of channel stacking and relationships between channel networks. A storey is defined as a deposit of a single channel bar and adjacent channel fill (Bridge and Mackey, 1993a). Multistorey successions (more than one vertically superimposed storey) record spatial and temporal trends in fluvial activity such as fining upward cycles or changes in the patterns of large-scale strata (macroform architecture). These trends indicate changes in fluvial style. Identifying storeys in stratigraphic sections involves defining elements and interpreting facies associations in consideration of allogenic forcing mechanisms, including climate, base level changes, tectonics, and sedimentation rates. Allogenic mechanisms ultimately affect avulsion frequency and the ability of a river to rework its channel-belt, as well as in-channel autogenic processes such as scouring.

Multistorey gravelly architecture, in outcrop, is typically seen as repeating sets of thicker gravel overlain by thinner sands and silts. The bartop sands are typically eroded into and overlain by another gravelly deposit. In these cases the vertically stacked gravelly deposits are unrelated as there is a lack of interfingering between the sediments and the contacts are depositional or erosional (Eynon and Walker, 1974; Smith, 1990). These contacts are delineated as storey boundaries and are normally demarcated by laterally continuous bartop sands. These prominent bounding surfaces differ from smaller-scale internal surfaces which isolate thin, discontinuous, sand lenses interstratified in thicker gravel, or individual gravelly bedload sheets interbedded in thicker bartop sands (Fig. 1.2E) (Morison and Hein, 1987).

Alternatively, multistorey character *within* a single channel-belt (such as is seen in Squamish and Fraser River profiles) records the vertical superposition of channel bars and fills before the channel-belt is abandoned (Bridge and Mackey, 1993a). Herein lies the problem of discriminating between bounding surfaces that delineate superimposed barforms and surfaces that merely represent growth increments within a macroform. For instance, upper bar sediments are likely to be discordant with lower bar sediments due to changes in flow direction over bars at high-stage flow (bankfull depths). Thus, changes in stratal orientation do not necessarily signify the occurrence of a separate barform. Rather, it is the case that because bars are built from flow patterns which change throughout the history of bar growth, that discontinuities between genetically related sediment can be expected within these solitary barforms. For example, not all scour surfaces identified in the Inner Channel site stratigraphy are interpreted as storey boundaries. Instead, storeys are defined from the scale of the depth of flow in the contemporary channel and other scour surfaces of lesser scale are considered internal growth elements. In a similar fashion, Massari (1983) interpreted scour surfaces within lithosomes as in-channel features rather than

major erosion surfaces separating different storeys within complex bodies. Massari's (1983) interpretation was based on the assumption that the scale of the largest preserved element indicated minimum water depths, and that smaller scale elements bounded by scour surfaces were simply the product of channel scour and subsequent in-channel deposition. Obviously, this raises questions about the scale of individual elements and determinations of paleochannel depth and width.

### 7.1.2 Estimating Paleochannel Depth and Width

#### *7.1.2.1 Paleochannel Depth*

The importance of being able to recognize complete, untruncated channel bars or channel fill successions is critical because their thicknesses are normally taken to represent the maximum bankfull channel depths, from which channel widths can be subsequently estimated (Bridge and Tye, 2000). Barform thickness cannot be less than the vertical thickness of major scour deposits or assemblages of downstream or laterally accreted sets of strata, whose thicknesses are between half, and just less than the total channel depth at bankfull stage (Bristow, 1987; Bridge and Tye, 2000).

The preserved thickness of channel bars is constrained by the aggradational regime and the manner of channel movement (Friend, 1983). If aggradation rates are low or channels migrate rapidly (such as in braiding rivers) paleochannel thickness may exceed bankfull depth, as rivers are able to progressively rework and scour a large portion of the channel-belt. In this case, there is no evidence of scour hollows. Alternatively, if aggradation rates are high or channels are stable, scour hollows are selectively preserved (Cowan, 1991; Siegenthaler and Huggenberger, 1993), and the average depth of flow controls the thickness of internal stratification packages. This is the case in the Fraser and Squamish Rivers, where lateral accretion deposits in Calamity Bar are the thickest channel bar sediments profiled and point to mean channel depths greater than 8 m. Also, isolated scour hollow deposits up to 16 m deep in Wellington Bar reveal the full depth of channel scour and probably show that the channel network is relatively stable.

Not only is it obvious that scouring is an important autogenic process promoting the downward thickening of sediment that preserves the channel fill, but the preservation of scour hollows also provides insights into the paleogeomorphology of river systems. For instance, preserved isolated scour hollows may indicate channel constriction (due perhaps to bar accretion choking the channel), tight channel curvature, or channel confluences (Salter, 1993). Stable meandering paleochannel stratigraphies are an exception to this, as they typically display flat bases with few scour hollows because, in general, bends migrate at a nearly constant pool depth across the channel-belt (Salter, 1993). In contrast to scouring, incision is an allogenic process that initiates downcutting without thickening.

#### *7.1.2.2 Paleochannel Width*

Paleochannel width is typically determined in one of three ways. Characteristic width-to-depth ratios determined from modern fluvial styles are used to calculate channel width once the depth of the paleochannel has been determined (Allen, 1983). Alternatively, paleochannel width can be measured directly from stratigraphic sections provided the 3D geometry of the channel-belt can be determined, as in the case of the Squamish River profiles. Lastly, empirical equations derived from modern rivers give estimates of channel width. Some equations employ the thickness and dip angle of lateral accretion deposits to determine width (Collinson, 1978), while others use the mean channel depth (Bridge and

Mackey, 1993b). Although the use of empirical equations is appealing, they can only be used to determine the width of the local channel that deposited the strata. In this sense, the width of the main channel of the Fraser River could be found, but it would not give any indication of the multiple channeled character of the river, nor its total bankfull width.

### 7.1.3 The Issue of Scale Invariance

Sambrook Smith *et al.* (*in review*) have been employing GPR data to determine the scale dependency of sand-bed braiding river deposition at three different scales of river channels: Calamus (~30 m wide), South Saskatchewan (~500 m wide), and Jamuna Rivers (~1000 m wide). In the two larger rivers, they found high-angle planar stratification associated with bar-margin slipface accretion and barfront progradation, but none in the more stable Calamus River. Low-angle planar stratification was found in Calamus River sediments, indicative of slow rates of bar migration. In contrast, the steeply dipping facies recorded the rapid accretion of bar-margins into deeper water and was proportionally scaled to the South Saskatchewan (up to 2 m thick) and Jamuna Rivers (up to 8 m thick) supporting the case for scale invariance (Sambrook Smith *et al.*, *in review*).

The issue of scale invariance is central to the building of architectural frameworks, whereby the internal geometry of facies is scaled to the size (width) of fluvial systems. Without scale invariance, facies models for different sizes of river would have to be developed. In this sense, Sambrook Smith *et al.* (*in review*) conclude that different braiding river models have to be developed, not for rivers of different size, but for rivers with different stability regimes.

The Squamish and Fraser Rivers provide an ideal test of scale invariance as they both are in the same stability regime (Desloges and Church's (1989) Fig. 3), and are roughly an order of magnitude different in size (100 and 500 m, respectively) and discharge (250 and 3400 $m^3s^{-1}$, respectively). GPR profiles of equivalent length and depth from each river provide a basis for comparing the scale of radar facies found in each river. Squamish River facies and elements are generally thinner and not as laterally extensive in character as Fraser River facies throughout the alluvial stratigraphy. This provides for a greater number of alluvial facies, both vertically and laterally within a profile and immediately suggests that the two river systems are of unequal size. The scale differences persist in storeys 1 and 2 in both rivers, signifying that these differences are indeed long-term and diagnostic of the two river systems.

The low-angle radar facies (lateral, downstream, and upstream accretion) approach the scale of the channel depth in both rivers, but local flow dynamics probably prevent individual facies from attaining equivalent thicknesses within their respective river networks. The steeply dipping facies (slipface accretion) is an anomalous case, as it shows similar thicknesses in both rivers, and more importantly does not build to the depth of flow. Thinner slipface deposits appear to be associated with bartop sedimentation and the building of highly mobile barforms. In contrast, thicker strata are related to deeper, in-channel sedimentation. It is unclear why there appears to be an upper limit to slipface heights, but it is likely related to issues of flow competence and sediment supply. Bar development is typically flow depth limited, which undoubtedly influences barfront sedimentation. Flow depth limitations cause flow to diverge over bartops resulting in the broadening of the bartop (Ashworth, 1996). This reduces sediment transport to the barfront and lessens barfront migration rates, in essence causing the barfront to stall. In turn, however, sediment is probably swept around developed slipfaces further

extending the barform downstream. Similar results are likely produced when sediment supply is limited, as in the case of the Fraser and Squamish Rivers. Alternatively the lack of well developed separation cells in the lee of barfronts causes sediment to accrete at lower angles, again reducing the height of slipface accretion deposits. In this regard, the condition of scale invariance does not seem to be met in wandering rivers. Alternatively, the finding of similar slipface thicknesses in both rivers may simply be a product of the sites profiled and not reflective of the full range of slipface heights present in the Fraser River.

# 7.2 Channel Bar Architecture

### 7.2.1 The Concept of Macroform Architecture

Defining macroforms is inherently interpretative because the recognition of them in stratigraphic sections hinges, in part, on defining and interpreting the bounding surfaces that enclose them. Further, ideas regarding the geometry, relative orientation of surfaces, and internal structures that comprise macroform architecture are merely speculative. The conceptual notion of macroforms is derived from Jackson's (1975) seminal work, which recognized the hierarchical arrangement of sedimentary bodies in alluvial systems. Jackson (1975) identified macroforms as large sedimentary bodies scaled directly to the spatial dimensions of the river (width), whose thicknesses are controlled by the depth of flow. Macroforms are not sensitive to synoptic and seasonal flow variations, as they exist for 10s of years, suggesting that multiple flow events contribute to the development of the barform. In this sense, their subsurface architectures are independent of formative annual flows, as there is no genetic affinity among individual packages of sediment (Allen, 1983). Yet, not all workers advance ideas similar to Allen (1983), for as Miall (2000) speculates:

> Macroforms consist of genetically related facies with sedimentary structures showing similar orientations and internal, minor bounding surfaces ($1^{st}$ to $3^{rd}$) that extend from the top to the bottom of the element, indicating that it developed by long-term lateral, oblique, or downstream accretion. A macroform is comparable in height to the depth of the channel in which it formed and, in width and length, is of a similar order of magnitude to the width of the channel. However, independent confirmation of these dimensions is difficult in multistorey sandstone bodies, where channel margins are rarely preserved and the storeys commonly have erosional relationships with each other.

Miall's (2000) statement ignores dissection and reworking of bar sediments as a mechanism whereby macroforms develop. Instead, he suggests that macroforms build only by the accretion of sedimentary packages. Brierley and Hickin's (1991) work on the alignment and juxtaposition of sandy bartop elements in braiding and wandering reaches in the Squamish River challenges Miall's (2000) notion that macroforms build through the steady, consistent growth of sediment. Instead, they found elements were randomly distributed across mid-channel bars in braiding reaches and were partially ordered across bank-attached, compound bars in wandering gravel-bed reaches. In contrast, elements were systematically aligned down, and across point bars in meandering reaches, which supports Miall's (2000) concept.

### 7.2.2 Macroform Architecture

Macroform architecture (equivalent to a storey) in TFLENT Bar, Squamish River, shows a complex juxtaposition of facies recording different flow directions and depositional styles. This pattern of

sedimentation is apparent in a small sampling of the barform, confirming Eynon and Walker's (1974) observation that macroform architecture demands the juxtaposition of genetically unrelated elements. They suggest that there is little reason to suppose that large kilometer-scale braid bars should display consistent facies or depositional patterns, where small portions of the sedimentary body are reworked at any one time. The extent and multiplicity of scour surfaces in the wandering Squamish River is undoubtedly less than is found in braiding rivers, but in both planforms they commonly separate units of contrasting sedimentary character within channel and bar deposits (Smith, 1985).

The three sites profiled on Queens Bar illustrate kilometer-scale disparity between synchronous sedimentation across the bar, and the inherently ambiguous nature of macroform architecture. Like TFLENT Bar, flow directions and the style of sedimentation differ between all three sites throughout the thickness of storey 2. In the upper portion of the storey, slipface accretion dominates the unit bars, but ill-defined internal growth increments make reconstructions identifying their simultaneous deposition upon the same macroform unlikely. In fact, to avoid the explicit demarcation of macroforms, some workers simply recognize them as compound barforms composed of a combination of multiple unit bar types (Karpeta, 1993).

Comparing the surficial morphology of a macroform at a single point in time to its subsurface architecture shows that there is little correspondence between the two images. For example, the tip of Wellington Bar appears as a simple, convex-up morphological unit, underneath which, however, its storey 2 shows radar reflections dipping in three directions with different dip angles. Yet, if the depositional history of the bar is charted since 1952 it becomes apparent that the internal structure of the bar does correspond to the morphological changes during that time period. This equivalence enables time-transgressive reconstructions of bar morphology.

### 7.2.3 Unit Bar Architecture

In contrast to macroforms, unit bars are small, mobile barforms typically composed of gravelly bedforms such as bedload sheets. Analysis of the unit bars attached to Queens Bar, Fraser River, at the Bar Tail site, and prograding down the Inner Channel site, shows there is equivalence between their surficial morphologies and subsurface stratigraphies. The radar stratigraphies show steeply dipping, inclined reflections that record the migration of bar-margin slipfaces, obvious at the edges of both bars. The equivalence is likely due to the short-lived transitory nature of unit bars, as there is little reworking of the sediment pile immediately following their emplacement. Instead, the geometry of the internal sedimentary structures, and their surficial morphology echo the flow conditions that transported and deposited them.

## 7.3 Wandering Gravel-Bed Architecture

The geometry, proportion, and spatial distribution of the five fluvial radar facies and two radar elements (Fig. 7.1 and Table 7.1) recognized in Squamish and Fraser River channel bars provide a glimpse into the alluvial architecture of wandering gravel-bed systems.

**radar facies 1** *vertical accretion deposits (stratified bedload sheets)*

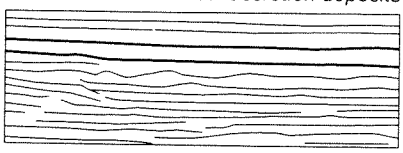

subhorizontal, continuous, subparallel reflections

flow and flow

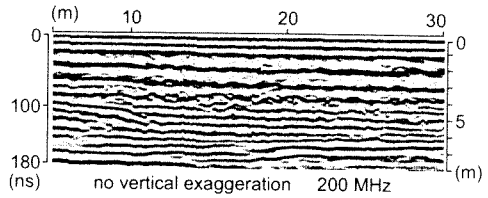


**radar facies 2** *lateral accretion deposits (stratified bedload sheets)*

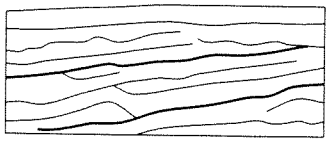

low-angle (<1 to 6°), cross-stream dipping, subparallel reflections

flow

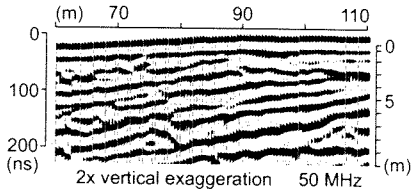


**radar facies 3** *downstream accretion deposits (stratified bedload sheets)*

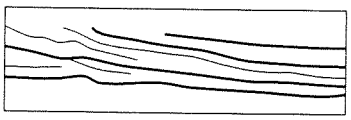

low-angle (2 to 8°), downstream dipping, subparallel reflections

flow

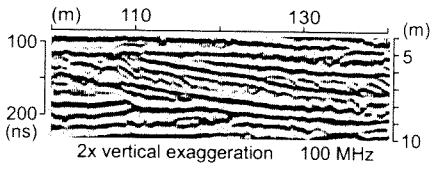


**radar facies 4** *upstream accretion deposits (stratified bedload sheets)*

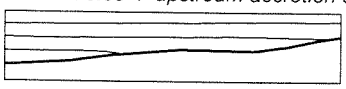

low-angle (<1°), upstream dipping, parallel reflections

flow

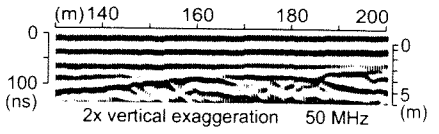


**radar facies 5** *bar-margin slipface deposits*

small- to medium-scale (0.5 to 3 m), steeply inclined (13 to 26°), oblique reflections

flow

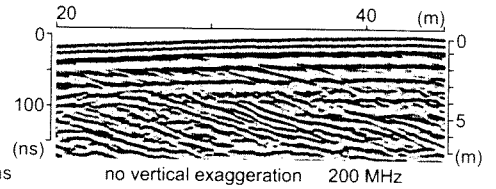


**radar facies 6** *delta foreset deposits*

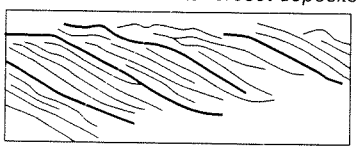

large-scale (4 to >6.5 m), steeply inclined (11 to 28°), oblique reflections

flow

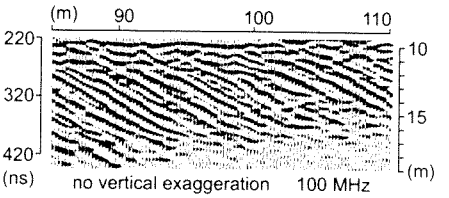


**radar element** I *channel and chute deposits*

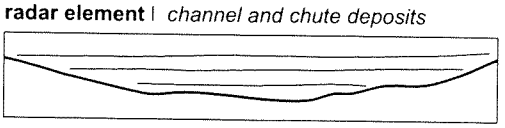

2D, basal, concave-up reflections

flow

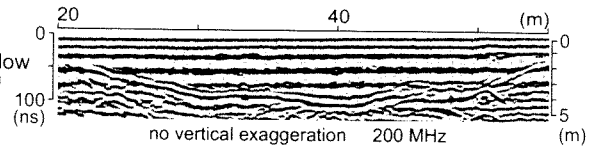


**radar element** II *scour hollow deposits*

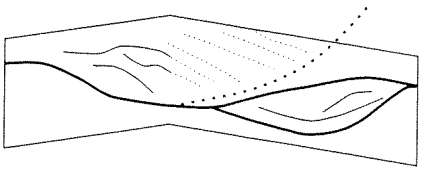

3D, basal, steep-sided (5 to 19°), scallop-shaped reflections

flow

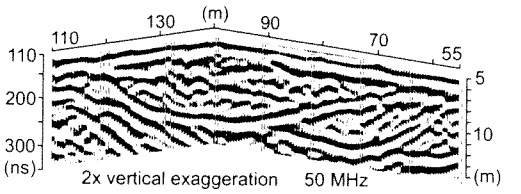


**Fig. 7.1** Radar configurations in wandering gravel-bed rivers. Radar facies 1 to 5 and radar elements I and II are typical channel bar reflection configurations. Radar facies 6 captures deltaic sedimentation.

**Table 7.1** Summary of radar facies and element parameters identified in TFLENT (TB), Calamity (CB), Queens (QB), and Wellington (WB) Bars. Reflection configurations are graphically defined in Fig. 7.1.

| Radar Facies or Element | Bar | Facies or Element Thickness (m) | Facies or Element Length (m) | Internal Reflection Configuration | Reflection Dip Angle (°) | Reflection Orientation | Spatial Extent |
|---|---|---|---|---|---|---|---|
| Facies **1** | TB | 1 to 3 | 20 to 80 | parallel to subparallel | ~0 | horizontal to subhorizontal | extensive |
| | CB | 3 to 5 | 50 to 150 | | | | moderate |
| | QB | 3 to 4 | 35 to 100 | | | | limited |
| | WB | 2 to 5 | >50 | | | | limited |
| Facies **2** | CB | 3 to 8 | >150 | parallel to subparallel | 3 to 5 | crossflow dipping | extensive |
| | QB | 1 to 5 | >55 | | 5 to 6 | | limited |
| | WB | 1 to 5 | >130 | | <1 | | extensive |
| Facies **3** | TB | 1 to 4 | 25 to 60 | divergent to subparallel | 3 to 5 | downflow dipping | moderate |
| | QB | 5 to 7 | >200 | | 4 to 8 | | moderate |
| | WB | 2 to 6 | >60 | | 2 to 3 | | limited |
| Facies **4** | WB | >6 | >200 | parallel | <1 | upflow dipping | extensive |
| Facies **5** | TB | 0.5 to 2.5 | 10 to 60 | parallel to subparallel oblique | 13 to 26 | cross- & downflow dipping | moderate |
| | CB | 0.5 to 3 | 40 to 60 | | 16 to 25 | | limited |
| | QB | 0.5 to 3 | 10 to 90 | | 16 to 26 | | extensive |
| | WB | 1.5 to 2.5 | >90 | | 14 to 20 | | moderate |
| Facies **6** | TB | 4 to 7 | 45 | parallel to subparallel oblique | 25 to 28 | downflow dipping | moderate |
| | WB | >6.5 | >200 | | 11 to 18 | | extensive |
| Element **I** | TB | 3 to 4 | 30 to 45 | complex fill | 6 to 10 | normal to flow | rare |
| | QB | 2 to 2.5 | 35 to 45 | | ~11 | | |
| Element **II** | WB | 6.5 to 16 | 30 to >150 long 50 to >180 wide | complex fill | 5 to 19 | cross- & downflow dipping | extensive |

Figures 7.2A and 7.2B compare the architectural arrangement of facies and elements in wandering rivers derived from Squamish and Fraser River data to Miall's (1996) depositional model. The depiction of Squamish and Fraser River architecture is a synthetic collage of representative subsurface and surficial elements illustrating some of the controls on channel bar development and in this sense it is a generalized simplification of naturally complex systems.

Both Figs. 7.2A and 7.2B show assemblages of lateral (LA) and downstream accretion (DA) strata. Although they are prominent stratal geometries in the stratigraphy of wandering rivers, they are only two of the four varieties of stratified, gravelly sheet-like deposits found in this study. Vertical accretion can only be identified from the presence of subhorizontal, subparallel reflections in three-dimensions, because the 2D, flow-normal signatures of lateral, downstream, upstream, and slipface accretion also reveal geometrically similar reflections. The four facies (vertical, lateral, downstream, and upstream accretion) expose the low-angle character of bar surfaces, for together they tend to dominate the thicknesses of the radar stratigraphies.

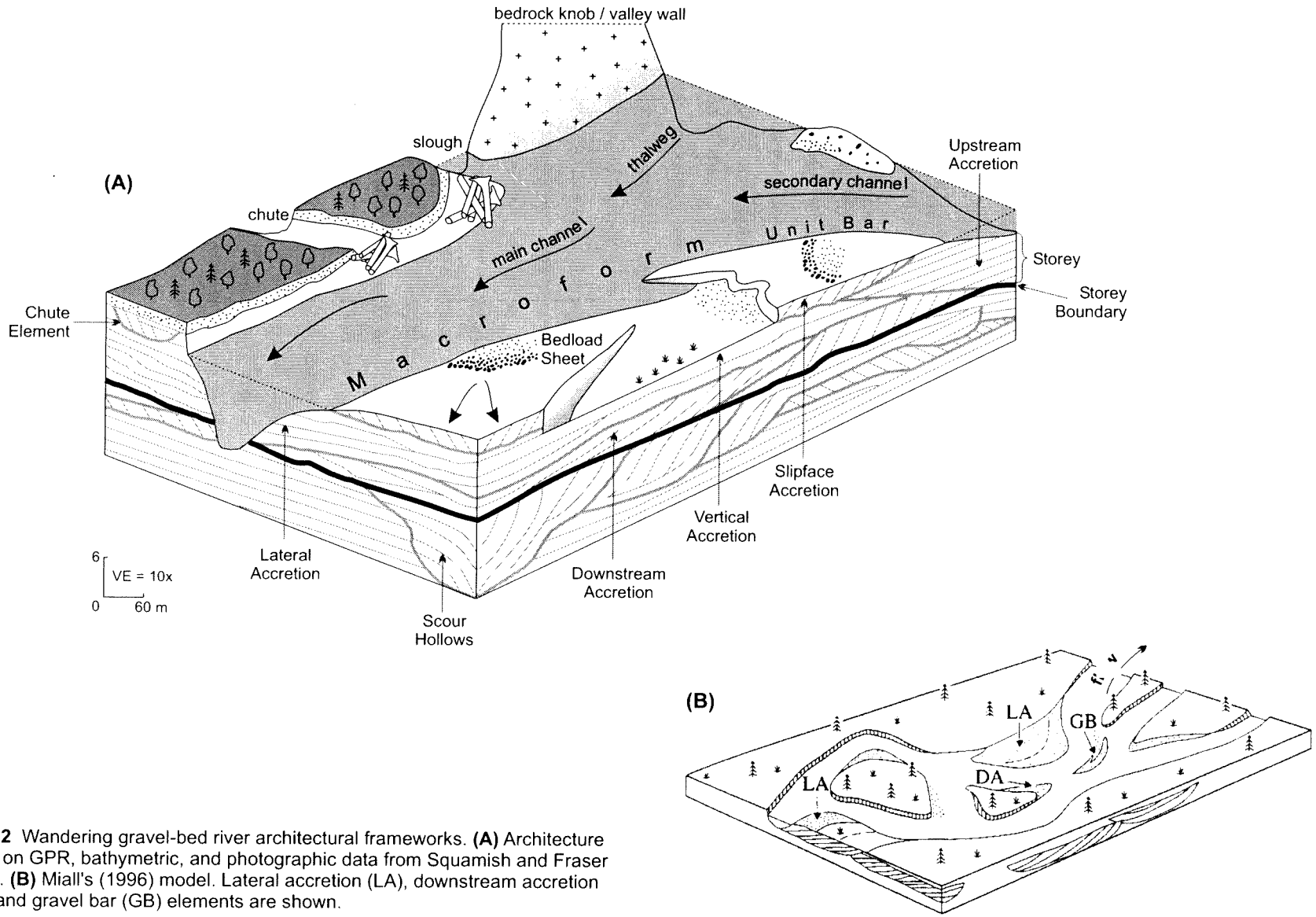


**Fig. 7.2** Wandering gravel-bed river architectural frameworks. **(A)** Architecture based on GPR, bathymetric, and photographic data from Squamish and Fraser Rivers. **(B)** Miall's (1996) model. Lateral accretion (LA), downstream accretion (DA), and gravel bar (GB) elements are shown.

Lateral and downstream accretion facies are identified in this study with respect to the known/modern orientation of the channel-belt. In the rock record, distinguishing the two facies without directional indicators such as well defined channel margins, scour hollows, or upstream accretion deposits would be problematic. Lateral accretion deposits dominate point bars (Calamity Bar) and are scaled to the depth of flow. Yet the facies is also found in mid-channel bar sediments (Wellington Bar), indicating that lateral accretion deposits cannot be used to uniquely reconstruct the position of barforms. Downstream accretion deposits typically thicken the downstream margin of barforms and in many cases grade out of slipface deposits. In this sense, they are the distal expression of barforms and can be used to reconstruct the transition from barforms into channel floor deposits. Both downstream and lateral accretion facies are characterized by offlapping reflection terminations. The occurrence of onlapping reflections in the upstream accretion facies serves to differentiate it from those two facies.

Roberts *et al.* (1997) also found lateral and downstream accretion radar facies to dominate the architecture of a small bar in the wandering gravel-bed Rhone River (Fig. 7.3A). The stratal geometry profiled was coincident with the lateral position of the bar, but the stratigraphy also showed scour surfaces extending over the entire bar surface. This implies that distinct stages of sedimentation contributed to the multi-directional growth of the barform, unlike Miall's (1996) conception of unidirectional growth being accomplished through the lateral accretion of sediment (Fig. 7.2B).

Channel and chute elements are rarely imaged. The absence of channel forms in Fraser River profiles is an artifact of the limited area profiled with GPR. For example, Fraser River channels are ~500 m wide and the longest GPR profile was 225 m. A further reason is the lack of paleochutes in the areas profiled. These conclusions become apparent from consideration of Squamish River profiles, in which channel and chute forms were profiled. The Squamish River is ~100 m wide, whereas GPR profiles were up to 260 m long, and paleochannels were evident in the photographic record on areas profiled with GPR.

Scour hollow elements are manifest on bathymetric soundings and subsurface profiles as isolated forms in the Fraser River, but are not imaged in Squamish River profiles. Although scour hollows persist in single thread Squamish River channels, the GPR profiles suggests that they do not over-deepen the stratigraphy to any noticeable extent in the former multiple channeled sections of the river. The downstream orientation of the element also records the regional paleoflow direction.

Bar-margin slipface deposits are found as discrete facies and also grading laterally into and out of horizontal sheet-like deposits as well as downstream accretion facies. The facies completely dominates some unit bars and is preserved in the deeper stratigraphies of some sites. Slipfaces clearly record local paleoflow directions, but determinations of regional paleoflow directions (with respect to the axis of the channel-belt) reveal either downflow or crossflow directions. In contrast, Miall's (1996) model shows minor amounts of slipface deposits within the gravel bars and bedforms (GB) architectural element (Fig. 7.2B). The element is a tabular body, in which horizontal to subhorizontal bounding surfaces separate massive or crudely stratified gravel from planar tabular cross-stratified gravel, or trough cross-stratified gravel. Sandy bedforms are commonly interstratified with the gravelly strata (Miall, 1988).

In all, Miall's (1996) depiction of gravel bars excludes the dynamic nature of mid-channel bar sedimentation, which records diverging flow directions and differential sedimentation in main and secondary channels on either side of the barhead. Further, the architecture is too simplistic as it does not accommodate issues of scour, the variable scale of facies, and the diversity of accretionary styles.

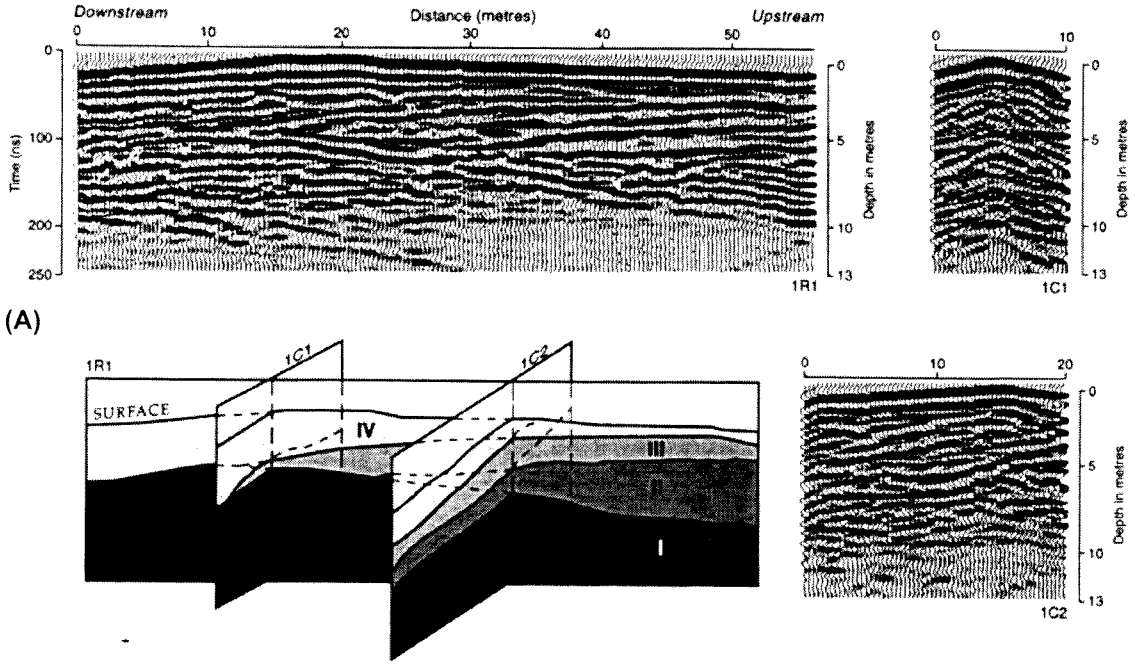


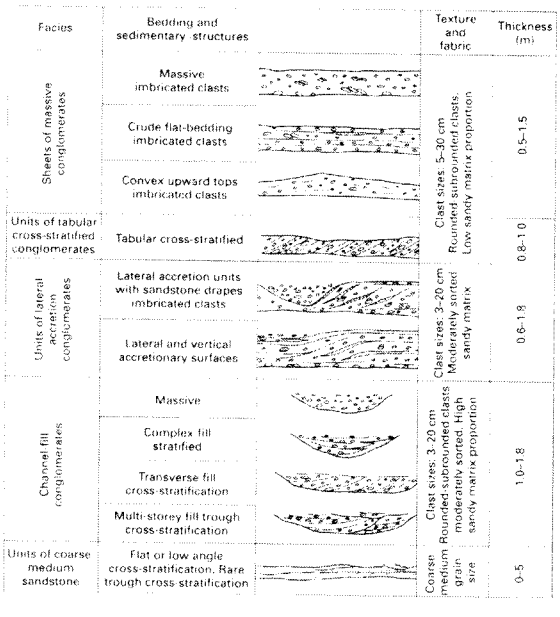


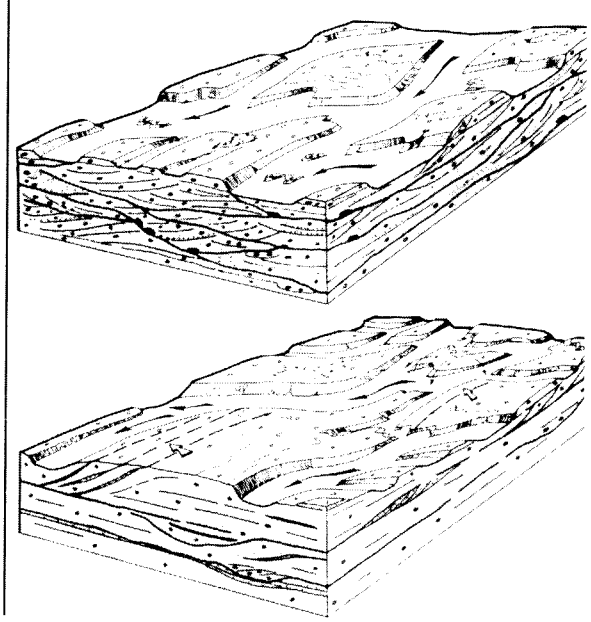


**Fig. 7.3** Wandering gravel-bed river GPR profiles, and braiding river stratification and architecture. **(A)** 100 MHz GPR profiles of a gravel bar in the wandering gravel-bed Rhone River, France. I through IV are inferred stages of bar development. Stage IV is the most recent stage of sedimentation (from Roberts *et al.*, 1997). **(B)** Conglomeratic stratification types interpreted as depositional facies in an ancient braiding river, and **(C)** its reconstructed architecture (from Ramos and Sopena, 1983).

## 7.4 Paleohydraulic Interpretations of Fluvial Style

Interpreting the paleohydraulic regime of gravelly successions in the subsurface is largely dependent on the selective preservation of radar facies, elements, and facies associations. The hydraulic regime of wandering rivers shows a multiple channeled planform of intermediate sinuosity, but does the stratigraphy of wandering rivers also confer these properties? Further, can wandering river deposits be distinguished from braiding and meandering river styles of sedimentation?

### 7.4.1 Multiple Channeled, Intermediate Sinuosity Depositional Style

To answer the question of multiple channels, evidence is found in the dip directions of inclined reflections which can differ from set to set by ~90° within, and between storeys. This points to multiple flow directions transporting sediment over a site during different stages of barform development. The sinuosity of the channel system cannot be readily determined due to the limited scale of the radar profiles. Still, the unidirectional orientation of continuous sets of migrating scour hollows and downstream accretion deposits (with respect to the channel-belt) do suggest deposition within low sinuosity river systems.

### 7.4.2 Wandering River Depositional Style

In order to determine if wandering rivers display a depositional style that is unique and different from braiding and meandering rivers, characteristic in-channel reflection configurations and facies associations are compared between the three planforms to differentiate depositional environments.

The assemblage of gravelly stratification types defined by Ramos and Sopena (1983) for braiding successions (Fig. 7.3B) is remarkably similar to facies and elements identified in this study (Fig. 7.1). The two river types can be differentiated, however, as braiding architectures lack the high proportion of slipface deposits found in wandering rivers (Fig. 7.3C). The wandering architecture depicts more geometrical relief within each element and facies, but this difference is likely attributable to differences in river scale rather than river style.

Braiding river deposits are dominated by concave-up strata, but also display limited sets of steeply dipping, inclined strata (Fahnestock and Bradley, 1973; Smith, 1974), which are common in wandering rivers. Steeply dipping, planar cross-stratification not only indicates the former positions of high relief bar-margins, but it also documents deeper flow regimes because bar-margin slipfaces only develop if the flow depth to grain-size ratio is >10 (Smith, 1985).

In contrast, multiple channeled braiding fluvial style in the rock record is usually interpreted for deposits displaying lenticular, massive conglomerate (typically interpreted as longitudinal bars) with numerous shallow (1 to 2 m thick) and narrow (2 to 15 m wide) concave-up forms that crosscut each other (Ori, 1982). Flow directions vary within sets, giving evidence of multiple flow directions at different stages.

Radar images of ancient (Vandenberghe and van Overmeeren, 1999) and modern (Ekes, 2000) braiding systems also show similar concave-up structures and an abundance of horizontal to subhorizontal reflection configurations (Figs. 7.4A and 7.4B). In general, such deposits are interpreted as extensive thin sheets deposited in unconfined, continuously shifting, shallow braiding streams (Minter, 1978) and are not found in meandering stream deposits.

Wandering river deposits are dominated to some extent by subhorizontal reflections and in this respect are very similar to braiding river deposits. It has been suggested that bedload sheets and low relief bedforms infilling channels or forming bars indicate shallow water depths and by consequence imply a braiding style of river development (Hein and Walker, 1977; Minter, 1978; Morison and Hein, 1987; Lunt *et al.*, 2001). Yet, bedload sheets are also identified on bar surfaces in deep, gravel-bed rivers, such as the Fraser River (Figs. 1.2B and 5.2A). This implies that they are ubiquitous deposits in gravel-bed rivers, and in this sense bedload sheets cannot be used to infer water depths as they also are found at all stratigraphic levels in ancient deposits.

Point bars, characterized by low-angle, lateral accretion surfaces, certainly dominate meandering river deposits (Nanson, 1980) and in effect serve to set them apart from braiding and wandering river stratigraphies. Point bars are also found in modern braiding streams (Smith, 1974; Lunt *et al.*, 2001), ancient braiding deposits (Ori, 1982), and in wandering rivers (*e.g.*, Calamity Bar), but they are limited features in these river types. For example, Ori (1982) found evidence of braid bar deposits intertonguing with gravelly, sigmoid, tabular bodies (1 to 4 m thick, dipping 5 to 13°, 10 to 50 m wide). Ori (1982) interpreted the tabular bodies as point bar deposits in a braiding river succession.

Although braiding rivers also contain moderate amounts of low-angle downstream accretion facies, it is the widespread and pervasive nature of high- and low-angle dipping strata that distinguishes wandering river stratigraphies from braiding and meandering river sediments. As can be seen from the previous discussion, wandering and braiding rivers deposit many of the same sedimentary facies, but it is the total sum of the facies and their spatial abundance that grants wandering rivers a unique style of deposition.

## 7.5 Late Quaternary Implications

The presence of large-scale (>6.5 m thick), steeply inclined (11 to 28°) reflections (radar facies 6), found beneath alluvial deposits in both the Fraser and Squamish Rivers are interpreted to be deltaic foresets. They record the former positions of delta fronts prograding down the flooded Fraser and Squamish Valleys. Raised deltas are present in many coastal valleys in southwest BC, and have been interpreted to represent deposition in the late Pleistocene deglacial period at a time when sea level was higher than at present (Friele *et al.*, 1999). The timing of deltaic sedimentation can be determined by matching the elevation of the top of the buried deltas to relative sea level curves spanning the deglacial period.

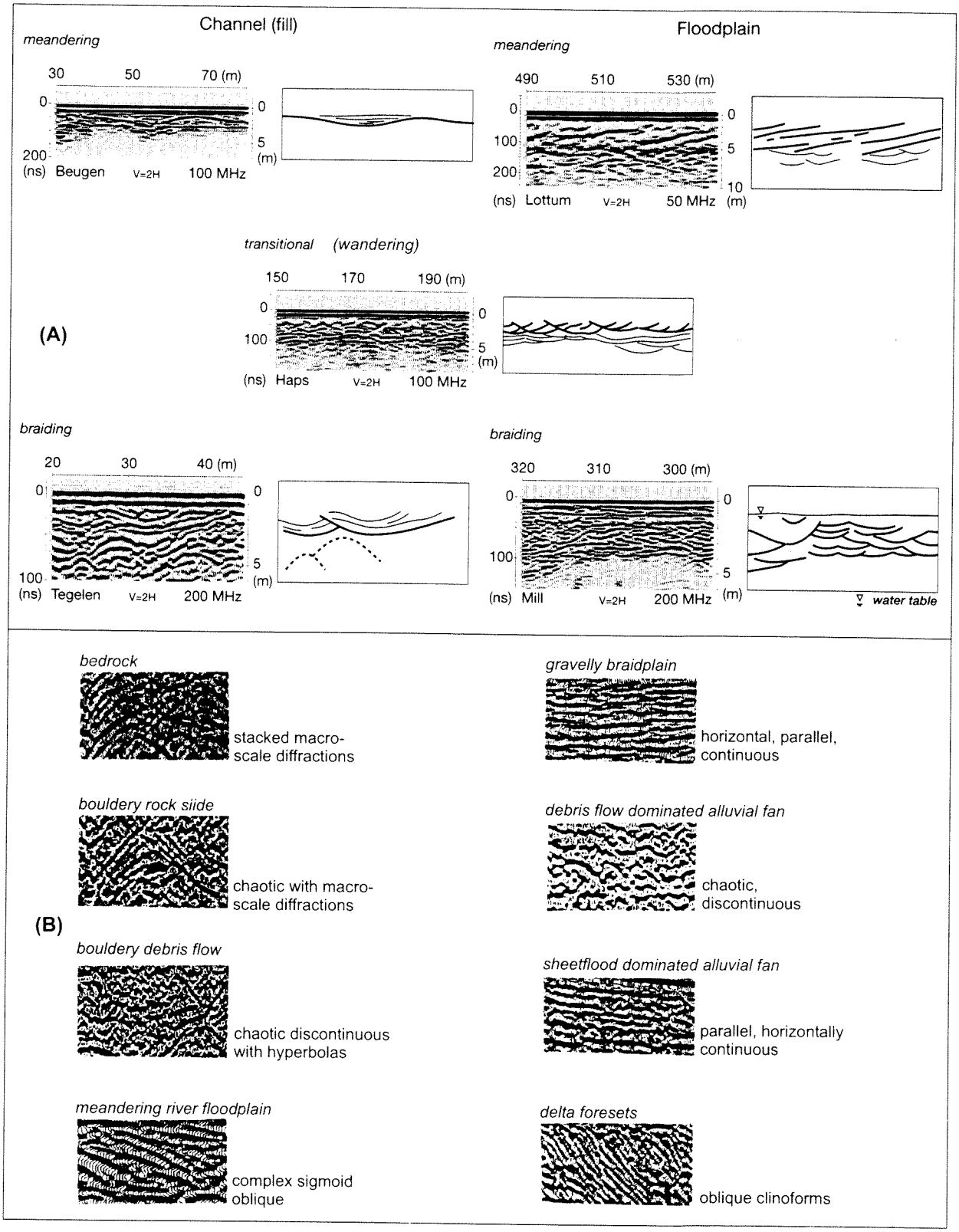


**Fig. 7.4** Radar images of braiding, meandering, and wandering river types. **(A)** Radar configurations imaged in braiding, meandering, and wandering river channel and floodplain sediments from the Maas Valley, Netherlands (from Vandenberghe and van Overmeeren, 1999). **(B)** British Columbia examples of alluvial and colluvial radar configurations including meandering, braiding, and deltaic depositional styles. Each image is 6 to 10 m thick (from Ekes, 2000).

### 7.5.1 Squamish River

The radar facies is similar to Ekes and Hickin's (2001) 10 to 20 m thick, steeply dipping (15° to 25°) oblique clinoform facies overlain by the Cheekye Fan. They interpreted the facies as delta foresets (Fig. 7.4B). Their results are significant because the paraglacial Cheekye Fan impinges on the Squamish River 20 km downstream from TFLENT Bar at the head of Howe Sound. This means that the deltaic sediments Ekes and Hickin (2001) documented were likely coeval with deglacial marine flooding and delta formation in the main trunk of the Squamish Valley. They found the top of the foresets (topset-foreset boundary) between 48 and -10 m elevation, reflecting delta progradation during relative sea level fall commensurate with glacial retreat. Friele *et al.* (1999) dated foresets at 45 m elevation at 11 900 years ago (10 200 $^{14}$Cyr BP; $^{14}$C ages calibrated using procedure of Stuiver *et al.* (1998)). It is interesting to compare this date with James *et al.* (*in press*) revised sea level curve for the Fraser Lowland, which shows sea level reached 45 m about 13 500 years ago (11 600 to 11 340 $^{14}$Cyr BP) (Fig. 7.5). The discrepancy in age implies that the Squamish Valley became ice-free more than 1300 years later than the Fraser Lowland. This is consistent with ideas regarding the differential decay of the Cordilleran ice sheet (Friele and Clague, 2002).

Friele and Clague (2002) indicate sea level stood at 30 m elevation about 11 200 years ago (9830 $^{14}$Cyr BP). This can be taken as the maximum date of delta formation at the 25.5 m elevation TFLENT site. Since that time ~8.5 m of alluvial sediment have been deposited, which gives a minimum alluvial aggradation rate of ~0.8 mm a$^{-1}$. The identification of delta foresets confirms Hickin's (1989) calculations (based on contemporary Squamish River sedimentation rates) that the Squamish River delta front was located at the Ashlu-Squamish confluence some 6000 ± 1500 years ago. This study furthers Hickin's (1989) predictions, in demonstrating that Howe Sound extended somewhat further upvalley (beyond the Ashlu River confluence) during the Holocene.

### 7.5.2 Fraser River

The depth to the top of the foresets beneath the Fraser River sediments is about -10 m elevation. This implies that the delta was building out at a time when relative sea level was lower than at present. The timing of relative sea level fall around -10 m elevation is not well defined on sea level curves (Fig. 7.5), but was likely reached between 11 400 and 10 200 years ago (10 000 to 9000 $^{14}$Cyr BP; Williams and Roberts, 1989; James *et al.*, *in press*). The foreset reflections appear to be truncated. This means that the delta was graded to a higher sea level when it was deposited, implying that sedimentation commenced slightly earlier. It is difficult to reconstruct the original upper surface of the foresets or to gain an approximation of the depth of fluvial incision. Yet if 5 m of foresets were eroded, the timing of deposition would be very similar to that stated above. Assuming that the Wellington Bar site was graded to sea level 10 200 years ago, fluvial sedimentation since that time has deposited ~17 m of sediment, giving an alluvial aggradation rate of ~1.7 mm a$^{-1}$.

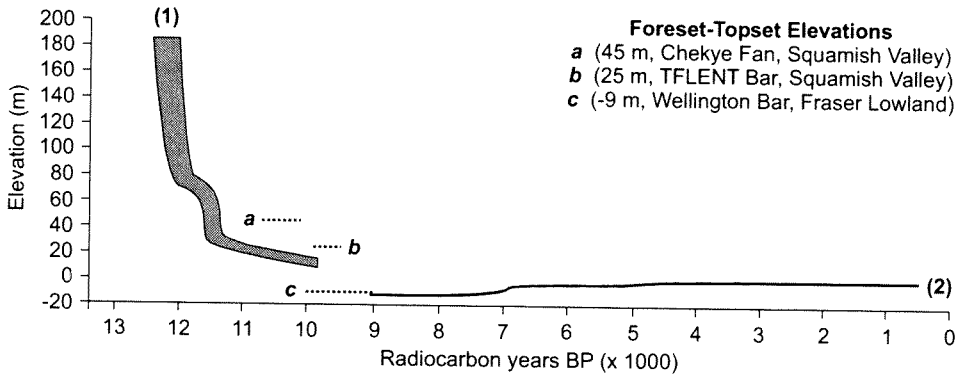


**Fig. 7.5** Age-elevation plot of inferred sea level curve (shaded) for the Fraser Lowland. Dashed lines indicate the approximate timing of the transition from deltaic to alluvial sedimentation (foreset-topset elevations) for Cheekye Fan and TFLENT Bar in the Squamish Valley, and Wellington Bar in the Fraser Lowland. Cheekye Fan sediments were dated at ~10 200 BP, indicating that deglaciation occurred later in the Squamish Valley than in the Fraser Lowland. Curve (1) redrawn from James *et al.* (*in press*) and curve (2) from Williams and Roberts (1989).

### 7.5.3 Preservation Potential

Morningstar (1987) and Passmore and Macklin (2000) provide evidence of floodplain building over the last 3000 years in wandering gravel-bed systems, while Desloges and Church (1987) postulate that the wandering style of the Bella Coola River has persisted during most of the Holocene. This postulation is confirmed by Squamish and Fraser River stratigraphies and is likely true of many coastal British Columbia gravel-bed river systems.

The style of sedimentation during this time does not appear to have varied much from its present form. Yet, climatic conditions, base level, and sediment supply have changed greatly. Although inferences about previous climatic regimes are typically interpreted from the style of channel deposits (*e.g.*, debris flow deposits; Miall, 1996), the radar stratigraphy records continuous alluvial sedimentation and does not capture the transition from a cool and moist climate (shortly following deglaciation), to warm and dry conditions (~10 000 years ago), and its return to cool and moist conditions (Lian and Hickin, 1996). It is questionable whether such transitions produced a change in the style of channel deposits in large, perennial rivers such as the Squamish and Fraser Rivers. Base levels have increased almost 13 m since alluvial sedimentation commenced and should have intimately affected the style of deposition. As relative sea level rose, channel slopes should have declined thus reducing the energy gradient and transport competence of the river systems (Schumm, 1993). This should have resulted in a fining-up trend from coarser-stratified channel deposits to finer-grained deposits. Systems like the Fraser River, however, are prograding alluvial fans, in which grain-size trends typically coarsen-up as the fan builds seaward. In either scenario it is unlikely the radar data could distinguish subtle grain-size trends without considerable time spent calibrating the GPR data. The supply of glacially derived sediment has declined measurably during the Holocene and should have led to a decline in channel switching and an increase in channel stability. This implies that both river systems evolved from braiding to wandering regimes, in which bed-material sediment discharge is intermediate between braiding and meandering rivers (Desloges and Church, 1987). Yet, there is little evidence of braiding architectures preserved in the alluvial successions.

The apparent lack of sedimentary evidence for these changes lies in the nature of basin subsidence and the aggradational regime of these rivers. When basin subsidence is low, sedimentation rates are also low and avulsion frequency declines giving more time for fluvial action to rework the channel-belt and bars (Ramos and Sopena, 1983). This results in more coarse-grained channel deposits and increases channel stacking densities (Ashworth *et al.*, 2001). In contrast, the storey architecture is largely depositional when tectonic uplift is the forcing mechanism. Uplift increases sedimentation rates, which in turn, causes channels to aggrade more rapidly, avulse more often, and cause a decline in channel stacking densities (Ashworth *et al.*, 2001).

Although the Bella Coola River has been in-place for almost 10 000 years, Desloges and Church (1987) suggest that its sedimentary deposits would not be prominent in the stratigraphic record because its non-aggradational nature results in long-term vertical stability. The Squamish and Fraser Rivers provide evidence in favor of Desloges and Church's (1987) ideas about the long-term vertical stability of these river systems, even in cases such as the Chilliwack Reach in the Fraser River, which is currently aggrading. The low aggradation rates and multistorey character of the alluvial fill suggest that sediments have been repetitively reworked in-channel, effectively removing any evidence of previous channel

behavior. The lateral instability of wandering rivers also reworks floodplain sediments and Morningstar (1987) showed that more than half of the Fraser River floodplain (the northern half) had been constructed within 2400 $^{14}$Cyr BP. Morningstar (1987) calculated floodplain migration rates between 2.1 and 2.8 m $a^{-1}$, which if extrapolated to the entire floodplain suggest that the floodplain is less than 5000 years old. These migration rates are very similar to the long term rate of lateral accretion measured at Calamity Bar (2.2 m $a^{-1}$), and floodplain migration rates determined by Desloges and Church (1987) for the Bella Coola River (3.0 to 3.5 m $a^{-1}$).

Sedimentation rates are very difficult to quantify as gravel tends to move in discrete pulses (waves) of sediment and gravel transport functions appear to behave exponentially above the critical threshold of motion for gravel (McLean *et al.*, 1999). This means that sedimentation rates likely vary regionally along the channel axis and by consequence so does avulsion frequency. Thus, the identification of low and high sedimentation rates from subsurface profiles may simply be a function of the timing of sediment waves migrating through the system and their resulting preservation.

Desloges and Church (1987) also hypothesize that during burial the gravel facies would be preserved, but the sand facies (that are diagnostic of wandering rivers) would be stripped during flood rendering inaccurate interpretations of the sedimentary record and of its wandering style. Clearly, the gravelly stratigraphic evidence presented rebukes this notion and suggests that gravelly in-channel wandering river deposits are distinct from other depositional environments preserved in the rock record.

## 7.6 Conclusions

The results presented here provide the first radar stratigraphic record of Holocene sedimentation and macroform development in the wandering gravel-bed Fraser and Squamish Rivers. Ground-penetrating radar profiles detail the alluvial architectures built on top of, and eroded into deltaic sediments likely deposited ~10,000 years ago when both coastal valleys were drowned by higher relative sea levels during deglaciation. The radar stratigraphy images the multistorey nature of macroform development, from basal scour surfaces to bartop deposits. The upper storeys are generally correlated to some 50 years of channel and bar changes (ending in 2001) mapped from bathymetric soundings and time-sequential aerial photographs. Equivalence between bar architecture and morphology implies that stratal configurations in the multistorey architecture reveal former flow and sediment transport directions. Deeper alluvial stratigraphic configurations are incongruent with the mapped morphological development of barforms, suggesting that bounding surfaces separate storeys that record the prior evolution of macroforms and paleochannels.

Storeys are composed of up to five radar facies and two radar elements. Elements and facies are *only* uniquely identified by their three-dimensional configurations, as many of the facies appear similar in two-dimensions. The alluvial facies record a style of deposition dominated by low-angle, sheet-like sedimentation, juxtaposed with steeply dipping bar-margin slipface deposits. Scour hollow, and channel and chute elements rarely occur in the stratigraphy. The scale and geometry of radar facies and elements between and within storeys is roughly similar (within each river system), implying that the style of sedimentation has remained largely unchanged throughout the last few hundred years. Scaling relationships are complicated by the fact that although sheet-like sediments and scour hollows largely

scale to the depth of flow, slipface deposits do not. Further, the variable lateral extent of facies also suggests a lack of scaling relationships. Instead, the lateral extent and thickness of facies reflect the degree of channel reworking and position of the sedimentary body in the channel.

The radar stratigraphy also shows different scales of channel bars. Smaller-scale unit bars can be differentiated from macroforms by the close correspondence between their architectures and morphologies. In this case, the sedimentary record of unit bars preserves genetically related sediments that are tied directly to their morphological expression enabling their geometries to be reconstructed, before they are reworked. Although macroforms are also morphologically distinct sedimentary bodies, their stratigraphy is ambiguous as it is composed of genetically unrelated strata. Macroforms are neither deposited nor reformed by singular flow events. Instead, their development proceeds serially by the attachment, agglomeration, and erosion of sediment, which fundamentally limits 3D reconstructions of past bar evolution.

This study extends Roberts *et al.* (1997) radar stratigraphy of channel bars in wandering gravel-bed rivers. The study also gives a coherent picture of the multistorey radar stratigraphy of unit bars and macroform architectures, integrated with the evolution of these barforms. In all, the radar stratigraphy provides a glimpse into gravelly macroform architecture and speaks to the difficulty of delineating discrete macroforms in stratigraphic sections, radar or conglomeratic. The facies assemblage and morphology of wandering systems clearly differentiate the planform from braiding or meandering rivers and position it as a gradational member in a continuum of channel types.

## 7.7 Future Work

Future work on wandering systems, in particular the Fraser and Squamish Rivers, needs to address the issue of geologic control to support inferences made from geophysical (GPR) data. Subsurface data from drill core together with some shallow exposures in trenches are needed to provide information on vertical and horizontal grain-size distributions. These data not only provide direct evidence of the sedimentary character of the deposits, but can also be used to corroborate sedimentary structures identified in the GPR profiles. In total, this work will better permit a fuller description of fluvial deposits, from which a better understanding of the processes can be gained.

More GPR work is also necessary to better resolve and image the shallow sedimentary structure of bartops as well as the deeper alluvial/deltaic features. This will give a regional perspective of how these river systems have evolved in the postglacial period. The shallow images require 900 MHz or 1GHz antennas and the deeper stratigraphy can only be resolved with 12.5 or 25 MHz antennas or shallow seismic profiling. The study area needs to be broadened to include channel bars in the eastern reaches of the Fraser River, such as Powerline Island, and in the more northerly section of the wandering Squamish River reach. This will provide for comparisons between the bars already studied (whose stratigraphies are predominately depositional in character), and other bars that show an episodic history of repetitive scour and fill. The larger data set should serve to determine if similar processes and the style of deposition is equivalent throughout the Fraser and Squamish River systems. From this, a more complete characterization of wandering gravel-bed architecture can be derived, together with a more detailed elucidation of bar-forming mechanisms.

# Appendix 1 GPR Profiles

Appendix 1 contains 50, 100, and 200 MHz GPR profiles shot on each bar (written to a CD in *.pdf format).

| | Line | Length (m) |
|---|---|---|
| TFLENT Bar *Squamish River* | a | 260 |
| | b | 260 |
| | d | 260 |
| | e | 50 |
| | f | 75 |
| | g | 85 |
| | h | 65 |
| | i. | 160 |
| | k | 160 |
| Calamity Bar *Fraser River* | a | 220 |
| | b | 145 |
| | d | 80 |
| | g | 130 |
| | h | 60 |
| | i. | 120 |
| | j | 120 |
| Queens Bar Inner Channel site *Fraser River* | h | 85 |
| | i. | 40 |
| | j | 224 |
| | k | 50 |
| | l | 105 |
| | m | 16 |
| | n | 45 |
| | o | 55 |
| | p | 45 |
| Queens Bar Bar Tail site *Fraser River* | a | 100 |
| | b | 100 |
| | r | 125 |
| | s | 140 |
| | t | 100 |
| | u | 40 |
| | v | 40 |
| | w | 125 |
| | x | 100 |
| | y | 155 |

| | Line | Length (m) |
|---|---|---|
| Queens Bar Mid Bar site *Fraser River* | d | 60 |
| | e | 70 |
| | f | 45 |
| | g | 45 |
| Wellington Bar *Fraser River* | a | 200 |
| | b | 80 |
| | d | 100 |
| | e | 80 |
| | f | 200 |
| | g | 100 |
| | h | 100 |
| | i. | 100 |
| | k* | 100 |
| | m* | 100 |

* 50 MHz profiles only (100 and 200 MHz profiles were not shot).

# References


Allen, J. R. L. (1983) Studies in fluviatile sedimentation: bars, bar-complexes and sandstone sheets (low-sinuosity braided streams) in the Brownstones (L. Devonian), Welsh Borders. *Sedimentary Geology*, **33**, 237-293.

Ashley, G. M. (1990) Classification of large-scale subaqueous bedforms: a new look at an old problem. *Journal of Sedimentary Petrology*, **60**(1), 160-172.

Ashmore, P. E. (1991) How do gravel-bed rivers braid? *Canadian Journal of Earth Sciences*, **28**, 326-341.

Ashmore, P. E. (1993) Anabranch confluence kinetics and sedimentation processes in gravel-braided streams. In: *Braided rivers* (Ed. by J. L. Best and C. S. Bristow), pp. 129-146. Geological Society Special Publication 75, London.

Ashworth, P. J. (1996) Mid-channel bar growth and its relationship to local flow strength and direction. *Earth Surface Processes and Landforms*, **21**, 103-123.

Ashworth, P., Jones, M. & Best, J. (2001) The influence of sediment supply and aggradation rate on the alluvial architecture of braided rivers. In: *Fluvial Sedimentology 2001, Seventh International Conference on Fluvial Sedimentology, Program and Abstracts*, pp. 48, Lincoln, Nebraska.

Bano, M., Marquis, G., Niviere, B., Maurin, J. C. & Cushing, M. (2000) Investigating alluvial and tectonic features with ground-penetrating radar and analyzing diffractions patterns. *Journal of Applied Geophysics*, **43**, 33-41.

Bennett, S. J. & Bridge, J. S. (1995) The geometry and dynamics of low-relief bed forms in heterogeneous sediment in a laboratory channel, and their relationship to water flow and sediment transport. *Journal of Sedimentary Research*, **A65**(1), 29-39.

Beres, M. & Haeni, F. P. (1991) Application of ground-penetrating-radar methods in hydrogeologic studies. *Ground Water*, **29**(3), 375-386.

Beres, M., Green, A., Huggenberger, P. & Horstmeyer, H. (1995) Mapping the architecture of glaciofluvial sediments with three-dimensional georadar. *Geology*, **23**(12), 1087-1090.

Beres, M., Huggenberger, P., Green, A. G. & Horstmeyer, H. (1999) Using two- and three-dimensional georadar methods to characterize glaciofluvial architecture. *Sedimentary Geology*, **129**, 1-24.

Best, J. L. (1987) Flow dynamics at river channel confluences: implications for sediment transport and bed morphology. In: *Recent developments in fluvial sedimentology* (Ed. by F. G. Ethridge, R. M. Flores and M. D. Harvey), pp. 27-35. Society of Economic Paleontologists and Mineralogists Special Publication 39.

Best, J. L. & Ashworth, P. J. (1997) Scour in large braided rivers and the recognition of sequence stratigraphic boundaries. *Nature*, **387**, 275-277.

Billi, P., Magi, M. & Sagri, M. (1987) Coarse-grained low-sinuosity river deposits: example from Plio-Pleistocene Valdarno basin, Italy. In: *Recent developments in fluvial sedimentology* (Ed. by F. G. Ethridge, R. M. Flores and M. D. Harvey), pp. 197-203. Society of Economic Paleontologists and Mineralogists Special Publication 39.

Boggs, S. (1995) *Principles of Sedimentology and Stratigraphy*. Prentice Hall, New Jersey, 774 pp.

Boniface, C. (1985) *Vegetation succession on mid-channel bars of the Fraser River, British Columbia*. MSc Thesis, Department of Geography, Simon Fraser University, Burnaby, 137 pp.

Bridge, J. S. (1993a) Description and interpretation of fluvial deposits: a critical perspective. *Sedimentology*, **40**, 801-810.

Bridge, J. S. (1993b) The interaction between channel geometry, water flow, sediment transport and deposition in braided rivers. In: *Braided rivers* (Ed. by J. L. Best and C. S. Bristow), pp. 13-71. Geological Society Special Publication 75, London.

Bridge, J. S. & Mackey, S. D. (1993a) A revised alluvial stratigraphy model. In: *Alluvial Sedimentation* (Ed. by M. Marzo and C. Puigdefabregas), pp. 319-336. International Association of Sedimentologists Special Publication 17, Oxford.

Bridge, J. S. & Mackey, S. D. (1993b) A theoretical study of fluvial sandstone body dimensions. In: *The geological modelling of hydrocarbon reservoirs* (Ed. by S. Flint and I. D. Bryant), pp. 213-236. International Association of Sedimentologists Special Publication 15, Oxford.

Bridge, J. S. & Tye, R. S. (2000) Interpreting the dimensions of ancient fluvial channel bars, channels, and channel belts from wireline-logs and cores. *AAPG Bulletin*, **84**(8), 1205-1228.

Bridge, J. S., Alexander, J., Collier, R. E. L., Gawthorpe, R. L. & Jarvis, J. (1995) Ground-penetrating radar and coring used to study the large-scale structure of point-bar deposits in three dimensions. *Sedimentology*, **42**, 839-852.

Bridge, J. S., Collier, R. E. L. & Alexander, J. (1998) Large-scale structure of Calamus River deposits (Nebraska, USA) revealed using ground-penetrating radar. *Sedimentology*, **45**, 977-986.

Brierley, G. J. (1984) *Channel stability and downstream change in particle size on Squamish River, B.C.* MSc Thesis, Department of Geography, Simon Fraser University, Burnaby.

Brierley, G. J. (1989a) *The character of channel planform control on the morphology and sedimentology of the gravel-bed Squamish River floodplain, British Columbia.* PhD Thesis, Department of Geography, Simon Fraser University, Burnaby, 304 pp.

Brierley, G. J. (1989b) River planform facies models: the sedimentology of braided, wandering and meandering reaches of the Squamish River, British Columbia. *Sedimentary Geology*, **61**, 17-35.

Brierley, G. J. (1991a) Bar sedimentology of the Squamish River, British Columbia: definition and application of morphostratigraphic units. *Journal of Sedimentary Petrology*, **61**(2), 211-225.

Brierley, G. J. (1991b) Floodplain sedimentology of the Squamish River, British Columbia: relevance of element analysis. *Sedimentology*, **38**, 735-750.

Brierley, G. J. & Hickin, E. J. (1985) The downstream gradation of particle sizes in the Squamish River, British Columbia. *Earth Surface Processes and Landforms*, **10**, 597-606.

Brierley, G. J. & Hickin, E. J. (1991) Channel planform as a non-controlling factor in fluvial sedimentology: the case of the Squamish River flooplain, British Columbia. *Sedimentary Geology*, **75**, 67-83.

Bristow, C. S. (1987) Brahmaputra River: channel migration and deposition. In: *Recent developments in fluvial sedimentology* (Ed. by F. G. Ethridge, R. M. Flores and M. D. Harvey), pp. 63-74. Society of Economic Paleontologists and Mineralogists Special Publication 39.

Bristow, C. S. (1993) Sedimentary structures exposed in bar tops in the Brahmaputra River, Bangladesh. In: *Braided rivers* (Ed. by J. L. Best and C. S. Bristow), pp. 277-289. Geological Society Special Publication 75, London.

Bristow, C. S. (1995) Facies analysis in the Lower Greensand using ground-penetrating radar. *Journal of the Geological Society, London*, **152**, 591-598.

Bristow, C. S., Skelly, R. L. & Ethridge, F. G. (1999) Crevasse splays from the rapidly aggrading, sand-bed, braided Niobrara River, Nebraska: effect of base-level rise. *Sedimentology*, **46**, 1029-1047.

Brooks, G. R. & Hickin, E. J. (1991) Debris avalanche impoundments of Squamish River, Mount Cayley area, southwestern British Columbia. *Canadian Journal of Earth Sciences*, **28**, 1375-1385.

Carling, P. A. (1990) Particle over-passing on depth-limited gravel bars. *Sedimentology*, **37**, 345-355.

Carling, P. A. (1996) Morphology, sedimentology and paleohydraulic significance of large gravel dunes, Altai Mountains, Siberia. *Sedimentology*, **43**, 647-664.

Carling, P. A. & Glaister, M. S. (1987) Rapid deposition of sand and gravel mixtures downstream of a negative step: the role of matrix-infilling and particle-overpassing in the process of bar-front accretion. *Journal of the Geological Society, London*, **144**, 543-551.

Church, M. (1983) Pattern of instability in a wandering gravel bed channel. In: *Modern and ancient fluvial systems* (Ed. by J. D. Collinson and J. Lewin), pp. 169-180. International Association of Sedimentologists Special Publication 6, Oxford.

Church, M. & Jones, D. (1982) Channel bars in gravel-bed rivers. In: *Gravel-bed rivers: fluvial processes, engineering and management* (Ed. by R. D. Hey, J. C. Bathurst and C. R. Thorne), pp. 291-338. John Wiley and Sons, Chichester.

Collinson, J. D. (1978) Vertical sequence and sand body shape in alluvial sequences. In: *Fluvial sedimentology* (Ed. by A. D. Miall), pp. 577-586. Canadian Society of Petroleum Geologists Memoir 5, Calgary.

Cowan, E. J. (1991) The large-scale architecture of the fluvial Westwater Canyon Member, Morison Formation (Upper Jurassic), San Juan Basin, New Mexico. In: *The three-dimensional facies architecture of terrigenous clastic sediments and its implications for hydrocarbon discovery and recovery* (Ed. by A. D. Miall and N. Tyler), pp. 80-93. Society of Economic Paleontologists and Mineralogists Concepts in Sedimentology and Paleontology 3, Tulsa.

Davis, J. L. & Annan, A. P. (1989) Ground-penetrating radar for high-resolution mapping of soil and rock stratigraphy. *Geophysical Prospecting*, **37**, 531-551.

Dawson, M. R. & Bryant, I. D. (1987) Three-dimensional facies geometry in Pleistocene outwash sediments, Worcestershire, U.K. In: *Recent developments in fluvial sedimentology* (Ed. by F. G. Ethridge, R. M. Flores and M. D. Harvey), pp. 191-196. Society of Economic Paleontologists and Mineralogists Special Publication 39.

Desloges, J. R. & Church, M. (1987) Channel and floodplain facies in a wandering gravel-bed river. In: *Recent developments in fluvial sedimentology* (Ed. by F. G. Ethridge, R. M. Flores and M. D. Harvey), pp. 99-109. Society of Economic Paleontologists and Mineralogists Special Publication 39.

Desloges, J. R. & Church, M. A. (1989) Canadian landform examples - 13: wandering gravel-bed rivers. *The Canadian Geographer*, **33**(4), 360-364.

Dietrich, W. E., Kirchner, J. W., Ikeda, H. & Iseya, F. (1989) Sediment supply and the development of the coarse surface layer in gravel-bedded rivers. *Nature*, **340**, 215-217.

Dinehart, R. L. (1989) Dune migration in a steep, coarse-bedded stream. *Water Resources Research*, **25**(5), 911-923.

Dix, C. H. (1955) Seismic velocities from surface measurements. *Geophysics*, **20**, 68-86.

Ekes, C. (2000) *Radar facies and architecture of alluvial fans and related sediments in high-energy alpine environments, British Columbia.* PhD Thesis, Department of Geography, Simon Fraser University, Burnaby, 217 pp.

Ekes, C. & Hickin, E. J. (2001) Ground penetrating radar facies of the paraglacial Cheekye Fan, southwestern British Columbia, Canada. *Sedimentary Geology*, **143**, 199-217.

Eynon, G. & Walker, R. G. (1974) Facies relationships in Pleistocene outwash gravels, southern Ontario: a model for bar growth in braided rivers. *Sedimentology*, **21**, 43-70.

Fahnestock, R. K. & Bradley, W. C. (1973) Knik and Matanuska Rivers, Alaska: a contrast in braiding. In: *Fluvial Geomorphology* (Ed. by M. Morisawa), pp. 220-250. Proceedings of 4th Geomorphology Symposia, State University of New York, Binghamton.

Forbes, D. L. (1983) Morphology and sedimentology of a sinuous gravel-bed channel system: lower Babbage River, Yukon coastal plain, Canada. In: *Modern and ancient fluvial systems* (Ed. by J. D. Collinson and J. Lewin), pp. 195-206. International Association of Sedimentologists Special Publication 6, Oxford.

Friele, P. A. & Clague, J. J. (2002) Readvance of glaciers in the British Columbia Coast Mountains at the end of the last glaciation. *Quaternary International*, **87**, 45-58.

Friele, P. A., Ekes, C. & Hickin, E. J. (1999) Evolution of Cheekye fan, Squamish, British Columbia: Holocene sedimentation and implications for hazard assessment. *Canadian Journal of Earth Sciences*, **36**, 2023-2031.

Friend, P. F. (1983) Towards the field classification of alluvial architecture or sequence. In: *Modern and ancient fluvial systems* (Ed. by J. D. Collinson and J. Lewin), pp. 345-354. International Association of Sedimentologists Special Publication 6, Oxford.

Gawthorpe, R. L., Collier, R. E. L., Alexander, J., Bridge, J. S. & Leeder, M. R. (1993) Ground penetrating radar: application to sandbody geometry and heterogeneity studies. In: *Characterization of fluvial and aeolian reservoirs* (Ed. by C. P. North and D. J. Prosser), pp. 421-432. Geological Society Special Publication 73, London.

Gottesfeld, A. S. & Gottesfeld, L. M. J. (1990) Floodplain dynamics of a wandering river, dendrochronology of the Morice River, British Columbia, Canada. *Geomorphology*, **3**, 159-179.

Gustavson, T. C. (1978) Bed forms and stratification types of modern gravel meander lobes, Nueces River, Texas. *Sedimentology*, **25**, 401-426.

Hein, F. J. & Walker, R. G. (1977) Bar evolution and development of stratification in the gravelly, braided, Kicking Horse River, British Columbia. *Canadian Journal of Earth Sciences*, **14**, 562-570.

Hickin, E. J. (1989) Contemporary Squamish River sediment flux to Howe Sound, British Columbia. *Canadian Journal of Earth Sciences*, **26**, 1953-1963.

Hickin, E. J. & Sichingabula, H. M. (1988) The geomorphic impact of the catastrophic October 1984 flood on the planform of Squamish River, southwestern British Columbia. *Canadian Journal of Earth Sciences*, **25**, 1078-1087.

Holbrook, J. (2001) Origin, genetic interrelationships, and stratigraphy over the continuum of fluvial channel-form bounding surfaces: an illustration from middle Cretaceous strata, southeastern Colorado. *Sedimentary Geology*, **144**, 179-222.

Huggenberger, P. (1993) Radar facies: recognition of facies patterns and heterogeneities within Pleistocene Rhine gravels, NE Switzerland. In: *Braided rivers* (Ed. by J. L. Best and C. S. Bristow), pp. 163-176. Geological Society Special Publication 75, London.

Huggenberger, P., Meier, E. & Beres, M. (1994) Three-dimensional geometry of fluvial gravel deposits from GPR reflection patterns; a comparison of results of three different antenna frequencies. In: *5th International Conference on Ground Penetrating Radar*, pp. 805-816, Kitchener, ON.

Jackson, R. G. (1975) Hierarchical attributes and a unifying model of bed forms composed of cohesionless material and produced by shearing flow. *Geological Society of America Bulletin*, **86**, 1523-1533.
James, T. S., Hutchinson, I. & Clague, J. J. (*in press*) Improved relative sea-level histories for Victoria and Vancouver from isolation basin coring. *Current Research*.
Jol, H. M. & Smith, D. G. (1991) Ground penetrating radar of northern lacustrine deltas. *Canadian Journal of Earth Sciences*, **28**, 1939-1947.
Judson, D. R., Schultz, P. S. & Sherwood, J. W. C. (1978) Equalizing the stacking velocities of dipping events via DEVILISH. In: *Presented at the 48th Annual International Meeting of the Society of Exploration Geophysics*. brochure published b Digicon Geophysical Corp., San Francisco.
Karpeta, W. P. (1993) Sedimentology and gravel bar morphology in an Archaean braided river sequence: the Witpan Conglomerate Member (Witwatersrand Supergroup) in the Welkom Goldfield, South Africa. In: *Braided rivers* (Ed. by J. L. Best and C. S. Bristow), pp. 369-388. Geological Society Special Publication 75, London.
Knighton, A. D. (1984) *Fluvial forms and processes*. Edward Arnold, London, 218 pp.
Kostaschuk, R. A. & McCann, S. B. (1983) Observations on delta-forming processes in a fjord-head delta, British Columbia, Canada. *Sedimentary Geology*, **36**, 269-288.
Leclerc, R. F. (1995) *Radar facies of a meandering river floodplain, North Thompson River, British Columbia*. MSc Thesis, Department of Geography, Simon Fraser University, Burnaby, 146 pp.
Leclerc, R. F. & Hickin, E. J. (1997) The internal structure of scrolled floodplain deposits based on ground-penetrating radar, North Thompson River, British Columbia. *Geomorphology*, **21**, 17-38.
Lewis, C. P. & McDonald, B. C. (1973) Rivers of the Yukon north slope. In: *Fluvial processes and sedimentation*, pp. 251-271. Proceedings of Hydrology Symposium, University of Alberta, Edmonton. National Research Council, Ottawa.
Leys, K. F. & Werritty, A. (1999) River channel planform change: software for historical analysis. *Geomorphology*, **29**, 107-120.
Lian, O. B. & Hickin, E. J. (1996) Early postglacial sedimentation of lower Seymour Valley, southwestern British Columbia. *Geographie physique et Quaternaire*, **50**(1), 95-102.
Livesey, J. R., Bennett, S., Ashworth, P. J. & Best, J. L. (1998) Flow structure, sediment transport and bedform dynamics for a bimodal sediment mixture. In: *Gravel-bed rivers in the environment* (Ed. by P. C. Klingeman, R. L. Beschta, P. D. Komar and J. B. Bradley), pp. 149-176. Water Resources Publications, LLC, Highlands Ranch, CO.
Lunt, I. A., Bridge, J. S. & Tye, R. S. (2001) A three-dimensional model of gravelly, braided river deposits based on trenches, cores, well logs, and ground-penetrating radar profiles. In: *Fluvial Sedimentology 2001, Seventh International Conference on Fluvial Sedimentology, Program and Abstracts*, pp. 181, Lincoln, Nebraska.
Massari, F. (1983) Tabular cross-bedding in Messinian fluvial channel conglomerates, Southern Alps, Italy. In: *Modern and ancient fluvial systems* (Ed. by J. D. Collinson and J. Lewin), pp. 287-300. International Association of Sedimentologists Special Publication 6, Oxford.
McLean, D. G. (1990) *The relation between channel instability and sediment transport on lower Fraser River*. PhD Thesis, Department of Geography, University of British Columbia, Vancouver, 272 pp.
McLean, D. G. & Church, M. (1999) Sediment transport along lower Fraser River. 2. Estimates based on the long-term gravel budget. *Water Resources Research*, **35**(8), 2549-2559.
McLean, D. G., Church, M. & Tassone, B. (1999) Sediment transport along lower Fraser River. 1. Measurements and hydraulic computations. *Water Resources Research*, **35**(8), 2533-2548.
Miall, A. D. (1985) Architectural-element analysis: a new method of facies analysis applied to fluvial deposits. *Earth-Science Reviews*, **22**, 261-308.
Miall, A. D. (1988) Reservoir heterogeneities in fluvial sandstones: lessons from outcrop studies. *American Association of Petroleum Geologists Bulletin*, **72**(6), 682-697.
Miall, A. D. (1994) Reconstructing fluvial macroform architecture from two-dimensional outcrops: examples from the Castlegate Sandstone, Book Cliffs, Utah. *Journal of Sedimentary Research*, **B64**(2), 146-158.
Miall, A. D. (1996) *The geology of fluvial deposits*. Springer, Berlin, 582 pp.
Miall, A. D. (2000) *Principles of sedimentary basin analysis*. Springer, Berlin, 616 pp.
Minter, W. E. L. (1978) A sedimentological synthesis of placer gold, uranium and pyrite concentrations in Proterozoic Witwatersrand sediments. In: *Fluvial sedimentology* (Ed. by A. D. Miall), pp. 801-829. Canadian Society of Petroleum Geologists Memoir 5, Calgary.
Mitchum, R. M., Vail, P. R. & Sangree, J. B. (1977) Seismic stratigraphy and global changes of sea level, Part 6: stratigraphic interpretation of seismic reflection patterns in depositional sequences. In: *Seismic stratigraphy - applications to hydrocarbon exploration* (Ed. by C. E. Payton), pp. 117-133. American Association of Petroleum Geologists, Memoir 26, Tulsa.

Moorman, B. J., Judge, A. S. & Smith, D. G. (1991) Examining fluvial sediments using ground penetrating radar in British Columbia. In: *Current Research, Part A*, pp. 31-36. Geological Survey of Canada, Paper 91-1A.

Morison, S. R. & Hein, F. J. (1987) Sedimentology of the White Channel gravels, Klondike area, Yukon Territory: fluvial deposits of a confined valley. In: *Recent developments in fluvial sedimentology* (Ed. by F. G. Ethridge, R. M. Flores and M. D. Harvey), pp. 205-216. Society of Economic Paleontologists and Mineralogists Special Publication 39.

Morningstar, O. R. (1987) *Floodplain construction and overbank deposition in a wandering reach of the Fraser River, Chilliwack, B.C.* MSc Thesis, Department of Geography, Simon Fraser University, Burnaby, 129 pp.

Naegeli, M. W., Huggenberger, P. & Uehlinger, U. (1996) Ground penetrating radar for assessing sediment structures in the hyporheic zone of a prealpine river. *Journal of the North American Benthological Society*, **15**(3), 353-366.

Nanson, G. C. (1980) Point bar and floodplain formation of the meandering Beatton River, northeastern British Columbia, Canada. *Sedimentology*, **27**, 3-29.

Neill, C. R. (1973) *Hydraulic and morphologic characteristics of Athabasca River near Fort Assiniboine.* Alberta Research Council, Edmonton, 23 pp.

Nemec, W. & Steel, R. J. (1984) Alluvial and coastal conglomerates: their significant features and some comments on gravelly mass-flow deposits. In: *Sedimentology of gravels and conglomerates* (Ed. by E. H. Koster and R. J. Steel), pp. 1-31. Canadian Society of Petroleum Geologists Memoir 10, Calgary.

Olsen, H. & Andreasen, F. (1995) Sedimentology and ground-penetrating radar characteristics of a Pleistocene sandur deposit. *Sedimentary Geology*, **99**, 1-15.

Ori, G. G. (1982) Braided to meandering channel patterns in humid-region alluvial fan deposits, River Reno, Po Plain (northern Italy). *Sedimentary Geology*, **31**, 231-248.

Paige, A. D. & Hickin, E. J. (2000) Annual bed-elevation regime in the alluvial channel of Squamish River, southwestern British Columbia, Canada. *Earth Surface Processes and Landforms*, **25**, 991-1009.

Passmore, D. G. & Macklin, M. G. (2000) Late Holocene channel and floodplain development in a wandering gravel-bed river: the River South Tyne at Lambley, northern England. *Earth Surface Processes and Landforms*, **25**, 1237-1256.

Pelpola, C. P. (2001) *Bed-material transport rate derived from delta progradation in a small alpine basin, Fitzsimmons Creek, Coast Mountains, British Columbia.* MSc Thesis, Department of Geography, Simon Fraser University, Burnaby, 153 pp.

Ramos, A. & Sopena, A. (1983) Gravel bars in low-sinuosity streams (Permian and Triassic, central Spain). In: *Modern and ancient fluvial systems* (Ed. by J. D. Collinson and J. Lewin), pp. 301-312. International Association of Sedimentologists Special Publication 6, Oxford.

Reynolds, J. M. (1997) *An introduction to applied and environmental geophysics.* John Wiley and Sons, Chichester, 796 pp.

Roberts, M. C. & Morningstar, O. R. (1989) Floodplain formation in a wandering gravel-bed river: Lower Franser River, British Columbia, Canada. *GeoArcheoRhein*, **2**, 63-70.

Roberts, M. C., Bravard, J.-P. & Jol, H. M. (1997) Radar signatures and structure of an avulsed channel: Rhone River, Aoste, France. *Journal of Quaternary Science*, **12**(1), 35-42.

Rust, A. C. & Russell, J. K. (2001) Mapping porosity variation in a welded pyroclastic deposit with signal and velocity patterns from ground-penetrating radar surveys. *Bulletin of Volcanology*, **62**(6/7), 457-463.

Salter, T. (1993) Fluvial scour and incision: models for their influence on the development of realistic reservoir geometries. In: *Characterization of fluvial and aeolian reservoirs* (Ed. by C. P. North and D. J. Prosser), pp. 33-51. Geological Society Special Publication 73, London.

Sambrook Smith, G. H., Ashworth, P. J., Best, J. L., Woodward, J. & Simpson, C. J. (*in review*) The morphology and facies of sandy braided rivers: some considerations of spatial and temporal scale invariance.

Schumm, S. A. (1993) River response to baselevel change: implications for sequence stratigraphy. *The Journal of Geology*, **101**, 279-294.

Sensors and Software (1996) *pulseEKKO IV User's Guide.* Sensors and Software Inc., Mississauga, ON, 59 pp.

Sichingabula, H. M. (1985) *Character and causes of channel changes on the Squamish River, southwestern British Columbia.* MSc Thesis, Department of Geography, Simon Fraser University, Burnaby, 156 pp.

Siegenthaler, C. & Huggenberger, P. (1993) Pleistocene Rhine gravel: deposits of a braided river system with dominant pool preservation. In: *Braided rivers* (Ed. by J. L. Best and C. S. Bristow), pp. 147-162. Geological Society Special Publication 75, London.

Smith, D. G. (1991) Canadian landform examples - 22: lacustrine deltas. *The Canadian Geographer*, **35**(3), 311-316.
Smith, D. G. & Jol, H. M. (1992) Ground-penetrating radar investigation of a Lake Bonneville delta, Provo level, Brigham City, Utah. *Geology*, **20**, 1083-1086.
Smith, D. G. & Jol, H. M. (1995) Ground penetrating radar: antenna frequencies and maximum probable depths of penetration in Quaternary sediments. *Journal of Applied Geophysics*, **33**, 93-100.
Smith, D. G. & Jol, H. M. (1997) Radar structure of a Gilbert-type delta, Peyto Lake, Banff National Park, Canada. *Sedimentary Geology*, **113**, 195-209.
Smith, G. A. (1987) Sedimentology of volcanism-induced aggradation in fluvial basins: examples from the Pacific Northwest, U.S.A. In: *Recent developments in fluvial sedimentology* (Ed. by F. G. Ethridge, R. M. Flores and M. D. Harvey), pp. 217-228. Society of Economic Paleontologists and Mineralogists Special Publication 39.
Smith, N. D. (1974) Sedimentology and bar formation in the upper Kicking Horse River, a braided outwash stream. *Journal of Geology*, **82**(2), 205-223.
Smith, N. D. (1978) Some comments on terminology for bars in shallow rivers. In: *Fluvial sedimentology* (Ed. by A. D. Miall), pp. 85-88. Canadian Society of Petroleum Geologists Memoir 5, Calgary.
Smith, N. D. (1985) Proglacial fluvial environment. In: *Glacial sedimentary environments* (Ed. by G. M. Ashley, J. Shaw and N. D. Smith), pp. 85-134. Society of Paleontologists and Mineralogists SEPM Short Course 16, Tulsa.
Smith, S. A. (1990) The sedimentology and accretionary styles of an ancient gravel-bed stream: the Budleigh Salterton Pebble Beds (Lower Triassic), southwest England. *Sedimentary Geology*, **67**, 199-219.
Sohn, Y. K., Rhee, C. W. & Kim, B. C. (1999) Debris flow and hyperconcentrated flood-flow deposits in an alluvial fan, northwestern part of the Cretaceous Yongdong Basin, Central Korea. *The Journal of Geology*, **107**, 111-132.
Steel, R. J. & Thompson, D. B. (1983) Structures and textures in Triassic braided stream conglomerates ('Bunter' Pebble Beds) in the Sherwood Sandstone Group, North Staffordshire, England. *Sedimentology*, **30**, 341-367.
Stephens, M. (1994) Architectural element analysis within the Kayenta Formation (Lower Jurassic) using ground-probing radar and sedimentological profiling, southwestern Colorado. *Sedimentary Geology*, **90**, 179-211.
Stouthamer, E. (2001) *Holocene avulsions in the Rhine-Meuse delta, The Netherlands*. PhD Thesis, Faculty of Geographical Sciences, Utrecht University, Utrecht, 211 pp.
Stuiver, M., Reimer, P. J. & Braziunas, T. F. (1998) High-precision radiocarbon age calibration for terrestrial and marine samples. *Radiocarbon*, **40**(3), 1127-1151.
Tillard, S. & Dubois, J.-C. (1995) Analysis of GPR data: wave propagation velocity determination. *Journal of Applied Geophysics*, **33**, 77-91.
Todd, S. P. (1989) Stream-driven, high-density gravelly traction carpets: possible deposits in the Trabeg Conglomerate Formation, SW Ireland and some theoretical considerations of their origin. *Sedimentology*, **36**, 513-530.
Todd, S. P. (1996) Process deduction from fluvial sedimentary structures. In: *Advances in fluvial dynamics and stratigraphy* (Ed. by P. A. Carling and M. R. Dawson), pp. 299-350. John Wiley and Sons, Chichester.
van Dam, R. L. (2001) *Causes of ground-penetrating radar reflections in sediment*. PhD Thesis, Faculty of Earth Sciences, Vrije Universiteit, Amsterdam, 110 pp.
van Dam, R. L. & Schlager, W. (2000) Identifying causes of ground-penetrating radar reflections using time-domain reflectometry and sedimentological analyses. *Sedimentology*, **47**, 435-449.
van Overmeeren, R. A. (1998) Radar facies of unconsolidated sediments in The Netherlands: a radar stratigraphy interpretation method for hydrogeology. *Journal of Applied Geophysics*, **40**, 1-18.
Vandenberghe, J. & van Overmeeren, R. A. (1999) Ground penetrating radar images of selected fluvial deposits in the Netherlands. *Sedimentary Geology*, **128**, 245-270.
Whiting, P. J., Dietrich, W. E., Leopold, L. B., Drake, T. G. & Shreve, R. L. (1988) Bedload sheets in heterogeneous sediment. *Geology*, **16**, 105-108.
Williams, H. F. L. & Roberts, M. C. (1989) Holocene sea-level change and delta growth: Fraser River delta, British Columbia. *Canadian Journal of Earth Sciences*, **26**, 1657-1666.
Willis, B. (1993) Ancient river systems in the Himalayan foredeep, Chinji village area, northern Pakistan. *Sedimentary Geology*, **88**, 1-76.